Dynamic Modeling of Multi Stage Flash (MSF) Desalination Plant

by

Hala Faisal Al-Fulaij

Department of Chemical Engineering

University College London

Supervisors: Professor David Bogle

Thesis submitted for the degree of Doctor of Philosophy (Ph.D.)

at University College London (UCL)

July 2011

I, Hala Faisal Al-Fulaij, confirm that the work presented in this thesis is my own. Where information has been derived from other sources, I confirm that this has been indicated in the thesis.

Hala F. Al-Fulaij

Acknowledgments

This Ph.D. was carried out between March 2007 and January 2011 at the Chemical Engineering department, University College London (UCL).

This work was supervised by Professor David Bogle (UCL) and Professor Hisham Ettouney (Kuwait University). I take this opportunity to thank both of my supervisors for general guidance throughout the project and their great help, support and insight. I also thank Professor Giorgio Micale and Doctor Andrea Cipollina from University of Palermo who expended their time and made significant contribution to my knowledge especially in the computer tools field.

Also, I am grateful for the love and support of my family, especially my mother, father, husband and sisters. Their patience and encouragement have given me the strength to complete my thesis study.

Finally I would like to dedicate this thesis to my lovely children (Rayan, Maryam, AbdulWahab and Najat) hoping them the most of health, success, and happiness.

Abstract

The world population is increasing at a very rapid rate while the natural water resources remain constant. During the past decades industrial desalination (reverse osmosis (RO) and multistage flash desalination (MSF)) became a viable, economical, and sustainable source of fresh water throughout the world. In the MSF units, the flashing of seawater involves formation of pure vapour, which flows through a wire mesh demister to remove the entrained brine droplets and then condenses into product water.

The study presented in this thesis is motivated by the absence of detailed modelling and analysis of the dynamics of the MSF process and the demister. A detailed dynamic model can be used in design, control, startup/shutdown and troubleshooting. Most of the previous studies on MSF plant focused on model development and presented limited amount of performance data without any validation against plant data. Literature models of the MSF demister are either empirical or semi-empirical. This motivated use of a computational fluid dynamics (CFD) software to design a new demister that will reduce the pressure/temperature drop in the vapour stream without affecting the separation efficiency of brine droplets and allows the optimal design of complete MSF units.

Lumped parameter dynamic models were developed for the once through (MSF-OT) and the brine circulation (MSF-BC) processes. The models were coded using the gPROMS modelling program. The model predictions for both MSF-OT and MSF-BC in steady state and dynamic conditions showed good agreement against data from existing MSF plants with an error less than 1.5%. Dynamic analysis was made to study plant performance upon making step variations in system manipulated variables and identify stable operating regimes. New stable operating regimes were reached upon changing the cooling water flow rate by $\pm$ 15% and increasing the recycle brine flow rate by 15% and decreasing it by 7%. This was not the case for the steam temperature where its variation was limited to $\pm$ 2-3 %. This behavior is consistent with the actual plant data.

The FLUENT software was used to model the MSF demister using different combinations of Eulerian and Lagrangian approaches to model the vapour and the

brine droplets. This provided the open literature with novel and new methodologies for design and simulation of the MSF demister using CFD.

A new demister design was made upon varying the wire diameter. This led to an efficient design with low pressure drop and high separation efficiency. This design was used in the MSF/gPROMS model to predict its effect on the heat transfer area. The new design provided reductions of 3-39% in the condenser heat transfer area without affecting dynamic performance. Since the tubing system accounts for almost 70% of the capital cost, then this would reduce the plant capital cost and product unit cost.

The modelling approach presented in this thesis enables design of thermal desalination units to determine optimal heat transfer area and optimized operating conditions.

Table of Contents

List of Figures

List of Tables

Chapter 1
Introduction and motivation

The world population is increasing at very rapid rates while the natural water resources such as rivers, lakes, subsurface, and aquifers remain constant. Global resources of fresh water are scarce, unevenly distributed, and in many cases require some form of treatment and handling (Harvey & Mercusot, 2007). Thus, water shortage problems are found in more than 120 countries around the world. As a result, in many arid zones, costal or island, desalination of sea or brackish water can be the only solution for supply of fresh water. Currently, desalination is the life line in all of the Gulf states, Cyprus, Malta, Southern Italy, Spain, Greece, the Caribbean islands, southern California, western Florida, western Australia, Singapore, etc. (IDA, 2006). In addition, desalination is used on a wide scale in the USA, Japan, and Korea either to desalinate low salinity water or seawater for industrial use (Hinkebein & Price, 2005).

Desalination processes are classified into thermal and membrane desalination processes. Thermal desalination processes include multistage flashing (MSF), multiple effect evaporation (MED), and mechanical vapour compression (MVC) (Cipollina, Micale, & Rizzuti, 2009). On the other hand, membrane desalination is dominated by reverse osmosis (RO), while the electrodialysis (ED) process is found on a very limited scale (Cipollina, Micale, & Rizzuti, 2009). In the Gulf countries, MSF dominates the desalination industry and this is due to its reliable performance and its large unit capacity. The MSF processes include the once through (MSF-OT) and the brine recycle (MSF-BC) systems. The most common MSF process is the brine recycle system (MSF-BC).

A review of the desalination literature shows that mathematical modeling is an essential element in design, performance simulation, and development of better understanding for various elements of the process. As a result, process development and progress have taken place over the past 50 years and since the inception of desalination on industrial scale in the early 1960’s. The study presented in this thesis focuses on modeling and analysis of the MSF process, which accounts for more than

80% of fresh water supplies in the Gulf countries (Khawaji, Kutubkhanah, & Wie, 2007).

The aim of this thesis is: (1) the ability to improve the understanding of the design and operation of the MSF plants (2) integration of complex systems which consistute the MSF process, i.e., vapour flashing, orifice flow, thermodynamic losses, demister flow, vapour condensation etc. (3) establish basis for design and operation through the development of accurate models capable of simulating the system physics.

Three specific objectives are undertaken in this thesis. The first is detailed dynamic modeling of the MSF process, the second is detailed design of the MSF demister and the third integrates the first and second tasks. The MSF dynamic model was coded and solved using the gPROMS software. This work is motivated through extensive literature review which showed that most of the previous studies were done for older MSF units with production capacities below 32,000 m^3/d. Also, most of the studies were limited to model development and presented a small amount of data on system dynamics and without any validation of model results against plant data. The proposed model was applied to new MSF units with capacities above 50,000 m^3/d. In addition, the study focused on detailed analysis of the system dynamics upon making step changes in the plant manipulated variables. The analysis focused on determining regimes of stable and unstable operation. The models developed and presented in this thesis provide an inexpensive tool for system design and simulation. Also, it helps in better understanding of process details, design elements, and performance characteristics.

The second task focused on detailed modeling of the MSF demister by using the FLUENT computational fluid dynamics (CFD) software. This work was motivated by lack of such studies in the literature and the fact that most of the MSF demister studies are either empirical or semi-empirical in nature. The MSF demister has a strong effect on capital investment for the process and product quality. Optimum performance of the demister results in product with salinity close to zero. Also, the resulting pressure drop and associated temperature drop across the demister becomes

very small. As a result, the driving force for the heat transfer in the condenser tubes will increase and the required heat transfer area of the condenser tubes becomes smaller. In turn this reduces the process capital cost (70% of the plant capital cost is for the tubes) because of the reduction in the required heat transfer area for the condenser tubing. In addition, reduction in the amount of entrained brine droplets would reduce the frequency of maintenance and cleaning cycles of the flashing stages and the outside surface of the condenser tubes.

The third task integrates the first and second tasks, where the simulation results of the demister are used to simulate steady state operation of the MSF process. This analysis focused on the effect of using different demister designs on plant performance. This type of analysis is novel to the literature where combined analysis is performed using lumped parameter model of the plant and CFD model of the demister. This work is motivated by absence of such studies in the literature and the strong effect of the demister on the performance of the MSF process.

In Chapter 2, water shortage problems around the world and the need for water desalination are discussed. Also it includes a brief summary of different water desalination technologies followed by a detailed description of two types of multi stage flash desalination, MSF-OT and MSF-BC. Next, Chapter 3 presents a literature review on different types of modeling MSF processes. It starts with simple mathematical model, followed by detailed steady state and dynamic mathematical modeling. Next, in chapter 4, the MSF dynamic model is developed together with the gPROMS computer code for solving the model equations. At the end of this chapter, a brief description of the gPROMS modeling language is presented. Chapter 5 starts with validation of the dynamic model against steady state and dynamic data of industrial MSF plants. The dynamic model is then used to study operational stability as a function of step change disturbances in major operating conditions. In chapter 6, the Computational Fluid Dynamics (CFD) tool is used to model the demisters within the flashing stage. This chapter starts with description of the demister followed by development of the mathematical model and different approaches used to model the demister. At the end a brief summary of the CFD code is presented. CFD model results are validated against experimental data and real plant data for a large scale

plant and that is shown in Chapter 7. In this chapter, results of each approach and the effect of the new designed demister on the pressure drop and separation efficiency are presented. The chapter ends with a comparison between different demisters geometries. Chapter 8 combines the gPROMS dynamic study and the CFD demister model through studying the effect of the newly designed demister on the MSF plant heat transfer area, water quality and system dynamics. Chapter 9 presents the conclusion of this thesis and summarizes some important avenues of future work within the scope of this work.

Chapter 2
Water Desalination

2.1 Introduction

Although it contains no nutrients, water is a vital component of our diets. It is essential for the growth and maintenance of our bodies, as it is involved in a number of biological processes. But most of the people around the world don't get nearly enough water (UN, 2010a). Water comprises 50 to 70 per cent of an adult's total body weight, and without regular top-ups, our body's survival time is limited to a matter of hours or days. This chapter is divided into 8 sections. First, water shortage problems and reasons will be presented. The next section will talk about sources and distribution of fresh water around the globe. Then, water types and properties will be presented. That will be followed by a section which shows the seawater composition and how the water salinity would affect its properties. At this point, the need for water desalination will appear as a solution to provide fresh water. In this section, the desalination technologies are discussed to present the countries shares in the desalination market. Classification of desalination technologies will be discussed in detail in the following section. Finally, a detailed study on the MSF process types is shown with explanation of the details of the flashing stage. At the end of this chapter, general conclusions will be presented.

2.2 Water Shortage Problem

The world population is increasing at a very rapid rate; while, the natural water resources remain constant. Natural water resources are found in rivers, lakes, subsurface, and aquifers. Figure 2.1 shows a bar chart for the population development over the past 200 years and forecast for the next 50 years (UN, 2010b).

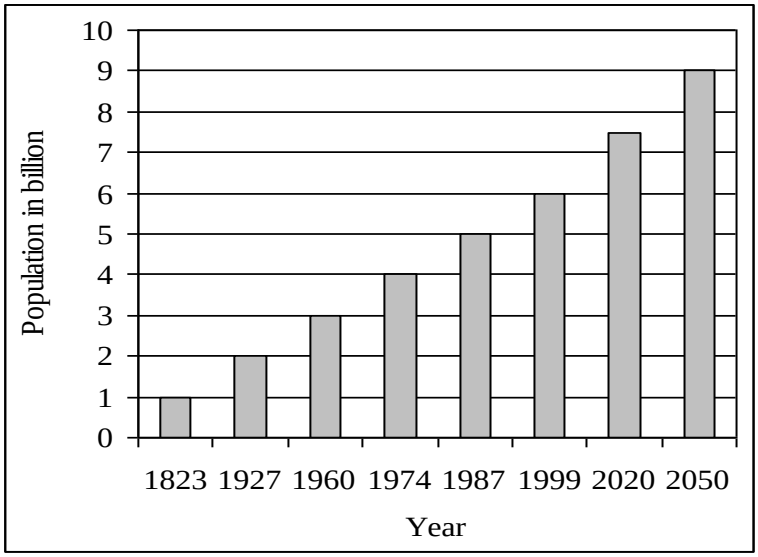

Figure 2.1 Variation in world population from 1823 to 2050 (UN,2010b)

As shown in Figure. 2.1, since 1823 and up to 2050 the world population has increased by almost one order of magnitude; while the natural water resources have not changed. Ninety-six percent of world population increase now occurs in the developing regions of Africa, Asia and Latin America, and this percentage will rise over the course of the next quarter century. At present, about 40% of the world's population is suffering from serious water shortages. By the year 2025, this percentage is expected to increase to more than 60%. This is because of the rapid increase of population, changes in the life-style, increased economic activities, and pollution that limit the use of fresh water resources. Moreover, common use of unhealthy water in developing countries causes 80-90% of all diseases and 30% of all deaths.

The combined effect of the continuous increase in the world population, changes in life style, and the limited natural resources of fresh water makes industrial desalination of seawater a major contender for providing sustainable source of fresh water for arid zones and during drought periods. This solution is also supported by the fact that more than 70% of the world population lives within 70 km of seas or oceans. During the second half of the twentieth century, desalination of seawater proved to be the most practical and in many cases the only possible solution for many countries around the globe, i.e., the Gulf States, Mediterranean and Caribbean Islands. At the

turn of century, desalination is being considered by a larger number of countries as the most viable and economical solution for providing fresh water.

2.3 Sources of Fresh Water

Global resources of fresh water are scarce, unevenly distributed, and in many cases it requires some form of treatment and handling. The water content on the earth is classified according to the following (Cipollina, Micale, & Rizzuti, 2009):

- Total amount of water is equal to 1.4×10^9 km^3.
- Percentage of salt water of the total amount is 97.5%. This is equal to 1.365×10^9 km^3.
- The remaining 2.5% is fresh water. This amount is equal to 3.5×10^7 km^3
- Frozen water in the icecaps (on mountain tops), glaciers (frozen rivers on high altitudes), and frozen soil moisture (in cold climates such as Siberia, Alaska, Northern Canada, etc.). The total amount of frozen water is equal to 80% of the total amount of fresh water. These forms are not easily accessible for human use.
- About 20% of the total amount of fresh water or 0.5% the total amount of fresh and seawater is found in lakes, rivers, or aquifers.

Table 2.1 gives volumes and percentages of various water resources, which includes atmospheric water, glaciers, rivers, lakes, marshes, soil moisture, and oceans (Shiklomanov & Rodda, 2003). The global daily average of rainfall is 2×10^{11} m^3. This amount is poorly distributed across the globe (Al-Shuaib, Al-Bahu, El-Dessouky, & Ettouney, 1999).

Table 2.1: Distribution of water resources across the globe

Resource	Volume km^3	Percent of Total Water	Percent of Fresh Water
Atmospheric Water	12,900	0.001	0.01
Glaciers	24,064,000	1.72	68.7
Ground Ice	300,000	0.021	0.86
Rivers	2,120	0.0002	0.006
Lakes	176,400	0.013	0.26
Marshes	11,470	0.0008	0.03
Soil Moisture	16,500	0.0012	0.05
Aquifers	10,530,000	0.75	30.1
Lithosphere	23,400,000	1.68	
Oceans	1,338,000,000	95.81	
Total	1,397,000,000		

As mentioned before, the natural water resources are constant across the world. This has resulted in water shortages in 88 developing countries across the world containing 50% of the world population. By 2025, it is estimated that 1.8 billion people will be living in countries or regions with absolute water scarcity, and two-thirds of the world population could be under stress conditions (UN, 2006). Most countries in the Near East and North Africa suffer from acute water scarcity, as do countries such as Mexico, Pakistan, South Africa, and large parts of China and India. Water supplies in these countries cannot meet urban and industrial development as well as associated changes in the life style. Moreover, common use of polluted (sewage, industry waste, agriculture and drainage water) water in developing countries causes 80 to 90% of all diseases and 30% of all deaths (Ustun & Corvalan, 2006). Even in industrial countries, long spells of dry seasons and limited rainfall forces governments, states, and municipalities to adopt severe water restriction programs that affect the population. Such situations are reported on a frequent basis in several countries around the world. The current water shortage extends to include underground water supplies, previously considered to be an unlimited resource in many countries. In this regard, several cases are reported for well failure, decline of the water table, and seawater intrusion into the fresh water aquifers. This situation has

forced many countries, industrial and developing, to adopt active and efficient programs for reclamation of industrial and municipal wastewater.

2.4 Water Types

Classification of various types of water is based on the purpose for which the water is used. As shown in table 2.2 the first water grade is set for safe drinking, household purposes, and a number of industrial applications (El-Dessouky & Ettouney, 2002). This water category has a salinity range of 5 to 1000 ppm. This type of water is found in rivers and lakes and can be generated by industrial desalination processes. In large cities, various levels of water salinity are used, where water with salinity below 150 ppm is used for drinking while higher salinity water of up 1000 ppm is used for various household applications. This has proved to be more effective, because the average per capita consumption of the low salinity drinking water (150 ppm) is limited to 2 liters/day. On the other hand, the per capita consumption rate for other household purposes is 200-400 liters/day, which is used for cooking, washing, cleaning, gardening, and other purposes. At industrial scale, the most stringent water quality is set by the makeup water for boilers and applications related to the electronic industry and pharmaceuticals. The water quality for this application is limited to a maximum salinity of 0.1 ppm. This high degree of purity is achieved through the use of ion exchangers, which operates on low salinity river water or industrially desalinated water. Other industrial applications call for less stringent water quality than those used for boilers. Applications include chemical reactions, dairy and food, washing and cleaning, and cooling

The second water category has a salinity range of 1000-3000 ppm. This type of water is suitable for irrigation purposes and industrial cooling. This applies for higher salinity water, which includes brackish and seawater. The salinity range for brackish water is 3000-10000 ppm. As for the seawater its average salinity is 34,000 ppm. Water with salinity above 10000 ppm is termed as high salinity water. The salinity of seawater varies subject to local conditions, where it is affected by ambient and topographical conditions. For example, enclosed seas have higher salinity than

open seas and oceans. Also, seas, which are found in areas of high temperatures or that receive high drainage rates of saline water, would certainly have higher degree of salinity. For example, the salinity of the Gulf water near the shores lines of Kuwait, Saudi Arabia, and the United Arab Emirates may reach maximum values close to 50,000 ppm. On the other hand, the salinity of the Gulf water near the Western shores of Florida, USA, may reach low values of 30,000 ppm. This is because of the large amount of fresh water received from rivers and springs in that area.

Table 2.2: Water classification based on salinity content

Type	Total Dissolved solids (TDS)	Source
Fresh Water	Up to 1,000	Industrial-Rivers-Aquifers-Lakes
Brackish Water	1,000-10,000	Industrial-Aquifers-Lakes
Salt water	>10,000	Aquifers-Lakes
Seawater	10,000-50,000	Seawater
Standard seawater	35,000	Seawater

2.5 Sea Water Composition and Properties

The main ions found in seawater include Na^{-}, Ca^{++}, K^{+}, Mg^{++}, $(SO_4)^{-}$, and Cl^{-}. Of course, all other ions found in nature are present in the seawater, but at much smaller concentrations. The chemical composition of open sea is constant; however, the total dissolved amount of dissolved solids changes subject to local conditions. This is because the diffusion time for salts or the time required to obtain complete mixing of all seas and oceans is much smaller than the time required for complete filling or replenishment. Table 2.3 shows typical composition of seawater, which has a total salinity of 36000 ppm (El-Dessouky & Ettouney, 2002). In addition to the dissolved ions found in seawater the seawater includes a wide variety of fine suspended matter that include sand, clay, microorganisms, viruses, and colloidal

matter. The size of these compounds varies over a range of $5x10^{-2}$ to 0.15 μm. Table 2.4 shows main thermodynamic properties for both seawater (salinity = 36,000 ppm) and fresh water (salinity = 0 ppm) at 25 ^{o}C (El-Dessouky & Ettouney, 2002). As shown in this table, the thermodynamics properties of the water vary depending on its salinity. Thus using accurate thermodynamic properties for a specific salinity is important to evaluate the performance of MSF process more accurately.

Table 2.3: Typical composition of seawater with salinity of 36,000 ppm

Compound	Composition	Mass Percent	ppm
Chloride	Cl^-	55.03	19810.8
Sodium	Na^+	30.61	11019.6
Sulfate	$(SO_4)^{--}$	7.68	2764.8
Magnesium	Mg^{++}	3.69	1328.4
Calcium	Ca^{++}	1.16	417.6
Potassium	K^+	1.16	417.6
Carbonic Acid	$(CO_3)^{--}$	0.41	147.6
Bromine	Br^-	0.19	68.4
Boric Acid	$H_3BO_3^-$	0.07	25.2
Strontium	Sr^{++}	0.04	14.4
Total		**100**	**36000**

Table 2.4: Thermodynamic properties of seawater and fresh water at 25^{o}C

Thermodynamic Property	Seawater (Salinity = 36,000 ppm)	Fresh water (Salinity = 0 ppm)
Density [kg/m^3]	1023.8	997.0
Specific Heat [kJ/kg.^{o}C]	3.99543	4.186172
Viscosity [kg/ms]	0.960499	0.891807
Thermal conductivity (W/m.^{o}C)	0.608656	0.610584

2.6 Need for Water Desalination

In many arid zones, coastal or inland, desalination of sea or brackish water can be the only solution for supply of fresh water. Due to the strategic nature of the product, many countries prefer to adopt the relatively expensive desalination process, which proved to provide sustainable source (Schiffler, 2004). Adoption of the desalination industry by the Gulf countries as well as a number of industrial countries has resulted in rapid progress in the industry since its inception on industrial scale in the 1950's. Currently, the world desalination capacity is exceeding 26 x 10^6 m^3/d. It is expected that this amount will be doubled before the end of the first half of this century (IDA, 2006)

The market share of the desalination industry in the Gulf countries represents more than 50% of the total world production, see Figure. 2.2. This share has not changed since the eighties, when the desalination industry became the main source of fresh water for domestic, industrial, and agriculture use in the Gulf countries. The second producer of fresh water by desalination is the US with a global market share close to 20%. It should be noted that the majority of the US desalination plants are for low salinity and river water. The data shown in Figure 2.2 amounts to a total of 22.2x10^6 m3/d, the majority of the remaining world production is approximately divided among another 10-20 countries with capacities above 100,000 m^3/d but less than 1×10^6 m^3/d, for example, Algeria, Libya, China, Singapore, Cyprus, Australia, etc, (IDA, 2006).

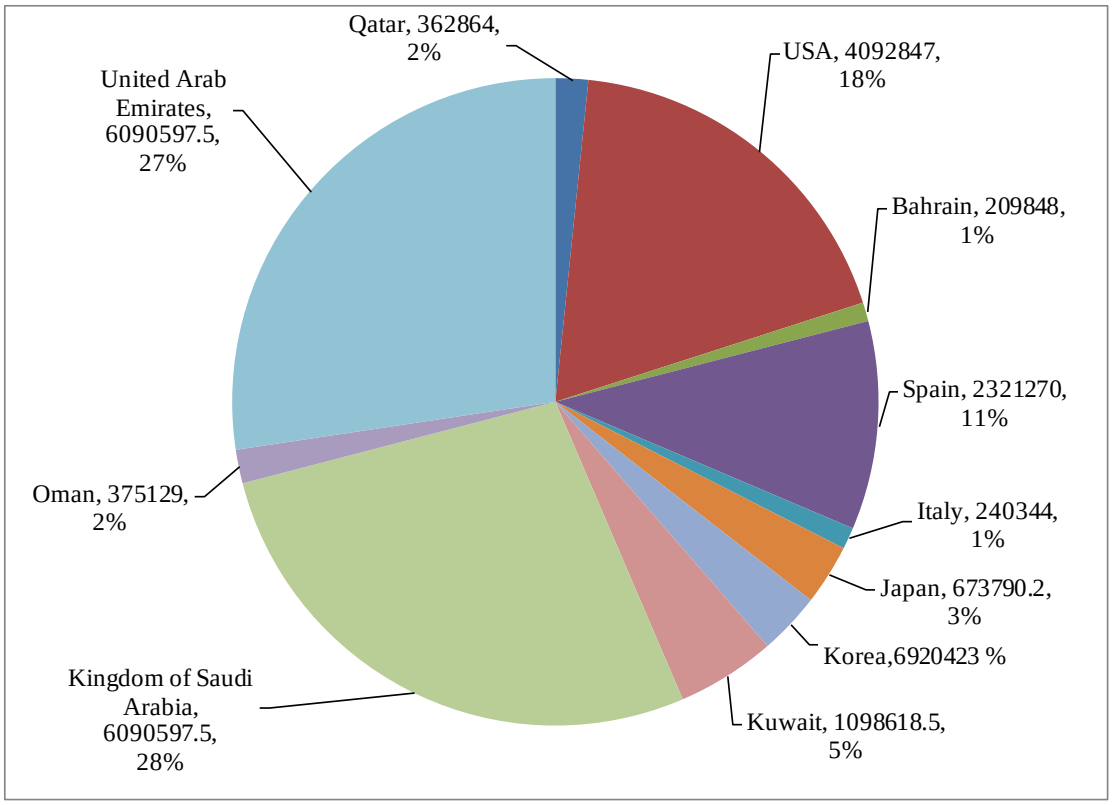

Figure 2.2 Desalination market shares of large producers (IDA,2006)

The MSF process is the workhorse of the desalination industry in the Gulf States as well as several other countries across the world. The main reason for the wide use of MSF plants is the high capacity output that they provide at relatively higher thermal efficiency and reliability, which leads to high performance and lower production costs (El-Bairouty, Fath, Saddiqi, & El-Rabghy, 2005). In addition, they are easy to operate and have almost the same characteristics as a power plant with which they are mostly combined. In the 1960's the MSF unit capacity was less than 5000 m^3/d. This capacity increased in the 1980's and 1990's to reach a unit average capacity of 30,000 m^3/d. During the current decade the unit capacity increased to reach a range of 50,000 m^3/d to 75,000 m^3/d (see Figure 2.3). The reverse osmosis process has a large portion of the desalination market. Mainly RO process is used for desalination of brackish water, river water, and reclaimed waste water. Although, RO consumes close to 25% of the total energy of MSF and multi effect evaporator (MED), but, its unit product cost is almost similar, when membrane replacement cost is considered. In addition, competitive tendering, pricing, and less restrictive system

design allowed for massive and economical increase in the unit capacity of the MSF and MED plants (Borsani & Rebagliati, 2005)

In 1960's MED processes were developed but it was facing many scaling problems on the outer surface of the tubes which makes it difficult to clean and decrease the operating period. Reverse osmosis and multi-stage flash are the techniques that are most widely used. The decision for a certain desalination technology is influenced by feed water salinity, required product quality as well as by site-specific factors such as labour cost, available area, energy cost and local demand for electricity (Fritzmann, Löwenberg, Wintgens, & Melin, 2007).

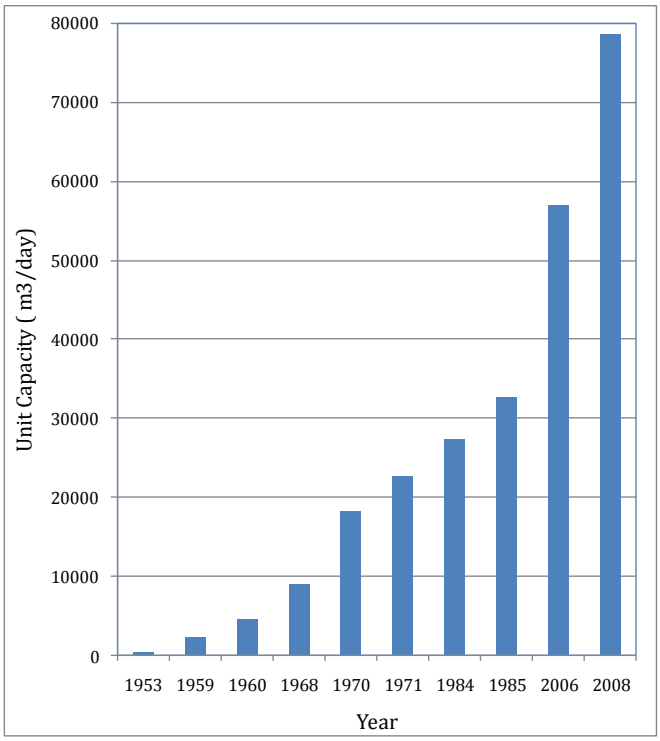

Figure 2.3 MSF unit capacity growth

Figures 2.4 and 2.5 show estimates for the market share for the main desalination processes, RO, MSF, and MED. Figure 2.4 is given for the entire desalination market, which includes desalination of river water, brackish water, and seawater. Figure 2.5 is for the desalination of seawater (IDA, 2006).

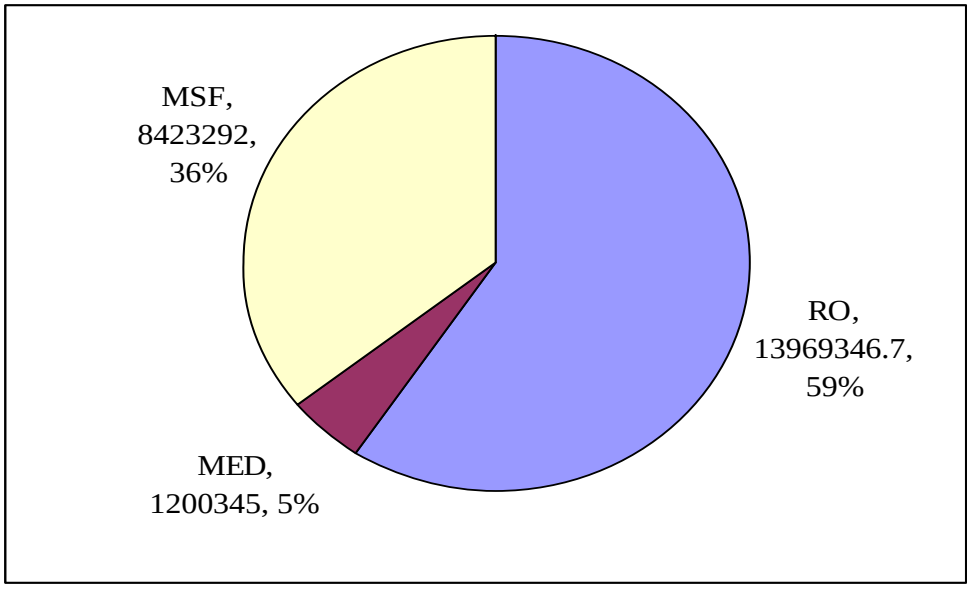

Figure 2.4 Market share of the main desalination process for desalination of river, brackish, and seawater (IDA,2006).

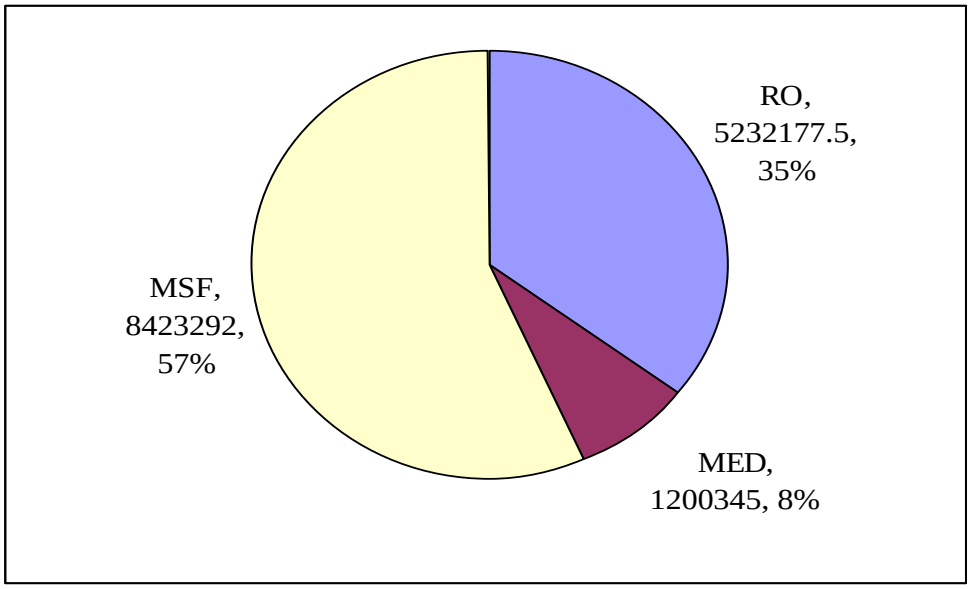

Figure 2.5 Market share of the main desalination process for desalination of seawater (IDA,2006)

Although, the MSF is found in several countries across the world, large scale MSF plants are only found in the Gulf countries. Cumulative increase for the MSF production capacity in the Gulf countries is shown in Figures. 2.6. The most striking feature in this data is rapid increase in the production capacity in the UAE to exceed that of Saudi Arabia (IDA, 2006).

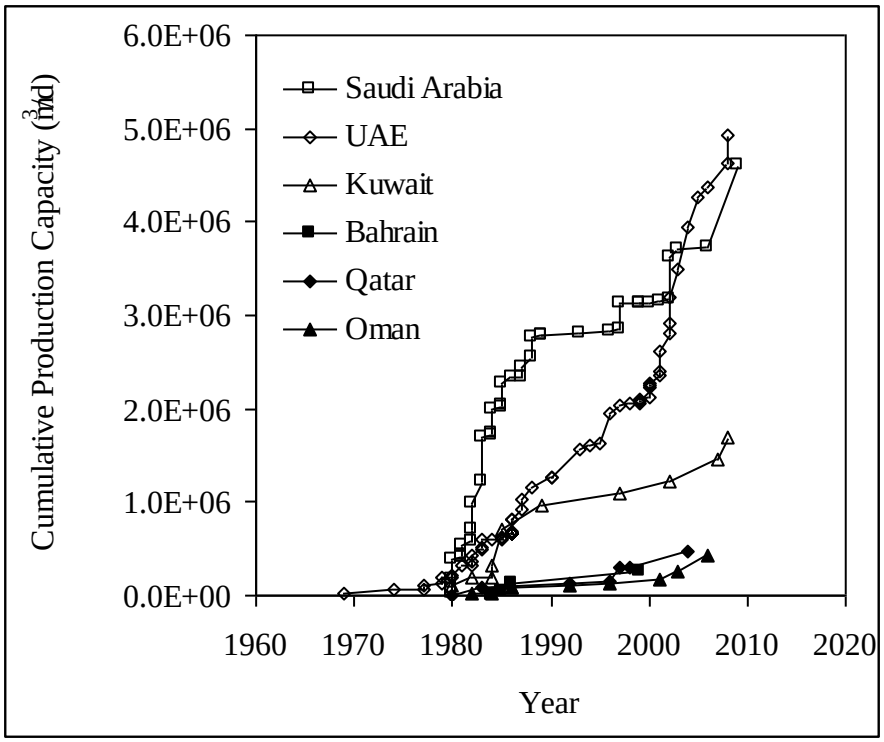

Figure 2.6 Cumulative production capacity of MSF plants in the Gulf countries

Examples of recent MSF desalination units constructed in the Gulf countries are shown in Table 2.5. The main features for these units are the increase in the unit production capacity to a range of 50,000-75,000 m^3/d and an increase in the operating temperature to a range of 105-112 ^oC instead of a lower range of 90-100 ^oC. However, the number of stages and the performance ratio remains well within those of older units with values of 20-24 stages and 8-10 performance ratio (amount of distillate produced per unit mass of steam used in the brine heater). Another feature is that all of the cited units are constructed either by Italian or Korean companies. Another important feature is the size of the entire plant, which has approached $1x10^6$ m^3/d (IDA, 2006).

Table 2.5: Examples of recent MSF installations in the Gulf countries

Plant	Year	Number of Units	Unit Capacity (m^3/d)	Total Capacity (m^3/d)	Number of Stages	Top brine Temperature (^oC)	PR	Manufacturer
Al Taweelah "B" (Abu Dhabi-UAE)	1995	6	57,600	345,600	20	112	8	Italimpianti
Al Hidd (Bahrain)	1999	4	37,000	148,000	21	107-112	9	Italimpianti
Ruwais (UAE)	2001	2	15,000	30,000	15	105-112	6	Italimpianti
Jebel Ali "K"(Dubai UAE)	2001	2	45,480	90,960	21	105	9	Italimpianti
Jebel Ali "K" 2 (Dubai UAE)	2003	3	60,530	181,590	19	105	8	Italimpianti
Mirfa (Abu Dhabi-UAE)	2002	3	34,000	102,000	21	110	8.9	Italimpianti
Umm Al Nar Station “B” (UAE)	2002	5	56,825	284,125	22	110	9	Doosan (Korea)
Fujairah (UAE)	2003	5	56,750	283,750	22	110	9	Italimpianti
Az Zour South (Kuwait)	1999	12	32,731	392772	24	110	8.8	Doosan (Korea)
Shuweihat (Abu Dhabi-UAE)	2004	6	75,670	454,000	21	111	9	Italimpianti
Subyia (Kuwait)	2007	12	56,825	681,900	23	110	9.5	Doosan (Korea)
Ras Laffan (Qatar)	2007	4	68,190	272,760	22	110	9.5	Doosan (Korea)
Sohar (Oman)	2008	4	37,504	150,018	24	110	9.5	Doosan (Korea)
Shoaiba (Saudi Arabia)	2009	12	73,645	883,742	22	110	9.5	Doosan (Korea)

2.7 Classification of Desalination Technologies

The industrial desalination processes involve the separation of nearly salt-free fresh water from sea or brackish water, where the salts are concentrated in the rejected brine stream. A simple classification of desalination processes can be made on the basis of the separation process used. Figure 2.7 shows classification of conventional thermal and membrane desalination processes.

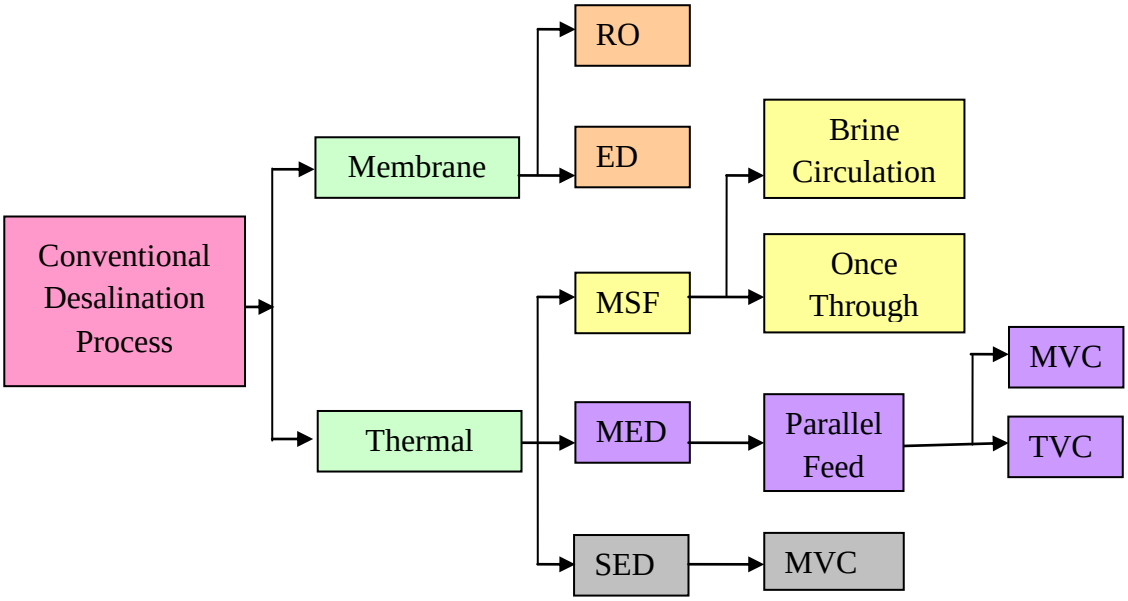

Figure 2.7 Conventional thermal and membrane desalination processes

2.7.1 Thermal processes

The thermal desalination processes include the multistage stage flashing (MSF), multiple effect evaporation (MED), and the single effect evaporation (SED). The only conventional process for the single effect evaporation is the mechanical vapour compression (MVC). As for the multiple effect evaporation, it includes two main systems. The first is the thermal vapour compression (TVC) and the second is the mechanical vapour compression (MVC). System design of the multiple effect evaporation allows for operation in the vapour compression or the stand-alone mode. The configuration of the conventional multiple effect evaporation system is the

parallel feed arrangement. Other configurations that include the feed forward or the feed backward system are not used in desalination processes. Also, most of the evaporation effects in single or multiple effect evaporation are the horizontal falling film type.

2.7.2 Membrane processes

The main membrane desalination process is reverse osmosis (RO), where fresh water permeates under high pressure through semi-permeable membranes leaving behind highly concentrated brine solution. The other membrane process is electrodialysis (ED) with very limited industrial applications. In this process the electrically charged salt ions are separated through selective ion exchange membranes leaving behind low salinity product water. Accordingly, a highly concentrated brine stream is formed on the other side of the membrane.

2.8 Multistage Flash Desalination Processes

The MSF desalination process was introduced in the early nineteen fifties. The first installation was constructed by Westinghouse and it included four flashing stages. This particular system was not a true flash desalination configuration. The patent of the multistage flash desalination configuration was made by Silver in 1957 (Silver, 1970). The main feature of this patent is the optimization of the number of stages versus the heat transfer area. Accordingly, it was found that use of a large number of stages, i.e., above 20, resulted in the optimum cost for the MSF process. Since then the MSF process went through a number of dramatic modifications and improvements. The early production capacity of a single unit was less than 500 m^3/d. In the late 1970's, several units with a larger capacity of 30,000 m^3/d were constructed and commissioned in the Gulf States. This large production capacity was a remarkable achievement for the MSF process. Another mile stone was reached through the construction and operation of the 50,000 m^3/d MSF units in Emirates. This achievement was made in the 1990's. Recently, further increase in the MSF production capacity was made by construction of the 75,000 m^3/d MSF units. In

addition to the dramatic increase in the production capacity, several other achievements were made in system design and operation. For example, use of demisters in all flashing stages was adopted in all MSF plants during the 1970's. This has resulted in reduction of the product salinity to values below 10 ppm. Also, developments of the on-line ball cleaning system has resulted in less frequent use of acid cleaning or plant shut down. Currently, MSF plants can be operated for periods varying from 2-5 years before a major overhaul is necessary (Ettouney, El-Dessouky, & Alatiqi, 1999), (Al-Shuaib, Al-Bahu, El-Dessouky, & Ettouney, 1999). Recent field experience shows that a large number of existing MSF plants has exceeded the intended life time (Al-Zubaidi, 1987), (Abu-Eid & Fakhoury, 1974). Several of these plants are going through rehabilitation. More efficient construction materials are used in the rehabilitation and newly designed and streamlined components. Such replacements are taking place in all areas of the plant, which may include venting system, demisters, tubing, partitions, and pumping units.

The MSF desalination plants are divided into two models, Once-through MSF (MSF-OT) and Brine recirculation MSF designs (MSF-BC). Comparative study was done in (Helal , 2004) that includes design, steady state modeling and optimization between the two designs. The Once-through MSF plants consist of an evaporation section (heat recovery section) and a brine heater and the condenser tubes arrangement will let the process be either Long-Tube (LT)- once through , or Cross-Tube (CT)- once through. The Brine recirculation MSF consists of brine heater, heat recovery section, and heat rejection section. The role of the rejection section is to remove the surplus thermal energy from the plant, thus cooling the distillate product and the concentrated brine to the lowest possible temperature. Also the condenser tubes arrangement will let the process to be either Long-Tube (LT)-brine recirculation, or Cross-Tube (CT)-brine recirculation.

The MSF field studies (Thirumeni & Deutsche, 2005), (Helal , 2003) show clearly the progress of the process over the years. The studies show adoption of various materials, cleaning and antiscalent agents, and controllers to improve the system performance. Also they show a gradual increase in the system capacity over

the years, continuous operation for long periods, high performance ratio, and more efficient operation.

2.8.1. Once through MSF process

The objective of the MSF-OT system is to overcome the main drawback of the single stage flash unit which is the low value of the system performance ratio. This is achieved by increasing the number of stages. Of course increasing the number of stages for the same flashing range would result in a reduction of the temperature drop per stage and in turn would reduce the driving force for heat transfer and consequently increases the total heat transfer area.

The physical processes that take place in the MSF-OT configuration are similar to those of the SSF (single stage flashing) process. This is except for using a larger number of flashing stages, where the same flashing process is repeated. The MSF-OT process has a simple layout, where all the feed seawater flows through the condenser tubes in the flash chambers. This results in energy recovery and increase of the seawater temperature before it is heated to the top brine temperature in the brine heater. Subsequently, flashing of the hot brine stream and formation of the distillate product takes place across the flashing chambers. A process schematic is shown in Figure 2.9. Process details are described in the following points:

- The feed seawater (M_f) is de-aerated and chemically treated before being introduced into the condenser/preheater tubes of the last flashing stage in the heat recovery section.
- As the seawater flows across the tubes from stage (n) to stage (1), its temperature increases due to absorption of the latent heat of the condensing fresh water vapour.
- The feed seawater (M_f) enters the brine heater tubes, where the heating steam (M_S) is condensed on the outside surface of the tubes. The feed seawater (M_f) absorbs the latent heat of condensing steam and its temperature increases to its maximum design value known as the top

brine temperature (T_o). This value depends on the nature of chemicals used to control the scale formation.

- The feed seawater (M_f) enters the flashing stages, where a small amount of fresh water vapour is formed by brine flashing in each stage. The flashing process takes place due to a decrease in the stage saturation temperature that causes the reduction in the stage pressure.
- In each stage, the flashed off vapour condenses on the outside surface of the condenser tubes, where the feed seawater (M_f) flows inside the tubes from the cold to the hot side of the plant. This heat recovery improves the process efficiency because of the increase in the feed seawater temperature.
- The condensed fresh water vapour outside the condenser tubes accumulates across the stages and forms the distillate product stream (M_d). This stream cascades in the same direction of the flashing brine from stage to stage and is withdrawn from the last stage.
- The flashing process and vapour formation is limited by the increase in the specific vapour volume at lower temperatures and difficulties encountered for operation at low pressures. Common practice limits the temperature of the last stage to range of 30 to 40^{o}C, for winter and summer operation, respectively. Further reduction in these temperatures results in drastic increase of the stage volume and its dimensions.
- In MSF, most of flashing stages operating at temperatures below 100 ^{o}C have vacuum pressure. This increases the possibilities of leakage of the outside air into the vessel. At such conditions, air and other dissolved gases in the flashing brine (not removed in the deaerator or formed by decomposition of $Ca(HCO_3)$) are non-condensable and their presence in the system may result in severe reduction in the heat transfer rates within the chamber, increase of the tendency for corrosion, and reduction of the flashing rates. This condition necessitates proper venting of the flashing stages to enhance the flashing process and to improve the system efficiency.

- Treatment of the feed seawater (M_f) is limited by simple screening and filtration. On the other hand, treatment of the feed seawater stream is more extensive and it includes dearation and addition of chemicals to control scaling, foaming, and corrosion.

2.8.2 Brine circulation MSF process

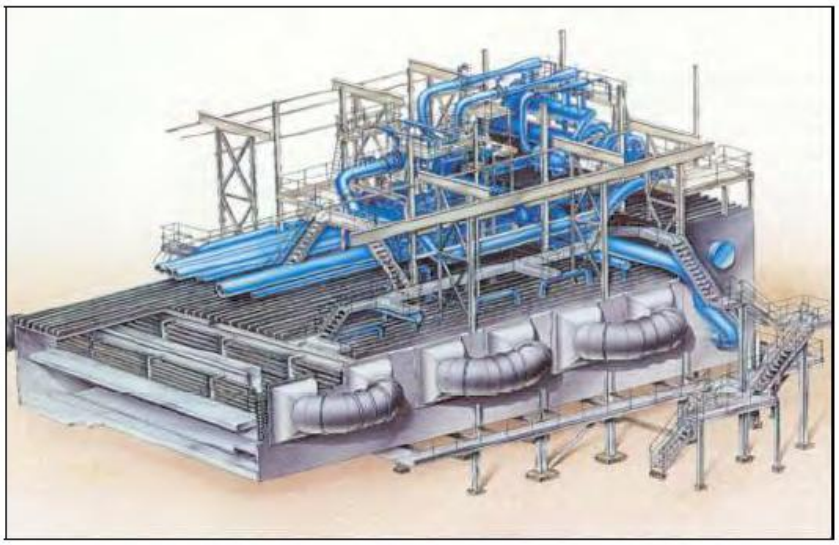

Figure2.8 View of a typical multistage flash desalination plant

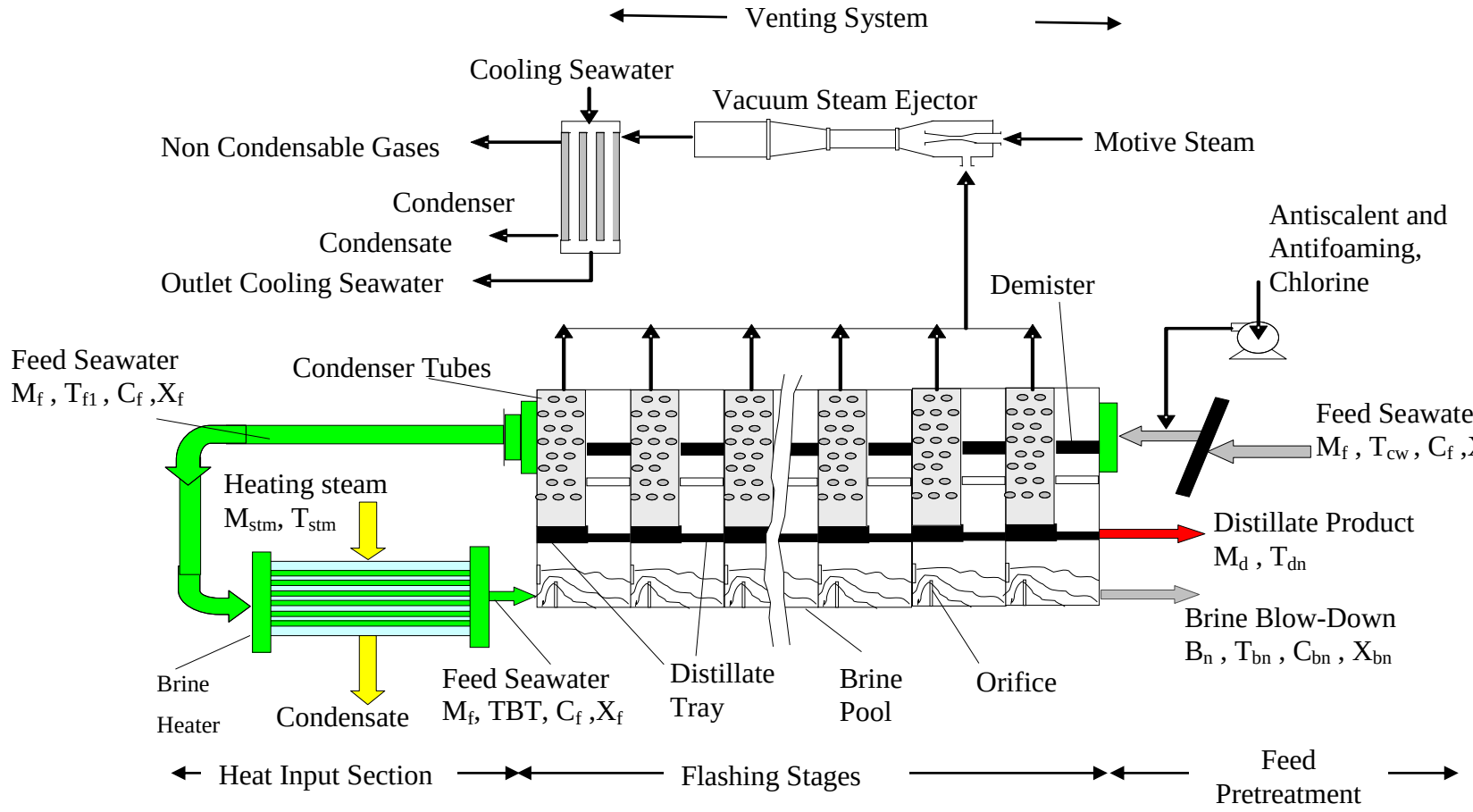

Figure 2.9 Multistage Flash Desalination Once through process (MSF-OT)

MSF-BC is a system where the brine is recycled as much more common. A schematic of the MSF-BC process is shown in Figure 2.10. Details of the MSF process are described below:

- The intake seawater stream (M_f+M_{cw}) is introduced into the condenser tubes of the heat rejection section, where its temperature is increased to a higher temperature by absorption of the latent heat of the condensing fresh water vapour.
- The warm stream of intake seawater is divided into two parts: the first is the cooling seawater (M_{cw}), which is rejected back to the sea and the second is the feed seawater (M_f), which is deaerated, chemically treated and then mixed in the brine pool of the last flashing stage in the heat rejection section.
- The brine recycle stream (M_r) is extracted from the brine pool of the last stage in the heat rejection section and is introduced into the condenser tubes of the last stage in the heat recovery section. As the stream flows in the condenser tubes across the stages it absorbs the latent heat of condensation from the flashing vapour in each stage.
- The brine recycle stream (M_r) enters the brine heater tubes, where the heating steam (M_s) is condensed on the outside surface of the tubes. The brine stream absorbs the latent heat of condensing steam and its temperature increases to its maximum design value known as the top brine temperature (T_o). Its value depends on the nature of chemicals used to control the scale formation.
- The hot brine enters the flashing stages in the heat recovery section and then in the heat rejection section, where a small amount of fresh water vapour is formed by brine flashing in each stage. The flashing process takes place due to decrease in the stage saturation temperature and causes the reduction in the stage pressure.
- In each stage of the heat recovery section, the flashed off vapour condenses on the outside surface of the condenser tubes, where the brine recycle stream (M_r) flows inside the tube from the cold to the hot

side of the plant. This heat recovery improves the process efficiency because of the increase in the feed seawater temperature.

- The condensed fresh water vapour outside the condenser tubes accumulates across the stages and forms the distillate product stream (M_d). This stream cascades in the same direction of the flashing brine from stage to stage and is withdrawn from the last stage in the heat rejection section.
- The flashing process and vapour formation is limited by increase in the specific volume of the vapour at lower temperatures and difficulties encountered for operation at low pressures. Common practice limits the temperature of the last stage to range from 30 to 40 ^{o}C, for winter and summer operation, respectively. Further reduction in these temperatures results in drastic increase of the stage volume and its dimensions.
- In MSF, most of the flashing stages operating at temperatures below 100 ^{o}C have vacuum pressure. This increases the possibilities of leakage of the outside air into the vessel. Also, trace amounts of dissolved gases in the flashing brine, which are not removed in the deaerator or formed by decomposition of $CaHCO_3$. At such conditions, air and other gases are non-condensable and its presence in the system may result in severe reduction in the heat transfer rates within the chamber, increase of the tendency for corrosion, and reduction of the flashing rates. This condition necessitates proper venting of the flashing stages to enhance the flashing process and to improve the system efficiency.
- Treatment of the intake seawater (M_f+M_{cw}) is limited to simple screening and filtration. On the other hand, treatment of the feed seawater stream is more extensive and it includes deaeration and addition of chemicals to control scaling, foaming, and corrosion.

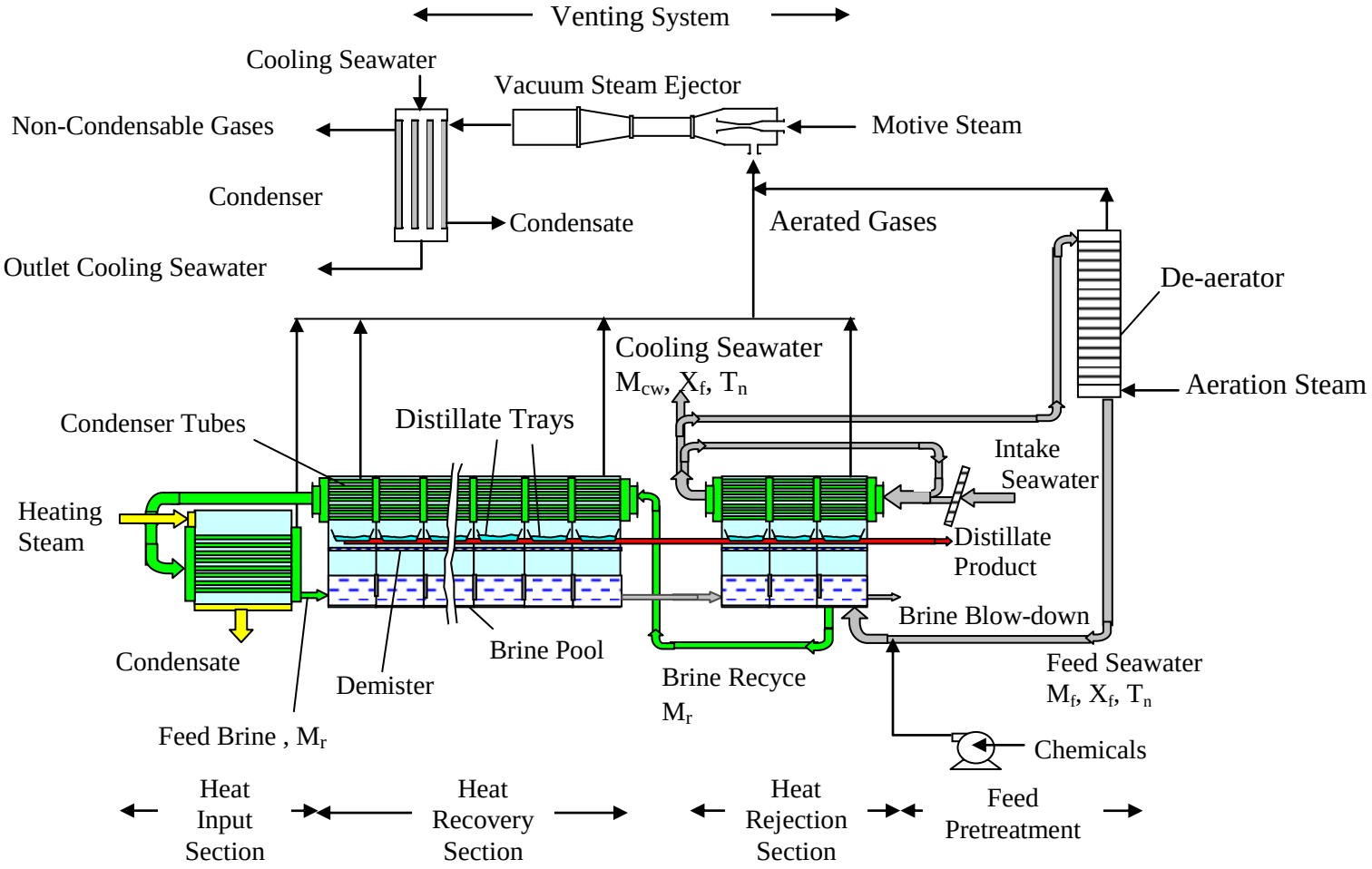

Figure 2.10 Multistage flash desalination with brine circulation (MSF-BC)

2.8.3 Comparison between MSF processes

The most common multistage flash desalination process is the brine recycle system (MSF-BC). As for the once through system (MSF-OT) its use is found on a very limited scale. This is because the (MSF-BC) has the following advantages:

1- In MSF-OT there is no control of the feed sea water temperature. In MSF-BC control of the sea water temperature takes place in the last stage of the heat rejection section.
2- The flow rate ratio of the feed to product in the MSF-OT process is approximately 10:1. On the other hand, this ratio in the brine circulation MSF is 2.5:1. This means that the amount of feed sea water in the MSF-OT system is close to 4 times higher than the amount of feed sea water in the MSF-BC system. This requires use of larger equipment for chemical treatment and higher dosing rates of various treatment chemicals (scale and foam) (Ettouny & El-Dessouky, 1999).
3- The gain output ratio or performance ratio (amount of distillate produced per unit mass of steam feed to the brine heater) of MSF-BC remains constant as the seawater temperature drops from 25^{o}C (summer) to 15^{o}C (winter) and that is due to the winter loop operation which controls the intake seawater temperature before entering the plant. While MSF-OT reduces the gain output ratio to low values of 3 as the seawater temperature drops from 25^{o}C (summer) to 15^{o}C (winter). That is because more steam will be required to heat the seawater to the same top brine temperature (Ettouney, El-Dessouky, & Al-Juwayhel, 2002).
4- Maintaining the gain output ratio at a value of 8 would require decrease in the brine blow down temperature, which is associated with drastic increase in the stage dimensions (to limit the vapour velocity to 4 m/s) (Ettouney, El-Dessouky, & Al-Juwayhel, 2002).
5- Low temperature of the reject brine in the MSF-BC due to the mixing in the stage and high temperature of the reject brine in the MSF-OT

On the other hand, the MSF-OT use can be useful especially in equatorial regions, where the seawater temperature remains nearly constant throughout the year. The MSF-OT system has the following advantages over the MSF-BC system such as:

1- Reduction in the number of pumping units (MSF-OT has pumps for feed seawater, distillate product, and brine reject) and (MSF has additional pumps for brine recycle and cooling seawater) and that would reduce the number plant trips caused to the pumping units (50% of all MSF plant trips) (El-Dessouky & Ettouney, 2002).
2- In addition, the salinity of the brine recycle stream is much higher than that of the intake sea water (63000 ppm versus 42000 ppm). Therefore the tendency towards scale formation would be higher in the MSF-BC system than in MSF-OT, this would require an increase in the antiscalent dosing rate in MSF-BC Also, a higher frequency of acid cleaning of the condenser tubes is expected for the MSF-BC (Ettouney, El-Dessouky, & Al-Juwayhel, 2002).
3- Low brine salinity 36,000-45,000 ppm in MSF-OT will reduce the consumption rate of the antiscalent. High brine salinity 60,000-75,000 ppm in the MSF-BC will increase the consumption rate of the antiscalent (AlBahou, Al-Rakkaf, Zaki, & Ettouney, 2007)
4- Lower boiling point elevation in MSF-OT, which would increase the flashing vapour temperature and consequently the feed seawater temperature entering the brine heater. On the other hand, the increase in the recycle brine salinity will result in higher boiling point elevation, which would decrease the flashing vapour temperature and consequently the feed seawater temperature entering the brine heater.

Other factors to be taken into considerations:

1- The gain output ratio of the MSF-OT is similar to the MSF-BC.
2- The capacity of the MSF-OT is similar to the MSF-BC.
3- The specific heat transfer area (defined as the total heat transfer area per unit product flow rate) of MSF-OT is similar to MSF-BC

2.8.4 Flashing stage Description

For conventional MSF systems with capacities of 27,000 up to 32,000 m^3/d, the flashing stage has dimensions of 18x4x3 m in width, height, and length. A schematic of the MSF flashing stage is shown in Figure 2.11. As shown, the stage contains:

- Large brine pool with similar width and length of the flashing stage and a depth of 0.2 to 0.5 m.
- Demister formed of wire mesh layers and support system.
- Brine orifice.
- Condenser/preheater tubes.
- Venting line.
- Water boxes.
- Distillate tray.
- Partition walls.

Each part of the flashing stage has a specific function that contributes to proper operation and high performance of the flashing process. A summary of these functions includes the following (El-Dessouky, Ettouney, Al-Juwayhel, & Al-Fulaij, 2004):

- The demister function is to remove or reduce the entrained brine droplets from the flashed off vapour. This is essential to prevent increase in the salinity of product water or scale formation on the outer surface of the condenser/preheater tubes and walls of the flashing chamber.
- The brine orifice controls the brine flow rate across the stages. This in turn affects the process of bubble formation, growth and release rate. In addition, the brine transfer device between the stages is designed to enhance turbulence and mixing of the inlet brine stream. The gate height of the brine orifice and the height of the brine pool are adjusted to prevent leakage of the flashed off vapour across the stages.

- The flashed off vapour condenses on the outer surface of the tube bundle of the condenser/preheater tubes. The released latent heat of condensation results in heating of the brine recycle stream flowing inside the tubes. This energy recovery is essential to maintain high system performance. The heat transfer area of the the condenser tube is a major design feature that controls the temperature of the brine recycle entering the brine heater. Also, the condensation temperature of the vapour and consequently, the pressure inside the flashing chamber is controlled by the available heat transfer area in the flashing chambers. Overdesign of the heat transfer area may lead to subcooling of the condensate. Also, use of excessive heat transfer area may result in lower velocity of the brine recycle inside the condenser tubes, which may enhance the fouling process. On the other hand, use of small heat transfer area would result in low energy recovery and high brine velocity.
- Connections for venting system, which removes non-condensable gases (O_2, N_2, and CO_2), which are dissolved in the feed seawater, even after dearation. Also, CO_2 can be generated during decomposition of the bicarbonate compounds in the high temperature stages. Another important source for the non-condensable gases is air leakage from the ambient surroundings into the flashing stages operating at temperatures below 100^oC, which correspond to vacuum conditions. The intake of the venting line is located at the coolest point within the flashing chamber, which is close to the outer surface of the condenser tubes. Poor venting would result in increase of the partial pressure of the non-condensable gases within the flashing stage, which would result in enhancement of corrosion reactions, increase in the thermal resistance between the tube surface and the condensing vapour, and reduction of the condensation temperature. All these factors reduce the process efficiency and the production capacity.

- Distillate tray, where the condensed distillate product is collected and cascade though the stages. The distillate product is withdrawn from the tray of the last stage.
- Water boxes at both ends of the tube bundle to transfer the brine recycle stream between adjacent stages.

The MSF process operates over a temperature range of 110 to 30^{o}C. This implies that the majority of the flashing stages operate at a temperature below 100^{o}C or vacuum conditions. Therefore, all flashing stages are designed to withstand pressures close to absolute zero or full vacuum. However, the bottom of the flashing stages is exposed to the hydrostatic pressure of the brine pool. Therefore, the system is designed to withstand a maximum pressure of 2 bar.

Stainless steels are the largest tonnage alloy materials used for industrial and domestic purposes. The primary property, which determines their use in many applications, is their corrosion resistance in a wide variety of aqueous environments. There are many varieties of stainless steel, but in all cases they are essentially alloys of iron and chromium to which other elements are added to give specific properties. The addition of nickel results in the well known austenitic stainless steels, and the largest tonnage alloy is an iron chromium nickel alloy (18%Cr 10%Ni) UNS S30400, commonly referred to as Type 304. The corrosion resistance of this alloy is improved by the addition of 2-3% molybdenum giving the often used UNS S31600, commonly referred to as Type 316. This alloy is particularly useful in atmospheric marine environments, but when immersed in seawater it can suffer pitting and crevice corrosion. With this tendency to pit in chloride-containing environments, the use of stainless steels in distillation plants which handle hot concentrated seawater would seem unlikely. However, because the environment is well deaerated, the tendency to pit is greatly reduced and stainless steel grades such as UNS S31603, commonly referred to as Type 316L, are successfully used in most modem MSF plants (Oldfield & Todd, 1999). The walls, ceilings, and partitions of the flashing stages are constructed of carbon steel with stainless steel or epoxy cladding. Stainless steel cladding is used in locations where higher erosion or corrosion conditions can be

found. All stages are reinforced with a stainless steel structure and heavily insulated to minimize heat losses.

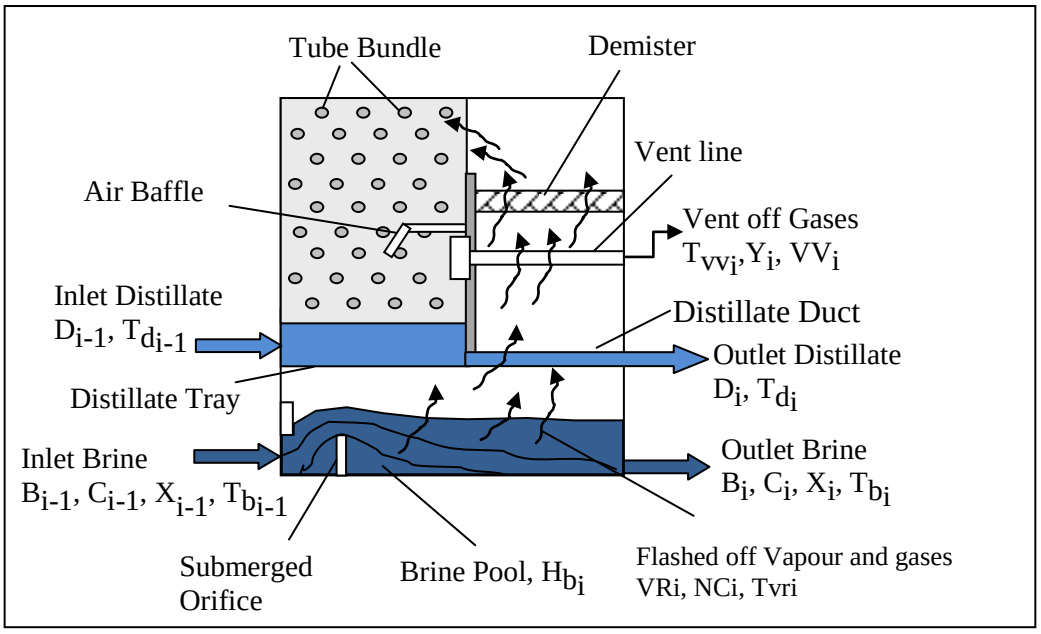

Figure 2.11 MSF flashing stage showing input and output variables

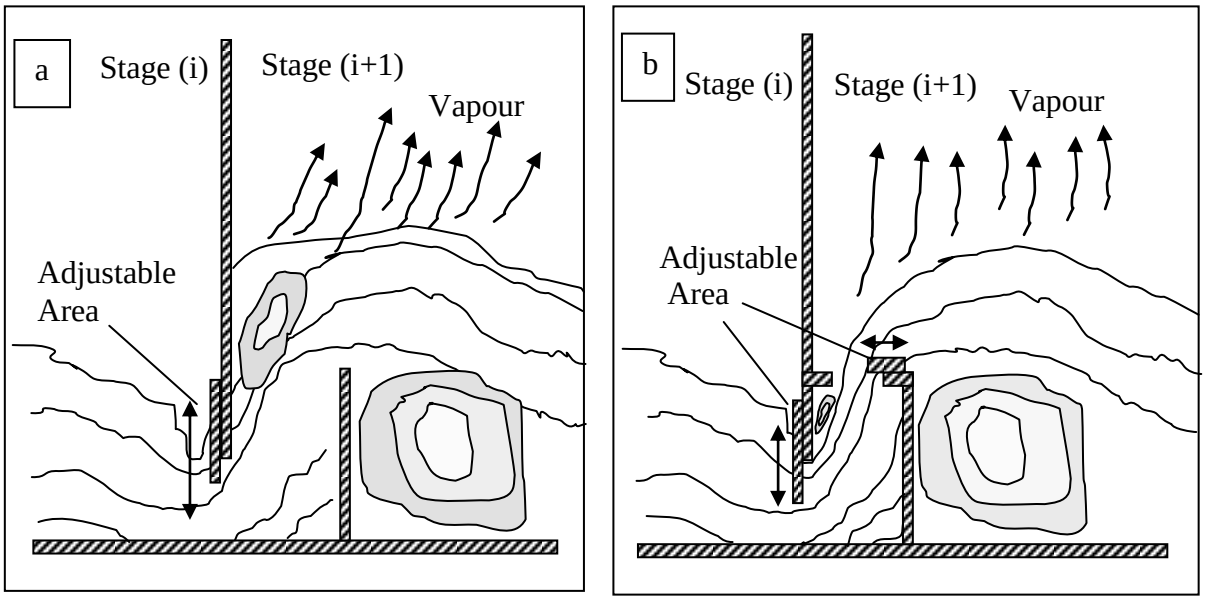

Figure 2.12 Two types of MSF orifices (a) Weir orifice (b) Flash box orifice

2.9 Conclusion

In the past 50 years, desalination proved that it is a feasible and economical process to solve the water shortage problem and to generate fresh water sufficient for large metropolitan areas and industrial use. Examples found in the Gulf States, Spain, USA, Italy, Australia, Singapore, etc. There are many desalination technologies available but MSF and RO are the leading techniques in the industry. MSF constitutes close to 50% of the desalination market. This is because of the large capacity of a single MSF plant, which ranges between 50,000 to 75,000 m^3/d. Forecast of the desalination market for the next 50 years shows that this process will continue to be one the major desalination technologies (IDA, 2006). This motivated the selection of MSF as the topic for research in this thesis. In the next chapter, a comprehensive literature review on different developed models for the MSF process will be presented showing the weakness and strength of each model.

Chapter 3
Modeling of MSF Processes: Literature Review

3.1 Introduction

A process system is a system in which physical and chemical processes are taking place. System definition requires specifications of its boundaries, inputs and outputs, and the physico-chemical processes taking place within the system. Process modeling is very important in process system engineering (PSE). It is used in order to design, optimize and control processes. In addition, it is a vital part of risk management, particularly consequence analysis of hazard. Modeling is not just about producing a set of equations. It is also about the reason behind the model, the scope and goal the modeler is looking for. Thus there is a difference between building a process model and analyzing models. Building process models follows the steps of a modeling procedure and it often starts from the most general case. Analyzing a process model for a given modeling goal releavant to this work includes (Cameron, Hangos, & Stephanopoulos, 2001):

1. Control and diagnosis where mostly lumped dynamic process model are used.
2. Static flow sheeting with lumped static process models.
3. Dynamic flow sheeting where again mostly lumped dynamic process models are in use.

In this chapter, comprehensive review on MSF literature studies including simple models for steady state analysis as well as detailed models for steady state and dynamic analysis. Critical evaluation and summary for the main features and outcome of these studies will be presented including full assessment of strength and weakness of each model.

3.2 Simple Mathematical Models

Simple mathematical models of the MSF process are very useful to provide quick estimates of the main process characteristics, i.e., performance ratio (defined as the amount of distillate product per unit mass of heat steam), heat transfer areas for the brine heater and condensers, and profiles of the temperature, pressures, salinity, and flow rate across the flashing stages. An important application for the short cut models is found in instruction of chemical and engineering courses. Examples include plant design, process synthesis, modeling and simulation, energy conservation, flow sheet analysis, and water desalination courses. The simplicity of the models makes it simple to grasp and understand various relations governing the systems. Also, the simplicity of the models allows for quick programming on hand calculators or computer spread sheets. The models provide major design and operating features of the system; however, care should be taken in interpreting the model results, especially performance charts, where the variations in the calculated design and operating variables will not simulate the actual behaviour of the system and are generated by the model assumptions and other simplifications. Therefore, use of the short cut models should be limited to obtaining rough and quick estimates of the main design and operating features.

Common assumptions among simplified mathematical models for the MSF system include the following:

- *Constant physical properties*: This assumption is invoked to simplify the solution of the energy balance equations. Therefore, assuming constant values for the specific heat at constant pressure for the flashing brine, the latent heat for evaporation, and the flow rate of the flashing brine results in a linear temperature profile for the flashing brine and inside the condenser tubes (Darwish, 1991). Constant physical properties assumption is motivated by the fact variations in the specific heat of the flashing brine, the water flowing inside the condenser tubes, and the latent heats are relatively small between flashing ranges of 110-30 ^{o}C (El-Dessouky & Ettouney, 2002).

- *Constant overall heat transfer coefficient*: This assumption is a direct result of the previous assumption. The heat transfer coefficients for brine flow inside the condenser tubes or for vapour condensation on the outside surface of the tubes depends on the physical properties of the stream, which includes viscosity, density, and thermal conductivity. The main drawback of this assumption is the inability to predict dependence of the condenser heat transfer area on the system temperature.
- *Constant thermodynamic losses*: Keeping the thermodynamic losses constant throughout the flashing stages simplicities calculations of the temperature of the flashed off and condensed vapour. This is because actual measurements of the thermodynamic losses show dependence on stream flow rate, temperature, and the brine salinity ((El-Dessouky, Ettouney, Al-Juwayhel, & Al-Fulaij, 2004), (El-Dessouky & Ettouney, 2002)).
- *Negligible heat losses to the surroundings*: This assumption is common among simple and detailed mathematical models. The direct effect of this assumption is the need to increase the design value of the heat transfer area to take into consideration the heat losses. The rate of increase is proportional to the percentage of heat losses, which may vary between 2-5% (Hassan, et al., 1998). Modeling of the external heat losses requires knowledge of the outside heat transfer area of piping system and the flashing stages. Also, a proper correlation is required to calculate for the heat transfer coefficient between the unit surface and the ambient air (Incropera, DeWitt, Bergman, & Lavine, 2006).
- *Negligible heat of mixing*: The heat of mixing for sodium chloride, which is the main solute in seawater and brackish water, is 278 kJ/kg (Omar, 1983). Since, the salt concentration in the feed seawater and the rejected brine are 40 and 70 kg/m^3, respectively, therefore, the amount of released energy due the heat of mixing is 8340 kJ/m^3. This amount is much smaller than the energy required for vapour evaporation for 1 m^3 of flashing water. Approximately, the amount of vapour formed is 33% of each 1 m^3 of flashing water or 333 kg. Therefore, the total amount of latent heat required for water flashing is 792,540 kJ/m^3. This value is based on average latent heat of evaporation of 2380 kJ/kg.

- *Negligible heat and vapour losses due to venting of non-condensable gases*: Approximately, 2-5% of the total amount of vapour formed in all flashing stages is vented to the ambient in order to prevent accumulation of non-condensable gases (El-Dessouky & Ettouney, 2002). Therefore, part of the product water vapour is lost in addition to heat losses. Accounting for these losses is made simple by increasing the design heat transfer area in order to increase the total amount of vapour formed in all stages.

The simple models developed by (Soliman, 1981), (Darwish, 1991), and El-Dessouky et al (1998) focused on obtaining closed form equations that can be used to determine various system features. The main outcome of the analysis presented by Darwish is the development of design equations for determining the brine circulation flow rate, the performance ratio, and heat transfer area. The analysis of Darwish captured several of the system features, for example:

- Decrease in the recirculation ratio upon the increase in the flashing range, which implies increase in the amount of vapour formed per unit mass of circulated brine.
- Increase in the performance ratio upon the increase in the number of flashing stages. This is because of the increase in the total heat transfer area and the corresponding increase in the amount of heat recovered by the recirculating brine.

El-Dessouky, et al. (1998) used simple models to determine the main features of the MSF systems which include single stage flashing, once through MSF, and MSF with brine circulation. The following are some of the main points discussed in their analysis:

- Efficient MSF units require the use of a large number of flashing stages. This is illustrated through the analysis of a single stage unit, which has a performance ratio of less than one. Increase in the number of flashing stages to a range of 20-24 gives a performance ratio in the range of 8-12.
- Increase in the top brine temperature improves the system performance ratio and reduces the required specific heat transfer area. Increase in the performance ratio is a result of increase of the flashing range (difference

between the top brine temperature and the rejected brine temperature); this is because the blow down temperature is always kept at 5-10 ^{o}C higher than the intake seawater temperature. Also, a decrease in the specific heat transfer area is caused by the increase in the value of the overall heat transfer coefficient and the increase in the temperature drop per stage and the temperature driving force for the heat transfer around in the condenser section. However, the upper limit on the top brine temperature is set by the maximum allowable temperature for safe use of the antiscalent material which stands at 115 ^{o}C (AlBahou, Al-Rakkaf, Zaki, & Ettouney, 2007)

- Three main advantages are gained in the MSF process with brine recycle. In this process the flashing stages are divided into two sections that include heat recovery and heat rejection. The first feature gives a good control on the temperature of the brine recycle into the heat recovery section. The second feature provides means for controlling the intake sea water temperature during winter operation. This is made by mixing part of the cooling seawater stream with the intake seawater. The third feature is the reduction of the amount feed seawater (makeup) stream. This will reduce the consumption rate of chemical additives.
- Minimum number of stages in the heat rejection section required to heat the intake seawater to the same temperature as that of the brine of the last stage. This is essential to prevent thermal shock upon mixing of the streams in the last stage. The thermal shock causes the decomposition of the bicarbonates salts and formation of carbonate precipitates and carbon dioxide gases which will reduce the heat transfer efficiency around the condenser tubes and has harmful effect on the steam jet ejector.

The main drawback of simple models is their inability to capture or provide an accurate account for the entire physical performance of the process. In other words, a simple model may give a good representation for one element of the system without being able to provide a good picture for the entire process. Therefore, the simple models must be used with care and their results (especially performance charts) cannot be used to analyze system performance. This is because of the fact that some

of the generated data can be labelled as numerically generated because of the difficulty in predicting the actual physical behaviour.

3.3 Detailed Mathematical Models

3.3.1 Steady State Models

Detailed steady state models are thought to predict accurate performance charts and to determine additional design and operating characteristics. The detailed mathematical models take into consideration dependence of the physical properties of various streams on temperature and salinity. Also, the detailed models include comprehensive correlations for evaluation of the physical properties, stage variation in the amount of flashed off vapour, thermodynamic losses, and the heat transfer coefficients. Detailed models solve iteratively the material (mass) and energy balance equations as well as the heat transfer equations in each flashing stage or in each fluid phase.

In the steady state modeling, the following simplifying assumptions were used:

1. Steady state operation is the common assumption among all studies. Although, system operation may experience seasonal temperature variations of the intake sea water, such variations are slow and the system parameters are adjusted accordingly. During real operation the plant goes through a slow transient due to accumulation of fouling and scaling materials which results in the increase of the thermal resistance for heat transfer. This effect is offset by the increase in the amount of heating steam and the use of on-line ball cleaning system or tube acid cleaning, which restores conditions to near clean operation (Abdel-Jabbar, Qiblawy, Mjalli, & Ettouny, 2007).
2. The distillate product from every stage is free of salt. This is validated by the fact that the distillate salinity on average is below 20 ppm. On the other hand, the brine and feed salinity varies between 40,000-70,000 ppm. Therefore, the effect of the distillate salinity on the salt balance equation will be negligible.

3. Heat losses from the plant are negligible. As mentioned previously, in reality, heat losses from the plant amounts to less than 5% of the total input heat. That is because the surface to volume ratio of the MSF plants is very small. Also, the temperature of the low temperature stage is very close to the ambient temperature, which reduces the rate of heat transfer to the surroundings (Abdel-Jabbar, Qiblawy, Mjalli, & Ettouny, 2007). Therefore, final system design should account for these losses by the increase in the heating steam load or the heat transfer area in each flashing stage.
4. Heat from mixing is negligible. This is because of the low of heat of mixing for NaCl, which constitutes more than 85% of all salts dissolved in seawater. The heat of solution for NaCl is 278 kJ/kg, which is much smaller than the latent heat of evaporation, which averages 2380 kJ/kg
5. The condensate produced in the brine heater is not sub cooled and flows through the brine heater at a constant temperature
6. The change of vapour enthalpy above and below the demister in the flashing chambers is neglected.
7. Non-condensable gases are neglected in mass and energy balances, as well in the equilibrium equations.
8. For MSF-OT system, the flow rate of the recycle streams are null (in particular the flow rate of the seawater to the reject seawater splitter of the reject seawater recycle, and of the recycle brine), this implies that in practice there is no distinction between the heat recovery and the heat rejection sections.
9. Constant brine holdup and constant brine flow rate along the unit (Steady State).
10. Constant heat transfer area in each section of the plant. In practice, it is not economical to design MSF plants to have uniform interstage temperature differences over the entire flash range. It is therefore usual to design and construct all of the stages in each section with identical heat transfer area (El-Dessouky & Bingulac, 1996).

In some models, correlations were used to predict the required parameters such as non-equilibrium allowance (NEA), boiling point elevation (BPE), overall heat transfer coefficient (U), and the discharge coefficient (Cd) and in some average values were used for simplicity.

Table 3.1 gives a summary of different solution methods used in detailed steady state models. As is shown, three methods were mainly used to perform the steady state modeling. One is Newton's method which allows solution of the entire system's mass balance and energy balance equations simultaneously. It is also known as Newton-Raphson method and it is an open method that finds the root (x) of a function such that $f(x) = 0$. It uses the first few terms of the Taylor series of a function in the vicinity of a suspected root (Chapra & Canale, 2006)

Second is the successive approximations method. It is a method of solving mathematical problems by means of a sequence of approximations that converges to the solution and is constructed recursively. That is, each new approximation is calculated on the basis of the preceding approximation, the choice of the initial approximation is to some extent arbitrary. The main feature of this method is the simplicity to code this procedure (Chapra & Canale, 2006)

Last is the tridiagonal matrix method (TDM), where the matrix has nonzero elements only in the main diagonal, the first diagonal below this, and the first diagonal above the main diagonal. Solution of the TDM equation system is rather simple and involves straightforward computer coding (Horn & Johnson, 1985).

The steady state models proved to be quite reliable (El-Dessouky & Ettouney, 2002). They aim to analyze different trends of operating parameters and to optimize the process. In addition, steady state models could be used to get an initial guess required to start the dynamic model solution. For example in (Rosso, Beltramini, Mazzotti, & Morbidelli, 1997) the effect of the stage numbers, steam temperature and sea water temperature was studied on the Gain Output Ratio (GOR), distillate flow rate, and brine temperature.

Therefore, detailed steady state models can predict accurately design and operating features of the system. The design includes the stage dimensions, tube bundle length, the demister length. The operating features include the flow rate and temperature profiles (Abdel-Jabbar, Qiblawy, Mjalli, & Ettouny, 2007). Performance charts can be used for accurate system design and simulation. Some authors didn't account for orifice geometry and for the fluid dynamics aspects of the process while other (El-Dessouky & Ettouney, 2002) considered the fluid-dynamic parameters, accounted for the brine gates geometry and the calculation of the discharge coefficient. Tanvir & Mujtaba (2006a) used the artificial neural network approach (ANN) to develop correlations for predicting the boiling point elevation as a function of boiling point and salinity. Later Tanvir & Mujtaba (2006b) used these correlations to simulate steady state performance of the MSF gPROMS. The model used in their study was based on Rosso et al. (1996).

Table 3.1: Summary of different solution methods used in detailed steady state models

Reference	Modeling and Solution Method
El-Dessouky & Ettouney (2002)	Each flashing stage is modeled by a set of mass and energy balance equations. Used Newton's method to solve simultaneously the entire set of mass and energy balance equations in all flashing stages.
El-Dessouky H. T., Ettouney, Al-Fulaij, & Mandani (2000)	
Ettouney, El-Dessouky, & Al-Juwayhel (2002)	
Abdel-Jabbar, Qiblawy, Mjalli, & Ettouny (2007)	
El-Dessouky & Bingulac (1996)	
Omar (1983)	Each flashing stage is modeled by a set of mass and energy balance equations. Successive approximation is used to solve the system's equations (stage-to-stage calculations)
Rosso, Beltramini, Mazzotti, & Morbidelli (1997)	
El-Dessouky, Shaban, & Al-Ramadan (1995)	

Table 3.1 (Continued): Summary of different solution methods used in detailed steady state models

Reference	Modeling and Solution Method
Helal, Medani, Soliman, & Flower (1986)	Decomposition of large set of equations into smaller subsets followed by iterative sequential solution of these subsets. Reduced the equations to generate a tri-diagonal matrix (TDM) and used an efficient method of solution based on Thomas algorithm (a modification of Newton's method).
Husain, et al. (1994)	
Thomas, Bhattacharyya, Petra, & Rao (1998)	
Al-Mutaz & Soliman (1989)	Orthogonal collocation method where, the selected stages are chosen to be at the roots of a suitable orthogonal polynomial.

3.3.2 Dynamic Models

Other MSF models include system dynamics. They are based on a detailed physico-chemical representation of the process, including all the fundamental elementary phenomena. Specific to the dynamic model are the description of mass and energy accumulation in the different stages and the use of correlations to determine the hydrodynamics behaviour between stages. This is used to analyze the stability of steady state regimes, to choose the proper start up and shut down procedures, and to study system transient behaviour (includes problems such as control strategies, stability assessment, process interactions, trouble shooting, start-up, load changes and shut down scheduling) and to optimize and develop system controllers for industrial units. That is because the successful development of a control system requires an appropriate definition of the control structure (i.e., selection of output, input and disturbance variables) and an efficient dynamical model on which the design, analysis and evaluation can be carried out ((Mazzotti, Rosso, Beltramini, & Morbidelli, 2000), (Thomas, Bhattacharyya, Petra, & Rao, 1998)).

The uses of the dynamic model for off-line simulation include the following:

- Creation of simulation facilities for the purpose of training operation personnel (off-line simulator of a plant enables the operator to gain

experience of operating problems and take timely corrective action. Also it is cheaper and less risky than training on the job).

- Investigation of the plant behaviour under dynamic conditions.
- Creation of an off-line simulator for design purposes and performance evaluation.

The utility of the dynamic model for on-line simulation is used to assist the automatic and individual control of the desalination plant (Husain, Hassan, Al-Gobaisi, Al-Radif, Woldai, & Sommariva, 1993).

Most of the assumptions made in steady state models are also made in the dynamic models. The dynamic modeling additional assumptions (Cipollina, 2004-2005) include:

1. Lumped parameters (no spatial variations in physical properties). Also In principle each industrial process is dynamic in nature, that is variation or fluctuations with time will always be present in the process parameters with time. If these variations are small enough, they can be ignored and the process can be considered as operating at a steady state, in this instance time will not be a variable and the model will consist of algebraic equations. (Husain, Hassan, Al-Gobaisi, Al-Radif, Woldai, & Sommariva, 1993)
2. Kinetics of condensate duct flashing neglected. This is the flashing of the distillate in the condensate duct as it cascade from stage to stage.
3. Equilibrium exists between vapour and liquid at the stage temperature and pressure.
4. Flashing efficiency accounted by a non-equilibrium parameter dependent on brine temperature and concentration.
5. Neglecting the effect of the non-condensable gases and blow through phenomenon across brine orifices

Early 1970 work on a dynamic model of an MSF-process was done by Glueck and Bradshaw. This model includes a differential energy balance combining vapour

space and distillate in the flash stage given as consequence an over-specified model. Drake (1986) applied empirical correlations for the evaporation rates but the non-condensable gases in the vapour were not taken into consideration. Simulations carried out with this model by Ulrich (1977) showed significant deviations in the cooling water flow rate. In 1989, a model was predicted without brine recycling (Rimawi, Ettouny, & Aly, 1989). But in 1993, a model was presented with flashing and cooling brine dynamics (Husain, Hassan, Al-Gobaisi, Al-Radif, Woldai, & Sommariva, 1993). The model was improved in 1994, considering the system dynamics (Husain, Reddy, & Woldai, 1994). In 1995, a model was developed including the brine recirculating (Reddy, Husain, Woldai, & Al-Gopaisi, 1995). In the same year, (Aly & Marwan, 1995) used a combination of Newton-Raphson and Runge-Kutta method to obtain the transients of the system profiles. The system analysis is limited to very short transient periods. Thomas et al. in 1998 developed a very detailed and comprehensive model but review for some of the simulation data reveal that the absence of pressure control in the last stage causes unlimited increase in the brine level.

The model contains differential equations for the mass and heat balances in all phases (liquid and vapour). And the model contains constitutive equations to calculate physical properties, equilibrium relations between pressure and temperature and heat transfer coefficient in the condensing zone. More constitutive equations are used to calculate the brine flow rate through the orifices depending on the pressure drops and on the brine level, whereas vapour flowing in the venting line is considered constant.

For the lumped parameter system, the dynamic behavior is described by ordinary differential equations (ODE's), and of the distributed parameter system by partial differential equations (PDE's).

The dynamic simulation can be carried out either off-line (no connection to the real plant; the input data are fed from a file) or on-line (the input data are directly received from the actual operating plant) (Husain, Hassan, Al-Gobaisi, Al-Radif, Woldai, & Sommariva, 1993).

The solution methods are the simultaneous approach (equation oriented) where the whole problem is treated as a global set of equations pertaining to all process unit and stage by stage (sequential) approach where the analysis proceeds from module to module (Cameron, Hangos, & Stephanopoulos, 2001). Subsequently, a combination of sequential and simultaneous approach became more popular, in which the equations associated with a recycle loop are solved simultaneously (Husain, Hassan, Al-Gobaisi, Al-Radif, Woldai, & Sommariva, 1993). Another model which includes detailed account of variations in physical properties as a function of temperature and concentration as well as thermodynamic losses was presented by Mazzotti et al in 2000. Model results show non-linear response to variations in steam and sea water temperatures. This indicates the necessity of using this type of models for development of an optimal control strategy. Next in 2001, a comprehensive model and discussion of various forms of probable system faults, which might be caused by pumps, valves, heaters, controllers, and heat exchangers was done by Tarifa & Scenna, (2001).

A dynamic model was developed using gPROMS ((Bogle, Cipollina, & Micale, 2009), (Cipollina, 2004-2005)). In this work, a comprehensive dynamic model of the MSF with many details was presented. The model details include temperature losses, blow through mechanism, and correlations for the heat transfer coefficients, transport properties, and thermodynamic properties (except for the specific heat of the brine stream, which is assumed constant). The model does not account for demister losses and distillate flashing. Also, values for the discharge coefficient are defined as a function of the stage pressure. Correlations for the discharge coefficient are more complex and depend on the orifice dimensions, pressure drop between the two stages, inlet brine flow rate, stage temperature, brine height, densities of the vapour and brine, and flashing rate.

In these studies the model is represented by differential and algebraic equations. They are used to solve the transient phase, process interaction, trouble shooting and it’s necessary to implement advanced control, supervision, fault detection and recovery strategies and dependable systems. Calculation of hold-ups in

brine and product tray is necessary for dynamic modeling of MSF desalination plants as they affect the inertia of the plant (Thomas, Bhattacharyya, Petra, & Rao, 1998).

A new method called heuristic selection (HS) (Tarifa, Humana, Franco, & Scenna, 2004) was used to develop algebraic equation system (AEs) models of process systems. For given AEs, the proposed method produces a set of decision variables, a set of subsystems, a set of variables for iteration, a set of equations for verification, and all of the possible calculation sequences. The method allows assigning degrees of preference to each variable. These degrees are considered when the method has to select an output variable for a given equation. The goal of the method is to select the decision variables and the calculation sequence that minimizes the size of the subsystems or minimizes the set of variables of iteration and, at the same time, selects the output variables in order to maximize the sum of the corresponding degree of preference. This method was used to develop a dynamic simulator for a MSF desalination plant. The application of the HS method to the model produced a robust, fast strategy to solve it (Tarifa, Humana, Franco, & Scenna, 2004).

Another novel method used for the simulation of MSF desalination process is based on a modular simulator, CAMEL. And it has been tested on both steady-state and unsteady state operating conditions (Falcetta & Sciubba, 1999).

From a wide look at the literature studies on the detailed steady state and dynamic models, these models were based on different assumptions. Some have a minor effect on the accuracy of the model predictions but others may cause weakness point in the model such as:

– All of the studies used lumped parameter analysis and ignored spatial variations. This assumption simplifies the system model because it reduces the model to an algebraic form for steady state analysis and a set of ordinary differential equations for dynamic analysis. Although, the lumped parameter analysis loses spatial details within the flashing stage, it still provides sufficient and useful information to design and analyze the system performance and dynamics. On the other hand, distributed systems provide insights into variations within the

flashing chamber. This might reveal areas of high turbulence within the flashing brine or dead zones within the condensing vapour. Such information can be used to improve the internals layout.

- Distilled flashing (vapour formed as a result of distillate flow in the distillate tray from stage to stage) is ignored in the condensate duct. Taking this parameter into consideration results in up to 10% increase in the amount of flashed vapour and as a result a similar reduction in the heat transfer area and increase in the performance ratio (El-Dessouky & Ettouney, 2002).
- Modeling of the temperature difference between the brine and flashed off vapour varied considerably among literature studies. The most accurate approach is to consider correlations for boiling point elevation and non-equilibrium allowance. It should be stressed that available correlations for the boiling point elevation provide close estimates for this thermodynamic property as a function of the brine temperature and salinity. On the other hand, the non-equilibrium allowance depends heavily on the layout and geometry of the flashing stage. Therefore, use of different correlations may provide large differences in estimation of this property (Al-Fulaij, 2002).
- Non-condensable gases in the flashing stage have a strong effect on the flashing and condensation process. Most of the literature studies have neglected the presence of the non-condensable gases, except for the work of (Cipollina, 2004-2005). The non-condensable gases have a similar effect to fouling, since they reduce the value of the condensing vapour temperature around the condenser tubes. Reduction in the condensation temperature is caused by reduction in the vapour partial pressure due to the presence of the non-condensable gases.
- The demister losses also result in reduction of the temperature of the condensing vapour and as a result the condenser heat transfer area increases and the system performance ratio decrease (El-Dessouky , Ettouney, Al-Fulaij, & Mandani, 2000). Most of the literature studies ignore the demister losses because it varies over a range of 0.01-0.6 ^{o}C. However, a reduction of 0.6 ^{o}C in the low temperature effects would result in large increase in the heat transfer area and a similar decrease in the performance ratio.
- Modeling of vapour blow through is not found in most of the literature studies; however, the only study which has considered this phenomenon is by Cipollina

(2004-2005). The phenomenon is associated with reduction in the brine level below the orifice height connecting two stages. As a result, the system operation becomes unstable because of difficulties in increasing the feed temperature to the design value. This might put the system in a cyclic or a run-away situation.

– Models of the condenser heat transfer coefficient vary widely among literature studies. Several studies used temperature dependent correlations for the overall heat transfer coefficient. Other investigators estimated the overall heat transfer coefficient based on individual correlations for vapour condensation and brine flow inside the tubes. The first approach may not be all that accurate because such correlations are system dependent, unless it was based on data from various plants. The main drawback of the second approach is the applicability of the vapour condensation correlations. The applicability will depend on the ranges of the vapour velocity, temperature, amount of non-condensable gases, etc.

Table 3.2: Summary for different solution methods in detailed dynamic models

Reference	Solution Method
Husain, et al. (1994)	Decomposition of large set of equations into smaller subsets followed by iterative sequential solution of these subsets.(Newton's) Reduced the equations to generate a tri-diagonal matrix(TDM) and then an efficient method of solution based on Thomas algorithm is used.
Husain, Hassan, Al-Gobaisi, Al-Radif, Woldai, & Sommariva (1993)	The model was described by ordinary differential equations (ODE's) which are replaced by set of finite difference equations and partial differential equations (PDE's) which are replaced by difference-differential equations TDM. TDM is solved by applying a simple algorithm derived from the Gauss elimination method. For the inner loop, either Newton-Raphson or Muller's method is used (TDM-Method)
Thomas, Bhattacharyya, Petra, & Rao (1998)	
Mazzotti, Rosso, Beltramini, & Morbidelli (2000)	Used the commercial software (LSODA) to solve the combined system of ODE's and algebraic equations by

Table 3.2 (continued): Summary for different solution methods in detailed dynamic models

Reference	Solution Method
Gambier & Badreddin (2004)	Used the commercial software (Matlab/Simulink) to simulate and solve the MSF mathematical model.
El-Khatib, Eissa, & Khedr (2005)	
Bogle, Cipollina, & Micale (2009)	Hierarchical structure was used to combine lower model (flashing stage) and contains all chambers equations with higher level (MSF plant) model equations. Used the commercial software package (gPROMS) to solve the model equations simultaneously using Newton-Raphson method.
Cipollina (2004-2005)	
Rahbar (1993)	Used the commercial software (ASPEN PLUS) for steady state simulation and (SPEEDUP) for dynamic simulation of the MSF plant
Aly & Marwan (1995)	Solved the MSF dynamic using a stage-to-stage approach. Integrated the dynamic equations using the Runge-Kutta method. Used the Newton's method to perform iterations at each time step.
Shivayyanamath & Tewari (2003)	
Rimawi, Ettouny, & Aly (1989)	Used the commercial software (IMSL) and combination of the method of lines and Gears routines to solve the MSF-OT model equations.

3.4 Conclusion

From a wide look at the literature, many studies are available on modeling MSF plants. These models were simple steady state, detailed steady sate and dynamic models. Each type has its applications. For example, application of steady state modeling includes parametric studies such as design prediction for long term

operation and optimization. Application of dynamic modeling includes off-line and on-line simulation, like training simulation, investigation of dynamic behaviour, and implementation of advanced control strategies.

In the next chapter, a comprehensive dynamic mathematical model will be developed for both the MSF-OT and MSF-BC process which consider several new modeling features that were overlooked in previous literature studies. Importance of such features will be studied and illustration will be given on their effects on system design and performance evaluation. The comprehensive modeling approach adopted in the following chapter will contribute to advancement of knowledge and understanding of the process.

Chapter 4
Dynamic Modeling of MSF Plants

4.1 Introduction

The main objective of this chapter is to develop mathematical models for the MSF processes (MSF-OT) and (MSF-BC) that contribute to advancement of knowledge and understanding of the processes. The developed models will provide tools to obtain accurate system design, evaluate system performance, and explain complex phenomena within the flashing stage.

This work is motivated by the fact that most of the previous literature studies have been performed for small capacity MSF units, i.e., less than 32,000 m^3/d. There are no literature studies that can be found on modeling of dynamics for the new and larger MSF units, which have capacities ranging from 50,000 to 75,000 m^3/d. In addition, the newly developed dynamic model will include new features that were not included in previous literature studies and will lead to more reliable results as shown later in the results section. These new features include:

- distillate flashing
- demister losses
- venting system

In addition, utilized correlations developed from real plant data (Al-Fulaij, 2002) including the overall heat transfer coefficient, non-equilibrium allowance, and orifice discharge coefficient are used in the developed models.

The Chapter starts with the mathematical model of the once through multi stage flashing process and followed by the mathematical model of the brine circulating multi stage flashing process. Next gPROMS programming software used to implement the model will be described in a separate section.

4.2 Model Basis and Assumptions

Modeling begins with conservation relations. They can be developed for mass, component mass, energy and momentum. The general conservation equation for a lumped system is (Felder & Rousseau, 2000):

Input	+	generation	-	output	-	consumption	=	accumulation
(Enters through system boundaries)		(Produced by system)		(Leaves through system boundaries)		(Consumed within system)		(Buildup within system)

This will be applied for each phase (brine, vapour and distillate) in the flashing stage. Further constitutive relations will be required to model heat transfer rate, temperature drop, discharge coefficient, gain output ratio, physical properties and enthalpies, etc.

The main assumptions used to develop the MSF dynamic model include the following:

- *Lumped parameter analysis*: This assumes uniform properties in each phase within the stage, such as the flashing brine, the vapour and the non-condensable gases. For example, the flashing brine temperature and salt concentration within each flashing stage are assumed uniform. This assumption is valid because small variations occur in the stream variables within each flashing stage (El-Dessouky & Ettouney, 2002)
- *Negligible heat losses*: This is because of the small ratio of the surface area and volume for each stage. Also, all of the flashing stages are properly insulated. Estimates for heat losses to the surroundings vary over a range of 2-5% of the total energy of the system (Husain, et al., 1994a)
- *Salt free distillate*: The distillate product is assumed to have zero salinity. This assumption is valid because of the very high salinity of the feed or brine streams, which may range from 36,000 ppm up to 70,000 ppm. On the other hand, the product salinity is extremely small and may vary from 1 ppm up to 20 ppm (Al-Deffeeri, 2009). Performing a salt balance that takes into account

the product salinity would have very small effect on the accuracy of the overall system material balance.

- *Subcooling and Superheating*: Negligible effects of subcooling or superheating on the system energy balance. For example, subcooling of the vapour condensate may occur over a range of less than $1^{o}C$. Similarly, the heating steam might be introduced with a small degree of superheating. In both cases, the heat associated with the subcooling or super heating is much smaller than the latent heat of condensation (Al-Deffeeri, 2009).

4.3 Model Structure

The MSF model is divided into two levels which are called the “Flashing stage” and the “MSF plant”, see Figure 4.1. The "Flashing stage" is the lower model of the hierarchical structure and “MSF Plant” is the higher level.

In this model the “flashing stage” is divided into three main phases: brine phase, distillate phase and vapour phase. The mathematical model consists of a system of differential algebraic equations and constitutive equations describing each phase. The differential algebraic equations include mass and energy balances for each phase in each flashing stage.

The "MSF plant" is the higher model of the hierarchical structure and describes the connection between the stages and other plant elements such as the brine heater. The mathematical model contains equations, which relate output/input stream between stages such as the brine, distillate and vented gases streams. Also it includes constitutive equations for interstage process parameters, such as the non-equilibrium allowance (NEA), discharge coefficient (Cd), outlet flow rate of brine from each stage, control loop for the brine height and pressure in the last stage, and venting rate of non-condensable gases and vapour.

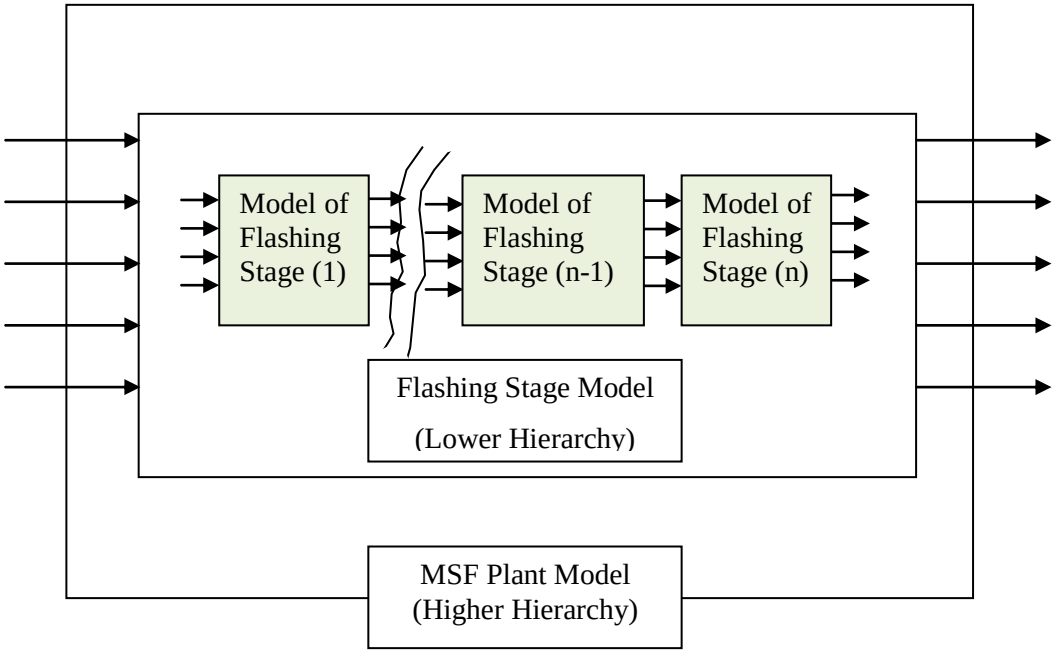

Figure 4.1 Hierarchical structure of lower hierarchy flashing stage model and higher hierarchy MSF plant model

4.4 Once through MSF process (MSF-OT)

4.4.1 Mathematical equations

The mathematical model was built in hierarchical structure as was mentioned in the previous section. The lower level model (Flashing Stage Model) mathematical model equations will be presented first. That will be followed by the mathematical model of the higher level model (MSF Plant).

The definitions of variables used in the system model are given in the nomenclature list. Also, the correlation used to calculate the physical properties such as specific heat (Cp), density (ρ), dynamic viscosity (μ), latent heat of water evaporation (λ), saturation pressure of water vapour (P), and boiling point elevation (BPE), are given in the appendix.

4.4.1.1 Lower Level Model (Flashing Stage Model)

Figure 4.2(a) shows schematics for the system variables between stages (i) and (i+1) and Figure 4.2(b) shows the overall input/output variables for the flashing stages and the brine heater. The following equations are developed for stage (i). First, the dynamic mass balances for the brine, distillate and vapour phase will be presented. That will be followed by the dynamic energy balances for all phases. All of the following equations were used in system modeling.

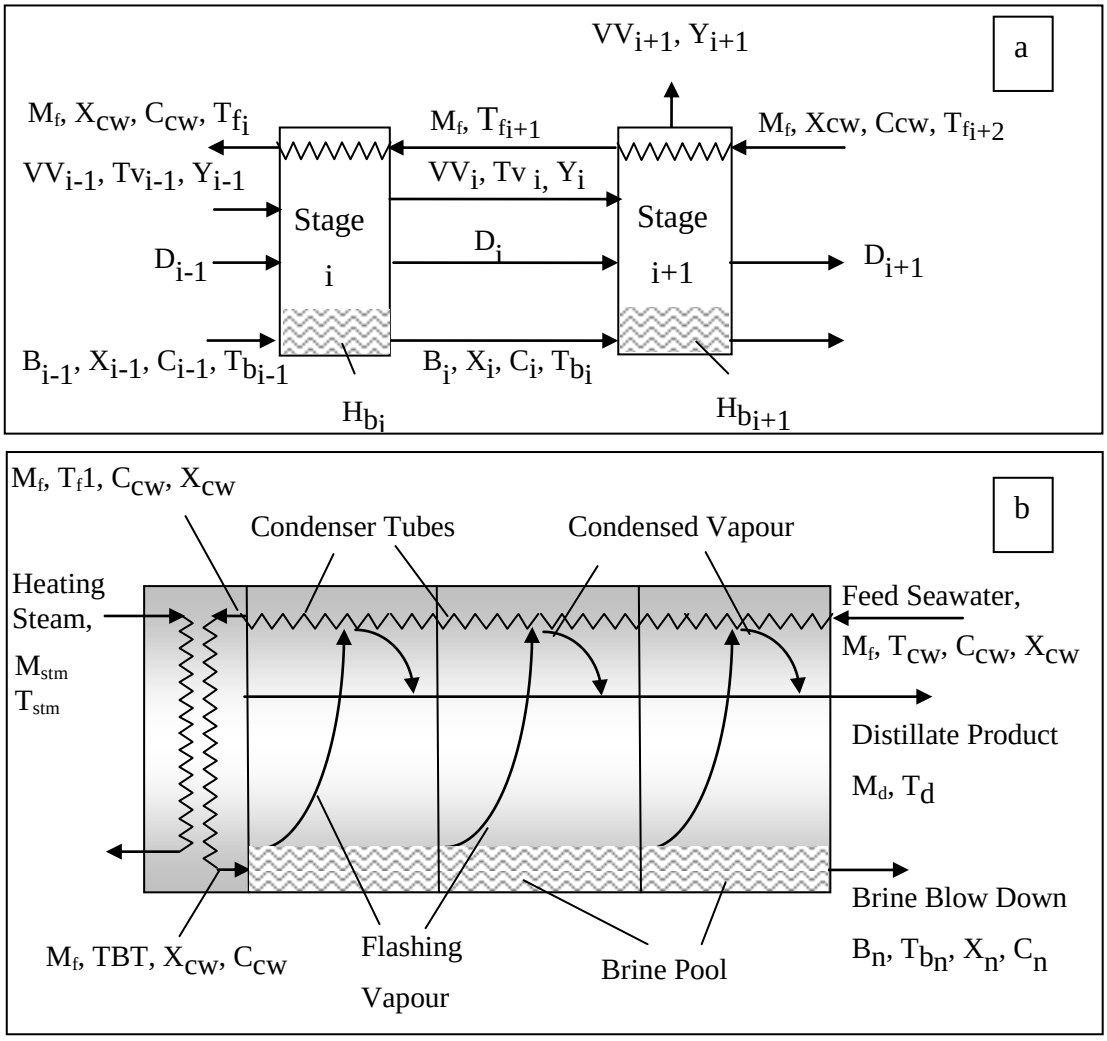

Figure 4.2 Process variables in MSF-OT process (a) variables between stages (i) and (i+1) and (b) overall variables

As the brine flows into the flashing stage, part of it flashes including both vapour and non condensable gases. Applying total mass balance for the brine phase gives the following:

$$\frac{dM_{b_i}}{dt} = B_{i-1} - B_i - VR_i - NC_i \quad (4.1)$$

where B_{i-1} refers to the brine flow rate entering the stage, B_i is the brine flow rate leaving the stage, VR_i is the mass flow rate of released vapour and NC_i is the released non-condensable gases mass flow rate.

The mass of the vapour phase is formed of the balance of flashed off vapour and non-condensable gases from the brine, the input and output flow rates of the distillate stream, and input and output flow rates of vented vapour and non-condensable gases. The total mass balance describing the vapour space is:

$$\frac{dM_{V_i}}{dt} = VR_i + NC_i + D_{i-1} + VV_{i-1} - D_i - VV_i \quad (4.2)$$

The mass balance of the distillate stream relates the input flow rates of distillate and vented vapour from the previous stage, the flow rate of the flashed off vapour from the brine within the stage, and the output flow rates of the distillate and the vented vapours. This balance is:

$$\frac{dM_{D_i}}{dt} = D_{i-1} - D_i + [VR_i - VV_i(1 - Y_i)] + VV_{i-1}(1 - Y_{i-1}) \quad (4.3)$$

Since the height of the distillate tray is small. Then we can neglect the transient term in the above equation and the steady state form is:

$$D_i = D_{i-1} + [VR_i - VV_i(1 - Y_i)] + VV_{i-1}(1 - Y_{i-1}) \quad (4.4)$$

Applying salt mass balance in the brine pool will result:

$$\frac{dM_{S_i}}{dt} = B_{i-1}\, C_{i-1} - B_i\, C_i \quad (4.5)$$

where C_{i-1} and C_i are the salt concentrations in the brine flow entering and leaving the stage respectively.

Applying mass balances of the non-condensable gases in vapour space results:

$$\frac{dM_{nc_i}}{dt} = NC_i + VV_{i-1}\, Y_{i-1} - VV_i\, Y_i \qquad (4.6)$$

This equation also results from substracting equation (4.3) from equation (4.2).

Applying mass balance on the non-condensable gases in the brine pool results:

$$\frac{dM_{bg_i}}{dt} = B_{i-1}X_{i-1} - B_iX_i - NC_i \qquad (4.7)$$

where Y_{i-1} and Y_i are mass fraction of non-condensable gases in the vented vapour entering and leaving the stage. X_{i-1} and X_i are mass fraction of gases in the brine flow rate entering and leaving the stage.

The energy balance equations are derived for the vapour phase and the brine pool. The enthalpy balance for vapour space is:

$$\begin{aligned}\frac{dE_{v_i}}{dt} = {} & VR_i\ e_{vr_i} + NC_i\ e_{ncr_i} + VV_{i-1}Y_{i-1}\ e_{ncr_{i-1}} \\ & + VV_{i-1}(1 - Y_{i-1})\ e_{vv_{i-1}} + D_{i-1}\, e_{d_{i-1}} - D_i\, e_{d_i} \\ & - VV_i\, Y_i\ e_{ncr_i} - VV_i(1 - Y_i)\ e_{vv_i}\end{aligned} \qquad (4.8)$$

The first four terms on the right hand side present the energy entering the vapour phase with the flashed off vapour, released non condensable gases, non-condensable gases vented from previous stage and vapour vented from the previous stage respectively. The difference between the fifth and sixth term, represents the amount of energy released by the distillate flashed from the distillate tray in the stage. The last

two terms represent the amount of energy leaving the vapour phase with the vented non condensable gases and vented vapour.

Enthalpy balance for the brine pool is:

$$\frac{dE_{b_i}}{dt} = B_{i-1}\, e_{b_{i-1}} - B_i\, e_{b_i} - VR_i e_{vr_i} - NC_i e_{ncr_i} \qquad (4.9)$$

The first term on the right hand side is the energy entering with the brine from the previous stage to the control volume (brine pool). The next three terms presents the energy leaving the brine pool with the brine, flashed off vapour and released non condensable gases respectively.

In addition, the following algebraic identities and constitutive equations are used in the model. Equations (4.10-4.16) define total mass and total volume in various phases within the flashing stage. The subscript (i) is omitted from these equations. The equations are as follows:

Mass of brine pool

$$M_b = \rho_b\, V_b \qquad (4.10)$$

Volume of brine pool

$$V_b = A_{st}\, H_b \qquad (4.11)$$

Mass of vapour space

$$M_v = \rho_v V_v \qquad (4.12)$$

Volume of vapour space

$$V_v = A_{st}\left(H_{st} - H_b\right) \qquad (4.13)$$

Mass of salt in the brine pool

$$M_s = C\, M_b \qquad (4.14)$$

Mass of gases in the brine pool

$$M_{bg} = X\, M_b \tag{4.15}$$

Mass of gases in the vapour

$$M_{nc} = Y\, M_v \tag{4.16}$$

The non condensable gases stripping rate is given by the following relation (Cipollina, 2004-2005):

$$NC = B\left(X - X_e\right)\gamma \tag{4.17}$$

$\gamma = 0.80$ (efficiency of degassing process)

The specific enthalpy used in the model equations (4.8,4.9) for the brine, distillate, vapour and non condensable gases is given by the relation:

$$e = C_P\,(T - T_{ref}) \tag{4.18}$$

where T is the phase temperature and C_P is the phase specific heat at constant pressure, and T_{ref} is the reference temperature.

The temperature of the released vapour from the flashing brine (T_{vr}) is less than the brine temperature (T_b) by the boiling point elevation (BPE) and the non-equilibrium allowance (NEA). The boiling point elevation is defined as the raising of the normal boiling point of a pure liquid by the presence of a dissolved substance (salts in the seawater). The non-equilibrium allowance represents the difference between the temperature of the brine pool and the temperature corresponding to thermodynamic equilibrium with the flashed off vapour (Al-Fulaij, 2002). This implies that the flashed vapour and brine pool do not reach thermodynamic equilibrium. This relation is

$$T_{vr} = T_b - BPE - NEA \tag{4.19}$$

As the vapour flows through the demister, its temperature drops because of the pressure losses caused by the demister. Thus, the vented vapour temperature (T_{vv}) is less than the released vapour temperature by the demister and the friction temperature losses

$$T_{vv} = T_{vr} - \Delta T_p - \Delta T_{fr} \tag{4.20}$$

The term ΔT_{fr} accounts for friction losses around the condenser tube bundle. In the current study this term is set to zero because of its negligible effects (El-Dessouky & Ettouney, 2002). The term ΔT_p is obtained by calculating the demister pressure loss ΔP_p and then finding the corresponding temperature drop using Antoine equation (El-Dessouky & Ettouney, 2002).

$$\Delta P_p = 3.9\,(\rho_p)^{0.38}(V_v)^{0.81}(d_w)^{-1.56} \tag{4.21}$$

The ranges of the experimental variables were V_v (0.98-7.5 m/s), ρ_p (80.32-208.16 kg/m^3), d_w (0.2-.32 mm).

The distillate temperature (T_d) is less than the released vapour temperature by the demister, friction and the condensation losses.

$$T_d = T_{vr} - \Delta T_p - \Delta T_{fr} - \Delta T_c \tag{4.22}$$

The terms ΔT_c accounts for condensation losses around the condenser tube bundle. In the current study this term is set to zero because of its negligible effects (El-Dessouky & Ettouney, 2002).

The model equations for the condenser tube include the heat transfer and the heat balance equations. Around the condenser tube, balance of heat is made between the feed seawater inside the condenser tubes, the condensed vapour outside the tubes, and the non-condensable gases outside the tubes. The condensed vapour includes: (1) flashed vapours from the distillate, (2) flashed vapours from the brine pool less amount of vapour vented form the stage (3) part of vapours vented from previous stage. The non-condensable gases (either flashed off from the brine or found in the vented stream from the previous stage) give off part of their sensible heat to the feed seawater stream inside tubes.The heat balance equation is:

$$D_{i-1}\left(e_{d_{i-1}} - e_{d_i}\right) + \left(VR_i - VV_i(1 - Y_i)\right)\lambda_{V_i} + VV_{i-1}(1 - Y_{i-1})\left((e_{VV_{i-1}} - e_{VV_i}) + \lambda_{V_i}\right) + VV_{i-1}\, Y_{i-1}\left(e_{ncv_{i-1}} - e_{ncv_i}\right) = M_f\, Cp_{b_i}(T_{f_i} - T_{f_{i+1}}) \quad (4.23)$$

The heat transfer equation is

$$D_{i-1}\left(e_{d_{i-1}} - e_{d_i}\right) + \left(VR_i - VV_i(1 - Y_i)\right)\lambda_{V_i} + VV_{i-1}(1 - Y_{i-1})\left((e_{VV_{i-1}} - e_{VV_i}) + \lambda_{V_i}\right) + VV_{i-1}\, Y_{i-1}\left(e_{ncv_{i-1}} - e_{ncv_i}\right) = U_i A_{t_i}\left[\frac{\left(T_{VV_i} - T_{f_{i+1}}\right) + \left(T_{VV_i} - T_{f_i}\right)}{2}\right] \quad (4.24)$$

where U_i is the overall heat transfer coefficient and A_t is the heat transfer surface area which is defined as:

$$A_t = N_t\, \pi\, D_{to}\, L_t \quad (4.25)$$

N_t is the total number of tubes in the stage, D_{to} is the tube outer diameter and L_t is the tube length.

The following are the correlations used to describe various properties (U_i and NEA) within the stage. These correlations are extracted from the study of (Al-Fulaij, 2002). The correlations are based on real data from 6 large MSF plant with different designs (number of stages) and operating at different conditions, which include:

- The rated unit capacity varies between 25,000 and 32,000 m^3/day
- Data are obtained for minimum load operation, which are collected over a period of 3 h and account for 70–75% of the normal design load;
- Data are obtained for overload operation, which are collected over a period of 3 h and account for 110–115% of the normal design load;
- High and low temperature operations; with top brine temperature (TBT) range of 91.1–106.55^{o}C; and brine blow down temperatures of 30.5–40.6^{o}C;
- Brine velocity inside the tubes varies over a range of 1.32–2.34 m/s

Non equilibrium allowance has two correlations, one for the flash box orifice and other of the weir orifice. In the first nine stages with flash box NEA has been calculated by the following correlation, (Al-Fulaij, 2002):

$$\mathrm{NEA} = 1667 \times 10^5 \quad T_{b_i}^{-4.84124} \times \left(T_{b_{i-1}} - T_{b_i}\right)^{-0.04486} \quad H_{b_i}^{1.150576} \quad Re_{1_i}^{-0.18218} \quad Re_{2_i}^{0.204095} \tag{4.26}$$

Applicable for the following parameter ranges:

$56.3 \leq T_{b_i} \leq 106.3\ ^{O}C$

$0.10 \leq h_i \leq 0.85$ m

$0.616 \leq (T_{b_{i-1}} - T_{b_i}) \leq 12.26\ ^{O}C$

$582{,}079 \leq Re_{1i} \leq 3{,}903{,}019$

$189{,}201 \leq Re_{2i} \leq 2{,}805{,}319$

For the remaining stages with weir orifice its correlation is (Al-Fulaij, 2002):

$$\mathrm{NEA} = 6998 \quad T_{b_i}^{-3.13716} \times \left(T_{b_{i-1}} - T_{b_i}\right)^{-0.02106} \quad H_{b_i}^{0.682908} \quad Re_{1_i}^{0.174489} \quad Re_{2_i}^{0.042234} \tag{4.27}$$

Applicable for the following parameter ranges:

$36 \leq T_{b_i} \leq 79\ ^{O}C$

$0.16 \leq hi \leq 0.95$ m

$0.88 \leq (T_{b_{i-1}} - T_{b_i}) \leq 3.2\ ^{O}C$

$348{,}444 \leq Re_{1i} \leq 1{,}383{,}353$

$65{,}987.5 \leq Re_{2i} \leq 1{,}177{,}950$

The overall heat transfer coefficient is (Al-Fulaij, 2002):

$$U_i = 0.107309 \times T_{v_i}^{0.773247} \times VL^{0.484958} \tag{4.28}$$

Applicable for $39.5\ ^{o}C \leq T_V \leq 105.1\ ^{o}C$ and 1.32 m/s $\leq VL \leq 2.28$ m/s.

4.4.1.2 Higher Level Model (MSF Plant)

A higher level model was required to relate two subsequent flashing stages in order to obtain the rest of the variables which are not possible to evaluate in the lower level model such as the stage outlet flow rates (B_i), the vented vapours and non condensable gases flow rate (VV_i) and the discharge coefficient (Cd). That is because each of these variables depends on the pressure and brine height in the next flashing stage.

An important fact should be mentioned that the behaviour of the real plant could be discontinuous due to the presence of the blow through phenomenon (Cipollina, 2004-2005) where vapours escape to the next stage through the brine orifice. This occurs when the brine level is lower than the gate height. Thus the equations describing the no-blow through condition will be presented followed by the equations modeling the blow through condition.

No- Blow through condition (the brine level is higher than the gate height)

Outlet flow rates of brine (Cipollina, 2004-2005):

$$B_i = Cd_i \left(W_i \, H_{g_i} \right) \sqrt{ABS\left(2 \left(P_i - P_{i+1} + (H_{b_i} - H_{b_{i+1}}) \, g \, \rho_{b_i} \right) \rho_{b_i} \right)} \times SGN\left(2 \left(P_i - P_{i+1} + (H_{b_i} - H_{b_{i+1}}) \, g \, \rho_{b_i} \right) \rho_{b_i} \right) \quad (4.29)$$

Equation (4.30) gives the vented vapour and non-condensable gases flow rate (Cipollina, 2004-2005)

$$VV_i = \alpha_i \sqrt{ABS\left(\rho_{v_i} \left(P_i - P_{i+1} \right) \right)} \times SGN\left(\rho_{v_i} \left(P_i - P_{i+1} \right) \right) \quad (4.30)$$

Blow through condition (the brine level is lower than the gate height)

Outlet flow rates of brine (Cipollina, 2004-2005):

$$B_i = Cd_i \left(W_i \, H_{b_i} \right) \sqrt{ABS\left(2 \left(P_i - P_{i+1} + (H_{b_i} - H_{b_{i+1}}) \, g \, \rho_{b_i} \right) \rho_{b_i} \right)} \times SGN\left(2 \left(P_i - P_{i+1} + (H_{b_i} - H_{b_{i+1}}) \, g \, \rho_{b_i} \right) \rho_{b_i} \right) \quad (4.31)$$

Equation (4.32) gives the vented vapour and non-condensable gases flow rate (Cipollina, 2004-2005)

$$VV_i = \left(\alpha_i + W_i \, \alpha' \left(H_{g_i} - H_{b_i} \right) \right) \sqrt{ABS\left(\rho_{v_i} \times \left(P_i - P_{i+1} \right) \right)} \times SGN\left(\rho_{v_i} (i) \left(P_i - P_{i+1} \right) \right) \quad (4.32)$$

where (i) refers to the stage under study and (i+1) refers to the next stage.

For the stages with direct venting such as stage 1, 7, 12 and 21, the variable P_{i+1} in equations (4.30,4.32) is replaced with the venting line pressure .

For the last stage, outlet pressure is fixed and a control loop is inserted to control the brine level in the last stage (Cipollina, 2004-2005) but the coefficient was changed from 0.85 to 0.9 which is the real plant condition:

$$K_{c-b} = 0.9\ MF \tag{4.33}$$

$$B_n = 0.9\ MF + K_{c-b}\left[\frac{H_{b_n} - H_{sp}}{H_{sp}}\right] \tag{4.34}$$

Similar to the NEA and U, the discharge coefficient is extracted from the study of (Al-Fulaij, 2002). For the flash box stages the correlation is given by:

$$Cd_i = 0.49 \times \left(\frac{H_{g_i}}{\left(\frac{\Delta P}{\rho_{b_i}\, g}\right) + H_{b_i}}\right)^{-0.058508} \times \left(\frac{v_1}{v_2}\right)^{0.187808} \times \left(\frac{\rho_{b_i}}{\rho_{m_i}}\right)^{-0.234325} \times \left(\frac{H_{1i}}{H_{2i}}\right)^{0.1997656} \tag{4.35}$$

Applicable for the following parameter ranges:

$57 \leq T_{b_i} \leq 106$ ^{O}C

$0.36 \leq v_1 \leq 1.77$ m/s

$0.165 \leq H_{g_i} \leq 0.45$ ^{O}C

$0.25 \leq H_{1i} \leq 0.56$ m

$0.36 \leq H_{2i} \leq 0.65$ m

$0.10 \leq H_{bi} \leq 0.85$ m

$2.94 \leq \Delta P \leq 11.84$ kPa

For the weir gate stages the correlation is given by:

$$Cd_i = 0.139938 \times \left(\frac{H_{g_i}}{\left(\frac{\Delta P}{\rho_{b_i}\, g} \right) + H_{b_i}} \right)^{0.147156} \times \left(\frac{v_1}{v_2} \right)^{1.33021} \times \left(\frac{\rho_{b_i}}{\rho_{m_i}} \right)^{0.36234} \qquad (4.36)$$

Applicable for the following parameter ranges:

$37 \leq T_{b_i} \leq 73$ ^{O}C

$0.58 \leq v_1 \leq 3$ m/s

$0.165 \leq H_{g_i} \leq 0.45$ ^{O}C

$0.32 \leq H_{bi} \leq 0.86$ m

$0.56 \leq \Delta P \leq 4.3$ kPa

ρ_m is the two phase mixture density (kg/m^3), which is defined as :

$$\rho_m = \frac{\rho_b}{\left[1 - \frac{Md}{Md+Mb}\left(1 - \frac{\rho_b}{\rho_v}\right)\right]} \qquad (4.37)$$

In the brine heater, the feed sea water temperature increases in the tubes as a result of steam condensation on the outer surface of the tubes. The brine heater heat balance is given by (El-Dessouky & Ettouney, 2002) :

$$M_{stm}\, \lambda_{stm} = M_f\, C_{P_b}\, (TF1 - TbT) \qquad (4.38)$$

The plant gain output ratio is defined as the mass flow rate ratio of the distillate product to heating steam. This ratio gives a measure for the plant efficiency and performance. It is desired to keep this ratio as high as possible (close the design value) (El-Dessouky & Ettouney, 2002). This relation is:

$$GOR = M_d / M_{stm} \quad (4.39)$$

4.5 Brine circulation MSF process (MSF-BC)

4.5.1 Mathematical equations

The mathematical model of MSF-BC was built in hierarchical structure same as the MSF-OT mathematical model. The lower level (Flashing Stage Model) mathematical model equations will be presented first. In the MSF-BC model, the lower level model is divided to two types. One is representing the heat gain section and other models the heat rejection section. That will be followed by the higher level mathematical model (MSF Plant).

4.5.1.1 Lower Level Model (Heat Gain Section Flashing Stage Model)

Comparing Figure 4.2 and Figure 4.3 shows that the only difference between the flashing stage of the heat gain section in the MSF-BC and that of MSF-OT is that in the MSF-OT the stream flowing in the condenser tubes is feed seawater (MF) while in the MSF-BC it is recycle brine (MR).

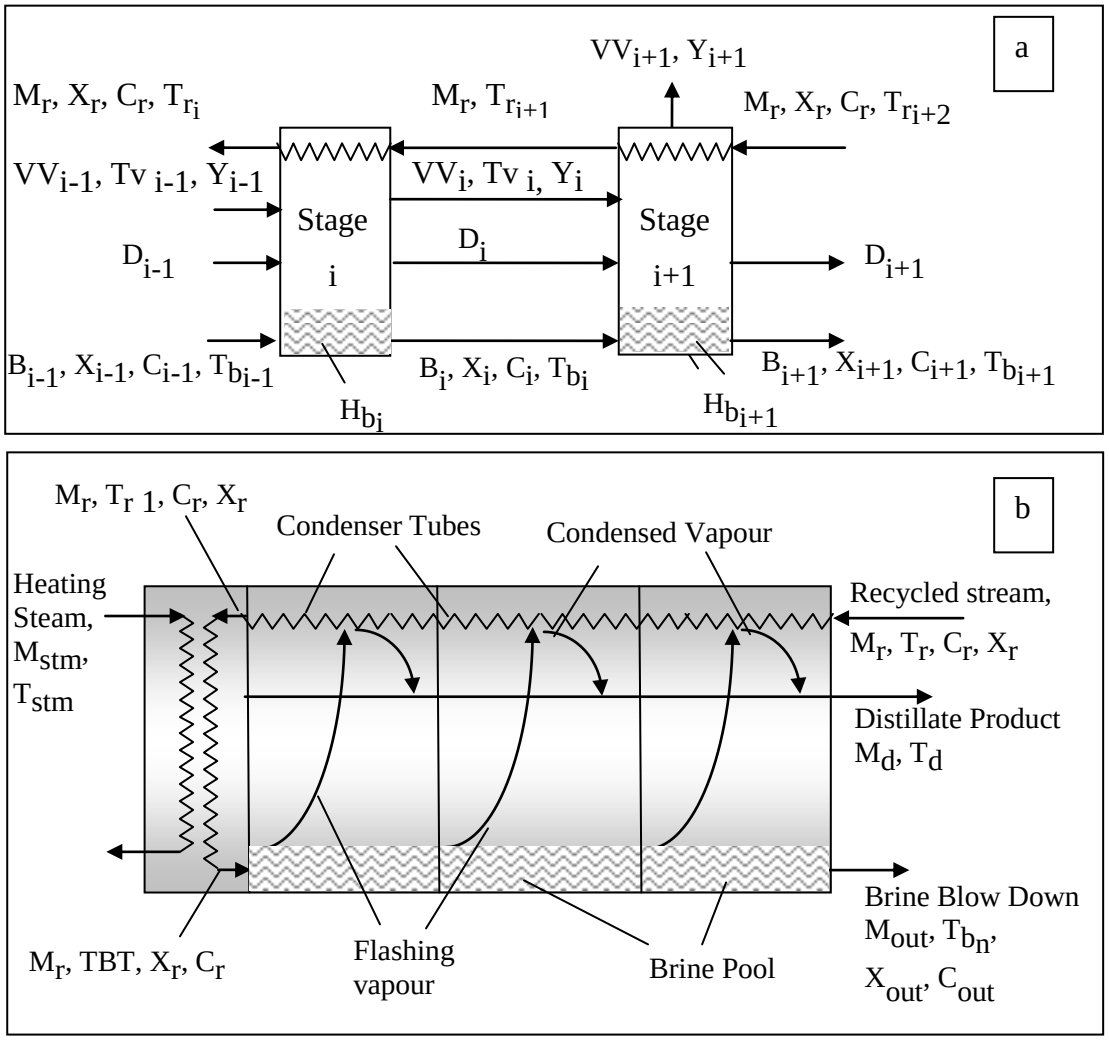

Figure 4.3 Process variables in MSF_BR process (a) variables between heat gain section stages (i) and (i+1) and (b) overall heat gain section variables

Thus, the dynamic model for each flashing stage in the heat gain section is same as that presented in section (4.4.1.1) of the flashing stage in the MSF-OT except for equations (4.23) which will be:

$$D_{i-1}\left(e_{d_{i-1}} - e_{d_i}\right) + \left(VR_i - VV_i(1 - Y_i)\right)\lambda_{V_i}$$
$$+VV_{i-1}(1 - Y_{i-1})\left((e_{VV_{i-1}} - e_{VV_i}) + \lambda_{V_i}\right)$$
$$+ VV_{i-1}\,Y_{i-1}\left(e_{ncv_{i-1}} - e_{ncv_i}\right) = M_r\;Cp_{b_i}\;(T_{r_i} - T_{r_{i+1}}) \qquad (4.40)$$

4.5.1.2 Lower Level Model (Heat Rejection Section Flashing Stage Model)

Figure 4.4.(a) shows schematics for the system variables between stages (i) and (i+1) and Figure 4.4.(b) shows the overall input/output variables for the heat rejection section.

The dynamic model for the brine, vapour and distillate in the flashing stage of the heat rejection section is quite similar to that presented in section (4.4.1.1) of the flashing stages in MSF-OT. The differences occur in the last stage where the makeup sea water (feed sea water less cooling water) is fed to the brine pool. The brine recycle is extracted from the brine pool in the last stage and fed into the condenser tubes of the last stage of the heat gain section. Thus equations (4.1, 4.5, 4.7 and 4.9) are modified in the following manner. Applying total mass balance on the brine pool gives:

$$\frac{dM_{b_i}}{dt} = B_{i-1} + (M_f - M_{cw}) - B_i - M_r - VR_i - NC_i \quad (4.41)$$

The salt mass balance in the brine pool is given by:

$$\frac{dM_{s_i}}{dt} = B_{i-1}\, C_{i-1} + (M_f - M_{cw})\, C_f - B_i\, C_i - M_r\, C_r \quad (4.42)$$

Mass balance of the non-condensable gases in the brine pool:

$$\frac{dM_{bg_i}}{dt} = B_{i-1}\, X_{i-1} + (M_f - M_{cw})\, X_f - B_i\, X_i - M_r\, X_r - NC_i \quad (4.43)$$

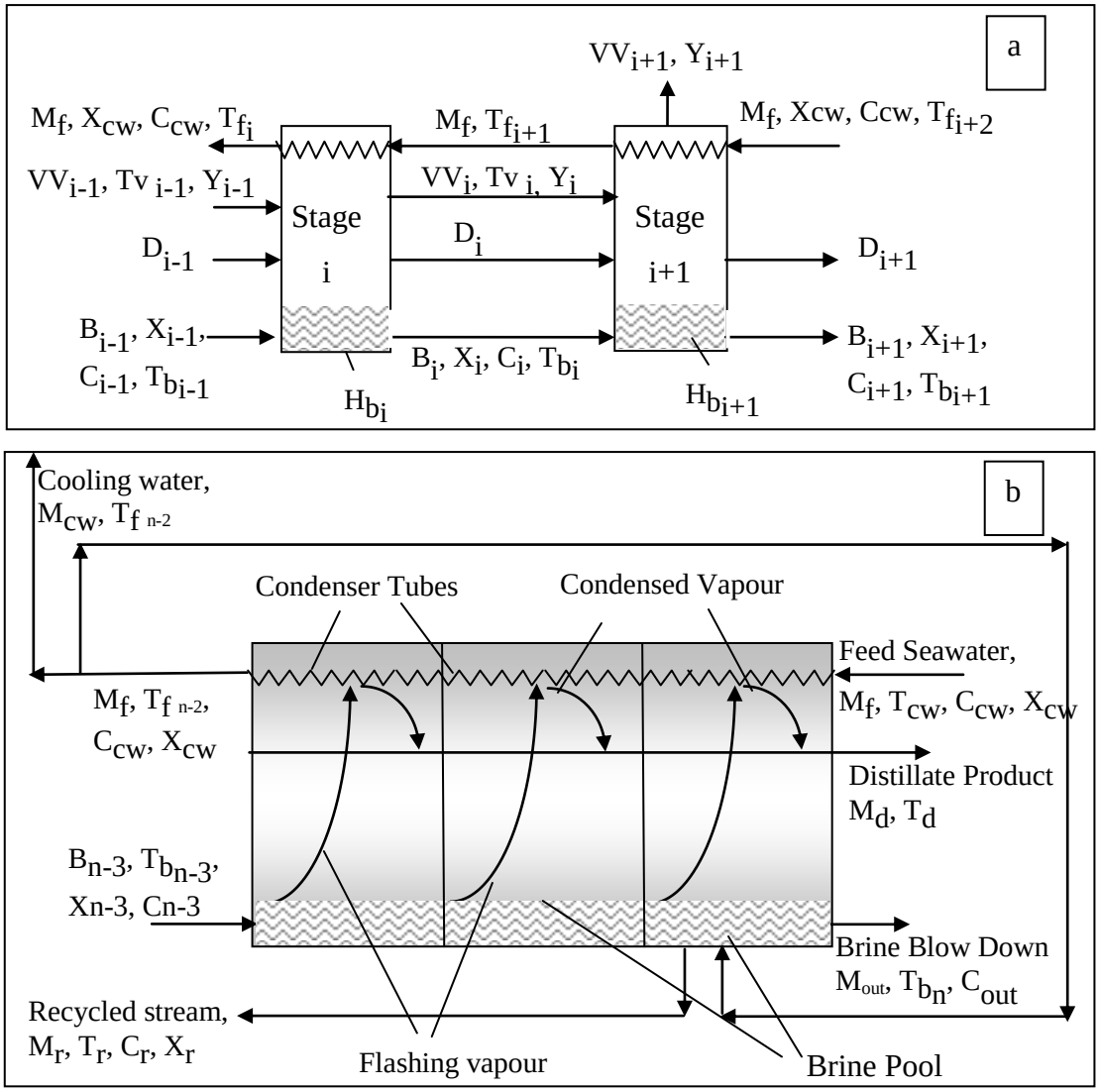

Figure 4.4 Process variables in MSF process (a) variables between heat rejection section stages (i) and (i+1) and (b) overall heat rejection section variables.

Enthalpy balance for the brine pool:

$$\frac{dE_{b_i}}{dt} = B_{i-1}\ e_{b_{i-1}} + (M_f - M_{cw})\ e_{f_{i-2}} - B_i\ e_{b_i} - NC_i\ e_{ncr_i} - VR_i\ e_{vr_i} - M_r\ e_{b_i} \quad (4.44)$$

The non-equilibrium Allowance will be obtained from Equation (4.26). The overall heat transfer coefficient will be evaluated from a correlation based on study by (Al-Fulaij, 2002):

$$U_i = 0.0225 \; T_{v_i}^{1.515} \; VL^{0.286} \tag{4.45}$$

This equation is applicable for $37^oC \leq T_V \leq 73\ ^oC$ and $1.32 \leq VL \leq 2.28$ m/s.

4.5.1.3 Higher Level Model

The higher level model of the MSF-BC model is the same as that of MSF-OT model (see section 4.4.1.2) except for the brine heater balance where M_f is replaced by M_r and T_{f1} is replaced by T_{r1}. In addition the following equation is used to evaluate the salinity of the brine recycle stream (C_r):

$$M_r C_r + (M_f - M_{cw} - M_d) C_{out} = ((M_f - M_{cw})) C_f + (M_r - M_d) C_{bn} \tag{4.46}$$

4.6 gPROMS Modeling Language

The simulators used for solving the mathematical models are divided into modular and equation oriented. The modular simulators are originally developed for chemical process industry (Aspen Technology, 2010). Most of these packages have modular elements for commonly known unit operations, which includes distillation, absorption, heat exchanger, etc. Although, these simulators have sufficient resources to simulate desalination processes, its use might be quite complex. This is because flow chart development would require extensive work. In addition, commercial simulators are expensive to acquire and have high maintenance cost.

Several software codes have been used to simulate and model the MSF plants. A popular tool in the academic and industrial communities is gPROMS (PSE, 1997). This system was developed specifically for chemical engineering systems. The system is introduced in a specific language which is close to the natural mathematical language. The system interprets this model and links together all the variables and

equations to powerful mathematical solver (Bogle, Cipollina, & Micale, 2009). gPROMS has a number of advantages over commonly used modular simulators.

The gPROMS is a complete software package for modeling and simulating processes in both lumped and distributed systems. It has many features such as the possibility of implementing models at different levels, which are included in a hierarchical structure, thus allowing the easy simulation of multi-stage system. It uses a purely declarative language, with the order in which equations are written being irrelevant. Single or multi-dimensional arrays for both variables and equations are allowed, to be used when describing multi-component or multi-stage systems. Also, it can be used for describing distributed parameters systems. It can be used to describe systems with significant gradients of all variables along the physical domain (Cipollina, 2004-2005).

For a moderately complicated process system, there is usually a set of different models for the same purpose that describes the system in different detail and/or at different levels. These models are not independent of each other but are related through the process system they describe and through their related modeling goals. Thus models could be arranged in a hierarchy ((Hangos & Cameron, 2001). This hierarchy can be easily modeled in gPROMS. In the MSF process, each flashing stage is described by its own equations and then all of the stages are related through the process system.

gPROMS is not only accepted by the academic researchers but also different pioneer companies (Shell Chemicals, Japanese Petrochemicals Producer, US Refinery Operator) that successfully implement gPROMS optimization tools to significantly improve their operation. gPROMS Model Builder can handle dynamic simulation with models of over 100,000 differential and algebraic equations (PSE, 1997). The gPROMS model builder was chosen because (Tanvir & Mujtaba, 2008):

- The model development time is reduced because the solution algorithm needs not to be written rather needs to be specified.
- The same model can be used for different simulation and optimization activity.

- The model does not have to be re-written with changing set of input specifications.
- The gPROMS model can be readily integrated with automation software, MS Office or any of the other standard tools (PROII, ASPUN PLUS, MATLAB, MATLAB Simulink, etc.) of the modern process manufacturing organization.
- gPROMS has an intelligent editors for easy construction and maintenance. Moreover, it allows complex conditional statements for discrete operation.

4.7 Conclusion

Detailed and comprehensive dynamic mathematical models are presented for both MSF-OT and MSF-BC processes. The new model includes many features which are not included in previous literature models such as distillate flashing, demister losses and venting system. These elements provide additional simulation and design details of the system, which can lead to more accurate system design, simulation, and control.

The mathematical model was based mainly on four assumptions including lumped parameter analysis, negligible heat losses to the surrounding, salt free distillate and negligible subcooling and superheating on the system energy balance. Elimination of these assumptions is possible; however, it will result in the increase in the size of the computer code, especially the lumped parameter assumption which has to be replaced with either one or two dimensional differential equation model through the flashing stages. This might not be possible or it will generate a very large computer code that needs to be programmed on very large computing facilities. Also, elimination of the subcooling/superheating assumptions and salt transport into the distillate stream requires development of new empirical relations to assist in the simulation process. The heat loss assumption is the simplest to model either through assignment of a constant loss value from the input heat to the system or through the use of heat losses to the surroundings from the outer surface of the flashing stages by natural convection.

The model was built in hierarchy structure where the lower hierarchy includes the flashing stages while the higher hierarchy includes combines the flashing stages together and the brine heater. The model is solved using gPROMS, which is an equation oriented simulator for the chemical engineering systems. gPROMS provides a large library for solution of algebraic and differential equations.

The next chapter includes the simulation results of the MSF dynamics and steady state models. The model predictions are validated against MSF-OT and MSF-BC plant data. Also, the system performance is analyzed for both dynamic and steady state for MSF-OT and MSF-BC processes.

Chapter 5
Validation and Results of Dynamic Modeling of MSF Plants

5.1 Introduction

The models presented in chapter 4 are lumped parameter dynamic modeling of the MSF processes both once through (MSF-OT) and brine circulation (MSF-BC) MSF plants. The models are validated against large production units operating at different conditions and of different designs (e.g. number of stages, orifice type and dimensions, stage dimensions, and condenser dimensions, etc.) to ensure generality of the model and prove that it can applied to any plant in the world.

First the MSF-OT plant computer solution using gPROMS is presented. It starts with model validation against data from existing MSF plants. Next, the steady state results are shown and finally the dynamic responses upon imposing changes in some operating or design parameters are presented. The same sequence was followed for the MSF-BC circulation plant.

The last part of this chapter includes calculations of variations in the heat transfer area as a function of the demister losses. In this regard two models are used, the first assumes zero losses in the demister and the second uses the losses predicted from an empirical relation. The results given in this part show the importance of proper modeling of the demister losses.

5.2 Modeling real MSF-OT plants

5.2.1 Cases investigated, assignment and initial conditions

Table 5.1 includes the design and operating conditions of MSF-OT plant installed in Kuwait and belongs to Ministry of Electricity and Water (MEW) used to validate the model. It includes 21 stage, the first 9 stages are having flash box orifice (see Figure 2.12. (b)) and the rest are having weir orifice (see Figure 2.12 (a))

Table 5.1: Parameters used in simulation of MSF-OT system for plant A (Kuwait-MEW)

Parameter	Value	Units
Number of stages (n)	21	
Stage width (Wst)	17.66	m
Stage length (Lst)	3.150	m
Stage height (Hst)	4.521	m
Number of condenser tubes (Nt)	1410	
Condenser tubes outer diameter (ODt)	0.0445	m
Condenser tubes inner diameter (IDt)	0.04197	m
Brine level set point in the last stage (Hst)	0.668	m
Top brine temperature(TBT)	91	^{o}C
Intake sea water flow rate (MF)	4027	kg/s
Intake sea water salinity (C_{cw})	40000	ppm
Intake sea water temperature (T_{cw})	37.7	^{o}C
Steam temperature (T_{stm})	111	^{o}C
Venting line pressure	7000	Pa
Non condensable gases concentration in feed seawater	18.1	mg/kg (ppm)

5.2.2 Model Validation Results:

Model validation was based on three aspects: the first is the model physics (to what extent the model gives an accurate description of the real physics of the system), the second is validation of the model predictions against measured data from experimental unit or real plants (whether values and trends of measured and predicted data are in agreement), the third is model expectations (this gives a measure of the detail level adopted in model development). A good example for the third aspect is modeling the heat transfer area using a constant overall heat coefficient against a more detailed model based on correlations of the inside and outside heat transfer coefficients. In this regard, the expectation is that the more detailed model would give more accurate results; however, in some cases the error involved using the simpler model might provide reasonable answers. These three aspects will be accounted for in

the discussion of results for each set of data. The validation was made against both steady state data and dynamic data of the plant in Table 5.1.

5.2.2.1 Steady State Validation Results

Comparison of the model predictions is made against field data for existing MSF plants (see table 5.1- Plant A).The comparison is for steady state data, which include variations in the flow rate, salinity, and temperature profiles of the brine stream across the stages.

As shown in Figure 5.1, from stage to stage the brine outlet temperature is decreasing due to the flashing process. Also, the brine flow rate is decreasing because of the distillate formed in each stage. Finally, the product salinity is increasing across the stages. That is due to the fact that the distillate is almost salt free in comparison with the brine so after flashing takes place the salt concentrates in the brine outlet as shown in equation (4.5) (Al-Mutaz & Soliman, 1989).

As shown in Figure 5.1, good agreement is obtained between model predictions and the plant data, especially for the brine flow rate and salinity, where the errors did not exceed 0.4% for both variables. On the other hand, the relative error in predicting the stage temperature is limited to a maximum of 0.62%.

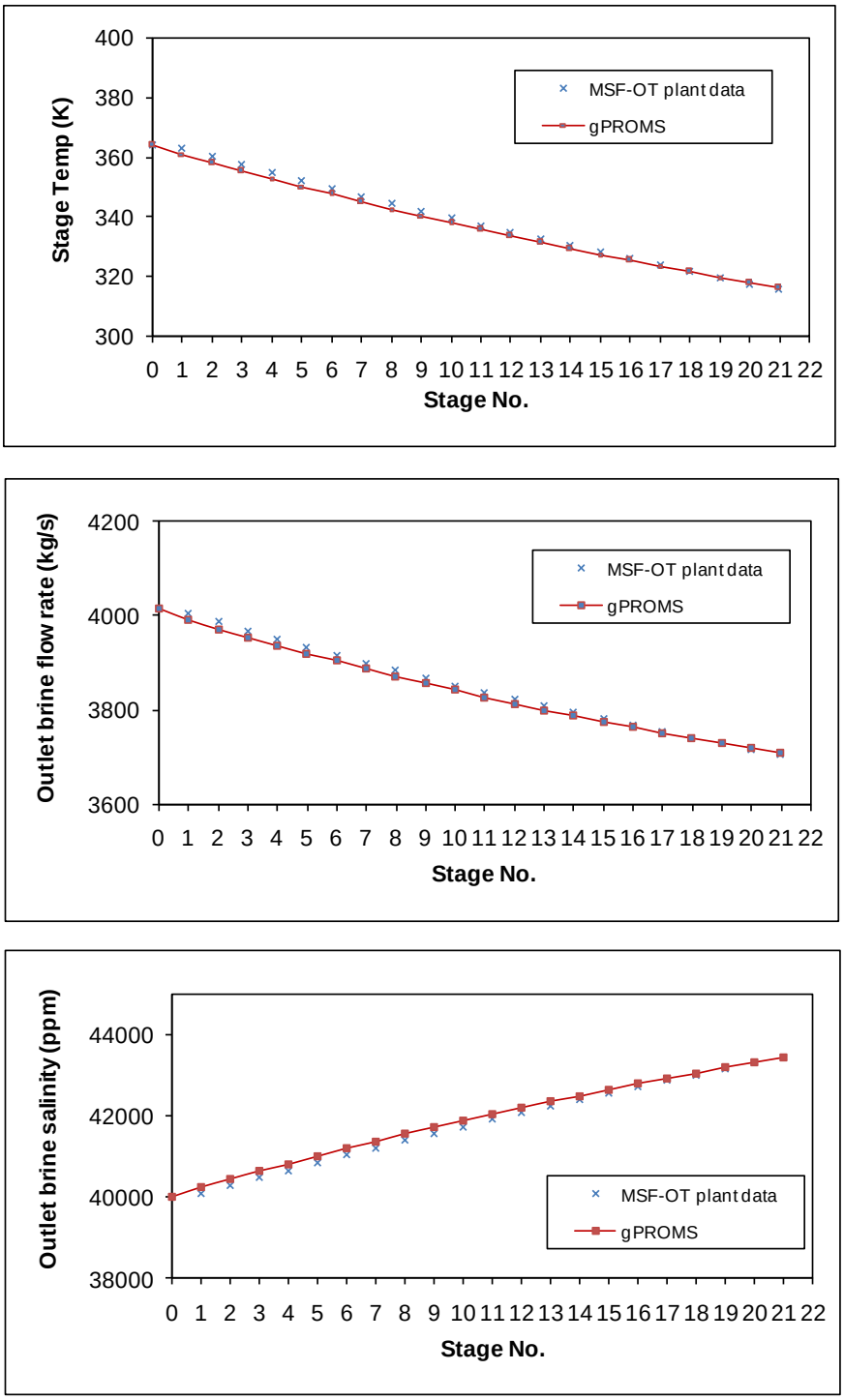

Figure 5.1 Comparison of gPROMS predictions and the field data for stage profiles of flow rate, salinity, and temperature of the brine stream leaving the stage.

5.2.2.2 Dynamic Validation Results

Comparison of the model predictions is made against field data for an existing MSF-OT plant (see Table 5.1). The comparison was made for data collected from daily operation, where small disturbances occur in operating parameters. These include the top brine temperature, the feed seawater flow rate, and intake seawater temperature. Summary of the plant operating parameters, which are made every four hours for a period of 24 hours, are shown in table. 5.2. As shown, small disturbances are found in this data, which are caused by daily fluctuations in solar insolation and heating steam pressure. The solar insolation affects the intake seawater temperature and the heating steam pressure affects the top brine temperature. As a result, small changes are made in the feed seawater flow rate in order to maintain the plant at the desired design conditions.

As shown in table 5.2, the top brine temperature and the intake sea water temperature are changing within a small range but the feed flow rate is changing by a big amount.

Table 5.2: Disturbances occurring in MSF-OT real plant over a period of 24 hours

time	Top brine Temp	M_f	Inlet seawater Temperature
hr	^oC	kg/hr	^oC
0	91.3	14491000	37.7298
4	91.4	14574000	37.8169
8	91.1	14491000	37.8016
12	91.1	14574000	37.8749
16	91	14450000	37.8601
20	91.3	14491000	37.6854
24	91.5	14533000	37.7061

As shown in Figures 5.2-5.4, for the gPROMS predictions, immediately following each disturbance a jump occurs and then the disturbance is reduced. That is because the simulator calculates the values for each second. While for the real plant data, values are measured every 4 hours. This trend can be seen clearly in Figures 5.3-

5.4 while for Figure 5.2, since the range is big (41000-42600 ppm) this trend is not clear.

Comparison of model predictions and plant data include the flow rate, salinity, temperature profiles and brine level of the brine stream across the stages. Results are shown in Figures 5.2.-5.5. As shown, good agreement is obtained between model predictions and the plant data, especially for the stage temperature where the errors did not exceed 0.81%. On the other hand, the relative error in predicting the brine flow rate and salinity is limited to a maximum of 2.5% for the brine flow rate and 0.63% for the brine salinity.

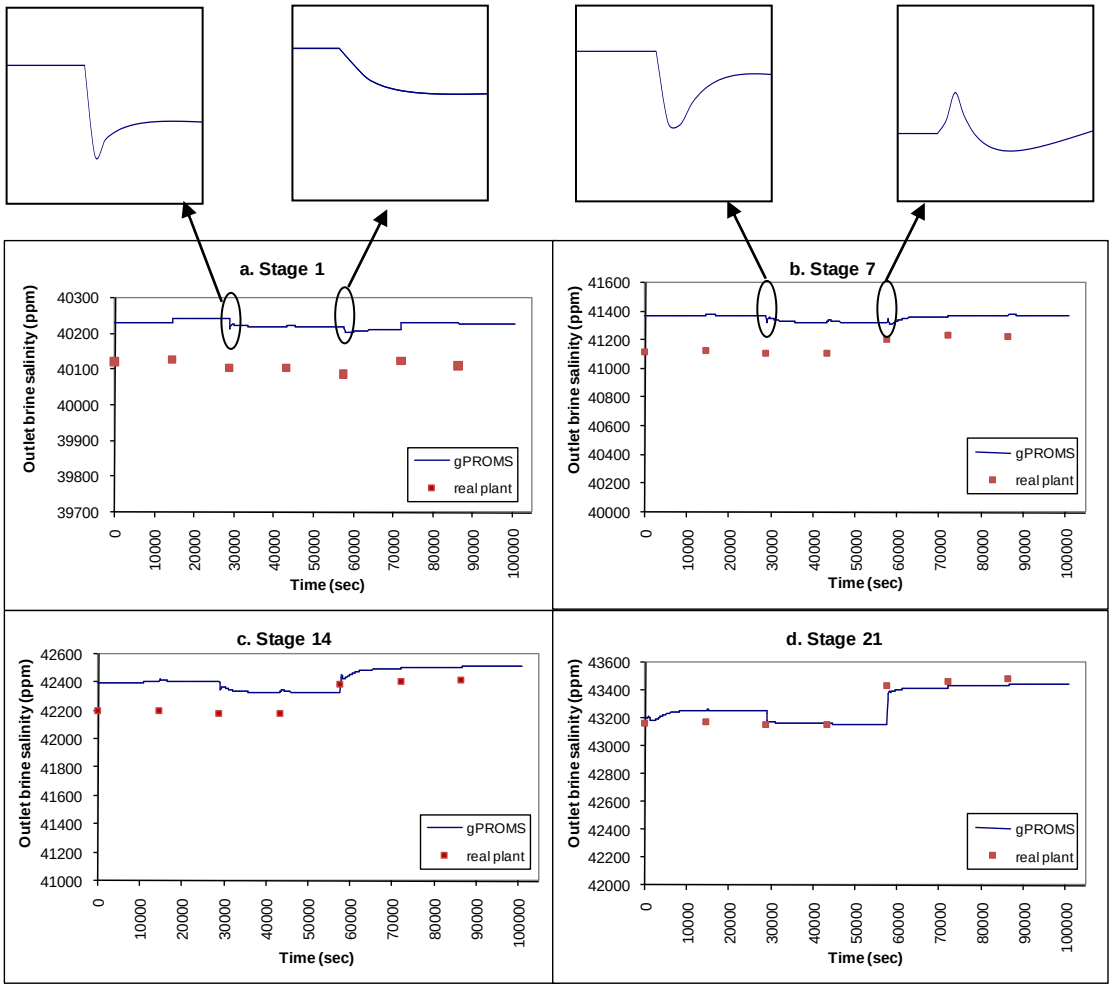

Figure 5.2 Comparison of gPROMS predictions and the field dynamic data for stage profiles of salinity of the brine stream.

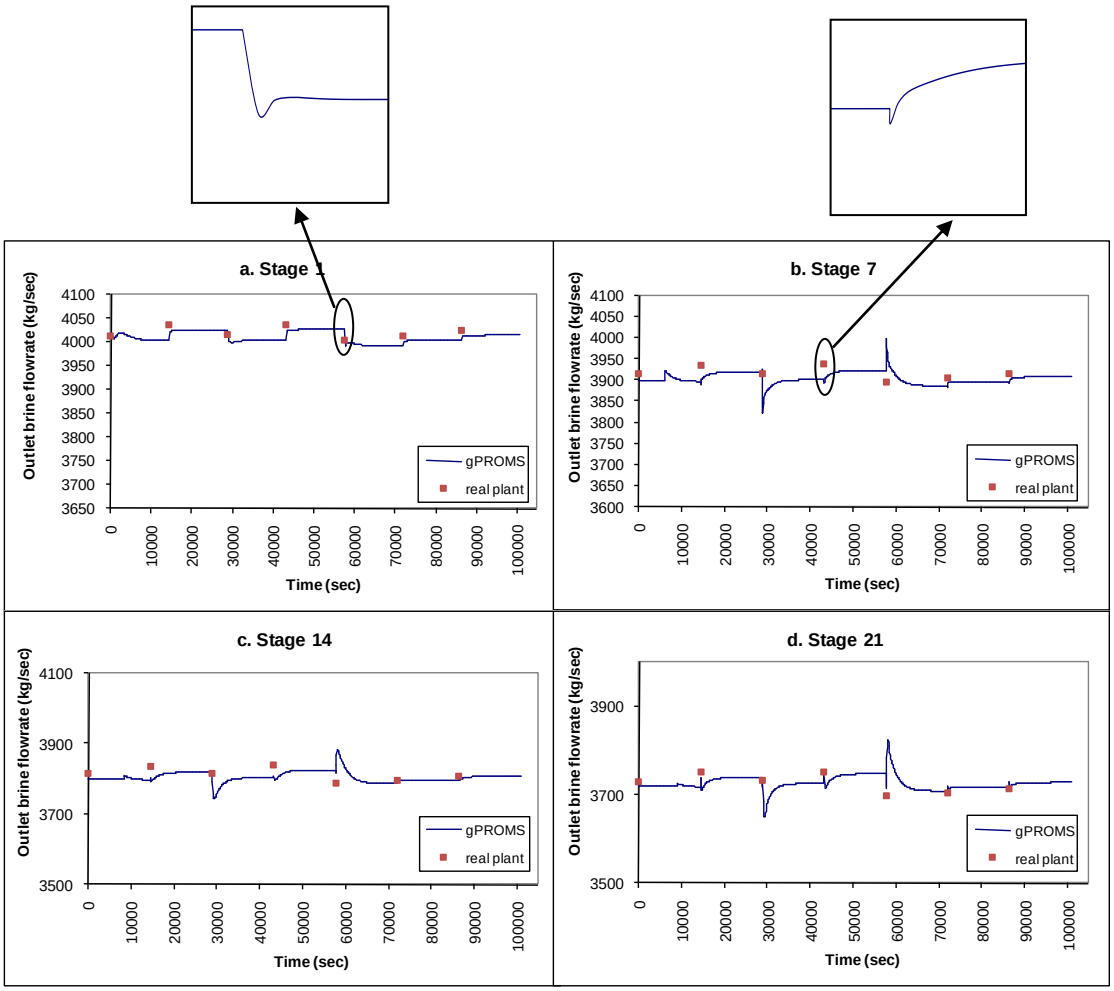

Figure 5.3 Comparison of gPROMS predictions and the field dynamic data for stage profiles of flow rate of the brine stream.

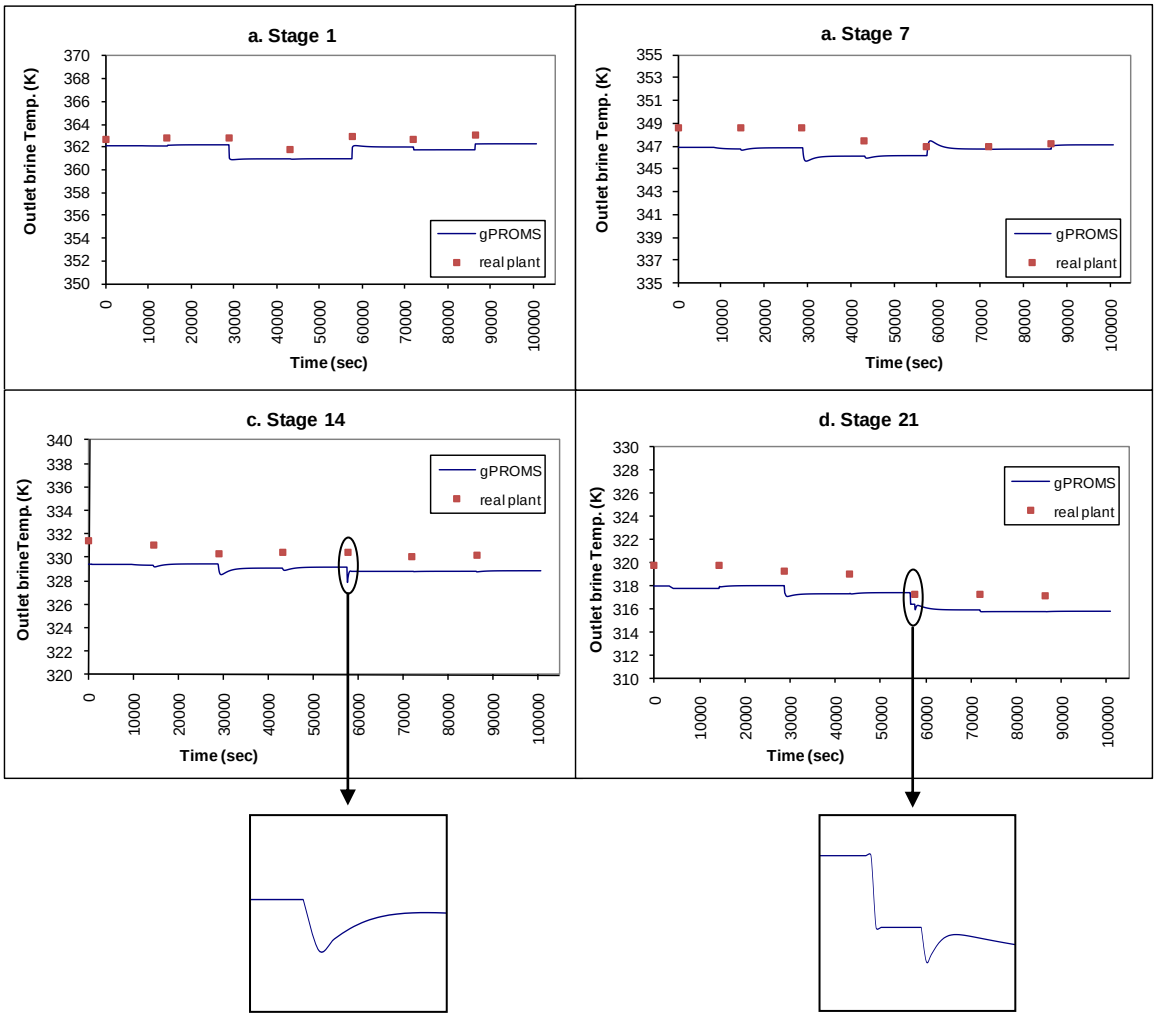

Figure5.4 Comparison of gPROMS predictions and the field dynamic data for stage profiles of temperature of the brine stream.

As shown in Figure 5.5, there is non-monotonic behaviour in the brine level. This is because the brine height depends on several parameters, which may result in its increase or decrease. For example, the brine height increases with the decrease of the discharge coefficient, stage pressure, temperature drop per stage, and gate height. A monotonic increase should have been observed in the brine height because of the monotonic decrease in the system temperature. However because of the unequal variations across the stages, the brine height changed in an uneven manner.

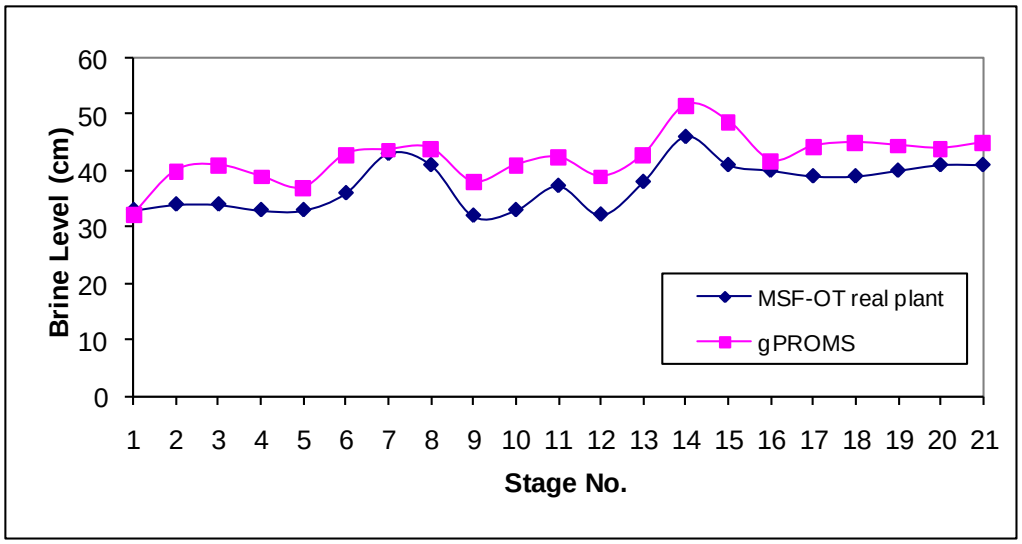

Figure 5.5 Non-monotonic behaviours in the brine level in the stages of MSF-OT plant.

5.2.3 Dynamic Response Results

The steady state and dynamic models have been validated and show good agreement with real plant data. Dynamic simulation is performed for the plant parameters shown in table 5.1 in order to explore its behaviour as a result of a certain change in the operating or design parameters within the real acceptable range.

Figures 5.6-5.8 illustrate the system transients after changing the seawater flow rate from 4048 kg/s to 4010 kg/s (Al-Deffeeri, 2009) and then changing it back to 4048 kg/s. Figures. 5.9-5.11. illustrate the system response after changing the top brine temperature (TBT) from 91^{o}C to 89^{o}C (Al-Deffeeri, 2009) and then restoring its value to 91^{o}C.

As shown in Figure 5.6, decrease of the feed flow rate results in drastic reduction in the brine level in all stages except for the last stage which is controlled. As mentioned previously, the feed flow rate is heated in the brine heater before entering the first flashing stage. That means that and increasing/decreasing the feed flow rate which is the brine inlet to the first stage will increase/decrease the inlet load

on the first stage and subsequently then rest of the stages causing an increase/decrease in the brine level in all stages. As shown in figure 5.7, decreasing the feed flow rate will reduce the amount of brine flowing from stage to stage. That in turn will reduce the flashed off vapour and the condensate rate in the stages. The opposite happens when increasing the feed flow rate.

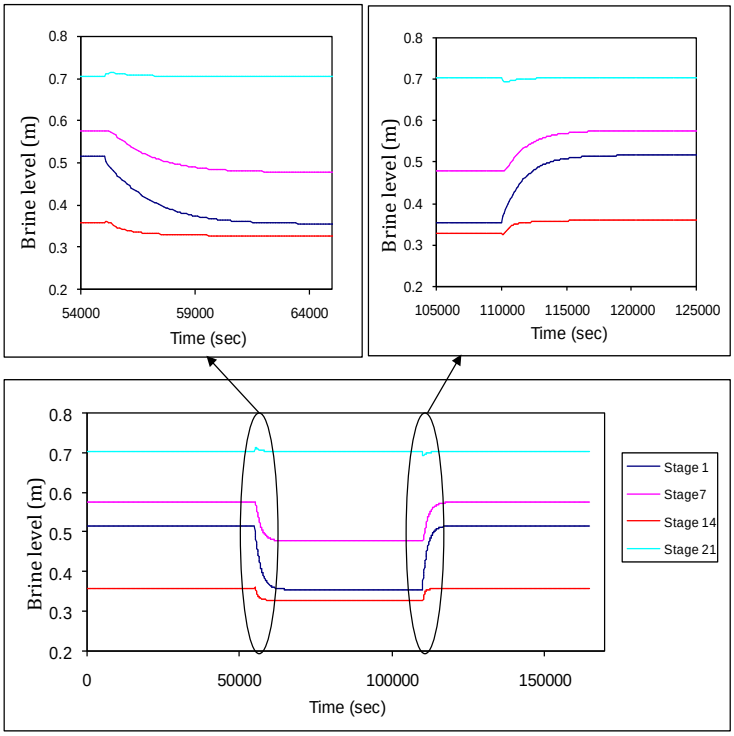

Figure 5.6 Dynamics of the brine level in stages 1, 7, 14, and 21 for step changes in the feed seawater flow rate (MF).

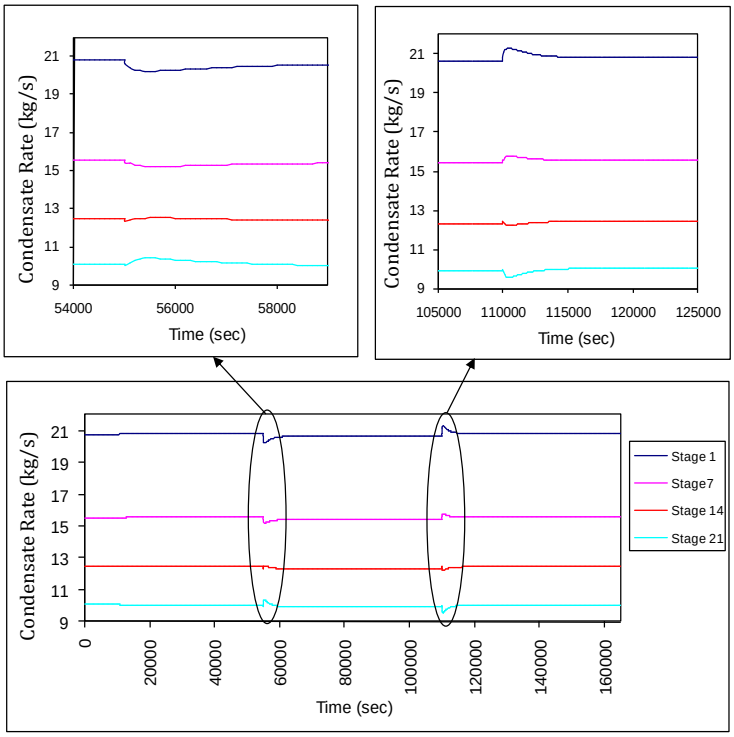

Figure 5.7 Dynamics of condensate rate in stages 1, 7, 14, and 21 for step changes in the feed seawater flow rate (MF)

Figure 5.8 shows the system dynamics for the plant gain output ratio (GOR) which is defined as the mass flow rate ratio of the distillate product to the heating steam. As shown it reaches a steady state value of 7.45. This is well below industrial standards and is caused by the use of small number of flashing stages and a small flashing range (difference between top brine temperature and brine reject temperature) (El-Dessouky & Ettouney, 2002). Use of 21 flashing stages results in a large difference between the outlet temperature of the feed seawater from stage 1 and the top brine temperature (TBT). This requires use of a larger amount of heating steam, which gives smaller GOR.

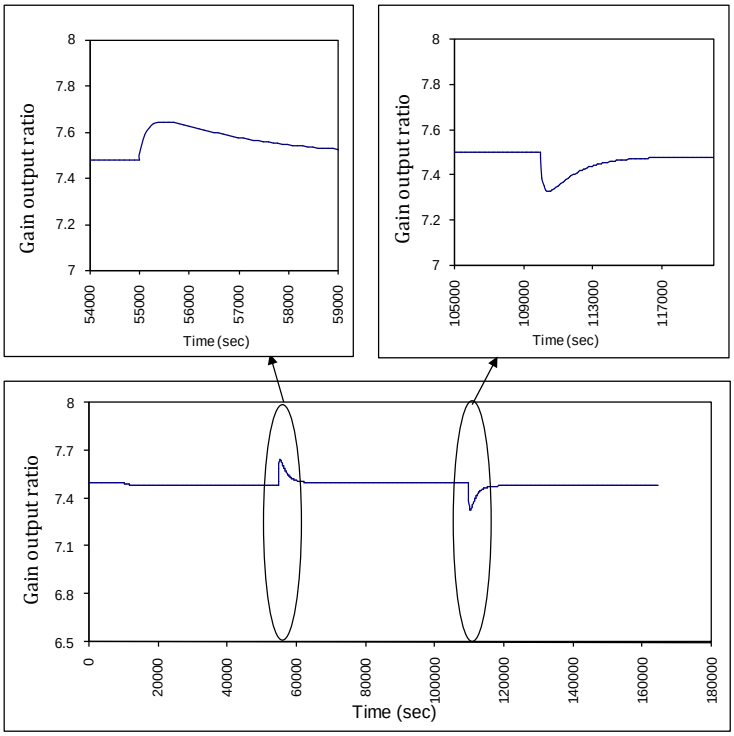

Figure 5.8 Dynamics in GOR in stages 1, 7, 14, and 21 for step changes in the feed seawater flow rate (MF)

Figures 5.9-5.10 show variations in the system variables upon step change in the top brine temperature (TBT) from 91^{o}C to 89^{o}C and then restoring the original conditions of 91^{o}C. Decrease in the top brine temperature reduces the flashing range which reduces the amount of vapour formed. This will result in an increase of the brine level in all stages except the last stage which is controlled and causes reduction in the condensation rate. As shown, the top brine temperature (TBT) has more drastic effect on the brine level especially in the first stage. This is because of the rapid and large change that occurs in the temperature and pressure of the stage.

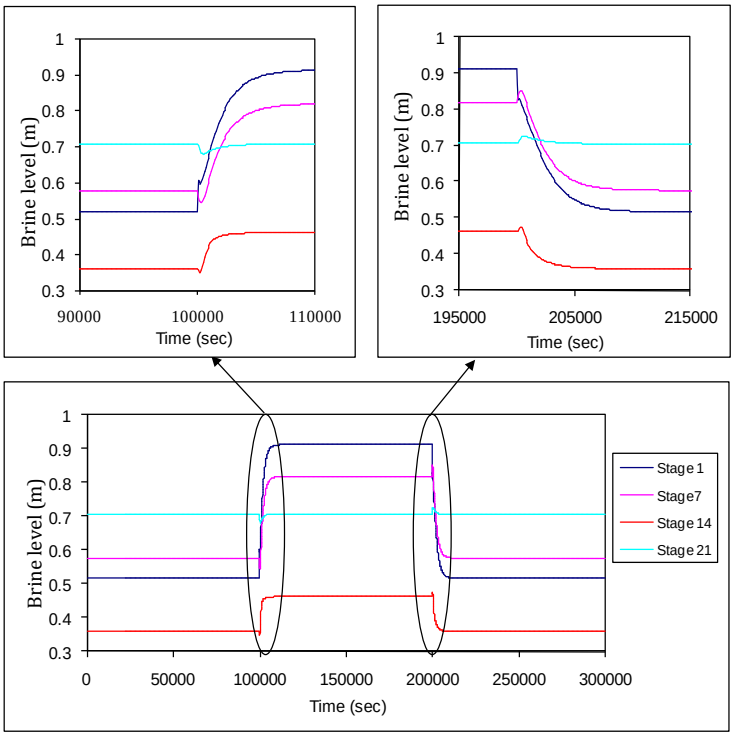

Figure 5.9 Dynamics of the brine level in stages 1, 7, 14, and 21 for step changes in the Top brine temperature (TBT).

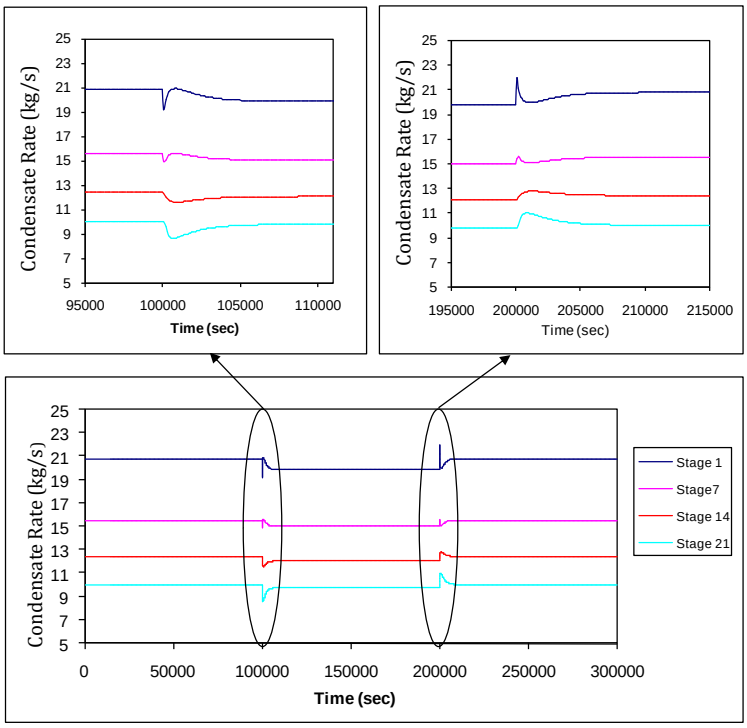

Figure 5.10 Dynamics of the condensate rate in stages 1, 7, 14, and 21 for step changes in the top brine temperature (TBT).

Plant gain output ratio (GOR) is other system variable which is affected, but, at a lesser magnitude. As shown in Figure 5.11, when the top brine temperature (TBT) decreases that means less amount of steam is used in the brine heater to heat the feed sea water. Also the reduction in the TBT will decrease the total productions rate and that is due to the reduction in the condensate flow in the stages. That in turn will keep GOR almost constant and unaffected.

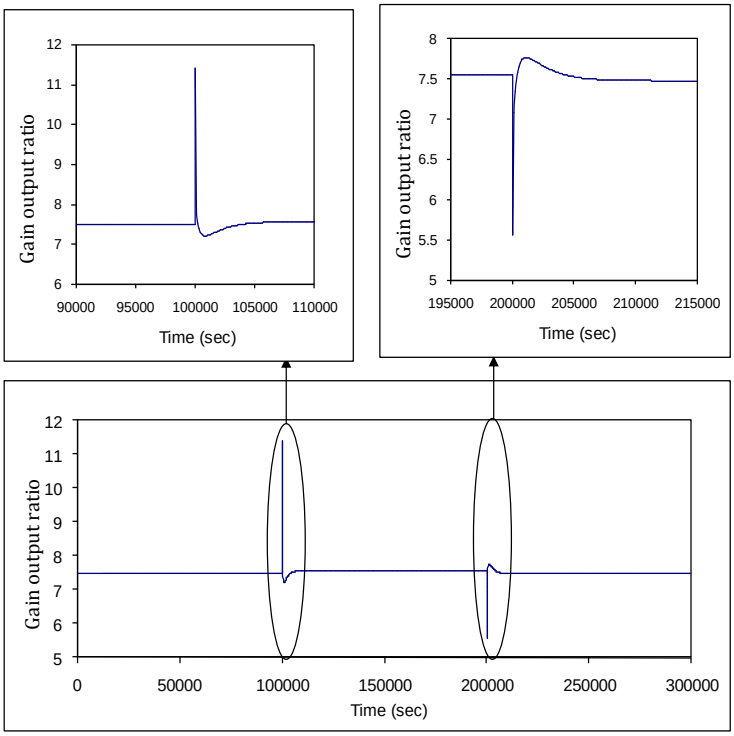

Figure 5.11 Dynamics of GOR in stages 1, 7, 14, and 21 for step changes in the top brine temperature (TBT).

5.3 Modeling real MSF-BC plants

5.3.1 Cases investigated, assignment and initial conditions

Tables 5.3 and 5.4 include the design and operating conditions of two MSF-BC plants installed in Kuwait and belongs to Ministry of Electricity and Water (MEW), which are used to validate the model. One has been used to validate the steady state model and other has been used to validate the dynamic model in order to

give the model more generality and strength since the two plants as shown in tables 5.3 and 5.4 have different operating and design conditions (different manufacturer).

Table 5.3: Parameters used in simulation of MSF-BC (plant B -Kuwait-MEW) operating at high temperature

Parameter	Value	Units
Number of stages (n):	24	
Heat Gain Section	21	
Heat Rejection Section	3	
Stage width (Wst)	17.66	m
Stage length (Lst)	3.150	m
Stage height (Hst)	4.521	m
Heat Gain Section:		
Number of condenser tubes (Nt)	1410	
Condenser tubes outer diameter (ODt)	0.0445	m
Condenser tubes inner diameter (IDt)	0.04197	m
Heat Rejection Section:		
Number of condenser tubes (Nt)	1992	
Condenser tubes outer diameter (ODt)	0.03175	m
Condenser tubes inner diameter (IDt)	0.02927	m
Brine level set point in the last stage (Hst)	0.66	m
Top brine temperature (TBT)	107.8	^{o}C
Recycled sea water flow rate (MR)	3389	kg/s
Intake sea water salinity (C_{cw})	40000	ppm
Intake sea water temperature (T_{cw})	27.3	^{o}C
Steam temperature (T_{stm})	120	^{o}C
Venting line pressure	7000	Pa
Non condensable gases concentration in feed seawater (C_{cw})	18.1	mg/kg (ppm)

Table 5.4: Parameters used in simulation of MSF-BC (plant C -Kuwait-MEW) operating at low temperature

Parameter	Value	Units
Number of stages (n):	26	
Heat Gain Section	23	
Heat Rejection Section	3	
Stage width (Wst)	16.528	m
Stage length (Lst)	2.850	m
Stage height (Hst)	4.150	m
Heat Gain Section Area:	3367	m^2
Heat Rejection Section Area:	3398	m^2
Brine level set point in the last stage (Hst)	0.66	m
Top brine temperature (TBT)	89.8	^oC
Recycled sea water flow rate (MR)	4028	kg/s
Intake sea water salinity (C_{cw})	40000	ppm
Intake sea water temperature (T_{cw})	34.9	^oC
Steam temperature (T_{stm})	100	^oC
Venting line pressure	7000	Pa
Non condensable gases concentration in feed seawater	18.1	mg/kg (ppm)

5.3.2 Model Validation Results

Model validation was based on three aspects which are the model physics, the validation of the model predictions against measured data from experimental unit or real plants and the model expectations. For more details about theses three aspects, refer to section 5.2.2. The validations were made against both steady state data and dynamic data of the plants in Tables 5.3 and 5.4.

5.3.2.1 Steady state model validation results

Comparison of the model predictions is made against field data for existing MSF-BC plants operating at high top brine temperature (see Table 5.3 – Plant B). The comparison was for steady state data, which includes variations in the flow rate, salinity, and temperature profiles of the brine stream across the stages. Results are shown in Figure 5.12. As shown, good agreement is obtained between model predictions and the plant data, especially for the brine flow rate and salinity, where the errors did not exceed 0.72% for both variables. On the other hand, the relative error in predicting the stage temperature is limited to a maximum of 1.19%.

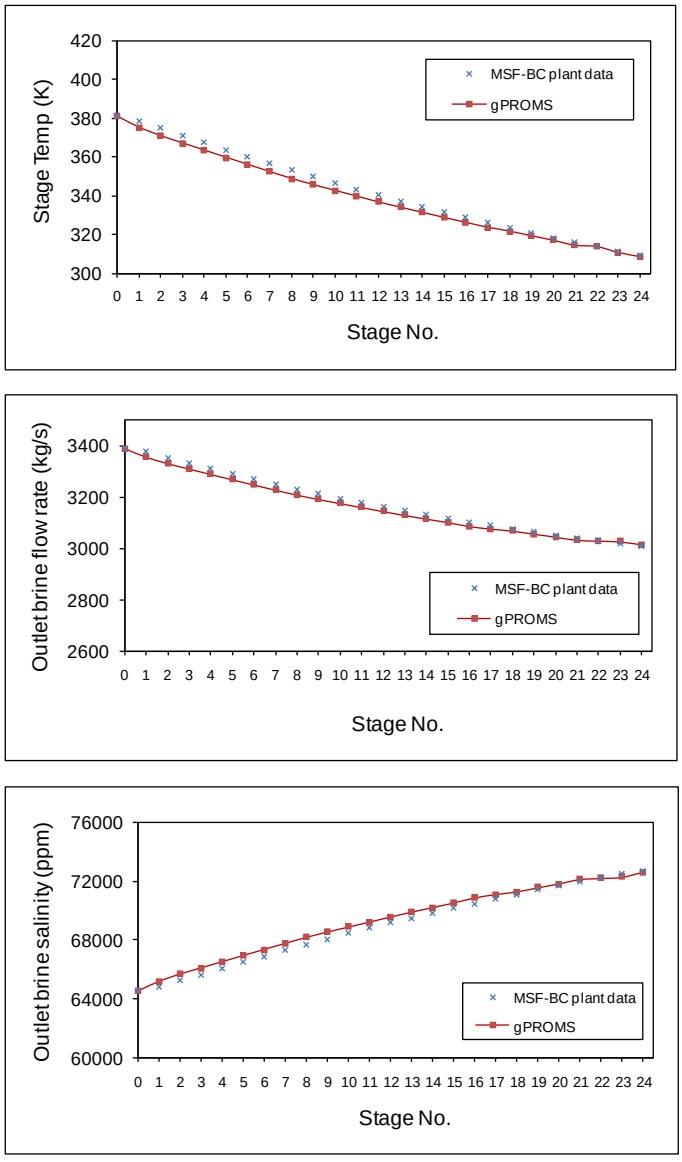

Figure 5.12 Comparison of gPROMS predictions and the field data from plant B for stage profiles of flow rate, salinity, and temperature of the brine stream.

5.3.2.2 Dynamic model validation results

Comparison of the model predictions is made against field data for existing MSF plant (see Table 5.4 – Plant C). In this plant, stages 1-14 are having a flash box and the rest have weir orifices. The comparison was made for data collected from daily operation, where small disturbances occur in operating parameters. These include the top brine temperature and intake seawater temperature. Summary of the plant operating parameters, which are made every three hours for a period of 24 hours, are shown in table 5.5. As shown, small disturbances are found in this data, which are caused by daily fluctuations in solar insolation and heating steam pressure. The solar insulation affects the intake seawater temperature and the heating steam pressure affects the top brine temperature.

Table 5.5: Disturbances occurring in MSF-BC plant (C) over a period of 8 hours

time	Top brine Temp	Intake seawater Temp.
hour	^{o}C	^{o}C
0	89.8	34.9
3	90.2	35.6
6	90.3	35.7
9	90.4	35.5
12	90	34.8
15	90	35.2
18	90	35
21	90.3	34.5
24	89.8	34.9

As shown in Figures 5.13-5.15, for the gPROMS predictions, immediately following each disturbance a jump occurs and then the disturbance is reduced. That is because the simulator calculates the values for each second. While for the real plant data, values are measured every 3 hours. This trend can be seen clearly in Figures 5.14-5.15 while for Figure 5.13, since the range is big (64600-65400 ppm) this trend is not clear. Comparison of model predictions and plant data include the flow rate, salinity, and temperature profiles of the brine stream across the stages. As shown in Figures 5.13-5.15, good agreement is obtained between model predictions and the

plant data for the stage outlet salinity, the brine flow rate and stage temperature where the errors did not exceed 0.6 %.

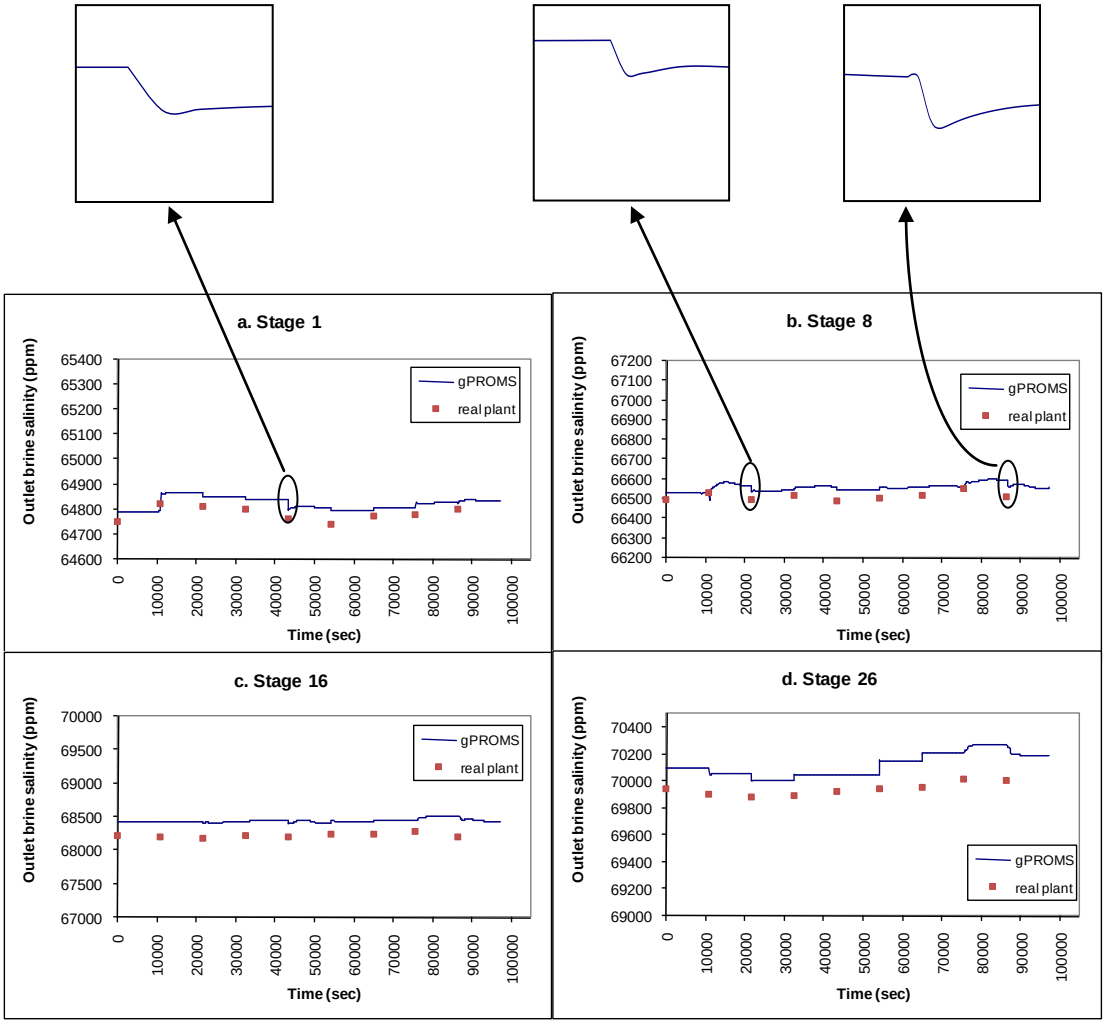

Figure 5.13 Comparison of gPROMS predictions and the field dynamic data from plant C for stage profiles of salinity of the brine stream.

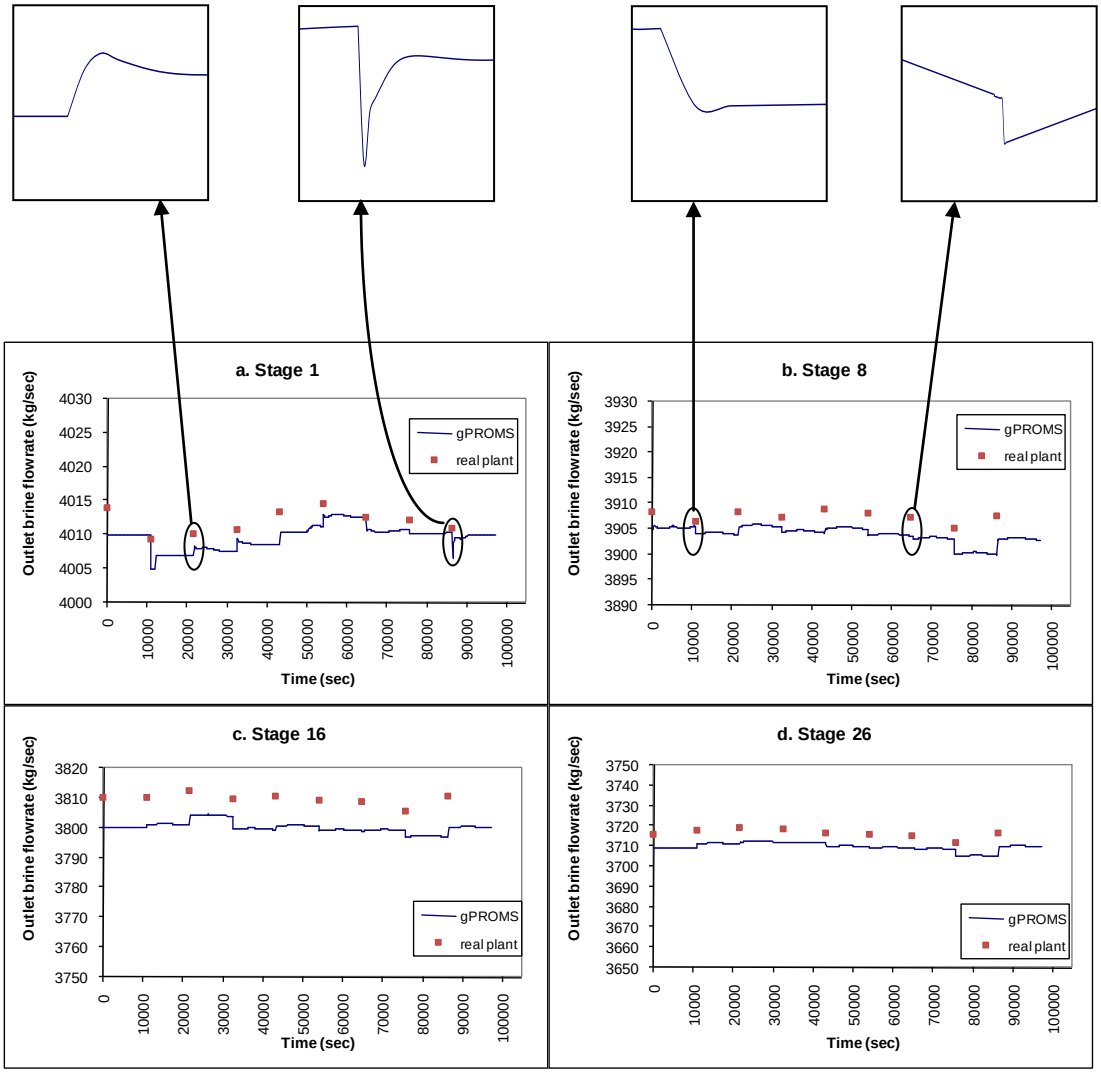

Figure 5.14 Comparison of gPROMS predictions and the field dynamic data from plant C for stage profiles of flowrate of the brine stream.

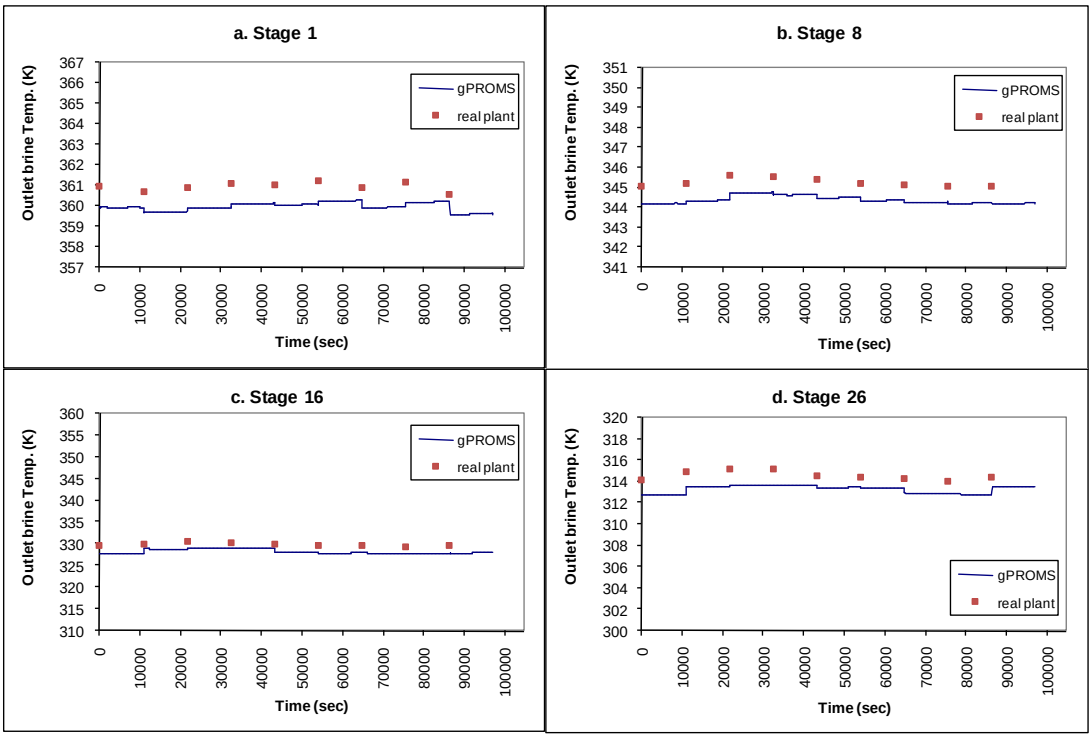

Figure 5.15 Comparison of gPROMS predictions and the field dynamic data from plant C for stage profiles of Temperature of the brine stream.

5.3.3 Dynamic Response Results

Dynamic simulation is performed for the plant parameters shown in table 5.3 for plant B in order to study the model response against changing some of the operating and design parameter and see how it agrees with the MSF-BC plant real behaviour. Figures 5.16-5.23 illustrate the system transients after increasing and decreasing the cooling seawater flow rate first by 5% and then by 10% and last by 15% (Alatiqi, Ettouney, El-Dessouky, & Al-Hajri, 2004). Before applying the disturbance the system was reset to the operating condition. Figures 5.24-5.31 illustrates the system transients after increasing the recycle brine flow rate first by 5% and then by 10% and last by 15% and decreasing it by 5% and then by 7 % (Alatiqi, Ettouney, El-Dessouky, & Al-Hajri, 2004). Again before applying the disturbance the system was reset to the operating condition. Figures 5.32-5.39 illustrates the system transients after increasing the steam temperature first by 1% and then by another 1%

and decreasing it by 1% and then by another 1 % and last other 1% (Alatiqi, Ettouney, El-Dessouky, & Al-Hajri, 2004). For the steam temperature disturbance, the system was not reset to the operating condition before applying the disturbance because it is impossible to change the steam temperature suddenly with big jumps.

Effect of increasing the cooling seawater flow rate on the brine level of selected stages is shown in Figure 5.16. As is shown, the increase in the outlet cooling seawater flow rate reduces the amount of makeup or feed seawater flow rate mixing with the brine in the brine pool of the last stage in the heat rejection section in order to provide the recycle brine flow rate (Alatiqi, Ettouney, El-Dessouky, & Al-Hajri, 2004). In turn, this reduces the brine level in all stages except last stage which is controlled. The reason behind this behaviour is that the brine level in the last stage is controlled as well as the recycle brine flow rate which is constant here. That in turn will cause a reduction in the brine level in the previous stages in order to keep the brine recycle flow rate constant. The opposite behaviour occurs when the cooling seawater flow rate is decreased as shown in Figure 5.17. Other effects of the cooling seawater flow rate on the stages condensate rate, the plant gain output ratio or total production rate are minimal as shown in Figures 5.18-5.23. The reason behind this behaviour is that as the amount of makeup or feed seawater reduces while the recycle flow rate is constant, more brine will be removed from the last stage to overcome the mass balance of the recycle stream (Equation 4.46).

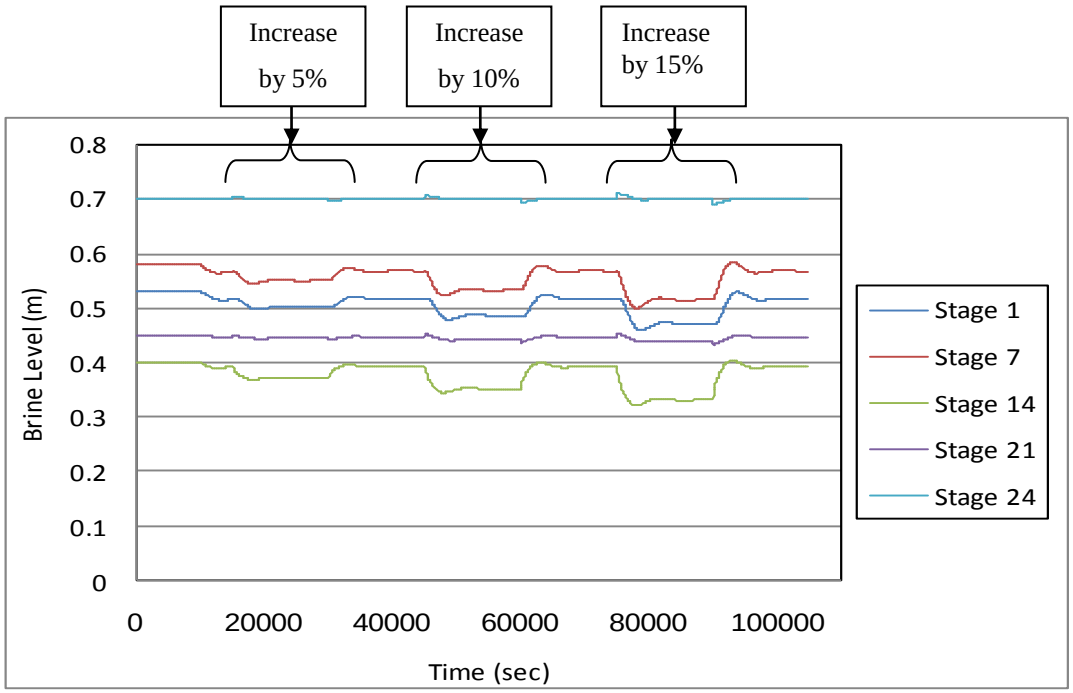

Figure 5.16 Simulation dynamics of the brine level in stages 1, 7, 14, 21and 24 for step increment in the cooling water flow rate.

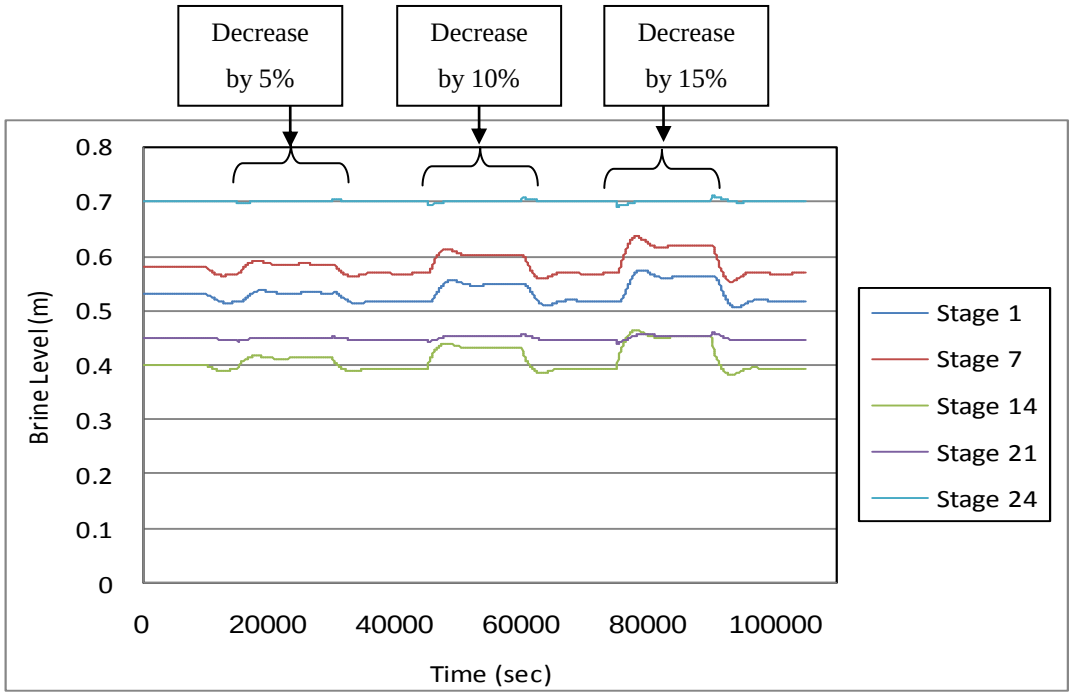

Figure 5.17 Simulation dynamics of the brine level in stages 1, 7, 14, 21and 24 for step reduction in the cooling water flow rate.

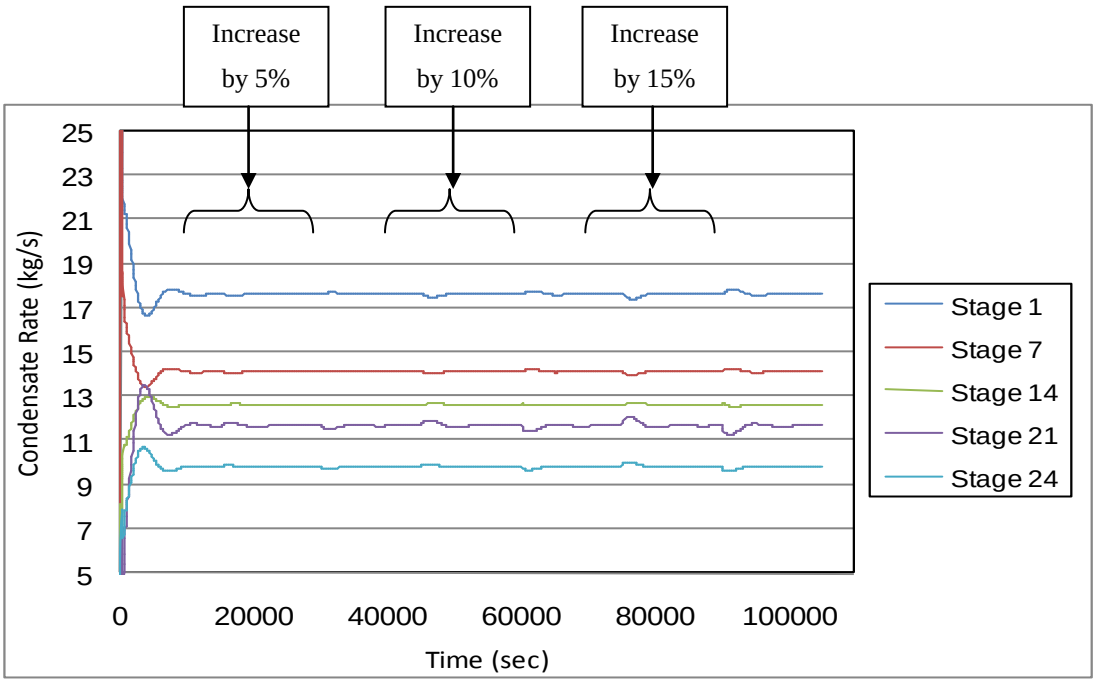

Figure 5.18 Simulation dynamics of the condensate rate in stages 1, 7, 14, 21and 24 for step increment in the cooling water flow rate.

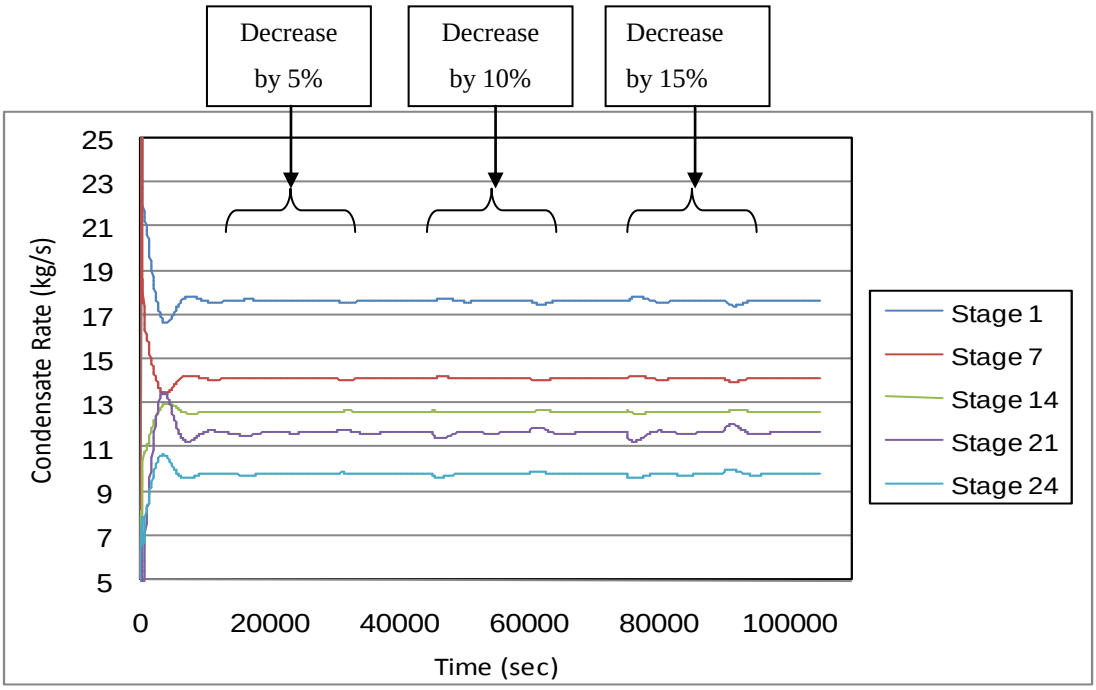

Figure 5.19 Simulation dynamics of the condensate rate in stages 1, 7, 14, 21and 24 for step reduction in the cooling water flow rate.

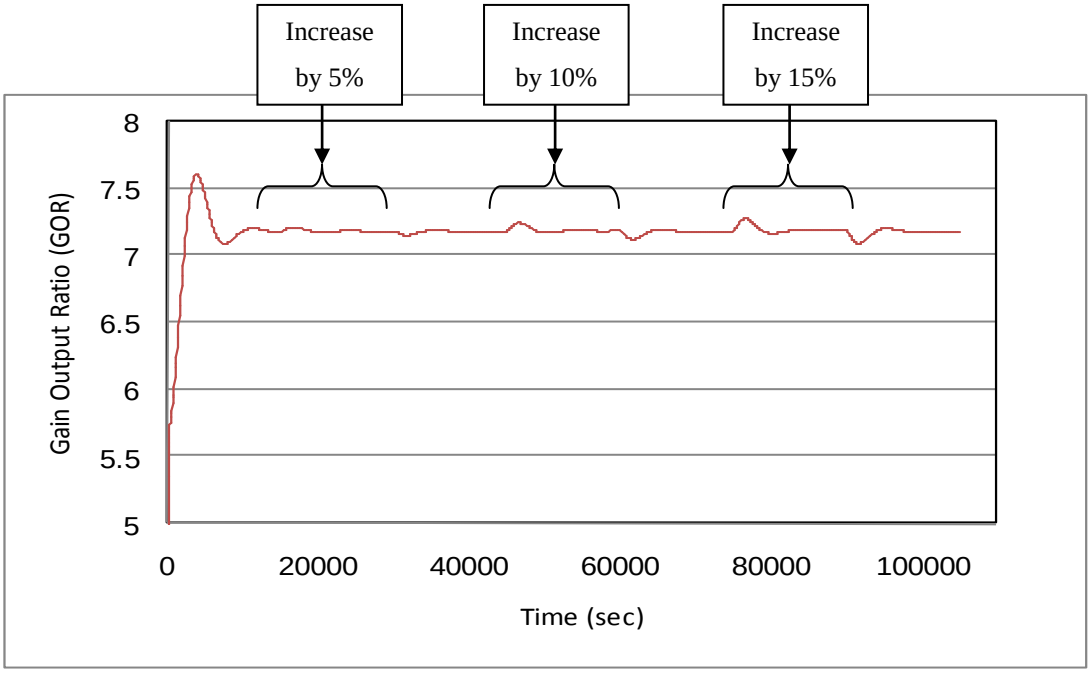

Figure 5.20 Simulation dynamics of the Gain Output Ratio (GOR) for step increment in the cooling water flow rate.

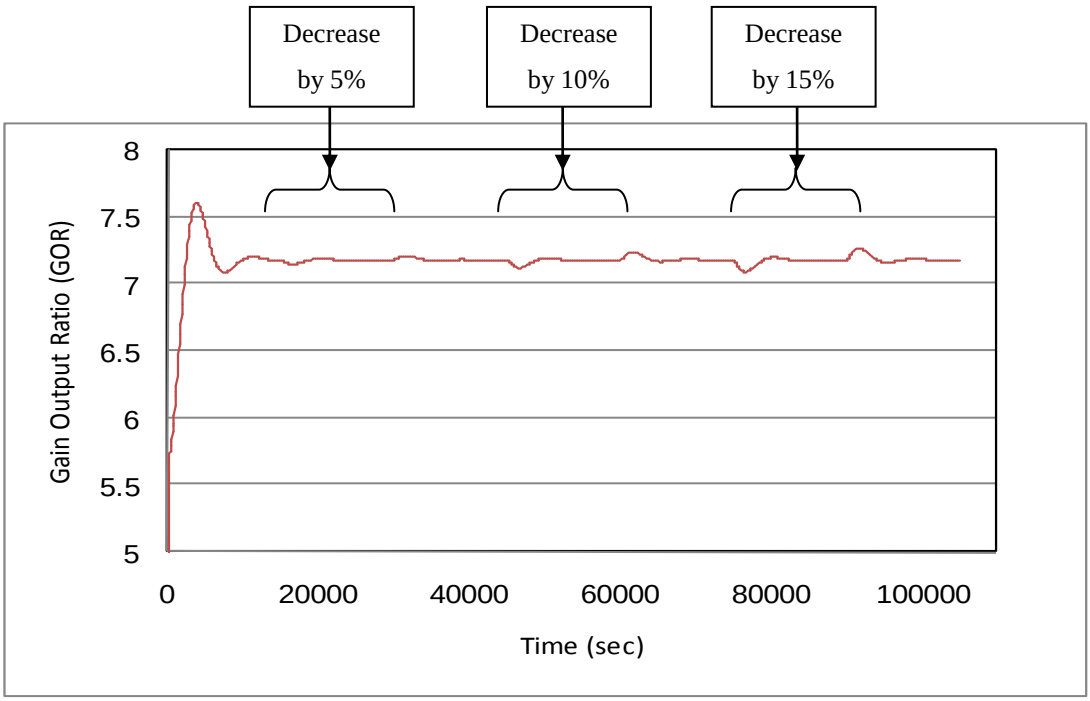

Figure 5.21 Simulation dynamics of the Gain Output Ratio (GOR) for step reduction in the cooling water flow rate.

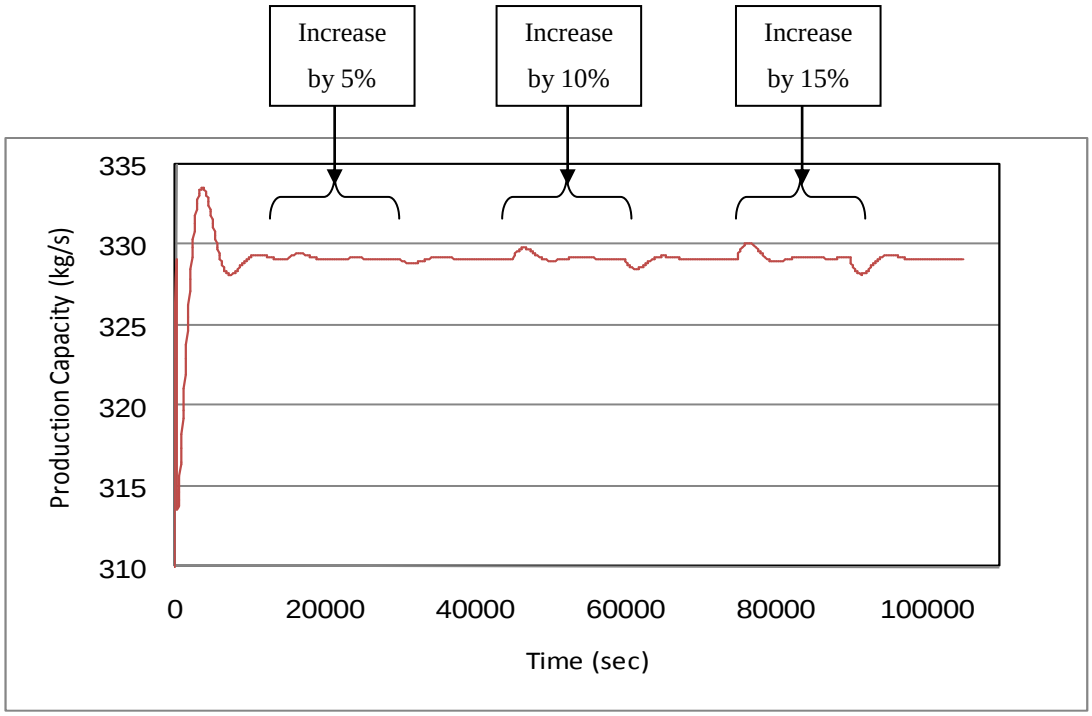

Figure 5.22 Simulation dynamics of the total production rate for step increment in the cooling water flow rate.

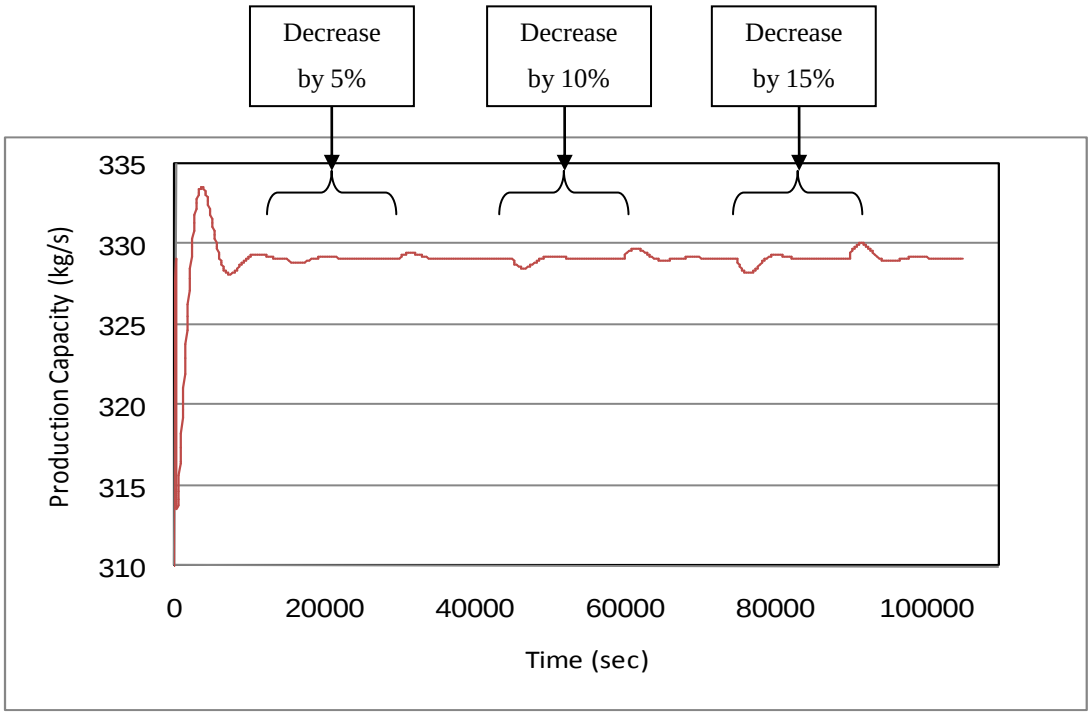

Figure 5.23 Simulation dynamics of the total production rate for step reduction in the cooling water flow rate.

Effect of increasing/decreasing the recycle brine flow rate on the brine level of selected stages is shown Figures 5.24-5.25. As is shown, the increase in the recycle brine flow rate increases the brine level in all stages except for the last stage which is controlled.

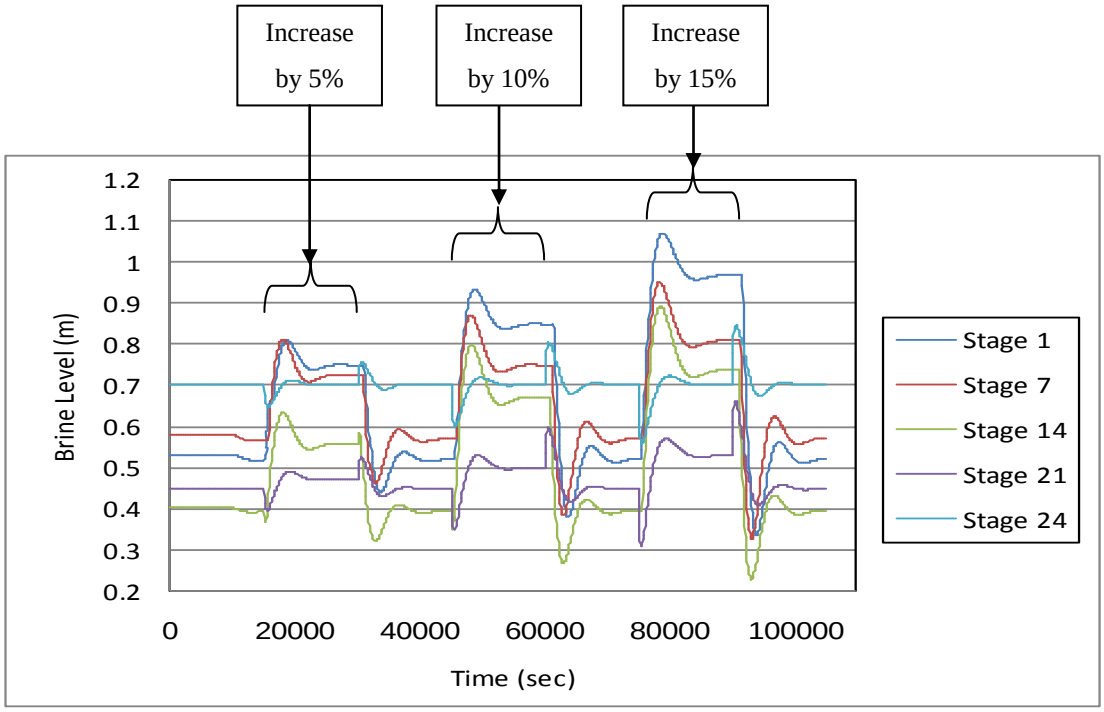

Figure 5.24 Simulation dynamics of the brine level in stages 1, 7, 14, 21and 24 for step increment in the recycle brine flow rate.

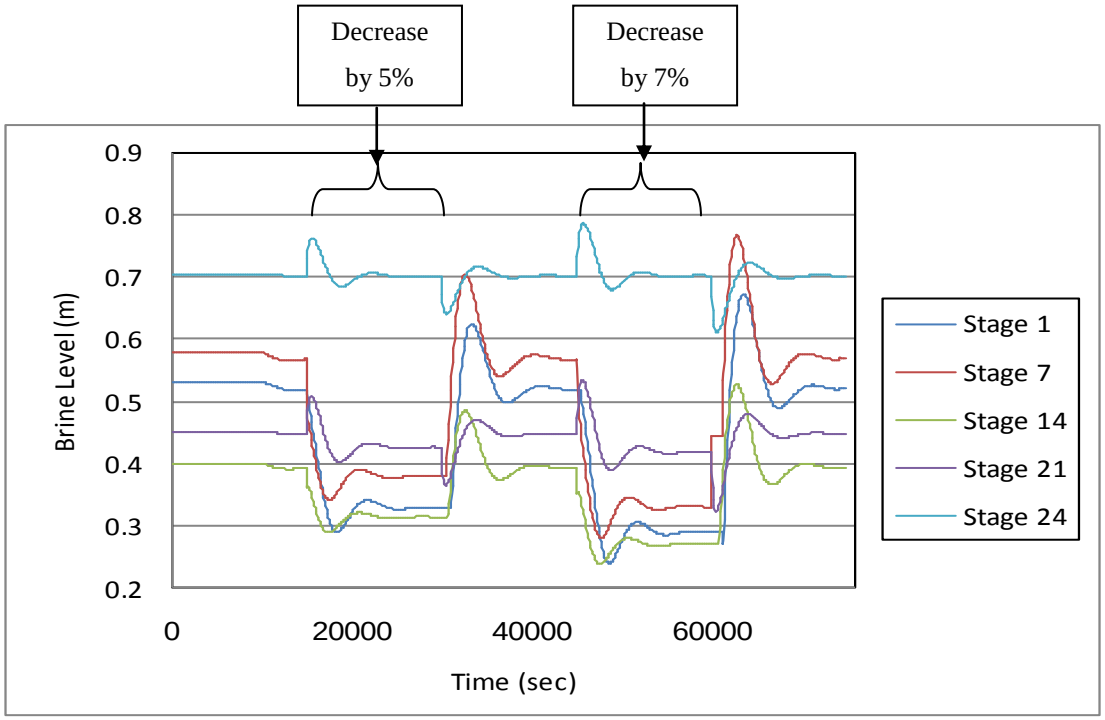

Figure 5.25 Simulation dynamics of the brine level in stages 1, 7, 14, 21 and 24 for step reduction in the recycle brine flow rate.

In addition, as shown in Figure 5.26 increasing the recycle brine flow rate increases the amount of condensate in each stage which caused by the fact that more feed is entering with the same input temperature so more vapour will flash off the brine and condensate in the flashing stages. That in turn will increase the plant total production (Figure 5.30) but will decrease the gain output ratio because more steam will be needed to heat the recycle brine flow rate to the same top brine temperature (Figure 5.28). The opposite behaviour occurs when the recycle brine flow rate is decreased (Figures 5.27, 5.29, 5.31). It was not possible to reduce the flow rate of the brine recycle below 7%. This is because the brine level in the flashing stages was less than the gate height of the stages which in turn causes the vapour blow through condition (vapour escape from one stage to the next) to occur and that will disrupt the flashing process and the simulator stops calculations.

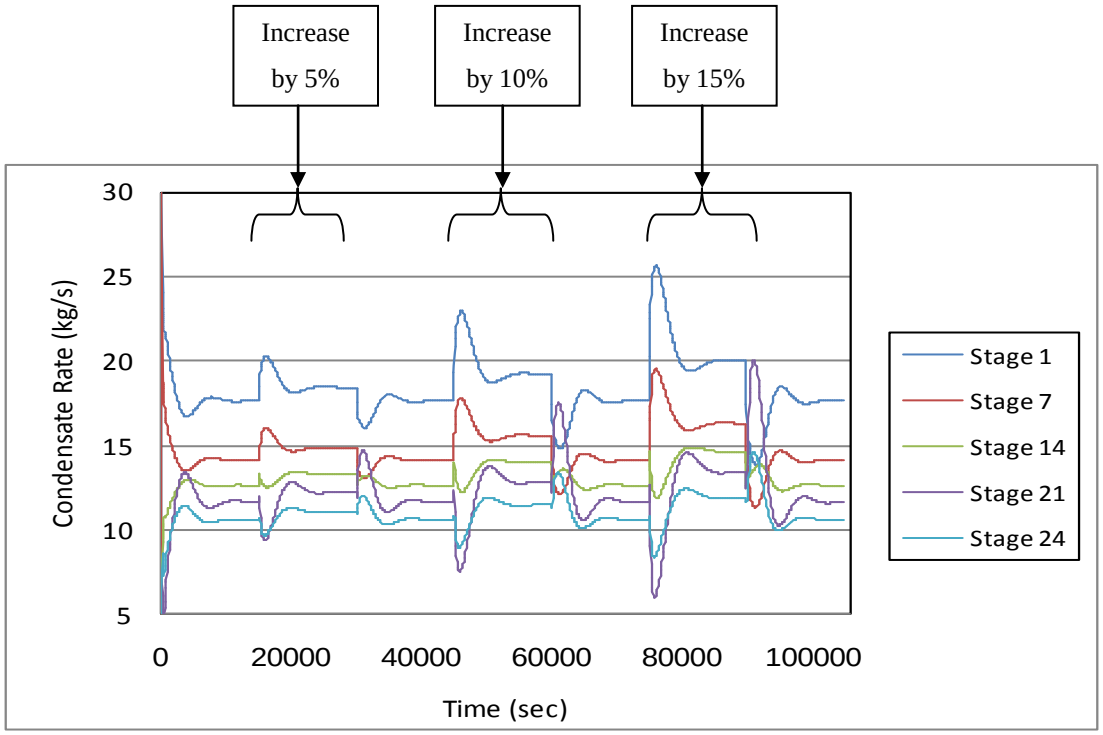

Figure 5.26 Simulation dynamics of the condensate rate in stages 1, 7, 14, 21and 24 for step increment in the recycle brine flow rate.

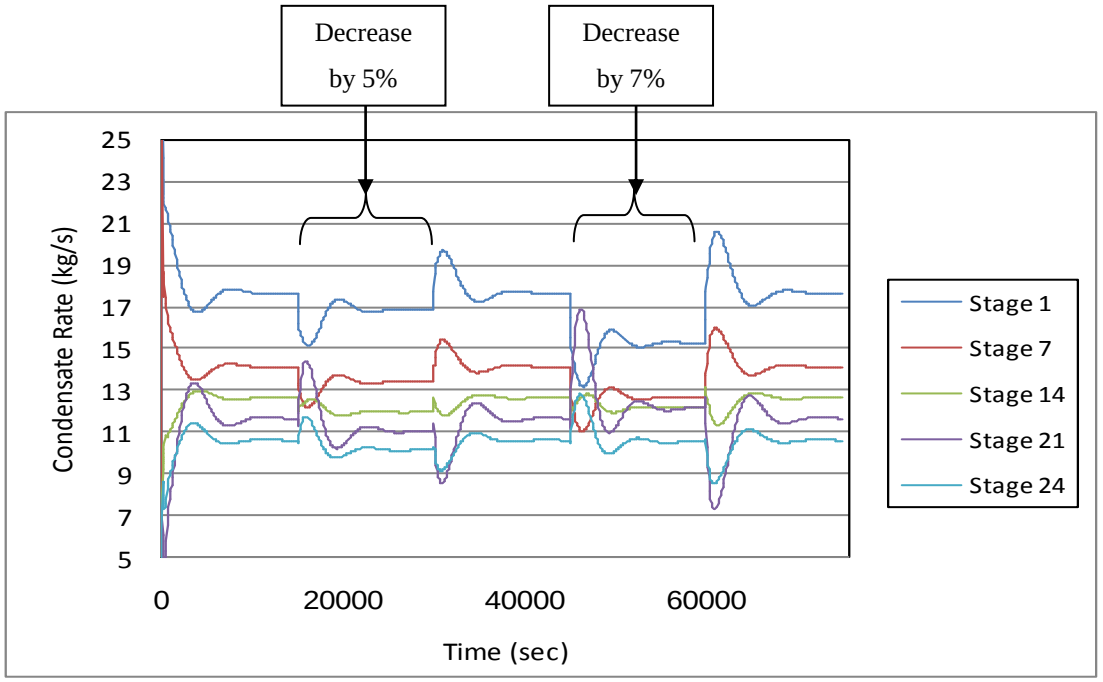

Figure 5.27 Simulation dynamics of the condensate rate in stages 1, 7, 14, 21and 24 for step reduction in the recycle brine flow rate.

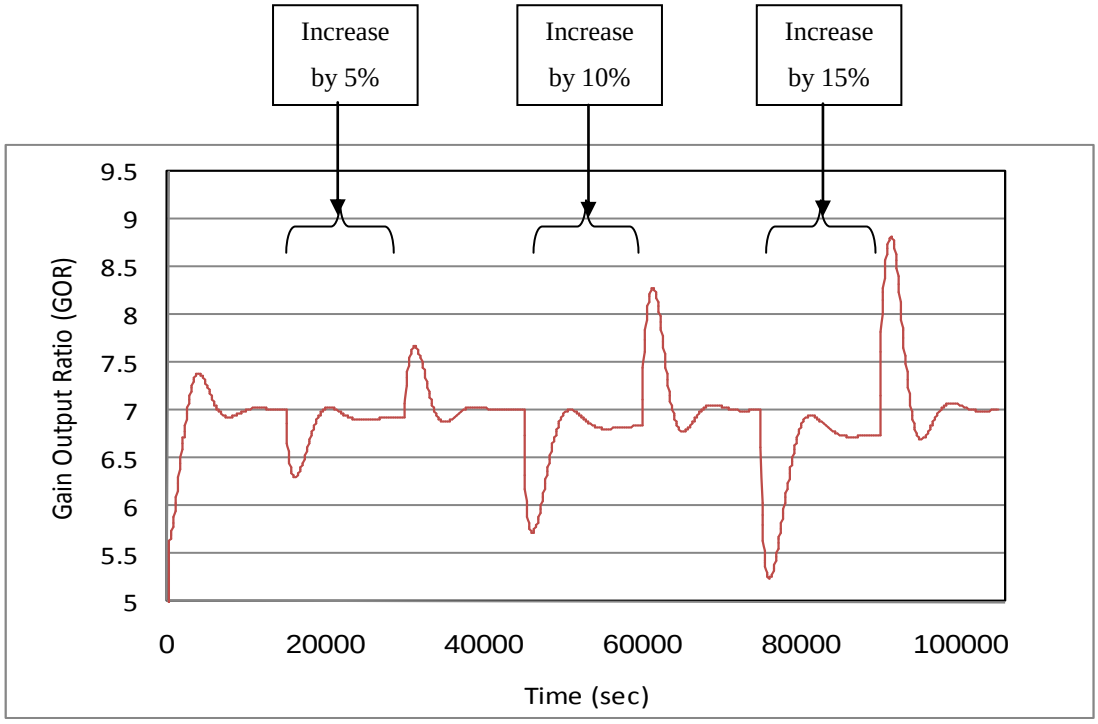

Figure 5.28 Simulation dynamics of the Gain Output Ratio (GOR) for step increment in the recycle brine flow rate.

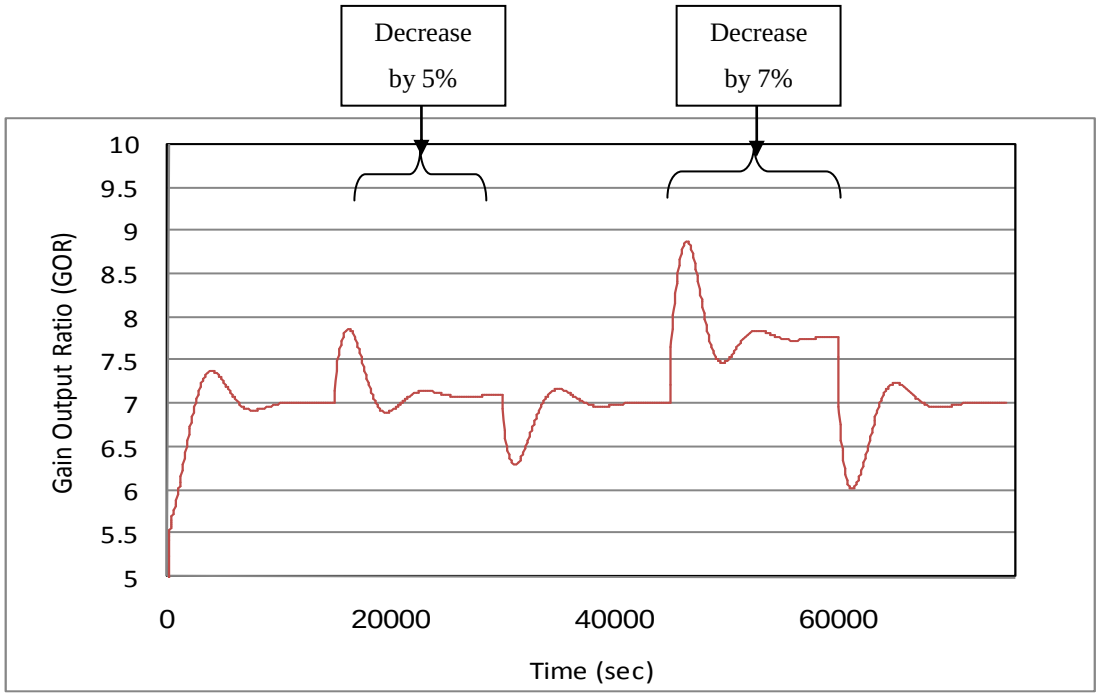

Figure 5.29 Simulation dynamics of the Gain Output Ratio (GOR) for step reduction in the recycle brine flow rate.

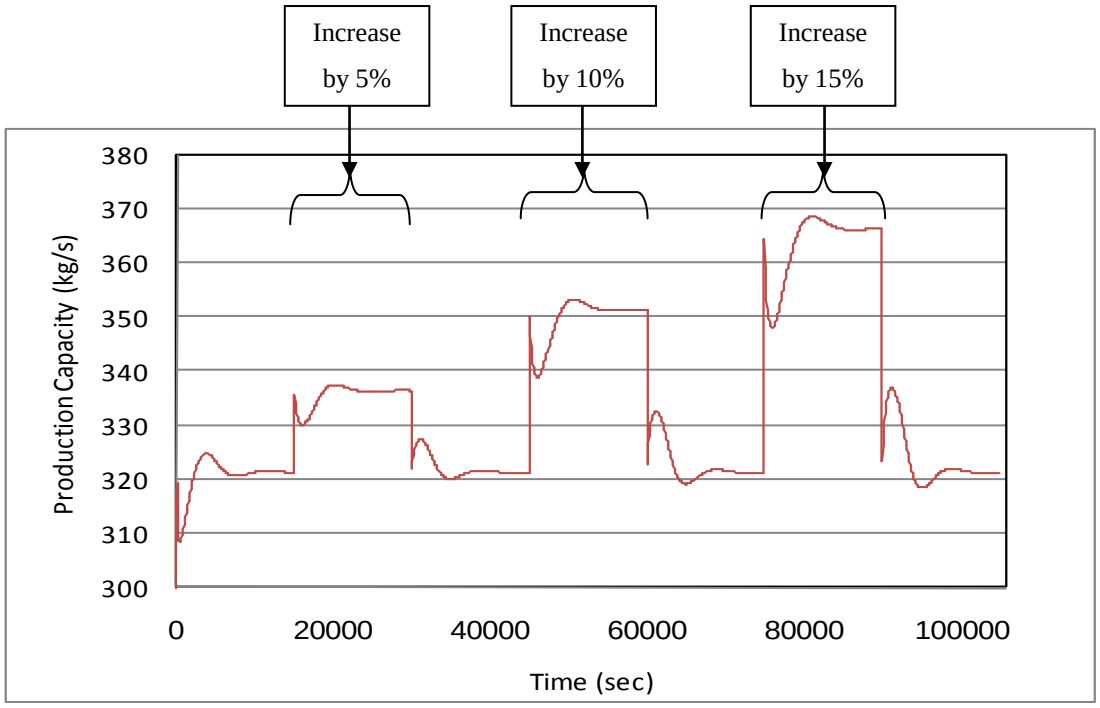

Figure 5.30 Simulation dynamics of the total production rate for step increment in the recycle brine flow rate.

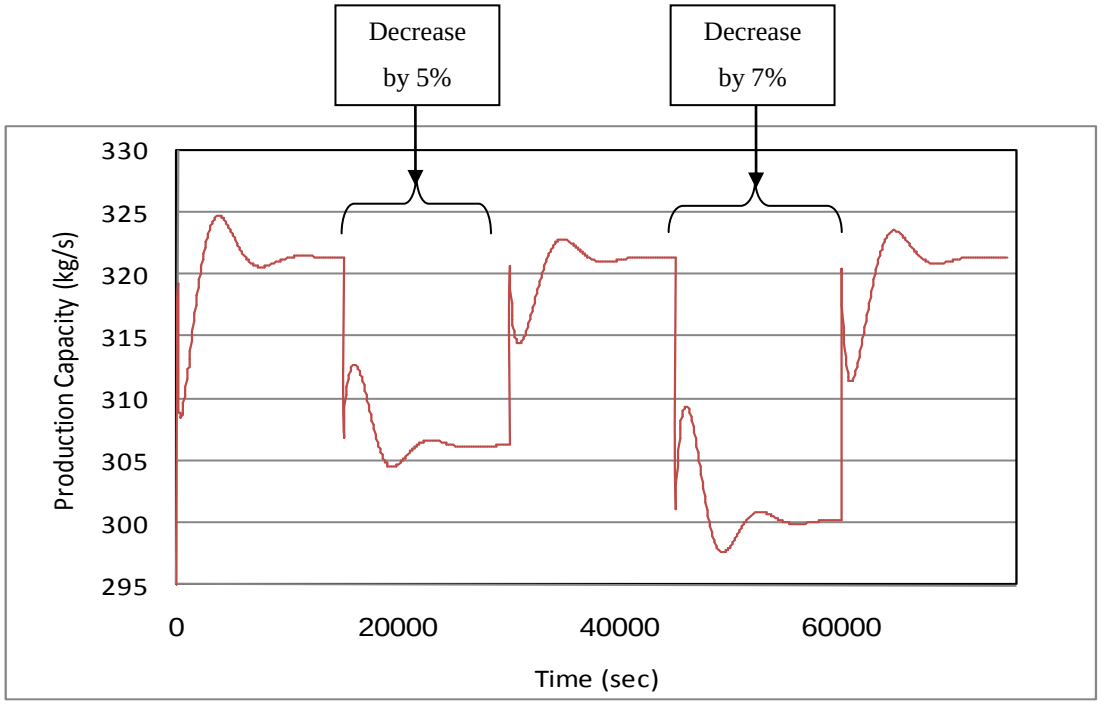

Figure 5.31 Simulation dynamics of the total production rate for step reduction in the recycle brine flow rate.

Effect of increasing/decreasing the steam temperature on the brine level of selected stages is shown Figures 5.32-5.33. As is shown, the increase in the steam temperature decreases the brine level in all the stages except for the last stage which is controlled. In addition, as shown in Figures 5.34-5.35, increasing the steam temperature increases the amount of condensate in each stage. That in turn will increase the plant total production (Figure 5.38-5.39) but will decrease the gain output ration because more steam will be needed to heat the recycle brine (Figure 5.36-2.37). The reason behind these behaviours is that as the steam temperature increases the top brine temperature increases. That will result in increasing the flashing rate in all stages which will form more vapour and reduce the brine level in all stages, except the last. Increasing the flashing rate will form more condensate and that results in an increase in the plant total production. On the other hand increasing the steam temperature will decrease its latent heat and more steam will be needed to heat the recycle brine to the desired top brine temperature and as a result the GOR will decrease.

The increase in the steam temperature was limited to 2% of the design value. That is because the brine level in the flashing stages was less than the gate height, which in turn causes the vapour blown through condition to occur and that will stop the flashing process and the simulator. Also, it was not possible to reduce the steam temperature by more than 3% because the brine level will increase until it fills the entire vapour space below the demister, which is not feasible during operation.

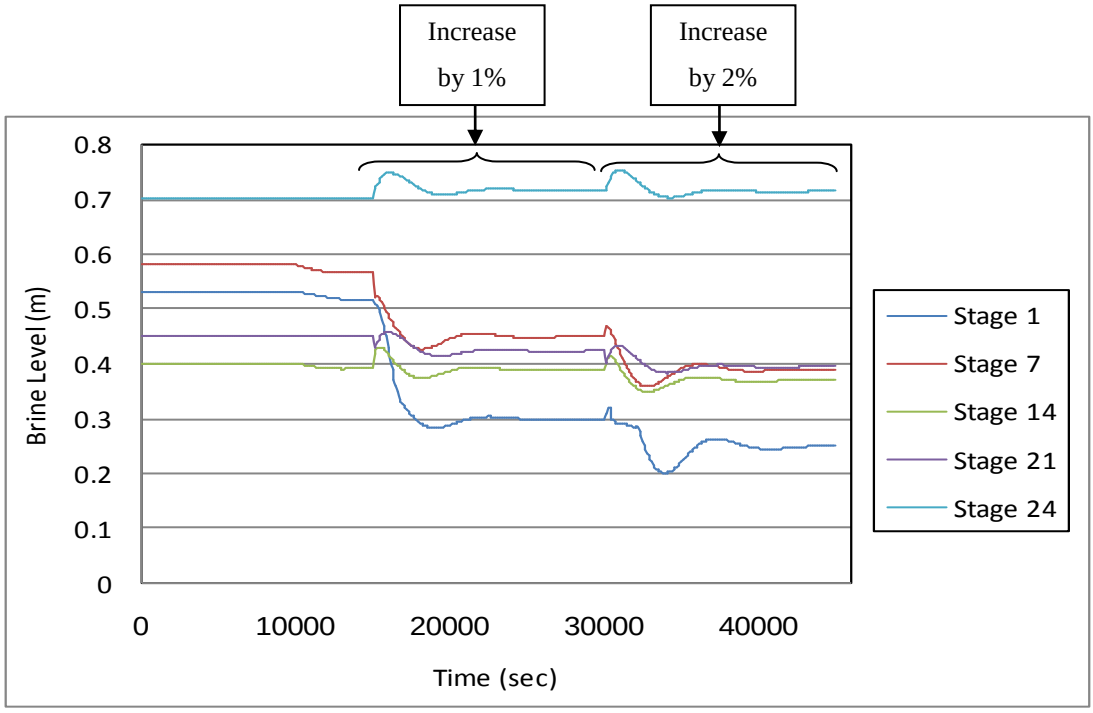

Figure 5.32 Simulation dynamics of the brine level in stages 1, 7, 14, 21and 24 for step increment in the steam temperature.

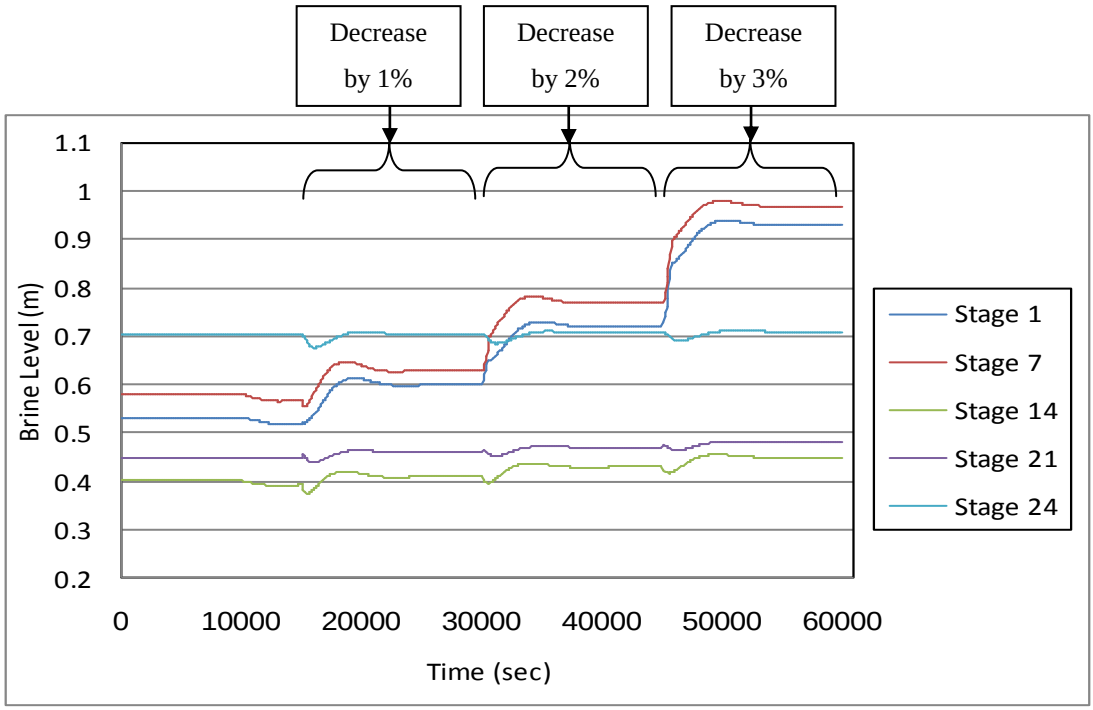

Figure 5.33 Simulation dynamics of the brine level in stages 1, 7, 14, 21and 24 for step reduction in the steam temperature.

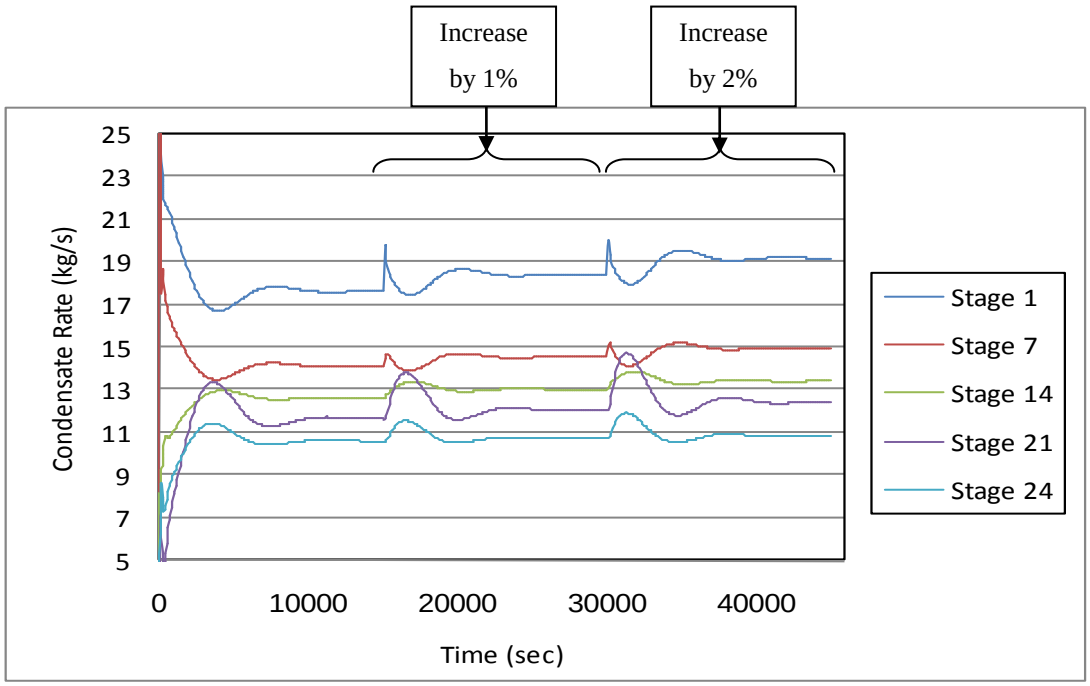

Figure 5.34 Simulation dynamics of the condensate rate in stages 1, 7, 14, 21and 24 for step increment in the steam temperature.

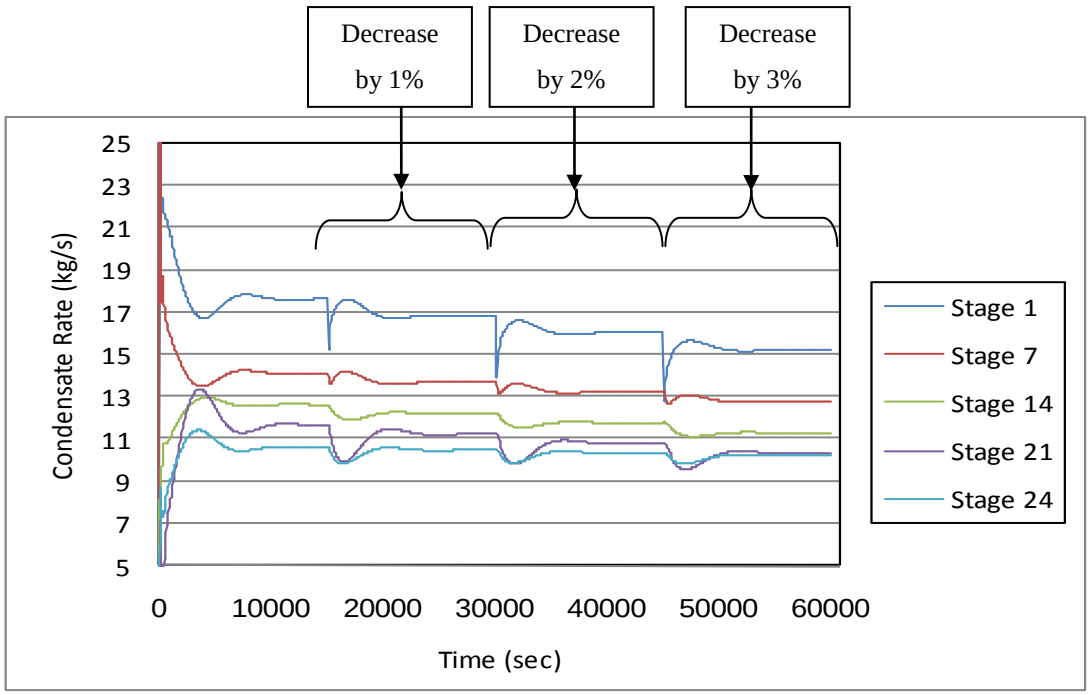

Figure 5.35 Simulation dynamics of the condensate rate in stages 1, 7, 14, 21and 24 for step reduction in the steam temperature.

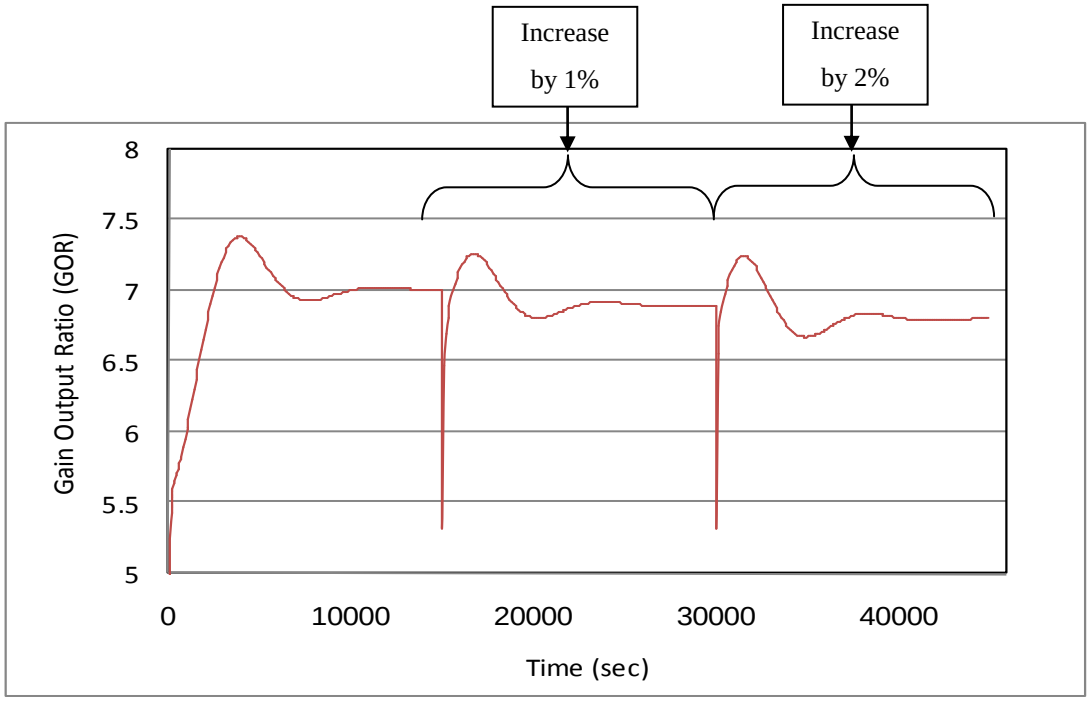

Figure 5.36 Simulation dynamics of the Gain Output Ratio (GOR) for step increment in the steam temperature.

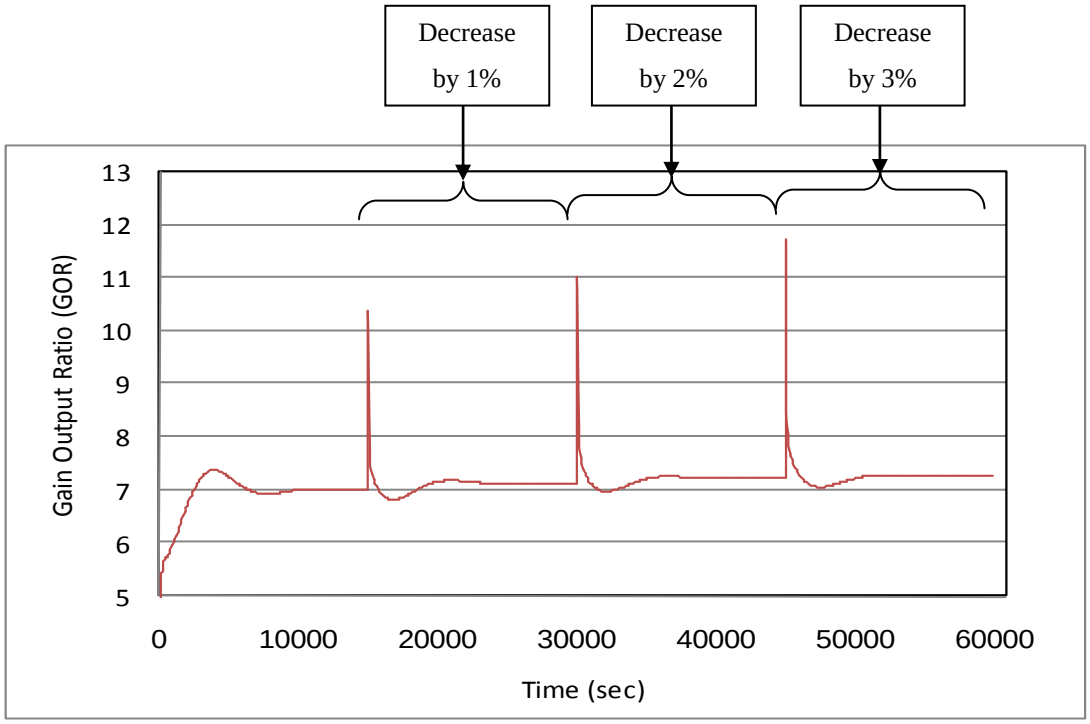

Figure 5.37 Simulation dynamics of the Gain Output Ratio (GOR) for step reduction in the steam temperature.

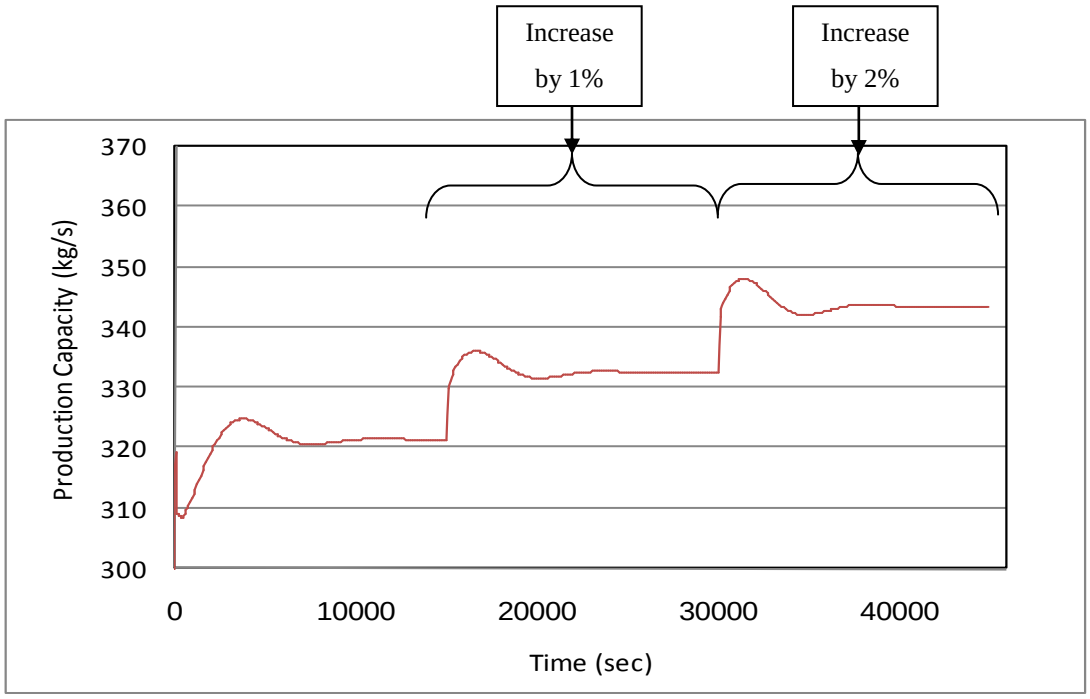

Figure 5.38 Simulation dynamics of the total production rate for step increment in the steam temperature.

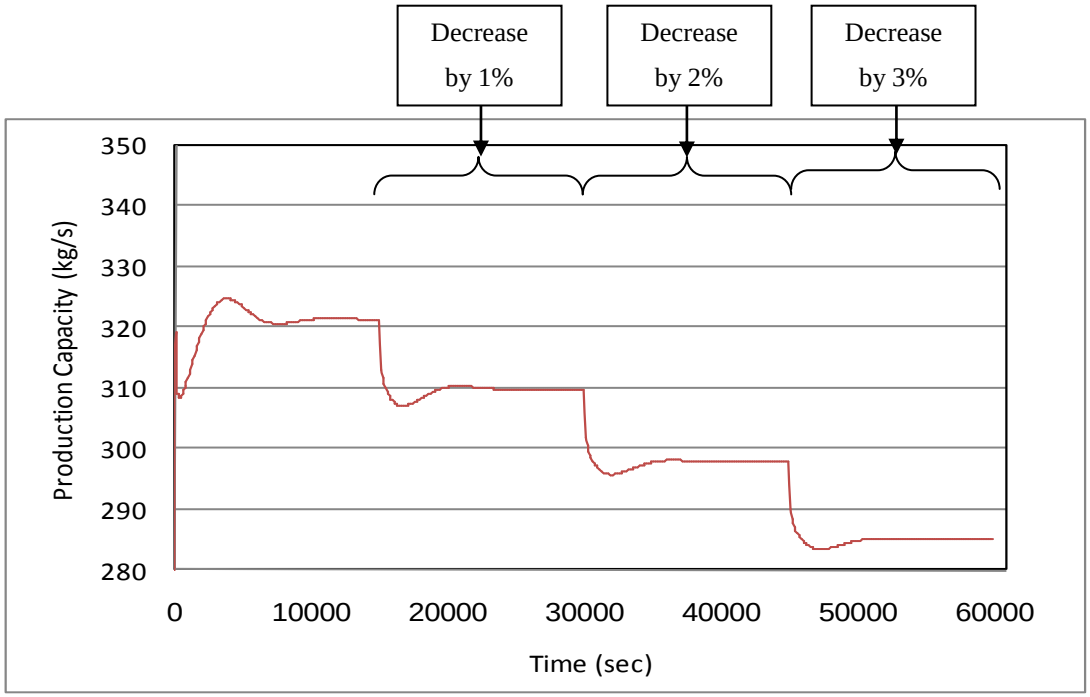

Figure 5.39 Simulation dynamics of the total production rate for step reduction in the steam temperature.

5.3.4 Effect of Demister losses on heat transfer area of the condenser tubes

The pressure drop across the demister causes the temperature to drop in the vapour passing through it. In this section, gPROMS is used to determine the variations in the required heat transfer area in MSF with/without the use a demister. As shown in tables 5.6 and 5.7, the demister causes a temperature drop in the vapour temperature, which ranges between 0.02-0.76 ^{o}C. Irrespective of this small change in the vapour temperature, a large decrease occurs in the heat transfer driving force in the condensing tube region. As a result an increase in the required heat transfer area occurs. On the other hand if the demister temperature drop was as small as possible that may reduce the required heat transfer area by almost 19-26 %. Since 70% of the plant capital cost is for the tubes so that will lead to a great decrease in the plant capital cost (Al-Zubaidi, 1987).

Table 5.6: Comparison of predicted heat transfer areas with and without the demister effect for high temperature operation unit

Stage	Tvapour below demister	Tvapour above demister	ΔT demister	Heat transfer area with demister effect	Heat transfer area without demister effect	% reduction in area
	˚C	˚C	˚C	m²	m²	
1	105.13	105.11	0.02	8277.08	8213.35	0.78
2	102.53	102.51	0.02	6480.35	6440.78	0.61
3	99.67	99.65	0.02	5843.70	5806.78	0.64
4	96.92	96.90	0.02	5211.63	5177.89	0.65
5	93.78	93.75	0.03	5238.22	5197.52	0.78
6	90.43	90.39	0.04	5627.19	5562.92	1.16
7	87.53	87.49	0.04	5349.36	5293.18	1.06
8	84.28	84.23	0.05	5662.92	5582.24	1.45
9	81.20	81.14	0.06	5757.80	5655.70	1.81
10	78.15	78.08	0.07	5842.92	5719.49	2.16
11	76.13	76.05	0.08	4571.87	4491.88	1.78
12	71.37	71.27	0.10	7816.49	7518.27	3.97
13	68.93	68.82	0.11	6532.15	6306.89	3.57
14	65.42	65.29	0.13	8194.23	7776.18	5.38
15	62.92	62.76	0.16	7108.08	6721.29	5.75
16	59.77	59.59	0.18	7959.37	7420.41	7.26
17	57.62	57.39	0.23	6300.76	5887.14	7.03
18	54.10	53.81	0.29	8319.23	7402.19	12.39
19	51.30	50.93	0.37	8602.75	7392.72	16.37
20	48.72	48.28	0.44	8142.93	6874.47	18.45
21	46.43	45.98	0.45	6821.50	5915.25	15.32
22	44.31	43.83	0.48	3776.14	3325.51	13.55
23	42.33	41.81	0.52	3150.55	2809.86	12.12
24	39.64	38.88	0.76	3331.74	2803.51	18.84

Table 5.7: Comparison of predicted heat transfer areas with and without the demister effect for low temperature operation unit

Stage	Tvapour below demister	Tvapour above demister	ΔT demister	Heat transfer area with demister effect	Heat transfer area without demister effect	% reduction in area
	˚C	˚C	˚C	m²	m²	
1	87.10	87.06	0.04	10267.62	10051.03	2.15
2	85.60	85.57	0.03	6570.77	6488.54	1.27
3	83.57	83.52	0.05	5708.51	5616.40	1.64
4	81.17	81.11	0.06	5681.62	5575.30	1.91
5	78.87	78.81	0.06	5523.68	5413.27	2.04
6	76.40	76.32	0.08	5795.05	5632.01	2.89
7	74.27	74.19	0.08	5424.97	5277.35	2.80
8	71.97	71.87	0.10	5491.49	5303.31	3.55
9	69.83	69.72	0.11	5307.89	5111.05	3.85
10	67.53	67.41	0.12	5486.94	5260.24	4.31
11	65.50	65.36	0.14	5240.00	5008.32	4.63
12	62.40	62.25	0.15	7847.57	7268.54	7.97
13	60.33	60.13	0.20	7841.38	7110.09	10.29
14	58.67	58.51	0.16	6354.78	5972.13	6.41
15	56.67	56.45	0.22	6387.34	5881.96	8.59
16	54.53	54.29	0.24	6762.97	6170.28	9.61
17	52.53	52.21	0.32	7024.36	6224.10	12.86
18	50.17	49.81	0.36	8561.52	7286.17	17.50
19	48.00	47.59	0.41	9934.33	8074.75	23.03
20	46.17	45.75	0.42	9491.60	7829.45	21.23
21	44.77	44.40	0.37	7528.83	6620.04	13.73
22	43.30	42.82	0.48	4021.83	3481.36	15.52
23	41.60	41.15	0.45	3874.30	3423.86	13.16
24	39.40	38.68	0.72	4892.77	3886.22	25.90

5.4 Conclusion

The models for both MSF-OT and MSF-BC processes were validated in steady state and dynamic operation against several sets of data obtained from large MSF plants. The validation results showed good agreement between measured and predicted data. This shows that the model developed and analyzed in this thesis is general and well suited for simulation of any MSF plant. It should be stressed that the measured dynamic data shown in this chapter was obtained during normal plant operation that may include variation in more than one operating parameter at a time. More proper dynamic data should involve variation in one operating parameter at time. However, this is almost impossible to acquire because of strict plant management and regulations (Al-Deffeeri, 2009).

The system dynamic response is predicted upon imposing disturbances in major operating conditions. This was done to study the plant behaviour and to determine the time required to reach new steady state condition. This model will also be useful when the details of flashing stage are studied.

Dynamic analysis was made to study plant performance upon making step variations in system manipulated variables and identify stable operating regimes. New stable operating regimes were reached upon changing the cooling water flow rate by $\pm$ 15% and increasing the recycle brine flow rate by 15% and decreasing it by 7%. This was not the case for the steam temperature where its variation was limited to $\pm$ 2-3 %. This behavior is consistent with the actual plant data and real operation in the plants.

At the end of this chapter, strong effect of the pressure/temperature drop within the stage demister on the heat transfer area in each stage is presented. Results show variations between 19-26% in the heat transfer area upon including the demister effects. This motivated the demister CFD modeling and analysis included in the next chapter. This includes designing and modeling a new demister with minimum pressure drop and unaffected droplets removal efficiency as will be shown in the next chapter.

Chapter 6
CFD Modeling of the Demister

6.1 Introduction

Removal of liquid droplets entrained in vapour or gas is essential in order to prevent equipment failure, product contamination or environmental pollution. Demisters are used in distillation, fractionation, gas scrubbing, evaporative cooling, evaporation, boiling, and trickle filters. Removal of mist droplets is desirable or even mandatory for different reasons, which includes ((Galletti, Brunazzi, & Tognotti, 2008), (Holmes & Chen, 1984), (Fabian, Van Dessel, Hennessey, & Neuman, 1993a)):

- Recovery of valuable products
- Improving emission control
- Protection of downstream equipment
- Improving product purity

There are several configurations used for demisting gases or vapours such as settling tanks, filters, cyclones, electrostatic precipitators, baffles/vanes, fibre filtering candles and wire mesh demisters. Each of these devices operates under different principles (McCabe, Smith, & Harriott, 2000). Selection among previous devices is controlled by the droplet/mist size, flow rate and temperature (Ettouney, 2005).

In multistage flash desalination, the flashed off fresh water vapour from large brine pools entrains brine in the form of fine mist droplets. The brine droplets must be removed before vapour condensation over the condenser tubes. If the demister does not operate efficiently, the entrained brine droplets will reduce the quality of the distilled water and will form salt scale on the outer surface of the condenser tubes. The first effect results in disposal of the distillate product because of limits imposed by the end user, especially if the product water is used as a makeup for boilers.

Scaling of the condenser tube reduces the heat transfer coefficient and enhances corrosion.

In the early days of evaporators, especially in the thermal desalination plants, solid vane type separators were used. The system suffers from the following drawbacks (El-Dessouky, Alatiqi, Ettouney, & Al-Deffeeri, 2000): (1) high pressure drop (which could result in the total loss of temperature driving force between stages) and (2) excessive brine carry over. In the late 1950's wire mesh mist eliminators were introduced to the desalination industry (Al-Zubaidi, 1987) because of their advantages such as: (1) low pressure drop (2) high separation efficiency (3) high capacity (4) low capital cost (5) minimum tendency for flooding and (6) small size. The demister consists of mats made up of many layers of wire mesh (is a simple porous blanket of metal wire that retains liquid droplets entrained by the water vapour), each staggered relative to the next. These mats are placed horizontally facing the stream of vertically rising vapour. As the vapour rises, the droplets collect on the mesh wires, merge into larger drops and drip from the bottom layer. The function of the wire mesh is to increase brine droplet sizes to a point where they are too large to be entrained by the rising vapour. Separators of this design present very little resistance to vapour flow and enable production of distillate with very low salinity, usually between 0 and 5 ppm (Al-Deffeeri, 2009)

The performance of wire mesh mist eliminators (Figure 6.1-6.2) depends on many design variables such as support grids, vapour velocity, wire diameter, packing density, pad thickness, and material of construction. Because the wire-mesh is not rigid, it must be supported on suitable grids. To obtain minimum pressure drop, maximum throughput, and maximum efficiency, the support grids must have a high percentage of free passage. To take full advantage of the 98% or so free volume in the wire-mesh, the free passage through the support grids should be greater than 90% of support grid area. If the free passage through the support grids is much below 90% of its area, the accumulated liquid is prevented from draining back through the support grids, causing premature flooding (Fabian, Van Dessel, Hennessey, & Neuman, 1993a).

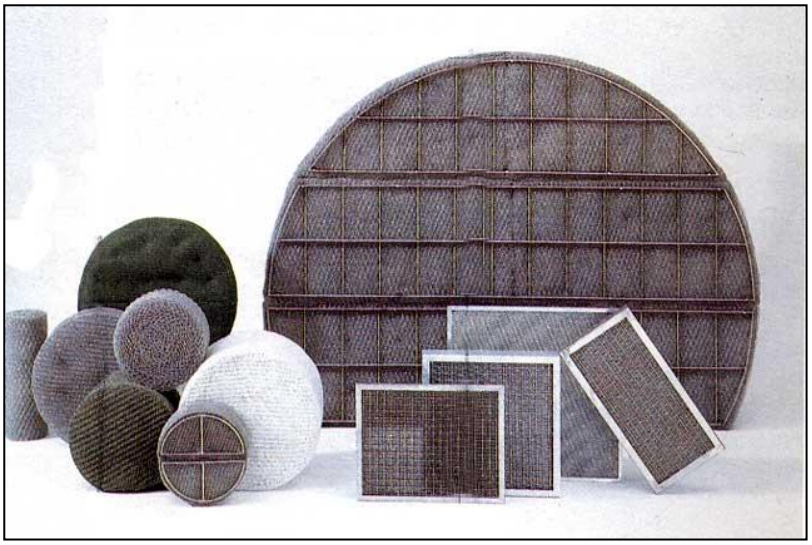

Figure 6.1 Wire mesh demister.

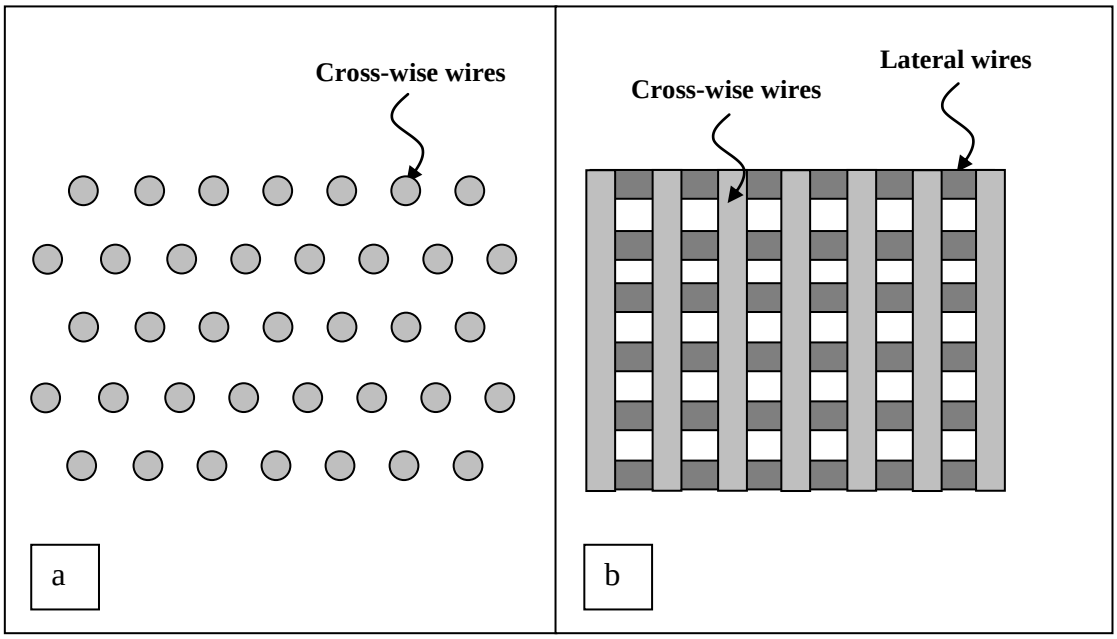

Figure 6.2 wire mesh demister (a) side view (b) top view.

Typically, maximum allowable velocity for a mist eliminator is limited by the ability of the collected liquid to drain from the unit. In the vertical up flow mesh demister, when the gas velocity increases past design levels, liquid begins to accumulate in the bottom of the unit. The liquid build-up results in re-entrainment of the brine droplets in the vapour stream. This is because the inertia of the incoming gas prevents the liquid from draining out of the unit. In horizontal units, the gas inertia

pushes the captured liquid toward the downstream face (Holmes & Chen, 1984). As a rule, smaller diameter wire targets collect smaller liquid droplets more efficiently. For example, a 10 μm wire removes smaller droplets than a 200 μm wire. However, a bed of 10 μm wires normally has the tendency to flood and re-entrain at much lower gas velocities than a bed of 200 μm wire. This is because the thinner wires provide dense packing that can trap the liquid by capillary action between the wires (Fabian, Van Dessel, Hennessey, & Neuman, 1993b). Interweaving of small diameter wires with larger diameter wire has been used often to tackle some of the most difficult mist removal problems. This design uses the metallic or plastic wires as a support structure to hold the fine wires apart. Even with this approach, the throughput capacity of the unit is limited, compared to that possible with conventional mesh. Special internal mesh geometry modifications are now available that allow these bi-component (that is, small-fiber and large-diameter wire mesh) configurations to operate at velocities essentially the same as conventional mesh designs. These ultra-high-efficiency designs can be substituted for conventional mesh and used, for example, in the dehydration towers of natural gas production plants, where even small losses of absorption chemicals, such as ethylene glycol, can be a significant operating expense (Lerner, 1986).

Construction materials for the wires include metal, fibre glass, plastics or polymers such as polypropylene or Teflon. Recently, three new alloys have been made available in wire form, which routinely provide three to five times the service lives of the traditional materials. They can offer improved service depending on the temperature and acid concentration of the gas stream (Fabian, Van Dessel, Hennessey, & Neuman, 1993a).

The main objective of this chapter is to use CFD software to model and design MSF demisters with maximum efficiency for removal of water droplets and minimum pressure drop, i.e., minimum temperature drop. This work is motivated by the strong effect of the demister performance on the capital and operating costs of the plant. The demister performance has strong effect on the total heat transfer area in the plant (see tables 5.6-5.7), which is strongly related to the plant capital cost (Al-Zubaidi, 1987). Also, the demister performance affects the product quality, which is strongly related

to the plant operating cost (Ettouney, El-Dessouky, & Faibish, 2002). In addition and as will be shown by the literature review in the next section, this study is novel and contributes to advancement of knowledge and understanding. The developed model will be validated against laboratory scale experimental results as well as actual plants data. As the model is validated, sensitivity analysis will be done to predict the effect of design and operating parameters on the demister efficiency and pressure drop.

This chapter starts with a description of the demister element and its physics. That will be followed by comprehensive literature review on demisters and relevant phenomena studies. The mathematical models are then presented for the three approaches used to model the demister, which are porous media, tube bank with multi phase flow and tube bank with discrete phase model. The first two approaches follow the Eulerian-Eulerian modelling method while the third approach follows the Eulerian-Lagrangian approach. Section 6.6 includes description of the CFD code which had been used to simulate the model. This is followed by discussion of model assumptions and boundary conditions used for each modeling approach. At the end of this chapter, the conclusion is presented.

6.2 Demisters Element Description

As mentioned in the introduction, demisters are used to minimize or prevent the carry over liquid droplet or mist from passing through it and effecting the condensate composition and quality. There are several configurations used for demisting gases or vapour such as settling tanks, filters, cyclones, electrostatic precipitators, baffles/vanes, fiber filtering candles and wire mesh demisters.

As the vapour/droplets flow through the demister, the droplets are captured and accumulated on the surface of the demister wires. The brine droplets are captured on the wires because of their larger density. The vapour stream can bend around the demister wires, while, the brine droplets would continue to flow in a straight line. As a result, the droplets would hit the demister wires and lose their momentum. Droplet accumulation might result in an increase of the droplet size or formation of a small

thin film. As the size of the droplets captured by the demister wires increases they may start to detach from the wire and drop back to the brine pool (see Figure 6.3).

There are three different mechanisms for capturing the entrained droplets by the wire mesh pad ((El-Dessouky, Alatiqi, Ettouney, & Al-Deffeeri, 2000); (Gerrard et al. 1986); (Holmes and Chen, 1984); (Feord et al., 1993)). These are diffusion, interception, and inertial impaction. The diffusion mechanism, driven by Brownian motion, is significant only for the capture of submicron droplets at a very low gas velocity. Interception occurs for droplets with dimensions similar to or higher than the wire diameter. Inertial impaction occurs when the vapour is forced to change its direction around an object. As the vapour and entrained liquid droplets pass through the mist eliminator, the vapour phase moves freely, but, the liquid, due its greater inertia, is unable to make the required sharp turns. Therefore, the droplets are impacted and collected on the surface of the mesh wires. The droplet momentum or inertia is proportional to their velocity, mass, and diameter. Droplets with sufficient momentum can break through the vapour streamlines and continue to move in a straight line until they impinge on the target. The second stage in the separation process is the coalescence of the droplets, which impinge on the wire surface. Subsequently, the droplets compound and form streams or rivulets, which drain back against the vapour flow. There are three different forces controlling the movement of the water droplets accumulated within the demister pad. These are the drag, the gravity, and the surface tension forces. When the gravity force is dominant, the droplets are detached from the wire and drained by gravity.

The separation processes in the wire mesh demisters (demister under study) undergoes the following three successive steps (El-Dessouky, Alatiqi, Ettouney, & Al-Deffeeri, 2000), which are as shown in Figure.6.3:

1- Accumulation (Figure 6.3(b)): Droplets impacting on the wire has a tendency to wet and stick to the surface. The contact usually creates a thin liquid film on the wire. Depending on the size of the wire, this thin film may either break up into smaller drops if the wire is small, or it may grow into a ligament hanging beneath the wire if the wire is large (Hung & Yao, 1999). Droplet accumulation on the

demister wires surface occurs by three main mechanisms: impaction, diffusion, and interception.

Inertia impaction: As the gas phase flows past the surface or around wires in the mesh pad the streamlines are deflected, but the kinetic energy of the liquid droplets associated with the gas stream may be too high to follow the streamline of the gas (Figure 6.3). As the droplets impact against the wires their momentum drops to zero (El-Dessouky, Alatiqi, Ettouney, & Al-Deffeeri, 2000). Also, it is called the disintegration mode. It occurs primarily when the droplets of moderate impacting velocity come into contact with a wire which is smaller than the incoming droplet. If the droplet velocity is very high, this mode would also happen even if the wire is larger than the droplet. When the droplets impact onto the surface of the wire, the wire serves as a shearing or cutting medium to the droplet. The minimal contact between the droplets and the wire causes a small surface tension effect at the interface. The water film being developed on the wire warps around the top portion of the wire and forms a "V" shaped fragment. It splits into two halves, one on each side. Each small fragment behaves like a small water jet and emerges directly outward. Eventually, each thin liquid jet disintegrates into even smaller drops (Hung & Yao, 1999).

Diffusion: The diffusion mechanism is significant only for the capture of sub-micron droplets at a very low gas velocity. Sub-micron droplets are the hardest to capture. They tend to follow the streamlines of the suspending fluid and collide with the drop only by virtue of their finite radii (Corbett, 1988).

Interception: The interception mechanism by which aerosol particles following the streamlines of the suspending fluid collide with the drop only by virtue of their finite radii, would then dominate the capture of particles in the size range of interest (Corbett, 1988). This mechanism occurs for droplets with dimensions similar to or higher than the wire diameter.

2- Coalescence Figure (6.3(c-d)): The droplets impinging on the surface of the wires coalesce to form larger size drops. In the momentum induced dripping mode, when the incoming droplets make contacts with the wire, a water film builds up consistently. The film runs off the contact point and wraps around the wire from both sides, and finally the film reattaches and forms a large fragment beneath the

wire. There are two reasons for which a longer and thicker fragment is formed. Firstly, the water film carries downward momentum from the top side of the wire; and secondly, droplets may impact on this ligament directly without hitting the wire. The shape of this fragment is very irregular (Hung & Yao, 1999).

3- Detachment (Figure 6.3(e)): In the vertical-flow installations, detached liquid drops drain back from the upstream face of the wire mesh pad. In the horizontal flow systems, collected liquid droplets drain down through the vertical axis of the mesh pad in a cross flow fashion (El-Dessouky & Ettouney, 2002). As the fragment becomes larger; it wriggles more vigorously under the influence of gravity as well as the momentum added by the impacting droplets. Finally, the surface tension at the interfacial contact can no longer sustain the combined effect of the weight and the downwards force of the impacting drops on the ligament. At this point, the drop detaches and falls off the wire. In the gravity induced dripping mode, the formation process of the dripping drops is very similar to the previous case. However, the shapes of the dripping drops are much more spherical (Brunazzi & Paglianti, 2000). When the ligament weight is large enough to overcome the surface tension at the wire interfacial surface, the drop detaches from the wire and drips off at gravity. The size of the dripping drops in this case is usually larger than the ones in the case of momentum induced dripping. Occasionally, there are some secondary drops formed when the primary pendent drop detaches from the wire (Hung & Yao, 1999).

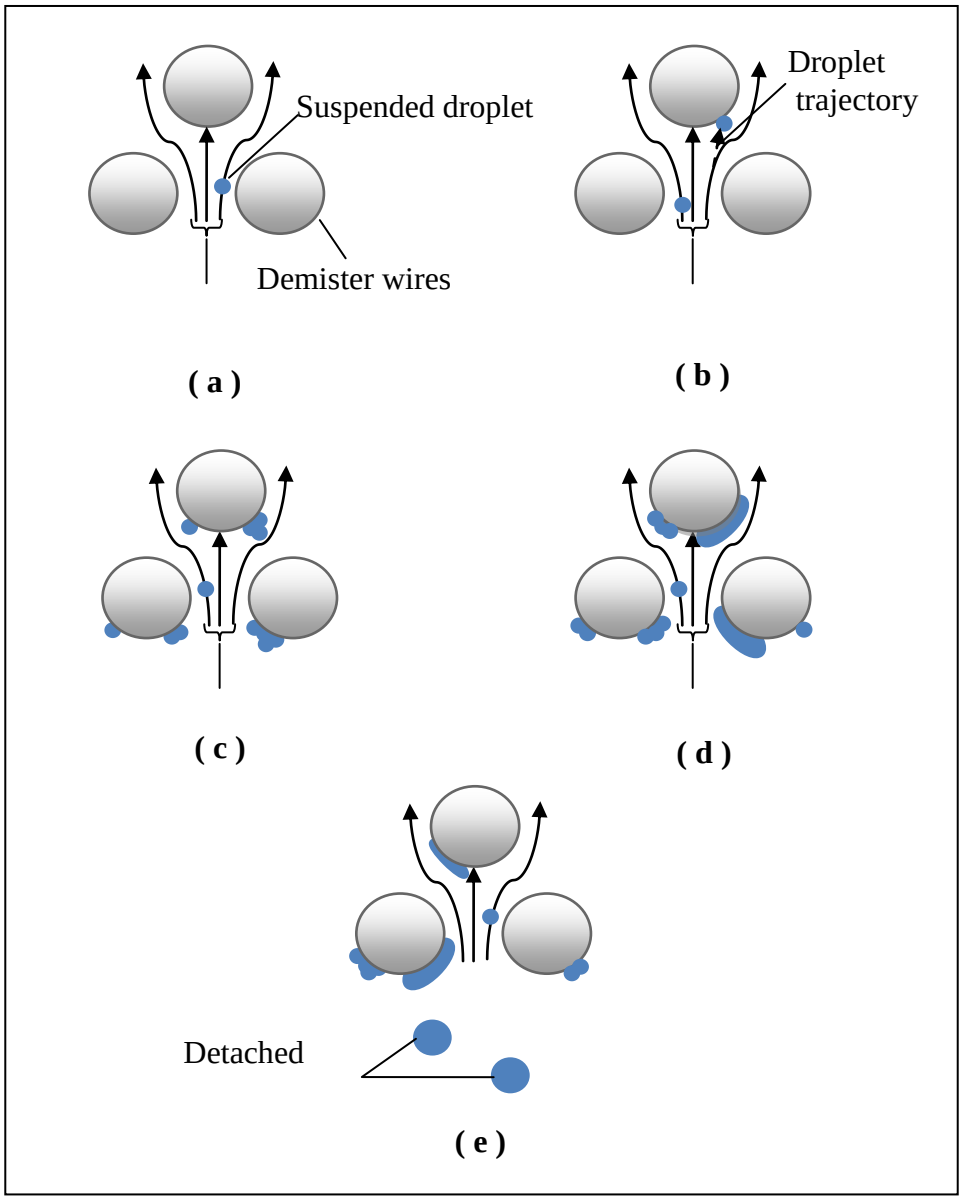

Figure.6.3. Steps of water droplets separation from vapour stream in the wire mesh demister (a) clean wire mesh, (b) accumulation, (c) and (d) coalescence, (d) detachment.

Consider a spherical droplet of diameter D_{do} and density ρ_l as shown in Figure.6.5 which is settling under gravity in a fluid (vapour phase) of density ρ_g and a viscosity μ_g. The droplet settling velocity and the critical droplet diameter (smallest droplet diameter that would settle by gravity within the flashing stage) are obtained through balance of forces on brine droplets travelling between the brine surface and the lower face of the demister. This requires a droplet force balance, which includes: drag, buoyancy, and gravity which is shown in Figure.6.4(a). This balance is given by:

$$\frac{\pi D_{do}^2}{8} C_{DC}\, \rho_g v_g^2 = \frac{1}{6}\, \pi\, D_{do}^3 (\rho_l - \rho_g)\, g \qquad (6.1)$$

The general form of the drag coefficient given in Equation.(6.1) is given by:

$$C_{DC} = \frac{24}{Re} + \frac{3}{Re^{0.5}} + 0.34 \qquad (6.2)$$

Several parameters affect the flow of brine droplets in the distillate vapour which include:

- Stage or vapour temperature
- Range of droplet diameter
- Salinity of the droplets

Several mechanisms affect the motion of the brine droplets upon their release from the surface of the flashing brine and until reaching the lower surface of the demister. Fine and small droplets may coalesce to form larger size droplets. Once the particle size exceeds a certain limit it will start to settle back to the brine pool. This is because its settling velocity would become larger than the vapour velocity, once its size exceeds a certain limit. Also, droplets may reduce their size as a result of water evaporation from their surface to the surrounding vapour.

Re-entrainment of brine droplets occurs when the vapour velocity exceeds a certain limit. As mentioned by Ettouney (2005), the vapour velocity is set by the stage dimensions and temperature. Since the stage dimensions are unaltered then the only

thing that would change the vapour velocity is the brine temperature. This occurs during winter operation, where, the feed water temperature may drop to values below 20^{o}C. This would result in reduction in the stage pressure and large increase in the vapour specific volume and the vapour velocity. As a result, the critical size for the droplets to settle increases. Also, the drag effects of the vapour flowing in the demister would increase to the point that droplets would detach from the wire surface and entrains in the rapidly moving vapour stream.

Various forms can be assumed for the liquid shape covering the demister wires. For example, a whole liquid drop can be assumed to be trapped within the demister wires. Also, a liquid film with a perfect or partial cylindrical shape can be assumed. The condition considered in the analysis is that for liquid droplet. Figure6.4(b) shows a brine droplet entrained by the demister wires. The droplet experiences the balance of the following forces: surface tension, drag, gravity, and buoyancy. For a droplet to be re-entrained in the vapour stream the drag and buoyancy must be equal to or greater than the gravity and surface tension adhesion. The force balance on a stationary droplet at this critical condition is given by:

$$\frac{\pi D_{do}^2}{8} C_{DC}\, \rho_g v_g^2 = \pi D_{do}\, \phi\sigma + \frac{1}{6}\, \pi\, D_{do}^3 \left(\rho_l - \rho_g\right) g \qquad (6.3)$$

In Equation (6.3), the drag coefficient is given by Equation (6.2). The parameter ϕ appearing on the right hand side of Equation (6.3) is used to define the fraction of the droplet perimeter which is attached to the demister wires. At the re-entrainment point the vapour velocity passing through the demister should be greater the vapour velocity obtained from Equation (6.3). It should be noted that Equations (6.3) and (6.2) would give a specific critical velocity, which applies to a specific droplet diameter. A Gaussian distribution for the droplet particle diameter can be used to obtain an average value for the critical velocity. The resulting ratio of the critical re-entrainment velocity together with the actual vapour velocity can be used to determine the fraction of re-entrained vapour.

At steady state conditions, the demister wire will be covered by a thin layer of liquid brine. The mass of liquid brine covering the demister wires can be obtained as a function of the demister specific area and by assume the fraction of the wires covered by the liquid brine and the thickness of the liquid film. Therefore, the mass of the brine covering the demister wires is given by (Ettouney, 2005):

$$m_b = \phi_2 A_p V_p \varphi_f \rho_b \tag{6.4}$$

In Equation (6.4), the parameter ϕ_2 defines the fraction of the demister area covered by liquid brine. The demister volume (V_p) is obtained through definition of the demister length, height, and width. A_p is defined as the demister specific area. φ_f is the thickness of the liquid film. ρ_b is the brine density.

The rate of brine re-entrainment is obtained by dividing the brine mass given by Equation (6.4) by the vapour residence time within the demister, which is given by (Ettouney, 2005):

$$\zeta = \frac{\rho_b L_p W_p H_p}{D_i} \tag{6.5}$$

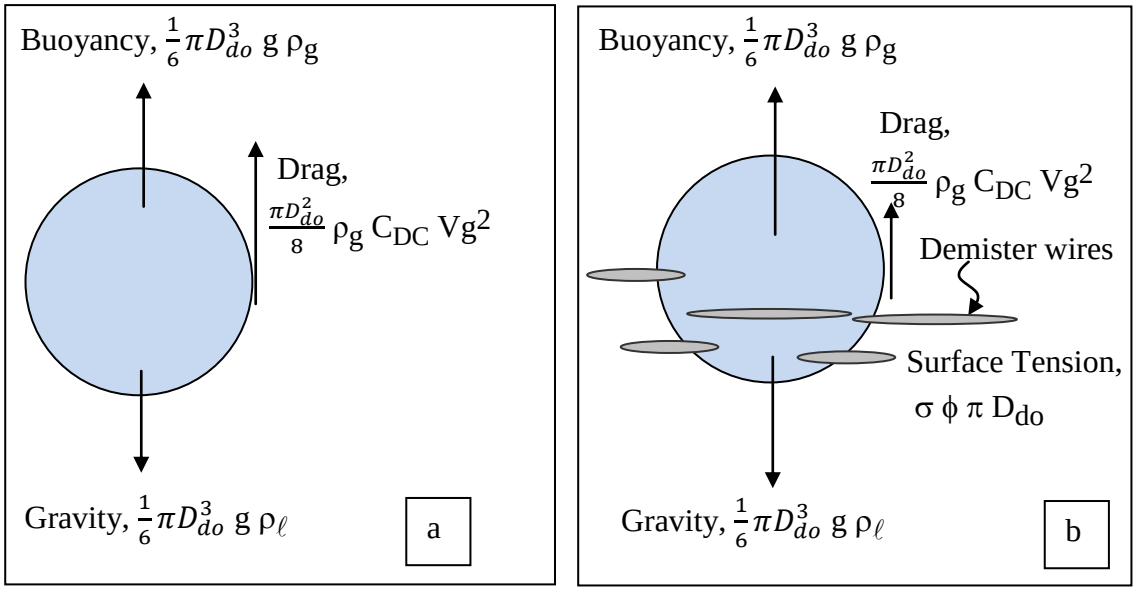

Figure 6.4(a) Balance of forces for a settling liquid droplet. (b) Balance of forces for a droplet attached to a demister wire (Ettouney, 2005).

6.3 Modeling of demisters: literature review

The literature review will be classified into three parts. The first part will focus on the semi-empirical correlation obtained for the removal efficiency and the pressure drop across the demister. The next part will focus on studies concerning the available models on the demister performance which are solved using CFD. That will be followed by models which are similar to the case under study such as tube banks system. At the end, conclusions from all the literature reviews will be presented.

A limited number of literature studies are found on demister performance evaluation. Research on evaluation of the performance of the wire mesh mist eliminator in operating conditions of MSF plants is still in an immature state. The available theoretical models devoted to simulation of the performance of the wire mesh pads are not adequate for implementation to industrial units (El-Dessouky, Alatiqi, Ettouney, & Al-Deffeeri, 2000). Due to complexity of the problem most of the previous research work was empirical. The common design procedure for vapour release velocity and the vapour velocity within the demister which according to the Souders-Brown relation, is given by:

$$V_{max} = K \sqrt{\frac{\rho_l - \rho_g}{\rho_g}} \tag{6.6}$$

where K is a constant which depends on the de-entrainment height (York, 1954) and on the physical properties of the working fluids. K values are reported equal to 0.058 and 0.078, for the vapour release velocity and vapour velocity within the demister, respectively (Wangnick, 1995). This method of designing wire mesh separators is very rough and is not practical because of the following reasons (Brunazzi & Paglianti, 1998):

- Requires prior knowledge of the K value
- Does not take into consideration the droplet size

An empirical correlation based on an experiment was developed by El-Dessouky et al. (2000) (Equation 4.20) for determination of the removal efficiency of large mist

droplets by wire mesh mist eliminator. The demister performance was evaluated by droplet separation efficiency, vapour pressure drop of wet demister, and flooding and loading velocities. These variables were measured as a function of vapour velocity, packing density, pad thickness, wire diameter, and diameter of captured droplets. This limits the correlation validity to the range of variables covered by the experiments. Buerkholz (1989) mentioned that in order to prevent any re-entrainment of the water droplets captured in the wire mesh pad, the gas phase velocity should be limited to 4-5 m/s. Also, he presented experimental data for the flooding load, the corresponding increase in pressure drop, and the fractional separation efficiency. In a dimensionless form the fractional degree of precipitation depends on the Stokes, the Reynolds, and Euler numbers. Experimental analysis shows that for large Reynolds numbers and in a large range of the Euler number, the inertial precipitation depends on a dimensionless precipitation parameter. Therefore, a simple approximation formula is given for the fractional degree of precipitation and the limiting droplet size for all types of separators (Buekholz, 1986). Brunazzi and Paglianti (1998) presented a semi-empirical model for the demister design, which is built on previous analysis presented by Langmuir and Blodgett (1946) and Pich (1966), who evaluated the inertial capture efficiency for a single wire, expressed in terms of a dimensionless Stokes number. The analysis for industrial wire mesh packing is presented by Carpenter and Othmer (1955) as a function of the demister pad thickness, the demister specific area, the stocks efficiency, and the number of mesh layers. A new model was presented by Brunazzi and Paglianti (2000) for predicting the removal efficiency of complex wire-mesh eliminators. This new model can be used for predicting separation efficiency of multilayer pads and composite separators.

More recently, a limited number of studies were found in the literature on demister modeling using computational fluid dynamics (CFD). The literature can be divided into two categories: wave-plate (vane type) demisters and wire-mesh demisters. Studies done by Verlaan (1991), Wang and Davies (1996), Gillandt et al. (1996), Wang and James (1998,1999), James et al. (2003,2005), Zhao et al. (2007) and Galletti et al. (2008) all concern the vane-type demisters with different droplet sizes which varies from 1 μm and up to 1000 μm. They used the standard k-ε model to describe the turbulence model. All the studies have neglected the turbulent

dispersion effects except the work done by Wang and James (1999), James et al. (2003,2005) and Galletti et al. (2008). Wang and Davies (1996), James et al. (2003) and Galletti et al. (2008) included drainage channels to remove the captured droplets. Verlaan (1991), Gillandt et al. (1996), Wang and James (1998,1999), Zhao et al. (2007) and Galletti et al. (2008) have compared the predicted results with experiments.

For the wire mesh demisters, Rahimi and Abbaspour (2008) predicted the pressure drop in a mist pad by CFD. The turbulence models based on the standard k-ε model was used to simulate the measurements of the pressure drop and was carried out for inlet velocity ranging 1-7 m/s. The CFD predictions agreed with experimental data and the El-Dessouky et al.(2000) empirical correlation. Also, the simulations show existence of a maximum in separation efficiency as a function of the vapour inlet velocity. This indicated that further increase in the velocity will result in droplet re-entrainment and carryover of fine droplets in the vapour stream.

A literature review on the modeling of the tube banks or condensers using CFD was done. That is because the wire mesh demister has geometry close to the tube banks but of course with a different mechanism. The numerical simulations of fluid flow and heat transfer in steam surface condensers have been conducted by few researchers. Davidson and Rowe (1981) and Al-Sanea et al.(1983) developed a single-phase two-dimensional model. In the first model the turbulent effect was neglected but in the second, the turbulent viscosity to the dynamic viscosity ratio was assumed to be constant. Zhang and Zhang (1993) used a quasi 3-D approach to simulate the single phase flow of two phase fluid and heat transfer in the condensers. that was followed by a study of Zhang and Bokil (1997) used a quasi 3-D approach to simulate the flow of two phase fluid and heat transfer in the shell-side of power plant condensers. Also in this model, the turbulent viscosity to the dynamic viscosity ratio was assumed to be constant. In other models, simple algebraic equations were used to determine the turbulent viscosity such as these done by Bush et al.(1990) and Malin (1997).

From the previous literature review the following conclusions can be drawn:

- A limited number of literature studies can be found on experimental analysis and simulation of wire mesh demisters.
- Recent progress in computing (software as well as hardware) has made it possible to simulate such complex problems that include two phase flow, transient effects, turbulence, two and three dimensional flow, and large computational domains. Such conditions were not possible to simulate a decade or two ago, as a result most of the available CFD studies are limited to the past two decades. These developments made it possible to execute the study presented in this work.
- CFD models of condenser tube banks have strong similarities with wire mesh demisters; this is irrespective of the inherent differences in model details. Review of these literature studies provided insights into development and understanding elements of CFD modeling of two phase flow around tube banks or porous media in demisters.
- There is no literature work on CFD modeling of the MSF wire mesh demisters. However, there is only one study found on CFD modeling of the wire mesh demisters by Rahimi and Abbaspour (2008) for a refinery reactor. Review of the manuscript does not clarify how the demister and flow of vapour and brine droples were modelled, i.e., porous media or tube bank. Also, the treatment of vapour/brine droplet flow is not clear, i.e., lagrangian or eulerian. In this study, almost 14% deviation occurs between the preidicted CFD results and the experimental data and as the velocity increases the difference increases which makes the model inaccurate for high vapour velocities (above 7 m/s).

6.4 Mathematical Model Equations (Eulerian-Eulerian method)

The Eulerian method prescribes the necessary properties (pressure, density, velocity, etc.) as functions of space and time. Therefore, information is obtained about the flow in terms of what happens at fixed points in space as the fluid flows through those points.

The Eulerian-Eulerian method treats the brine droplets and the vapour phase as two separate continuums. This requires solution of the appropriate continuum equations for each phase. Two approaches are followed to model the wire mesh demister by Eulerian-Eulerian method. First is the porous media approach. Second is the tube bank approach with multi phase flow. First the mathematical model and boundary conditions for the porous media with multi phase flow approache will be presented. Next, the mathematical model and boundary conditions for the tube banks with multi phase flow approache will be presented.

6.4.1 Porous Media with Multi Phase Flow

The mathematical model equations for the vapour phase will be presented first followed by these for the brine droplets.

Mass amd Momentum Conservation

The general mass conservation equation for constant density, two dimensional vapour flow is:

$$\rho_g \left[\frac{\partial \psi_g}{\partial \mathrm{t}} + \frac{\partial}{\partial x}\left(\psi_g\, u_g\right) + \frac{\partial}{\partial y}\left(\psi_g v_g\right)\right] = 0 \qquad (6.7)$$

The momentum conservation equations for the gas phase in two dimensional model (x-direction, horizontal) and (y-direction, vertical) are:

$$\frac{\partial(\psi_g \rho_g\, u_g)}{\partial t} + \frac{\partial}{\partial x}\left(\psi_g \rho_g\, u_g\, u_g\right) + \frac{\partial}{\partial y}\left(\psi_g \rho_g\, v_g u_g\right) =$$
$$\frac{\partial}{\partial x}\left(\psi_g \mu_{eg} \frac{\partial\, u_g}{\partial x}\right) + \frac{\partial}{\partial y}\left(\psi_g \mu_{eg} \frac{\partial\, u_g}{\partial y}\right) + \frac{\partial}{\partial x}\left(\psi_g \mu_{eg} \frac{\partial\, u_g}{\partial x}\right) + \frac{\partial}{\partial y}\left(\psi_g \mu_{eg} \frac{\partial\, v_g}{\partial x}\right) -$$
$$\frac{2}{3}\frac{\partial}{\partial x}\left[\psi_g \mu_{eg}\left(\frac{\partial\, u_g}{\partial x} + \frac{\partial\, v_g}{\partial y}\right)\right] - \psi_g \frac{\partial P}{\partial x} + S_{gx} - R_{gx} \qquad (6.8)$$

$$\frac{\partial(\psi_g \rho_g v_g)}{\partial t} + \frac{\partial}{\partial x}(\psi_g \rho_g u_g v_g) + \frac{\partial}{\partial y}(\psi_g \rho_g v_g v_g) =$$
$$\frac{\partial}{\partial \mathrm{x}}\left(\psi_g \mu_{eg} \frac{\partial v_g}{\partial x}\right) + \frac{\partial}{\partial \mathrm{y}}\left(\psi_g \mu_{eg} \frac{\partial v_g}{\partial y}\right) + \frac{\partial}{\partial \mathrm{x}}\left(\psi_g \mu_{eg} \frac{\partial u_g}{\partial y}\right) +$$
$$\frac{\partial}{\partial \mathrm{y}}\left(\psi_g \mu_{eg} \frac{\partial v_g}{\partial y}\right) - \frac{2}{3}\frac{\partial}{\partial y}\left[\psi_g \mu_{eg}\left(\frac{\partial u_g}{\partial x} + \frac{\partial v_g}{\partial y}\right)\right] - \psi_g \frac{\partial P}{\partial y} + S_{gy} - R_{gy} \qquad (6.9)$$

The first term on the left hand side represents the transient term (unsteady acceleration). The second and third terms represent the convective acceleration. On the right hand side, the first five terms represent the viscous terms (shear stress term). It should be noted that a Newtonian closure have been used for the stress. The sixth term represents the pressure gradient due to buoyancy force. The third term represents other body forces. S is the source term due to interphase friction between the gas phase and the liquid phase. R is the source term due to the distributed resistance, which is due to the tube bundle. μ_{eg} is the effective viscosity, which is the sum of turbulent viscosity μ_{t_g} and fluid viscosity μ_g.

The general mass conservation equation for constant density, two dimensional liquid droplets flow is:

$$\rho_l \left[\frac{\partial \psi_l}{\partial t} + \frac{\partial}{\partial x}(\psi_l u_l) + \frac{\partial}{\partial y}(\psi_l v_l)\right] = -\psi_l \dot{m} \qquad (6.10)$$

The porosity $\boldsymbol{\omega}$ is the volume of voids over the total volume. $\boldsymbol{u}$ is the velocity in the x-direction. $\boldsymbol{v}$ is the velocity in the y-direction $\dot{\boldsymbol{m}}$ is the mass rate of collected liquid droplet per unit volume.

$$\omega = \psi_g + \psi_l \qquad (6.11)$$

The momentum conservation equations for the liquid phase in two dimensional model (x-direction, horizontal) and (y-direction, vertical) are:

$$\frac{\partial(\psi_l \rho_l u_l)}{\partial t} + \frac{\partial}{\partial x}(\psi_l \rho_l u_l u_l) + \frac{\partial}{\partial y}(\psi_l \rho_l v_l u_l) = -\psi_l \frac{\partial P}{\partial x} + S_{lx} - R_{lx} - \psi_l \dot{m} u_l \quad (6.12)$$

$$\frac{\partial(\psi_l \rho_l v_l)}{\partial t} + \frac{\partial}{\partial x}(\psi_l \rho_l u_l v_l) + \frac{\partial}{\partial y}(\psi_l \rho_l v_l v_l) = -\psi_l \frac{\partial P}{\partial y} + S_{ly} - R_{ly} - \psi_l \dot{m} v_l + \psi_l \rho_l g \quad (6.13)$$

In the last equations the stress tensor is zero.

Interface friction

The interface friction forces between the gas phase and the liquid phase in the momentum equations are related to the interphase friction coefficient C_f which is given as (Zhang & Bokil, 1997):

$$C_{f_u} = \frac{1}{2}\rho_g f_d A_{do} |u_g - u_l| \quad (6.14)$$

$$C_{f_v} = \frac{1}{2}\rho_g f_d A_{do} |v_g - v_l| \quad (6.15)$$

where f_d is the friction factor for spherical objects and is obtained from an empirical correlation given by Clift et al. (1978). A_{do} is the total projected area of droplets in a given control volume and is defined as:

$$A_{do} = \frac{1.5\,\psi_l V}{D_{do}} \quad (6.16)$$

The interface friction forces between the gas phase and the liquid phase in the momentum equations are (Hu & Zhang, 2007):

$$S_{gx} = -S_{lx} = C_{f_u}(u_l - u_g) \quad (6.17)$$

$$S_{gy} = -S_{ly} = C_{f_v}(v_l - v_g) \quad (6.18)$$

Distributed Resistance

The source term for the distributed resistance (local hydraulic flow resistance forces) due to the tube bundles for both phases (liquid and gas) are included in the momentum equations (Zhang & Bokil, 1997):

For the liquid phase in x-direction:

$$R_{lx} = (\psi_l \xi_{lx}\, \rho_l u_l U_l) \quad (6.19)$$

For the liquid phase in y-direction:

$$R_{ly} = \left(\psi_l \xi_{ly}\, \rho_l v_l U_l\right) \quad (6.20)$$

For the vapour phase in x-direction:

$$R_{gx} = \left(\psi_g \xi_{gx}\, \rho_g u_g U_g\right) \quad (6.21)$$

For the vapour phase in y-direction:

$$R_{gy} = \left(\psi_g \xi_{gy}\, \rho_g v_g U_g\right) \quad (6.22)$$

where ξ is the pressure loss coefficient. The expression is given by Rhodes and Carlucci (1983) for the x and y direction as:

$$\xi_x = 2\left(\frac{f_x}{P_t}\right)\left(\frac{P_t\ \omega}{P_t - D_{ot}}\right)^2\left(\frac{1-\omega}{1-\omega_{td}}\right) \quad (6.23)$$

$$\xi_y = 2\left(\frac{f_y}{P_t}\right)\left(\frac{P_t\ \omega}{P_t - D_{ot}}\right)^2\left(\frac{1-\omega}{1-\omega_{td}}\right) \tag{6.24}$$

where

$$f_x = \begin{cases} 0.619\ Re_x^{-0.198} & ;\ Re_x < 8000 \\ 1.156 Re_x^{-0.2647} & ; 8000 \le Re_x < 2\times 10^5 \end{cases} \tag{6.25}$$

$$f_y = \begin{cases} 0.619\ Re_y^{-0.198} & ;\ Re_y < 8000 \\ 1.156 Re_y^{-0.2647} & ; 8000 \le Re_y < 2\times 10^5 \end{cases} \tag{6.26}$$

Mass source term

The mass source term $\dot{m}$ is the collected entrained brine droplets. The collection takes place on the wires as mentioned previously. For simplification it was assumed to be constant and equal to a percentage of the inlet liquid flow rate depending on the demister separation efficiency. In this model, for both approaches (tube bank and porous media) it is assumed to have uniform mass sink distribution for the water droplets only across the demister fluid zone.

Turbulence model

Standard *k-ε* model is used in this study for all the simulation. This model includes two equations: the turbulent kinetic energy *k* and the turbulent dissipation rate *ε*. For the gas phase the model has the following form:

$$\frac{\partial}{\partial t}\left(\psi_g\,\rho_g k_g\right) + \frac{\partial}{\partial x}\left(\psi_g\,\rho_g u_g k_g\right) + \frac{\partial}{\partial y}\left(\psi_g\,\rho_g v_g k_g\right) = \frac{\partial}{\partial x}\left(\psi_g\,\left(\mu_g + \frac{\mu_{t_g}}{\sigma_k}\right)\frac{\partial k_g}{\partial x}\right) + \frac{\partial}{\partial y}\left(\psi_g\,\left(\mu_g + \frac{\mu_{t_g}}{\sigma_k}\right)\frac{\partial k_g}{\partial y}\right) + \psi_g\left(G_g - \rho_g\varepsilon_g\right) + S_{k_g} \tag{6.27}$$

$$\frac{\partial}{\partial t}\left(\psi_g\,\rho_g\varepsilon_g\right) + \frac{\partial}{\partial x}\left(\psi_g\,\rho_g u_g\varepsilon_g\right) + \frac{\partial}{\partial y}\left(\psi_g\,\rho_g v_g\varepsilon_g\right) = \frac{\partial}{\partial x}\left(\psi_g\,\left(\mu_g + \frac{\mu_{t_g}}{\sigma_k}\right)\frac{\partial\varepsilon_g}{\partial x}\right) + \frac{\partial}{\partial y}\left(\psi_g\,\left(\mu_g + \frac{\mu_{t_g}}{\sigma_k}\right)\frac{\partial\varepsilon_g}{\partial y}\right) + \psi_g\,\frac{\varepsilon_g}{k_g}\left(C_1 G_g - C_2\rho_g\varepsilon_g\right) + S_{\varepsilon_g} \tag{6.28}$$

For the liquid phase the model has the following form:

$$\frac{\partial}{\partial t}(\psi_l \rho_l k_l) + \frac{\partial}{\partial x}(\psi_l \rho_l u_l k_l) + \frac{\partial}{\partial y}(\psi_l \rho_l v_l k_l) = \frac{\partial}{\partial x}\left(\psi_l \left(\mu_l + \frac{\mu_{t_l}}{\sigma_k}\right)\frac{\partial k_l}{\partial x}\right) + \frac{\partial}{\partial y}\left(\psi_l \left(\mu_l + \frac{\mu_{t_l}}{\sigma_k}\right)\frac{\partial k_l}{\partial y}\right) + \psi_l (G_l - \rho_l \varepsilon_l) + S_{k_l} \quad (6.29)$$

$$\frac{\partial}{\partial t}(\psi_l \rho_l \varepsilon_l) + \frac{\partial}{\partial x}(\psi_l \rho_l u_l \varepsilon_l) + \frac{\partial}{\partial y}(\psi_l \rho_l v_l \varepsilon_l) = \frac{\partial}{\partial x}\left(\psi_l \left(\mu_l + \frac{\mu_{t_l}}{\sigma_k}\right)\frac{\partial \varepsilon_l}{\partial x}\right) + \frac{\partial}{\partial y}\left(\psi_l \left(\mu_l + \frac{\mu_{t_l}}{\sigma_k}\right)\frac{\partial \varepsilon_l}{\partial y}\right) \psi_l \frac{\varepsilon_l}{k_l}(C_1 G_l - C_2 \rho_l \varepsilon_l) + S_{\varepsilon_l} \quad (6.30)$$

where μ_{t_g} is the turbulent viscosity of the gas phase and is defined as:

$$\mu_{t_g} = \frac{C_\mu \rho_g k_g^2}{\varepsilon_g} \quad (6.31)$$

And μ_{t_l} is the turbulent viscosity of the liquid phase and is defined as:

$$\mu_{t_l} = \frac{C_\mu \rho_l k_l^2}{\varepsilon_l} \quad (6.32)$$

The standard model was used without any modifications. The source terms S_k and S_ε are not considered in the mean of interphase turbulence exchange. The five constants of the model were set to the standard *k-ε* model and are σ_k = 1 and σ_ε = 1.3, C_1 = 1.44, C_2= 1.92, C_μ= 0.09 ((Rahimi & Abbaspour, 2008), (Hu & Zhang, 2007)).

Bounday Conditions

Each approach has its own boundary conditions which matches the models proposed previously. The porous media model incorporates an empirically determined flow resistance in a region of the model defined as “porous”. In essence, the porous media model is nothing more than an added momentum sink in the governing

momentum equations. In this model the effect of the porous medium on the turbulence field is only approximated.

The boundary conditions for the porous media approach include:

- Fluid Zone (Includes the porous media)
- Inlet conditions
- Outlet conditions
- Sides of the geometry
- Porous Jump Boundary Conditions at the inlet of the porous media

As shown in Figure 6.6., the system (was divided into three fluid zones which are inlet zone, porous media and outlet zone. The boundary conditions are as follow:

- **Flow Inlet Boundary Condition:** This condition is used to define the velocity and scalar properties of the flow at inlet boundaries. It is defined in the CFD code on the inlet surface as "Velocity Inlet". The following information should be entered for this boundary condition:

  - Velocity magnitude and direction or velocity components
  - Temperature (for energy calculations)
  - Outflow gauge pressure (for calculations with the density-based solvers)
  - Turbulence parameters (for turbulent calculations)
  - Mixture fraction and variance (for non-premixed or partially premixed combustion calculations)
  - Multiphase boundary conditions (for general multiphase calculations)

- **Pressure Outlet Boundary Condition:** This condition is used to determine the static pressure at flow outlets (and also other scalar variables, in case of back flow). It is defined in the CFD code on the outlet surface as "Pressure Outlet". The use of a pressure outlet boundary condition instead of an out flow condition often results in a better rate of convergence when back flow occurs

during iteration. Also, it should be noticed that the Outflow Boundary Condition which is more general cannot be used with multiphase model such as the model in this study. The following information should be entered for a pressure outlet boundary:

- Static pressure
- Back flow conditions which includes back flow direction specification method, turbulence parameters (for turbulent calculations), multiphase boundary conditions (for general multiphase calculations)

- **Symmetry Boundary Condition:** This is defined in the CFD code on the both sides of the geometry as "Symmetry". This condition is used when the physical geometry of interest, and the expected pattern of the flow/thermal solution, has mirror symmetry. FLUENT assumes a zero flux of all quantities across a symmetry boundary. There is no convective flux across a symmetry plane: the normal velocity component at the symmetry plane is thus zero. There is no diffusion flux across a symmetry plane: the normal gradients of all flow variables are thus zero at the symmetry plane. The symmetry boundary condition can therefore be summarized as follows:

  - Zero normal velocity at a symmetry plane
  - Zero normal gradients of all variables at a symmetry plane

- **Porous Media Condition:** the middle zone which includes the demister is defined in the CFD code as "Porous Media". In this model, a cell zone in which the porous media model is applied is defined and the pressure loss in the flow is determined via the inputs. The following information is required to define a porous media boundary:

  - Define the porous zone.
  - Identify the fluid material flowing through the porous medium

- Enable the Relative Velocity Resistance Formulation. By default, this option is already enabled and takes the moving porous media into consideration
- Set the viscous resistance coefficients and the inertial resistance coefficients, and define the direction vectors for which they apply. Alternatively, specify the coefficients for the power-law model.
- Specify the porosity of the porous medium. It was calculated from the packing density as:

$$\omega = 1 - \frac{Volume\ \ of\ wires}{total\ volume\ of\ demister} \quad (6.33)$$

$$\omega = 1 - \frac{mass\ of\ wire/\rho_w}{total\ volume\ of\ demister} \quad (6.34)$$

$$\omega = 1 - \frac{\rho_p}{\rho_w} \quad (6.35)$$

- Set any fixed values for solution variables in the fluid region (optional).
- Suppress the turbulent viscosity in the porous region, if appropriate.

– **Porous Jump Condition:** This condition allows accounting for the pressure drop across the porous media. Porous jump conditions are used to model a thin membrane. In this case it is the inlet of the porous media. The following information should be entered for a porous jump boundary:

- Identify the porous-jump zone.
- Set the Face Permeability of the medium(δ)
- Set the Porous Medium Thickness
- Set the Pressure-Jump coefficient C_2.

One technique for deriving the appropriate constants δ and C_2.involves the use of the Ergun equation (Ergun, 1952). In this technique the porous media is treated as packed bed. Semi-empirical correlation applicable over a wide range of Reynolds numbers and for many types of packing:

$$\frac{|\Delta P|}{H_p} = \frac{150\mu}{D_{do}^2}\frac{(1-\omega)^2}{\omega^3}v_\infty + \frac{1.75\rho}{D_d}\frac{(1-\omega)}{\omega^3}v_\infty^2 \quad (6.36)$$

When modeling laminar flow through a packed bed, the second term in the above equation may be dropped, resulting in the Blake-Kozeny equation (Ergun, 1952).

$$\frac{|\Delta P|}{H_p} = \frac{150\mu}{D_{do}^2}\frac{(1-\omega)^2}{\omega^3}v_\infty \quad (6.37)$$

In laminar flows through porous media, the pressure drop is typically proportional to velocity and the constant C_2 can be considered to be zero. Ignoring convective acceleration and diffusion, the porous media model then reduces to Darcy's Law:

$$\nabla P = -\frac{\mu}{\omega}\vec{v} \quad (6.38)$$

Comparing equations (6.36) and (6.37) with (6.38), the permeability and inertial loss coefficient in each component direction may be identified as:

$$\delta = \frac{D_{do}^2}{150}\frac{\omega^3}{(1-\omega)^2} \quad (6.39)$$

$$C_2 = \frac{3.5}{D_{do}}\frac{(1-\omega)}{\omega^3} \quad (6.40)$$

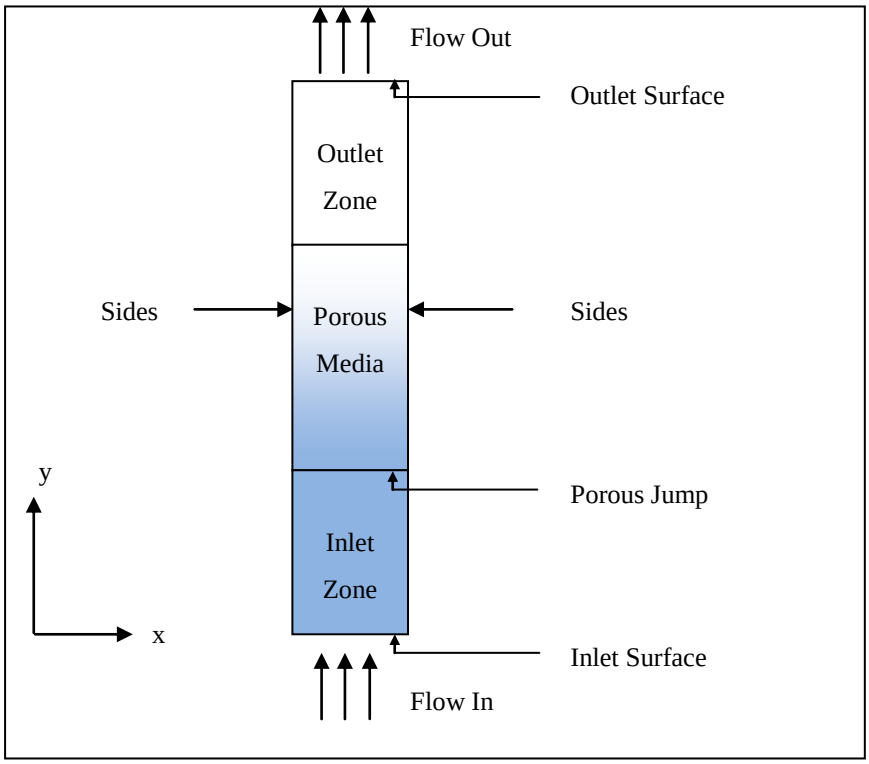

Figure 6.5 Schematic diagram of the porous media grid

6.4.2 Tube Banks with Multi Phase Flow

The mathematical model equations for the vapour phase will be presented first followed by these for the brine droplets.

Mass amd Momentum Conservation

The general mass conservation equation for constant density, two dimensional vapour flow is given by equation (6.7).

The momentum conservation equations for the gas phase in two dimensional model (x-direction, horizontal) and (y-direction, vertical) are:

$$\frac{\partial(\psi_g \rho_g u_g)}{\partial t} + \frac{\partial}{\partial x}(\psi_g \rho_g u_g u_g) + \frac{\partial}{\partial y}(\psi_g \rho_g v_g u_g) =$$
$$\frac{\partial}{\partial x}\left(\psi_g \mu_{eg} \frac{\partial u_g}{\partial x}\right) + \frac{\partial}{\partial y}\left(\psi_g \mu_{eg} \frac{\partial u_g}{\partial y}\right) + \frac{\partial}{\partial x}\left(\psi_g \mu_{eg} \frac{\partial u_g}{\partial x}\right) + \frac{\partial}{\partial y}\left(\psi_g \mu_{eg} \frac{\partial v_g}{\partial x}\right) -$$
$$\frac{2}{3}\frac{\partial}{\partial x}\left[\psi_g \mu_{eg}\left(\frac{\partial u_g}{\partial x} + \frac{\partial v_g}{\partial y}\right)\right] - \psi_g \frac{\partial P}{\partial x} + S_{gx} \qquad (6.41)$$

$$\frac{\partial(\psi_g \rho_g v_g)}{\partial t} + \frac{\partial}{\partial x}(\psi_g \rho_g u_g v_g) + \frac{\partial}{\partial y}(\psi_g \rho_g v_g v_g) =$$
$$\frac{\partial}{\partial \mathrm{x}}\left(\psi_g \mu_{eg} \frac{\partial v_g}{\partial x}\right) + \frac{\partial}{\partial \mathrm{y}}\left(\psi_g \mu_{eg} \frac{\partial v_g}{\partial y}\right) + \frac{\partial}{\partial \mathrm{x}}\left(\psi_g \mu_{eg} \frac{\partial u_g}{\partial y}\right) +$$
$$\frac{\partial}{\partial \mathrm{y}}\left(\psi_g \mu_{eg} \frac{\partial v_g}{\partial y}\right) - \frac{2}{3}\frac{\partial}{\partial y}\left[\psi_g \mu_{eg}\left(\frac{\partial u_g}{\partial x} + \frac{\partial v_g}{\partial y}\right)\right] - \psi_g \frac{\partial P}{\partial y} + S_{gy} \qquad (6.42)$$

The general mass conservation equation for constant density, two dimensional liquid droplets flow is given by :

$$\rho_l \left[\frac{\partial \psi_l}{\partial t} + \frac{\partial}{\partial x}(\psi_l u_l) + \frac{\partial}{\partial y}(\psi_l v_l)\right] = -\psi_l \dot{m} \qquad (6.43)$$

The right hand side term represents the mass sink value for the brine or liquid droplets. Actually, to get more accurate model and results this value should be zero and fluxes should be assigned at the boundry of the tubes.

$$1 = \psi_g + \psi_l \qquad (6.44)$$

The momentum conservation equations for the liquid phase in two dimensional model (x-direction, horizontal) and (y-direction, vertical) are:

$$\frac{\partial(\psi_l \rho_l u_l)}{\partial t} + \frac{\partial}{\partial x}(\psi_l \rho_l u_l u_l) + \frac{\partial}{\partial y}(\psi_l \rho_l v_l u_l) =$$
$$-\psi_l \frac{\partial P}{\partial x} + S_{lx} - \psi_l \dot{m} u_l \qquad (6.45)$$

$$\frac{\partial(\psi_l \rho_l v_l)}{\partial t} + \frac{\partial}{\partial x}(\psi_l \rho_l u_l v_l) + \frac{\partial}{\partial y}(\psi_l \rho_l v_l v_l) = -\psi_l \frac{\partial P}{\partial y} + S_{ly} - \psi_l \dot{m} v_l + \psi_l \rho_l g \quad (6.46)$$

In the last equations the stress tensor is zero.

Interface friction

The interface friction forces between the gas phase and the liquid phase in the momentum equations are mentioned previously in equations (6.14-6.18)

Mass source term

The mass source term $\dot{m}$ is the collected entrained brine droplets. The collection takes place on the wires as mentioned previously. For simplification it was assumed to be constant and equal to a percentage of the inlet liquid flow rate depending on the demister separation efficiency. In this model, for both approaches (tube bank and porous media) it is assumed to have uniform mass sink distribution for the water droplets only across the demister fluid zone.

Turbulence model for the gas-phase

Standard *k-ε* model is used in this study for all the simulation. This model includes two equations: the turbulent kinetic energy *k* and the turbulent dissipation rate *ε*. Equations (6.27-6.28) apply for the gas phase. Equations (6.29-6.30) apply for the liquid phase.

Bounday Conditions

The boundary conditions for the tube banks multi phase flow approach include:

- Fluid Zone
- Solid Zone

- Inlet conditions
- Outlet conditions
- Sides of the geometry

As shown in Figure 6.7., the system was divided into two zones which are: fluid zone, and solid zone (demister wires). The boundary conditions are as follow where the first three are similar to those mentioned previously in section 6.9.1:

- **Flow Inlet Boundary Condition:** this is defined on the inlet surface as Velocity Inlet.
- **Pressure Outlet Boundary Condition:** this is defined on the outlet
- **Symmetry Boundary Condition:** this is defined on the both sides of the geometry
- **Wall Boundary Condition:** The demister wires are defined as walls. Wall boundary condition is used to bound fluid and solid regions. In viscous flows, the no-slip boundary condition is enforced at walls by default. The shear stress and heat transfer between the fluid and wall are computed based on the flow details in the local flow field.

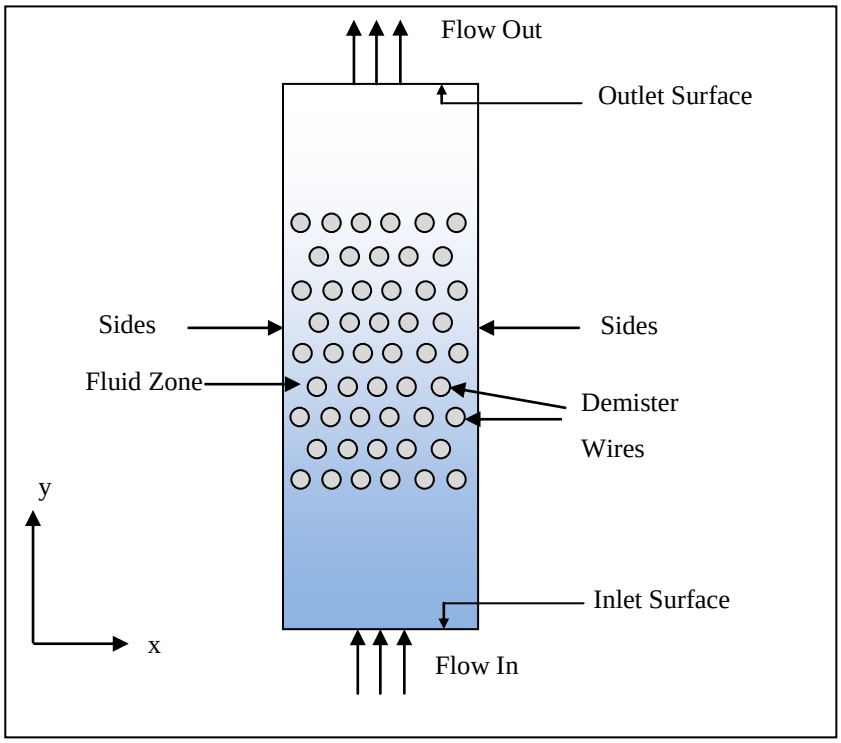

Figure.6.6 Schematic diagram of the tube bank grid

6.5 Mathematical Model Equations (Eulerian-Lagrangian method)

Eulerian-Lagrangian method treats the fluid phase (vapour) as a continuum and predicts the trajectory of a single droplet in the fluid flow as a result of various forces acting on the droplets. The Lagrangian approach has some advantages for predicting those particulate flows in which large particle (droplet) accelerations occur. The Eulerian approach seems to have advantages in flow cases where high particle concentrations occur and where high void fraction of the flow becomes a dominating flow controlling parameter (Durst, Miloievic, & Schonung, 1984). In other words, the Eulerian specification can be thought of as providing a picture of the spatial distribution of fluid velocity (and of any other flow quantities such as density and pressure) at each instant during the motion. While in the Lagrangian specification, the flow quantities are defined as a function of the time and of the choice of a material element of fluid and describe the dynamical history of this selected fluid element (Micale, 1993).

6.5.1 Tube Banks with Discrete Phase Model

Tube banks with a discrete phase model approach is another approach used to model the demister. This approach follows the Eulerian-Lagrangian method. The Lagrangian discrete phase model follows the Euler-Lagrange approach. The fluid phase is treated as a continuum by solving the time-averaged Navier-Stokes equations, while the dispersed phase is solved by tracking a large number of particles, bubbles, or droplets through the calculated flow field. The dispersed phase can exchange momentum, mass, and energy with the fluid phase. A fundamental assumption made in this model is that the dispersed second phase occupies a low volume fraction, even though a high mass is acceptable. The particle or droplet trajectories are computed individually at specified intervals during the fluid phase calculation.

The mathematical model can be divided into:

1. Lagrange approach for the discrete phase particles (water droplets)
2. Eulerian approach for the continuous phase (vapour stream) which includes:
   - Conservation equations which includes all the mass and momentum equations.
   - Auxiliary relationships which includes source terms for both momentum and mass terms.

Lagrangian Approach

Brennen, (2005) suggests a Eulerian-Lagrangian approach (Van Wachem & Almstedt, 2003) to model multiphase flows with a particulate volume fraction less than 10%, which is the case in this study (<<0.1%). In this approach, the flow field is first solved using a continuum approach and subsequently particles are tracked using a discrete phase model, which is derived from force balances based on Newton's (turbulent and transitional regimes) and Stokes' (laminar regimes) laws for particle motion

FLUENT predicts the trajectory of a discrete phase particle (droplet) by integrating the force balance on the particle, which is written in a Lagrangian reference frame. This force balance equates the particle inertia with the forces acting on the particle, and can be written (for the y direction in Cartesian coordinates) as:

$$\frac{dv_{pt}}{dt} = F_D\left(v_f - v_{pt}\right) + g_y\left(\frac{\rho_{pt}-\rho}{\rho_{pt}}\right) + F_y \qquad (6.47)$$

where the first term represents the drag force, the second represents the gravity and buoyancy effect and F_y is an additional acceleration (force/unit particle mass) term in the y direction, $F_D\left(v_f - v_{pt}\right)$ is the drag force per unit particle mass and for sub-micron particles, a form of Stokes' drag law is available (Ounis, Ahmadi, & McLaughlin, 1991). In this case, F_D is defined as

$$F_D = \frac{18\,\mu}{\rho_p D_{do}^2}\frac{C_{DC}Re}{24} \tag{6.48}$$

here ,v_f is the fluid phase velocity, v_{pt} is the particle velocity, μ is the molecular viscosity of the fluid, ρ is the fluid density, ρ_{pt} is the density of the particle, and D_{do} is the particle diameter. *Re* is the relative Reynolds number of the droplet, which is defined as:

$$Re = \frac{\rho D_{do}|v_{pt}-v_f|}{\mu} \tag{6.49}$$

An additional force arises due to the pressure gradient in the fluid:

$$F_y = \frac{\rho}{\rho_{pt}} v_{pi}\frac{\partial v}{\partial y_i} \tag{6.50}$$

The drag coefficient, C_{DC}, can be taken from (Morsi & Alexander, 1972) :

$$C_{DC} = a_1 + \frac{a_2}{Re} + \frac{a_3}{Re^2} \tag{6.51}$$

where a_1, a_2, and a_3 are constants that apply to smooth spherical particles over several ranges of *Re*

Eulerian Approach

The eulerian model of the vapour phase is the same as that for the vapour phase mentioned previously for the tube banks multi phase flow model. Thus equations (6.7, 6.14-6.18, 6.27-6.28, 6.41, 6.42, and 6.44) apply.

Boundary Conditions

The boundary conditions include:

– Fluid Zone

- Solid Zone (demister wires)
- Inlet conditions
- Outlet conditions
- Sides of the geometry

As shown in Figure 6.7, the grid was divided into two zones which are: fluid zone (void space of the demister and the vapour space above and below the demister), and solid zone (demister wires). The boundary conditions are as follow:

- **Flow Inlet Boundary Condition:** This is defined on the inlet surface. This condition is used to define the velocity and scalar properties of the flow at inlet boundaries. The following information should be entered for this boundary condition:
  - Velocity magnitude and direction or velocity components
  - Turbulence parameters (for turbulent calculations)
  - Discrete phase boundary conditions (for discrete phase calculations)
- **Pressure Outlet Boundary Condition:** this is defined on the outlet surface (see section 6.9.1).
- **Symmetry Boundary Condition:** this is defined on the both sides of the geometry (see section 6.9.1).
- **Wall Boundary Condition:** The demister wires are defined as walls. Wall boundary condition is used to bound fluid and solid regions. In viscous flows, the no-slip boundary condition is enforced at walls by default. The shear stress and heat transfer between the fluid and wall are computed based on the flow details in the local flow field. When a particle strikes a boundary face (wire surface), it will escape through the boundary. In this case, the particle is lost from the calculation at the point where it impacts the boundary. This similar to the real case where the particle accumulates on the wire surface and then it drops back to the brine pool.

6.6 Description of the CFD code

Computational Fluid Dynamics (CFD) is a branch of fluid mechanics that uses numerical methods and algorithms to solve and analyze problems that involve fluid flows, heat transfer and associated phenomena such as chemical reactions. Computers are used to perform the calculations required to simulate the interaction of liquids and gases with surfaces defined by boundary conditions. The fundamental basis of almost all CFD problems is the Navier–Stokes equations. CFD codes are structured around the numerical algorithm that can tackle fluid flow problems. In order to provide easy access to their solving power all commercial CFD packages includes sophisticated user interfaces to input problem parameters and to examine the results. All codes contain three main elements:

1. Pre-processor: Consist of the input of a flow problem to a CFD program.
2. Solver: There are three distinct streams of numerical solution techniques (1) finite difference (2) finite element (3) spectral methods.
3. Post processor: Consist of the output of the problem. Results, 2D and 3D surface plots, grid display, and particle tracking.

Most of the well-established CFD codes (CFX/ANSYS, FLUENT, PHOENICS and STAR-CD) are using the finite volume method which is a special finite difference formulation solver (Versteeg & Malalasekera, 2007).

Fluent is the world's largest provider of commercial (CFD) software and services (Fluent 6.3 Manual, 2006). Fluent offers general-purpose CFD software for a wide range of industrial applications, along with highly automated, specially focused packages. FLUENT provides complete mesh flexibility, including the ability to solve problems using unstructured meshes that can be generated about complex geometries with relative ease. Supported mesh types include 2D triangular/quadrilateral, 3D tetrahedral/hexahedral/pyramid/wedge/polyhedral, and mixed (hybrid) meshes. It also allows refining or coarsening the grid based on the flow solution. FLUENT is written in the C computer language and makes full use of the flexibility and power offered by

the language. Consequently, true dynamic memory allocation, efficient data structures, and flexible solver control are all possible. In addition, It uses a client/server architecture, which allows it to run as separate simultaneous processes on the desktop workstations and powerful computer servers. This architecture allows for efficient execution, interactive control, and complete flexibility between different types of machines or operating systems. All functions required to compute a solution and display the results are accessible in FLUENT through an interactive, menu-driven interface (Fluent 6.3 Manual, 2006).

FLUENT package includes the following products:

1. FLUENT, the solver.
2. GAMBIT, the pre-processor for geometry modeling and mesh generation.
3. TGrid, an additional pre-processor that can generate volume meshes from existing.
4. Boundary meshes.
5. Filters (translators) for import of surface and volume meshes from CAD/CAE packages such as ANSYS, CGNS, I-deas, NASTRAN, PATRAN, and others.

There are several advantages of CFD over experimental fluid dynamics (Micale, 1993):

1) Lead time in design and development is significantly reduced.

2) CFD can study systems whose flow conditions are difficult or impossible to reproduce in experimental model tests (e.g. very large or very small systems).

3) CFD can study systems under hazardous conditions at and beyond their normal performance limits (e.g. safety studies and accident scenarios).

4) CFD provides practically unlimited level of detail of results.

5) CFD is increasingly more cost-effective than experimental testing.

It has been observed on many occasions that even simple flows are not correctly predicted by advanced CFD codes, if used without sufficient insight in both the numeric and physics involved. Developing models for complicated phenomena such as turbulence, micro-mixing, multi-phase flows and coalescence, setting up the pertinent support equations, and solving the resulting set of partial differential equations numerically, by iteration, on a fine grid of discrete points is not an easy task (Micale, 1993)

Multiphase flow refers to the situation where more than one fluid may be present, each possessing its own flow field. Multiphase flows are very frequently encountered in many engineering problems, and particularly in many unit operations of chemical process industry.

The numerical solution technique employed in most of the CFD codes is the Finite Volume Methods (FVM). It requires (Micale, 1993):

1) Integration of the problem equations over each of the computational cells.
2) The conversion of the integral equations in a set of algebraic equations by means of a suitable discretization technique, that consists in the substitution of the differential convection, diffusion and source terms into finite difference approximations.
3) An iterative solution method of the resulting algebraic equations.

6.7 Model Assumptions

FLUENT provides the flexibility in choosing discretization schemes for each governing equation. The discretized equations, along with the initial and boundary conditions, were solved using the segregated solution method to obtain a numerical solution. Using the segregated solver, the conservation of mass and momentum were solved iteratively and a pressure-correction equation was used to ensure the conservation of momentum and conservation of mass. The k–ε model was used to

treat turbulence phenomena in both phases. Each modeling approach has its own assumptions. First the assumptions of the porous media model are presented. That will be followed with these of the tube banks multiphase model. At the end the assumptions of the tube banks with discrete phase model are shown.

6.7.1 Porous Media model

The following assumptions are made in the numerical model:

1) Pressure is assumed common to both phases.
2) The turbulent diffusivity is equal to the turbulent viscosity, i.e., Schmidt number is equal to one.
3) Constant mass sink term for brine droplets was set depending on the demister removal efficiency.
4) There is no heat transfer between the two phases.
5) Pressure drop from inlet to outlet for all sectors must be the same.
6) The effect of the porous medium on the turbulence field is only approximated.

6.7.2 Tube Banks– Multi phase model

The assumptions made in this model are same as those (1-5) made for the porous media model

6.7.3 Tube banks with discrete phase model

1) A fundamental assumption made in this model is that the dispersed second phase occupies a low volume fraction, even though high mass loading is acceptable. The particle or droplet trajectories are computed individually at specified intervals during the fluid phase calculation. This makes the model

appropriate for the modeling of spray dryers, coal and liquid fuel combustion, and some particle-laden flows, but inappropriate for the modeling of liquid-liquid mixtures, fluidized beds, or any application where the volume fraction of the second phase is not negligible. The discrete phase formulation used by FLUENT contains the assumption that the second phase is sufficiently dilute as mentioned previously that particle-particle interactions and the effects of the particle volume fraction on the gas phase are negligible. In practice, these issues imply that the discrete phase must be present at a fairly low volume fraction, usually less than 10-12% (Fluent 6.3 Manual, 2006).

2) Brine droplets behave as hard spheres.

3) The particles are assumed to vanish as soon as they touch the demister wires and do not accumulate on the outer surface.

6.8 Solution Methods of the CFD codes

The multiphase flow model, which is based on Eulerian-Eulerian approach, utilized the pressure based solver. It is suitable for low speed incompressible flows. The code adapted finite-volume discretization scheme to convert the scalar transport equations into algebraic equations that can be solved numerically. To ensure convergence, we discretized in space through a first-order upwind scheme, where cell-face quantities are determined by assuming that the cell-centre values of any field variable represents cell-averages that hold throughout the entire cells: thus, face quantities are identical to cell quantities, and are set equal to the cell-centre values in the upstream cells (relative to the direction of the normal velocity) (Mazzei, Casillo, Lattieri, & Salatino, 2010). The SIMPLE (Simultaneous Solution of Non-linearity Coupled Equations) algorithm was adopted to couple pressure and velocity. Under-relaxation factors of 0.3 were adopted for all the variables.

The discrete phase flow, which is based on Eulerian-Lagrangian approach, utilized a similar approach as given in the previous paragraph to solve the Eulerian

model of the vapour phase. The brine droplets, which form the discrete phase, are modelled by the Lagrangian approach. Calculations of the droplet trajectory using a Lagrangian formulation include the discrete phase inertia, hydrodynamic drag, and the force of gravity for transient flows. It also predicts the effects of the turbulence on the dispersion of particles due to turbulent eddies present in the continuous phase. The solution scheme for the vapour (continuous phase) and droplets (discrete phase) models was based on the same solution criterion given for the Eulerian-Eulerian approach discussed in the previous paragraph. It should be stressed that the continuous phase follows a steady state model while the discrete phase follows unsteady state model to track the particle movement with time.

6.9 Conclusion

This chapter focused on presenting a number of demister models. The first is the porous media approach and the second is the tube bank-multi phase flow model. These two approaches are modeled by Eulerian-Eulerian modeling method. In these models, a constant sink value was used in order to avoid droplet accumulation within the system. In other words a constant value is set to define the removal rate of captured droplets within the demister and this value depends on the demister removal efficiency which should be known in advance. This approach is useful for simulation purposes only and not for design purposes where the removal efficiency is still unknown and need to be determined.

The last approach is the tube bank- discrete phase model. This approach is more general and allows us to track the droplets motion since it is modeled by the Eulerian-Lagrangian combination. This approach is used for both simulation and design purposes as shown in the next chapter because it doesn’t need a prior knowledge of the demister removal efficiency.

The three approaches have been validated against experimental and data from real MSF plants. The validation results for the three approaches are shown in the next chapter. In addition, a number of new demister designs are analyzed using the third

approach to predict its removal efficiency and temperature/pressure drop across the demister. The new designs focused on evaluating their performance as a function of flashing stage conditions and wire diameter/spacing.

Chapter 7
Validation and Results of CFD Modeling of the Demister

7.1 Introduction

The mathematical models presented in chapter 6 were simulated using the Computational Fluid Dynamics (CFD) tool FLUENT and the results are presented in this chapter. In the first section, the Porous Media Approach model is simulated and the predicted results are validated against experimental and data obtained from real MSF plant. Next, the Tube Banks –Multi phase Approach model is presented. In this section, the model is validated against real and experimental data. In the third section, the Tube Banks –Discrete phase model Approach is simulated and after validating the model against experimental and real data from MSF plants (details in table 7.3, 7.10 and 7.11) new demisters geometries are designed and simulated by the same approach to obtain a demister with lower pressure drop and unaffected separation efficiency.

7.2 Porous Media – Multi Phase Model Approach

The porous media approach follows the Eulerian-Eulerian modeling method mentioned previously in section 6.4. In this approach a constant sink value (section 6.4.2) is set for the porous media in order to prevent brine droplets accumulation in the demister through simulations. This value depends on the design removal efficiency of the demister which should be known before running the simulator. Thus this approach is useful and important for simulation and troubleshooting purposes. An example is studying the effect of changing some of the operating parameters (velocity, brine droplet concentration and temperature) on the pressure/temperature drop across the demister. This approach is not applicable for design purposes where the removal efficiency is not known.

Before starting simulations of the runs, grid analysis should be done to see the effect of the number of grid points on the solution accuracy and to obtain the optimum number of grid points at which the results will remain the same as we increase the number of grid points. Next the simulation will be applied for an experimental demister and a demister installed in the flashing stages of real plants in order to validate the model. At the end of this section, the effect of some design and operating parameters on the demister performance (sensitivity analysis) will be shown.

7.2.1 Grid Sensitivity Analysis

The first step in the modeling procedure is constructing the geometry which represents the demister. The geometry was constructed using GAMBIT. The GAMBIT software package is designed to help analysts and designers build and mesh models for computational fluid dynamics (CFD) and other scientific applications (Gambit 2.3 Manual, 2006).

GAMBIT contains the following meshing schemes:

- Quad: Specifies that the mesh includes only quadrilateral mesh elements.
- Tri: Specifies that the mesh includes only triangular mesh elements.
- Quad/Tri: Specifies that the mesh is composed primarily of quadrilateral mesh elements but includes triangular corner elements at user-specified locations.

For the geometry in this study, a Quad scheme (Figure.7.1(b)) was selected because it is the most accurate and easiest to converge. Other schemes were chosen when the Quad scheme was not able to be used due to the complexity in the geometry.

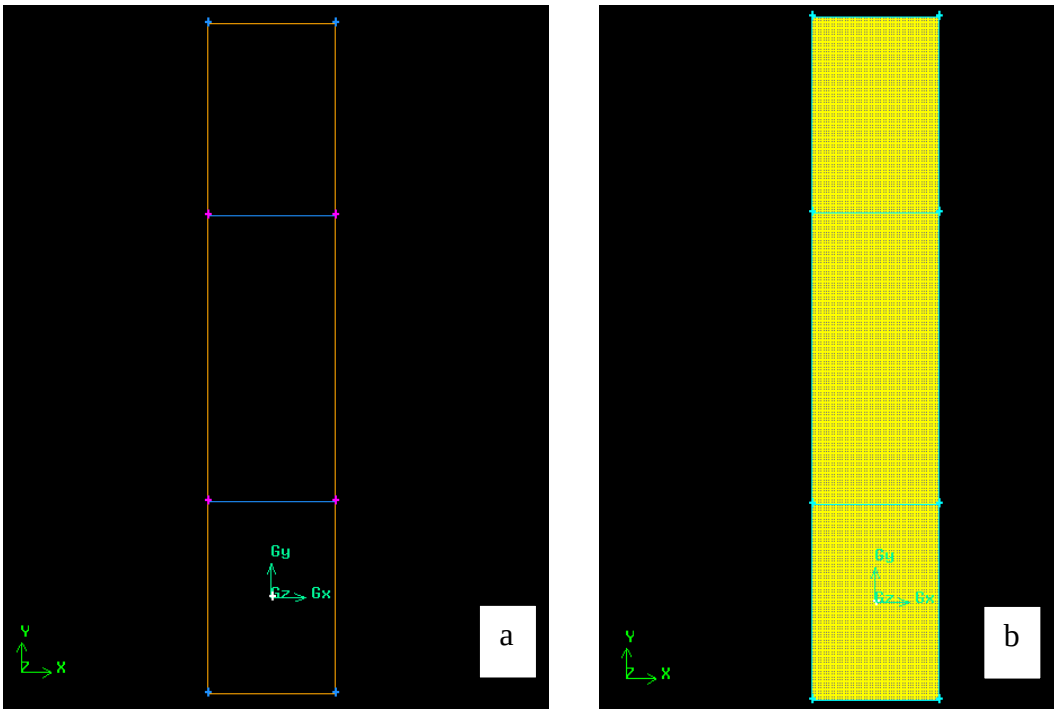

Figure.7.1 Schematic diagram of the porous media geometry (a) before meshing (b) after meshing

The grid analysis is done to predict the minimum number of grid points which should be used to get accurate results as mentioned previously. That was achieved by simulating the same geometry (demister) with the same boundary conditions and same operating variables with a different number of grid points.

The grid analysis was done using FLUENT for three different operating conditions (see table 7.1):

1- Lab scale demister ((El-Dessouky, Alatiqi, Ettouney, & Al-Deffeeri, 2000)
2- Demister installed in real MSF plant operating at high temperature (Table 5.3)
3- Demister installed in real MSF plant operating at low temperature (Table 5.1,5.4).

It should be noted that the industry use the same type of demister (material, packing density, and wire diameter) in all flashing stages. Also, in the laboratory

experiments the demister was obtained from the industry; therefore, the demister characteristics for the three data sets are exactly the same.

The predicted results include the separation efficiency, the pressure drop, and the x and y velocity components of the flow. The aim behind using these different conditions and comparing these different results is to ensure that the obtained optimum number of grid points is applicable for any set of conditions. Also it should be noticed that it is applicable to any type and size of plant since it doesn't depend on the size of the flashing stage but on the vapour flow temperature, pressure and concentration.

The model presented in section 6.4 is first simulated for steady state condition with a maximum number of iterations in each time step of 4. Next the same model is simulated for transient conditions with a time step = 0.0001 second, number of time steps =50000 which will result in a total time of 5 seconds. Both models (steady state and transient) are repeated for the same demister but with a different number of grid points. The obtained results include separation efficiency (brine droplets removal efficiency) and pressure drop between the inlet and the outlet of the geometry (demister) as well as the x and y velocity components of the flow.

Table 7.1: Input operating conditions and design parameter to the FLUENT code used for grid analysis.

	Lab scale demister	High Temperature Flashing Stage Stage (1)	Low Temperature Flashing Stage Stage (23)
Velocity range (m/s)	2.44	1.252	9.718
Packing density (kg/m^3)	80.317	80.317	80.317
Water droplet volume fraction in the inlet stream	7.34×10^{-5}	1.37×10^{-5}	3.78×10^{-5}
Droplet diameter	12 µm*	10 μm^{+}	8 μm^{+}
Porosity	0.9899	0.9899	0.9899
Temperature (K)	373.15	377.548	313.1

+ (Brunazzi & Paglianti, 1998)
* (Al-Deffeeri, 2009)

As shown in Figures (7.2-7.5), the separation efficiency, the pressure drop, and the x and y velocity components for both steady state and transient model remain constant and unaffected by the number of grid points at 52500 cells. The percentage error in prediction of all variables using different number of grid points remained below 0.1% for number of grid points greater than 52500. That means that the model can be simulated accurately with 52500 grid points. Using the minimum number of grid points will speed the simulation without affecting the results.

In all simulations, the residual values were set to a maximum value of 1×10^{-8}. For the steady state model the simulation stops when the residual is less than the set value. For the transient model, the simulations end up with a residual less than 1×10^{-13} which is very good.

As shown in Figures (7.2-7.5), there is negligible difference between the steady state model and the transient model results (maximum difference = 0.0115%) for the three different operating conditions. In other words, at the end of the simulation time and when no disturbance occurs in the operating condition (velocity, temperature and concentration) the transient model will approach the results of the steady state model. Thus, for simplicity and time saving, steady state model will be used to simulate all runs. This is because study of the demister dynamic responses to variations in the operating conditions is not the focus of this study. Also as shown in Figures (7.2-7.5) for the high temperature stage (specific volume is low) the velocity is lower than the low temperature stages and thus it has lower pressure drop and higher separation efficiency. On the other hand, the velocity in the experiment is lower than the velocity in the low temperature stages but has lower removal efficiency. The reason behind this is that the free space between the brine top surface and the demister bottom surface is much larger in the real plant (close to 1 meter) than in the experiment (less than 0.5 m); therefore, the real plant configuration allows for more efficient particle settling in the free board zone (Al-Deffeeri, 2009).

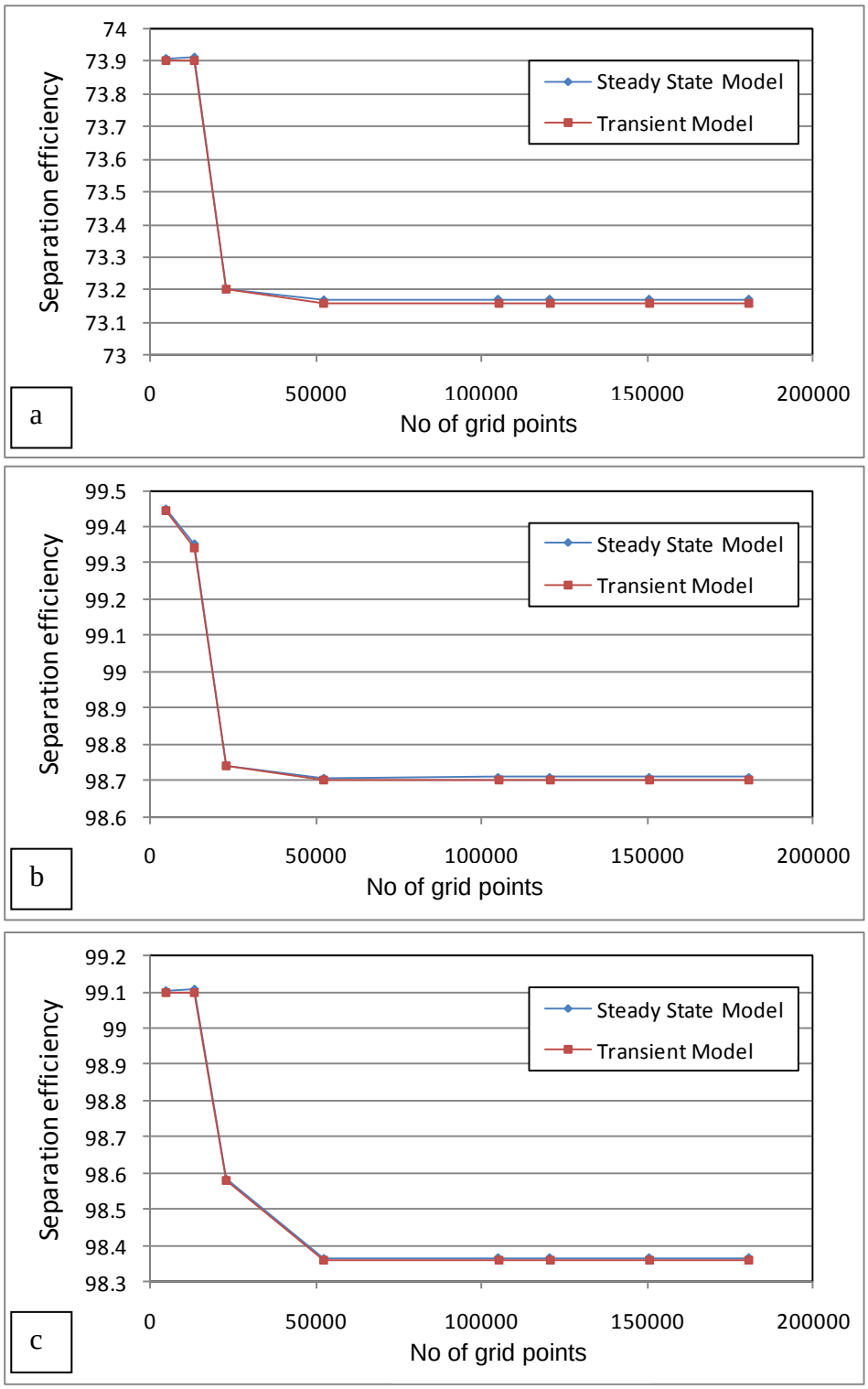

Figure 7.2 Separation efficiency values obtained for porous media geometry of different gird number (a) lab scale demister (b) high temperature stage demister (c) low temperature stage demister

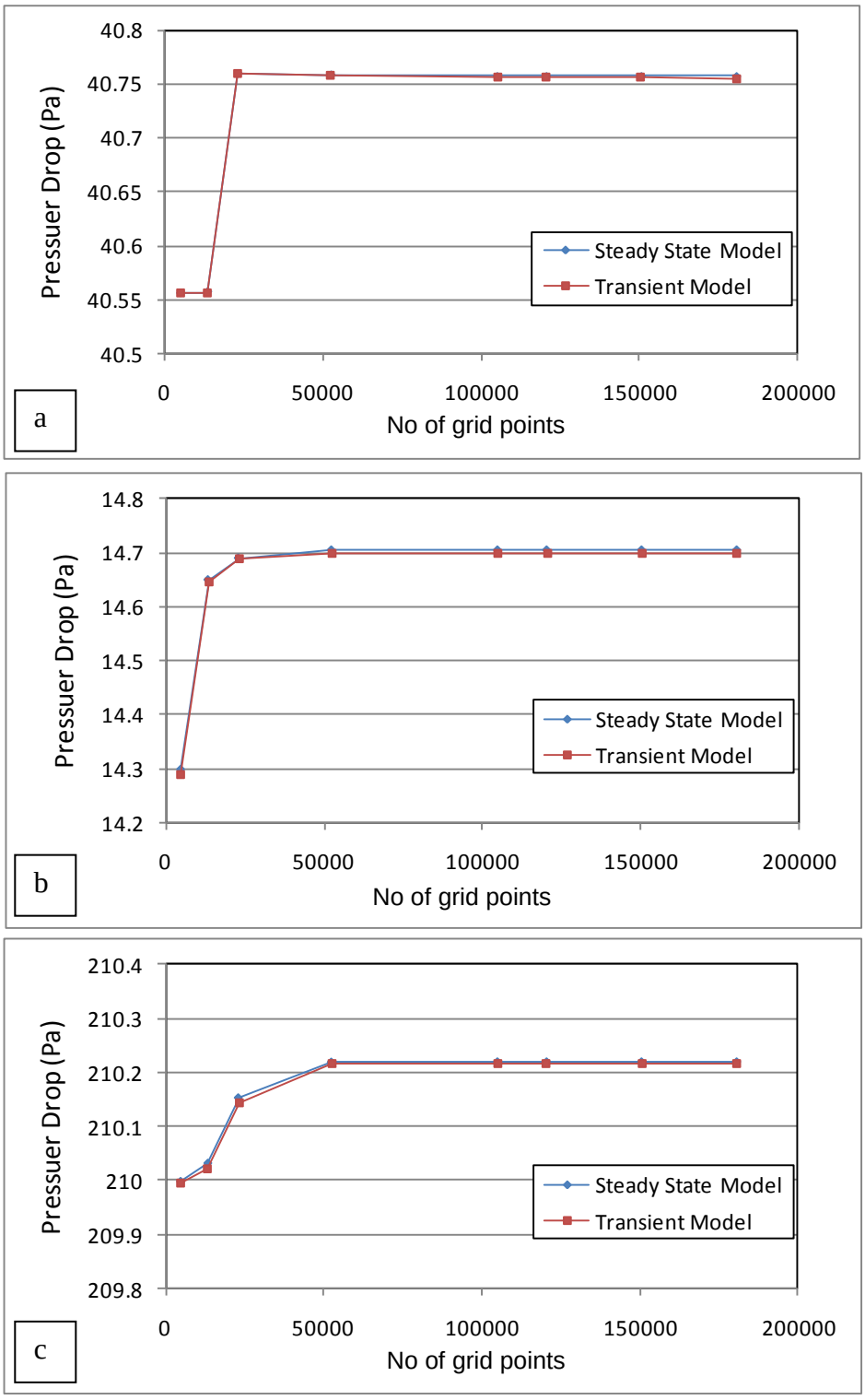

Figure 7.3 Pressure drop values obtained for porous media geometry of different gird number. (a) lab scale demister (b) high temperature stage demister (c) low temperature stage demister

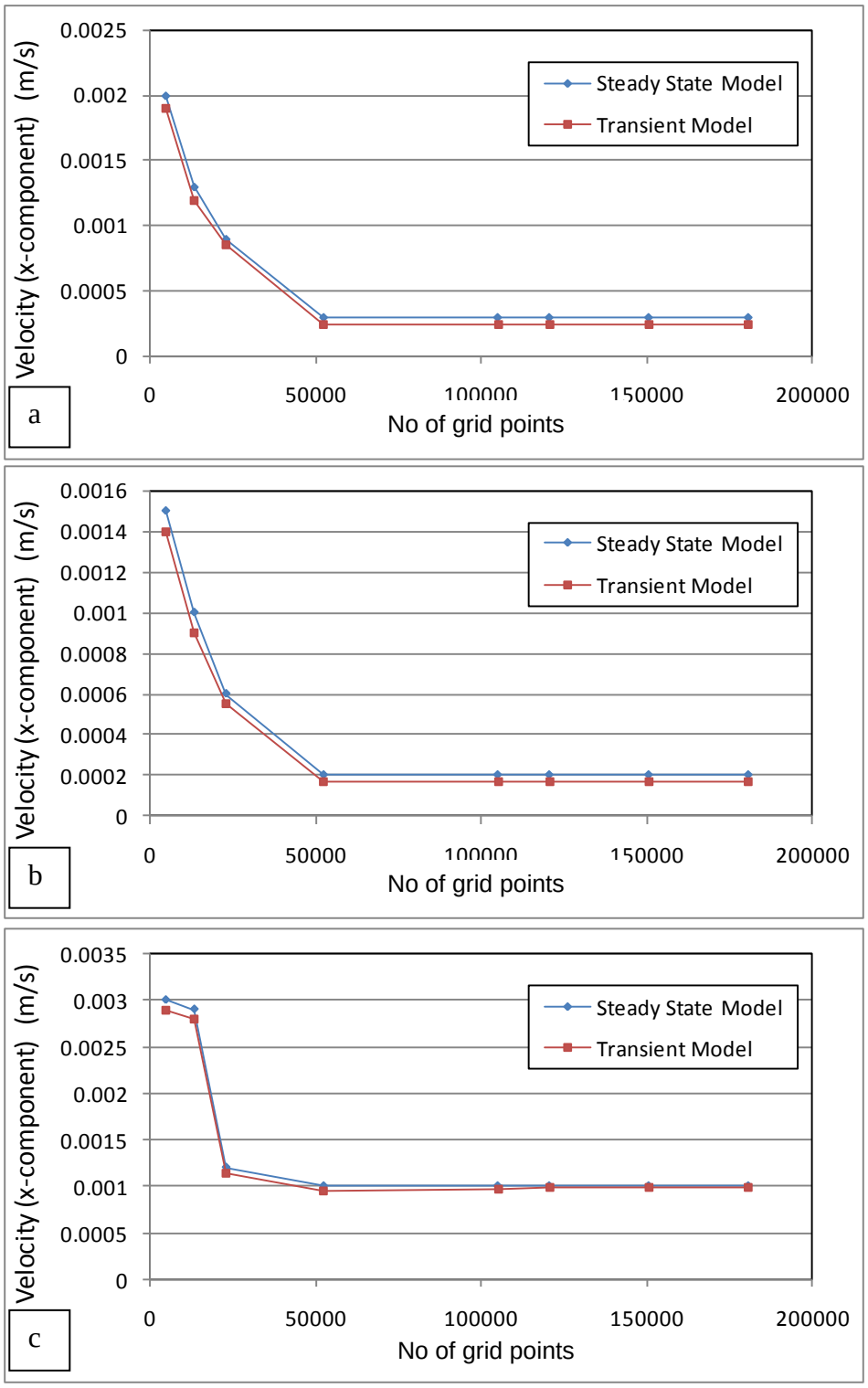

Figure 7.4 Velocity (x-component) values obtained for porous media geometry of different gird number. (a) lab scale demister (b) high temperature stage demister (c) low temperature stage demister

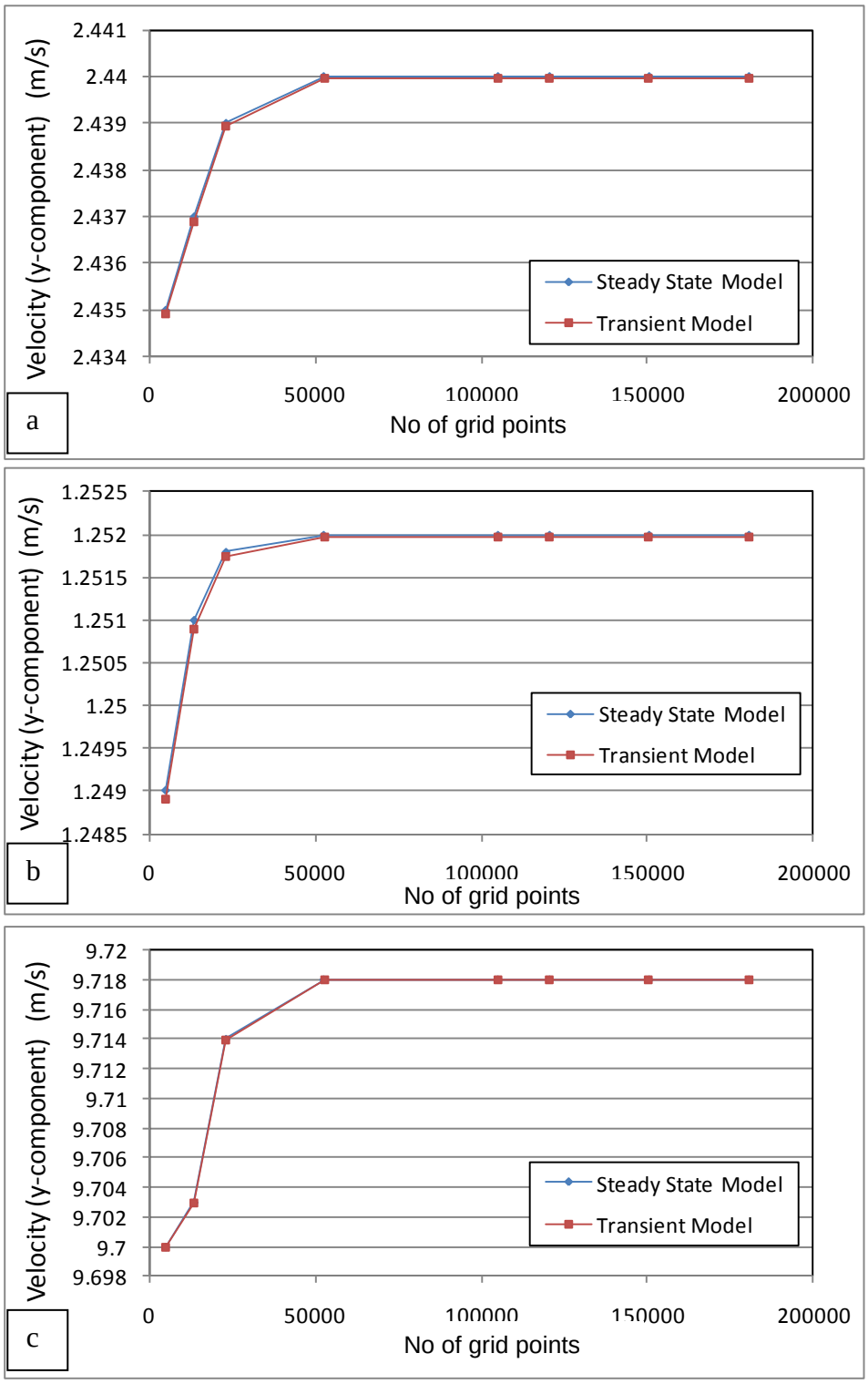

Figure 7.5 Velocity (y-component) values obtained for porous media geometry of different gird number. (a) lab scale demister (b) high temperature stage demister (c) low temperature stage demister

7.2.2 Cases investigated, geometries and boundary conditions

The CFD FLUENT code was used to simulate a lab scale wire mesh demister. The experiment was done by El-Dessouky et al. (2000), where an industrial type demister was used. All experimental measurements were taken at steady state conditions. The ranges of the experimental variables were as follows: 1) vapour velocity (0.98–7.5 m/s), 2) packing density (80.317–208.16 kg/m^3), 3) demister pad thickness (100–200mm), 4) wire diameter (0.2–0.32 mm), and 5) droplet size (1–5 mm). It should be noted that the above experimental ranges vary from high to intermediate temperatures of industrial scale flashing stages. The error analysis of the experimental data gave errors of 2.4% for temperature, 3.15% for flow rate, 2.73% for pressure drop, 2.31% for absolute pressure and 1.19% for liquid level. On the basis of these errors, the pressure drop of the wet demister, separation efficiency, and velocities for loading and flooding may depart by 4.6, 3.2 and 4.1% from the true values (El-Dessouky, Alatiqi, Ettouney, & Al-Deffeeri, 2000).

The CFD model is applied to each run in the experiment. Table 7.2 includes the operating conditions and design parameters of the demister which are used as input to the model.

Table 7.2: Input operating conditions and design parameter to the FLUENT code.

Velocity range (m/s)	1.13 – 10.4
Packing density (kg/m^3)	80.317-104.6-176.36-208.16
Water droplet volume fraction in the inlet stream	1.0E-5
Droplet diameter	10 μm = 10E-6 m
Porosity	Calculated for the packing density (0.974-0.9899)

Also, the CFD FLUENT code is used to simulate a wire mesh demister installed in an operating multistage flashing (MSF) desalination plant. The demister used in this plant has a packing density = 80.317 kg/m^3 and 0.28 mm wire diameter. Table 7.3 includes the operating condition of each flashing stages which is used as

input to the simulator. Each flashing stage represents a separate simulation condition because it has its own set of operating conditions. This wide range of conditions will make the model more general and applicable for any demister installed in any plant

Table 7.3: Operating conditions of the flashing stages of MSF-BC plant D (Kuwait – MEW) operating at low temperature

Stage	Vapour temperature below demister (K)	Vapour density (kg/m^3)	Droplet density (kg/m^3)	Flashed off Vapour Velocity (m/s)	Inlet Volume Fraction of Droplet in Flashed off Vapour
1	361.690	0.417	1013.3	1.829	3.181E-06
2	359.256	0.382	1015.1	2.805	2.898E-06
3	356.852	0.350	1016.8	3.006	2.638E-06
4	354.477	0.320	1018.5	3.183	2.402E-06
5	352.131	0.293	1020.1	3.408	2.186E-06
6	349.814	0.268	1021.7	3.649	1.990E-06
7	347.526	0.246	1023.2	4.051	1.813E-06
8	345.267	0.225	1024.7	4.183	1.650E-06
9	343.038	0.206	1026.2	4.498	1.501E-06
10	340.838	0.188	1027.6	4.587	1.365E-06
11	338.667	0.172	1029.0	4.630	1.242E-06
12	336.525	0.157	1030.3	4.724	1.132E-06
13	334.413	0.144	1031.6	4.777	1.030E-06
14	332.330	0.132	1032.8	4.925	9.391E-07
15	330.276	0.120	1034.0	5.015	8.543E-07
16	328.251	0.110	1035.2	5.553	7.778E-07
17	326.255	0.101	1036.4	5.923	7.086E-07
18	324.288	0.092	1037.5	6.318	6.458E-07
19	322.351	0.085	1038.5	6.637	5.896E-07
20	320.443	0.077	1039.6	7.178	5.378E-07
21	318.564	0.071	1040.5	7.628	4.910E-07
22	316.714	0.065	1041.5	8.305	4.484E-07
23	314.894	0.060	1042.4	8.612	4.107E-07
24	313.103	0.055	1043.3	9.718	3.756E-07

In the above table the values of the inlet volume fraction of droplet in flashed off vapour was calculated from the mass balance on the demister and by knowing the removal efficiency of the demister. It is mainly affected by the brine densilty and temperature.

7.2.3 Model validation

The porous media model has been simulated for the different conditions of the experiment done by El-Dessouky et al (2000) to validate the model. As shown in Figures (7.6-7.9), validation of the model showed very good agreement between the CFD results and the experimental data with an error less than 6%.

The wet demister in Figures (7.6-7.9) refers to the condition at which the water droplets are entrained inside the pad. The pressure drop for the dry demister is the lowest and is almost linearly proportional to the vapour velocity. The pressure drop for the dry demister is a measure of the relative resistance of the fluid flow through the pad. This arises from the viscous drag between the vapour and the wires forming the demister pad and also because of kinetic energy loss due to the changes of the flow direction. The specific pressure drop in wet demisters is caused by the dry pad and due to the presence of water droplets (El-Dessouky, Alatiqi, Ettouney, & Al-Deffeeri, 2000).

The pressure drop of the wet demister (Figures 7.6-7.9) is complicated and there are three contributions to this pressure drop. The first term represents the frictional pressure drop because of the slip between the vapour phase and the demister pad. The second term represents the pressure drop due to the vapour phase acceleration. The last term accounts for the gravitational effects, which is smaller than the other two terms and can be safely neglected (El-Dessouky et al, 2000). The frictional and acceleration pressure drops are strongly dependent on the vapour velocity. The vapour velocity inside the demister is changing as a result of variations in the system operating parameters or due to the hold-up of the liquid phase. As the liquid hold-up progressively increases, the free space area available for the vapour flow decreases and results in rapid increase in the flow resistance. The liquid hold-up may be either static or dynamic. Capillary action causes the static hold-up and occurs at high retention of the liquid within the demister pad. Dynamic hold-up takes place, as the settling velocity of the falling droplets becomes lower than the upward vapour velocity. The static hold-up increases with the increase of the wire surface area, which is directly related to the packing density. (El-Dessouky et al, 2000). As shown in table

7.4, comparison between the experimental data, CFD results and the empirical correlation values obtained by El-Dessouky et al (2000) (Equation 4.20) which is applicable for the whole range of the data, showed that the difference between the CFD results and the experimental data in all runs did not exceed 6% while for the empirical correlation it reached 32.49%. That makes the CFD model more accurate than the correlation.

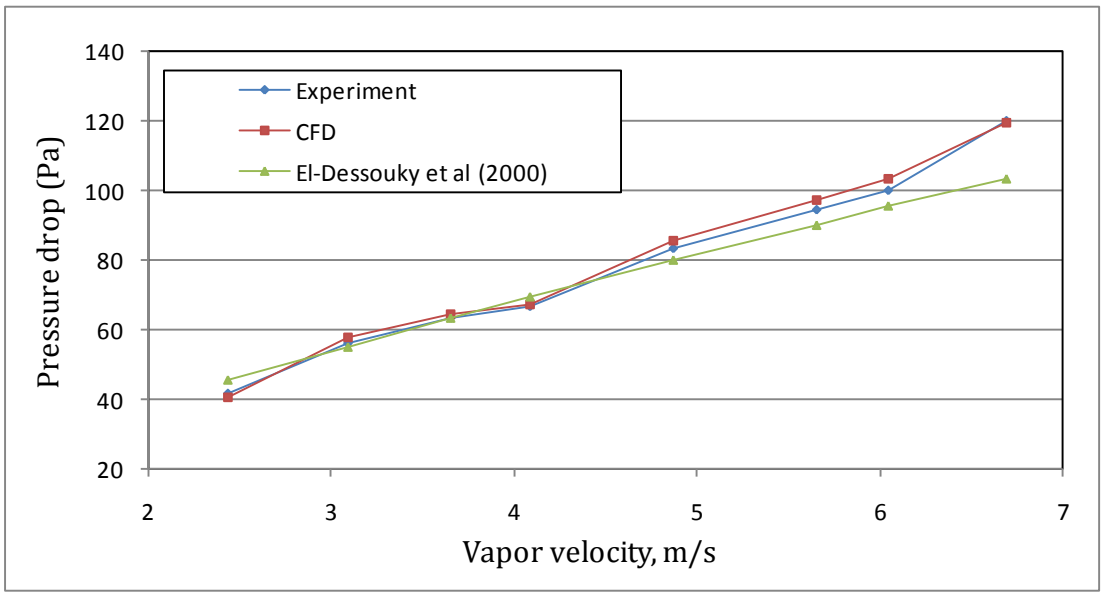

Figure 7.6 Variation in pressure drop as a function of vapour velocity for demister with packing density =80.317 kg/m^3

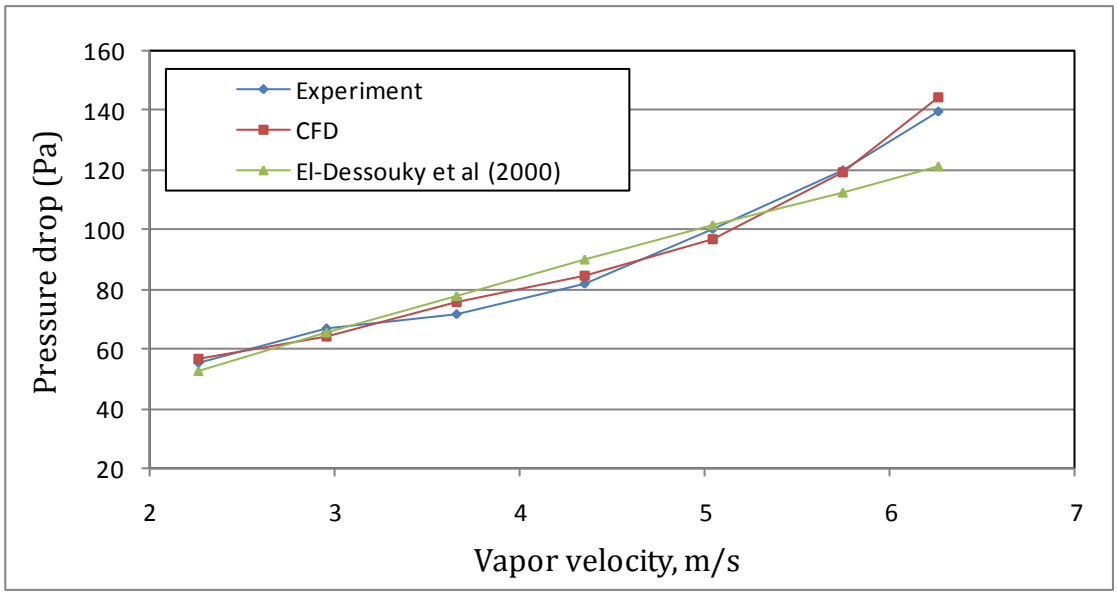

Figure 7.7 Variation in pressure drop as a function of vapour velocity for demister with packing density =140.6 kg/m^3

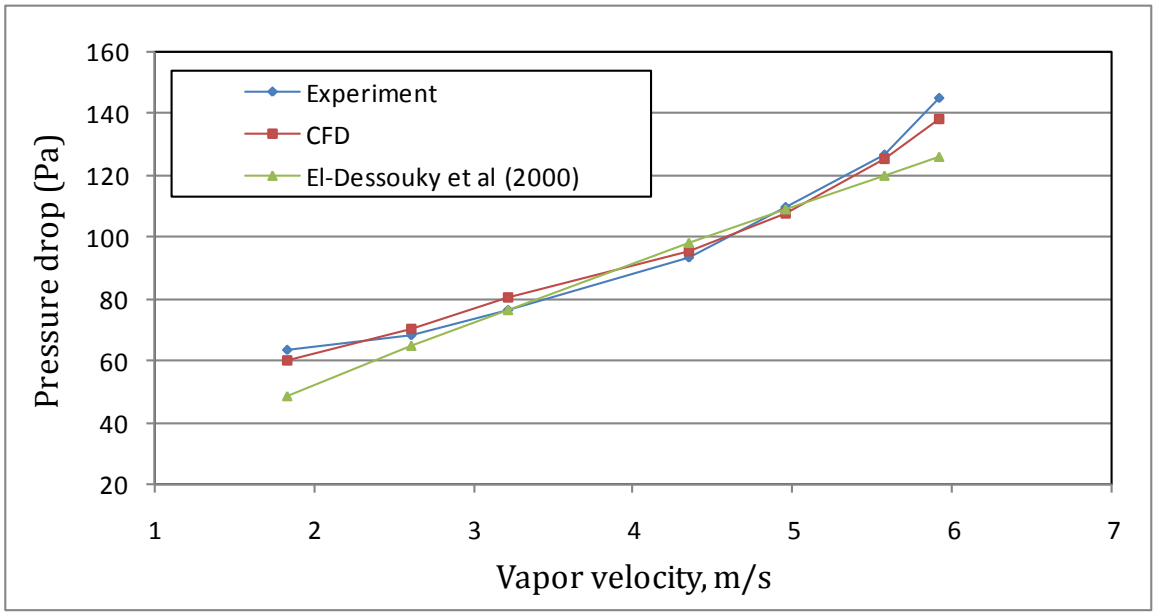

Figure 7.8 Variation in pressure drop as a function of vapour velocity for demister with packing density =176.35 kg/m^3

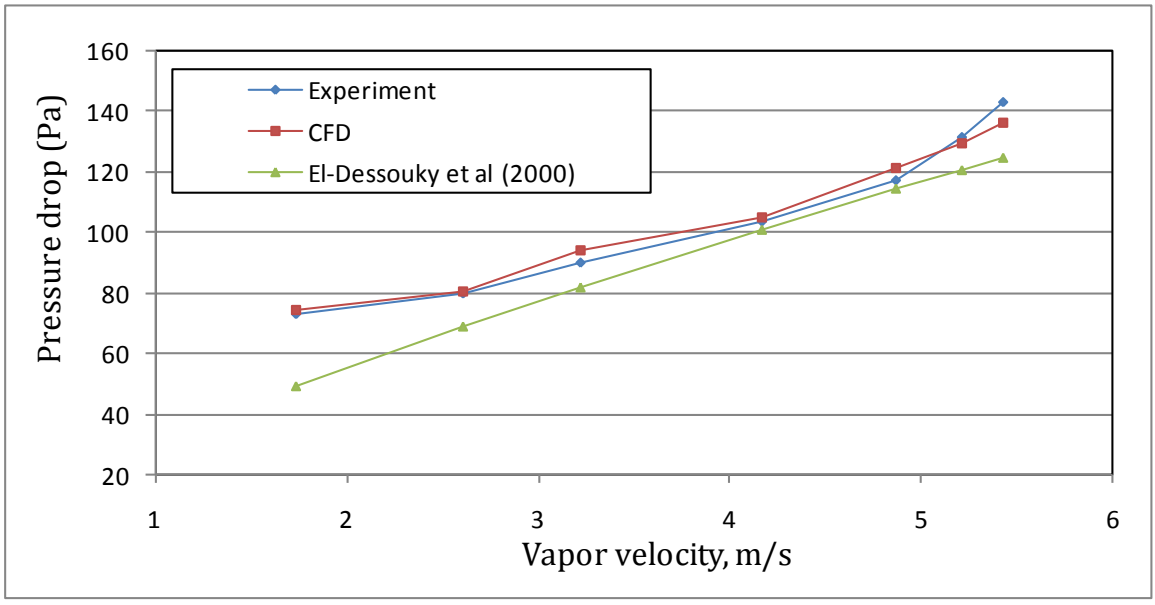

Figure 7.9 Variation in pressure drop as a function of vapour velocity for demister with packing density =208.16 kg/m^3

Table 7.4: Comparison between CFD porous media model results, empirical correlation results and experimental data

Packing Density	Vapour Velocity	Experimental El-Dessouky et al. (2000)	CFD (This Work)		Correlation El-Dessouky et al. (2000)	
kg/m^3	m/s	Pressure Drop (Pa)	Pressure Drop (Pa)	% Error	Pressure Drop (Pa)	% Error
80.317	2.435	41.667	40.750	2.200	45.527	9.264
	3.096	56.000	58.000	3.571	55.345	1.171
	3.652	63.333	64.620	2.031	63.308	0.040
	4.087	66.667	67.563	1.344	69.372	4.057
	4.870	83.333	85.863	3.035	79.994	4.008
	5.652	94.333	97.412	3.264	90.300	4.275
	6.052	100.000	103.681	**3.681**	95.463	4.537
	6.696	120.000	119.877	0.102	103.638	**13.635**
140.600	2.261	55.667	56.910	2.234	52.903	4.964
	2.957	66.667	64.432	3.353	65.799	1.301
	3.652	71.667	75.910	**5.921**	78.135	9.025
	4.348	81.667	84.576	3.562	90.037	10.249
	5.043	100.000	96.791	3.209	101.586	1.586
	5.739	120.000	119.017	0.819	112.841	5.966
	6.261	140.000	144.499	3.214	121.114	**13.490**
176.350	1.826	63.333	60.242	4.880	48.421	**23.546**
	2.609	68.333	70.111	2.601	64.713	5.298
	3.217	76.667	80.574	**5.097**	76.746	0.104
	4.348	93.333	95.391	2.204	98.038	5.041
	4.957	110.000	108.119	1.710	109.060	0.854
	5.565	126.667	125.763	0.713	119.832	5.396
	5.913	145.000	138.096	4.761	125.888	13.181
208.160	1.739	73.333	74.246	1.245	49.530	**32.459**
	2.609	80.000	80.836	1.045	68.875	13.907
	3.217	90.000	94.153	4.615	81.681	9.243
	4.174	104.000	104.879	0.845	100.935	2.947
	4.870	117.333	121.450	3.509	114.415	2.487
	5.217	131.667	129.511	1.638	121.017	8.088
	5.426	143.333	136.195	**4.980**	124.939	12.833

Next the porous media model was simulated for the demisters installed in the flashing stages of real MSF desalination plant. Each demister has different operating conditions (velocity, temperature and concentration). As shown in Table 7.5 and Figures 7.10-7.11, the model validation showed very good agreement between the CFD predicted results and real demister data with an error less than 9.6% except for the last stage it reached 28%. On the other hand the empirical correlation results were far away from the real data with an error which had exceeded 52%.

Table 7.5.: Comparison between CFD results obtained by porous media model, empirical correlation results and real plant (Plant D) unit data

Stage	Vapour Pressure below demister	Vapour Pressure above demister	ΔP demister (Real)	CFD (This Work)		Correlation El-Dessouky et al (2000)	
	kPa	kPa	Pa	Pressure Drop (Pa)	% Error	Pressure Drop (Pa)	% Error
1	66.377	66.352	25.442	23.842	6.288	36.076	41.798
2	60.421	60.386	35.277	38.632	9.510	51.086	44.812
3	54.981	54.938	43.462	43.486	0.053	54.037	24.330
4	50.017	49.973	44.161	45.414	2.837	56.606	28.179
5	45.488	45.432	55.600	51.944	6.576	59.839	7.625
6	41.359	41.290	68.419	70.425	2.932	63.258	7.543
7	37.596	37.526	69.445	70.563	1.611	68.870	0.828
8	34.168	34.095	72.791	71.293	2.058	70.697	2.876
9	31.047	30.967	80.542	79.354	1.475	74.999	6.883
10	28.207	28.121	86.621	81.437	5.984	76.205	12.025
11	25.624	25.532	91.236	91.335	0.109	76.784	15.840
12	23.274	23.169	105.062	103.526	1.462	78.044	25.716
13	21.139	21.032	106.465	106.171	0.276	78.750	26.032
14	19.199	19.083	115.871	119.533	3.160	80.740	30.319
15	17.436	17.305	131.285	123.786	5.712	81.931	37.593
16	15.836	15.700	135.978	137.718	1.280	89.012	34.539
17	14.383	14.223	159.851	145.555	8.943	93.805	41.317
18	13.065	12.879	185.376	170.222	8.175	98.860	46.670
19	11.868	11.680	188.249	178.255	5.309	102.895	45.341
20	10.783	10.583	200.225	188.312	5.950	109.676	45.224

Table 7.5 (Continued).: Comparison between CFD results obtained by porous media model, empirical correlation results and real plant (Plant D) unit data

Stage	Vapour Pressure below demister	Vapour Pressure above demister	ΔP demister (Real)	CFD (This Work)		Correlation El-Dessouky et al (2000)	
	kPa	kPa	Pa	Pressure Drop (Pa)	% Error	Pressure Drop (Pa)	% Error
21	9.799	9.595	204.146	190.012	6.923	115.224	43.558
22	8.907	8.701	206.173	195.782	5.040	123.478	40.110
23	8.098	7.879	219.094	199.495	8.946	127.183	41.950
24	7.365	7.071	293.358	210.221	**28.340**	140.308	**52.17**

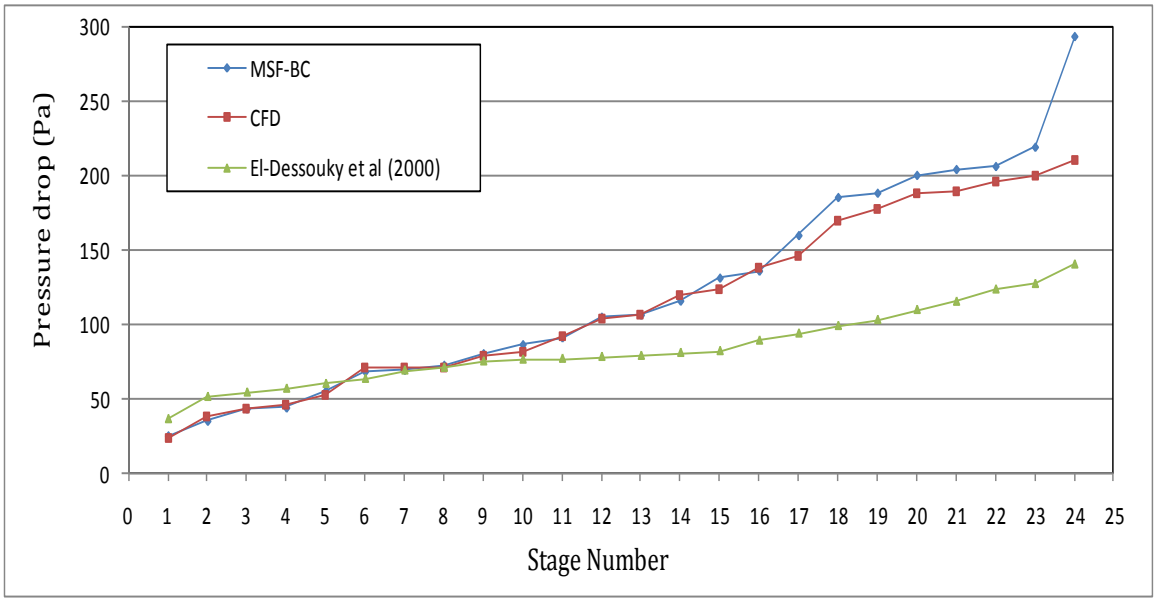

Figure.7.10 Variation in pressure drop as a function of MSF-BC stage number for demister with packing density =80.317 kg/m^3

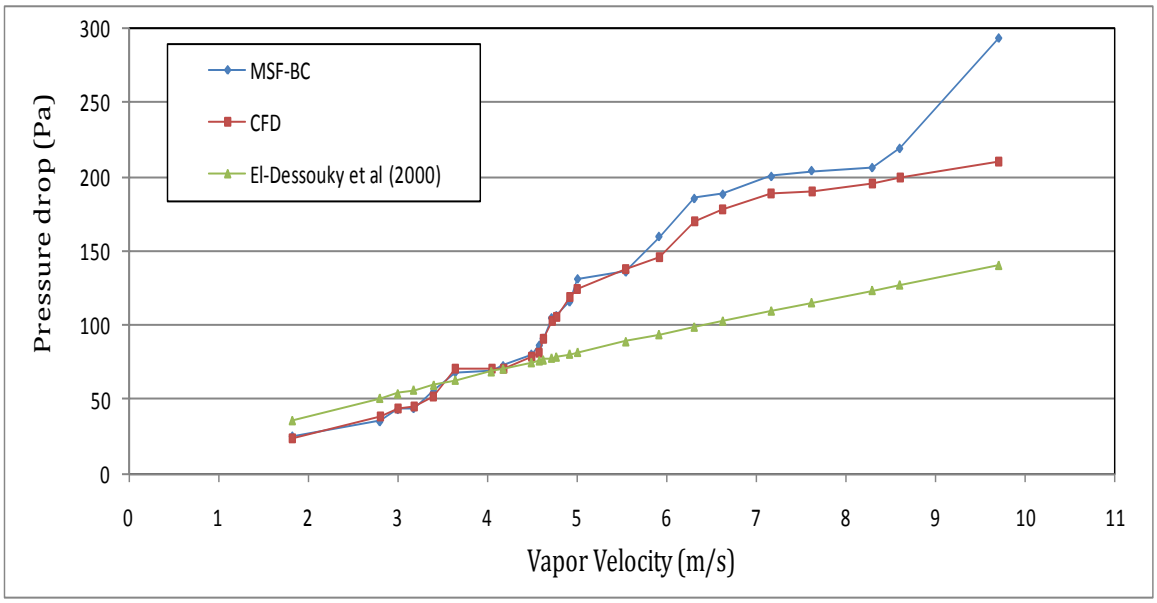

Figure 7.11 Variation in pressure drop as a function of MSF-BC stage vapour velocity for demister with packing density =80.317 kg/m^3

7.2.4 Modeling results and Discussion

The model has been validated against experimental data and real MSF plant data and showed a very good agreement. Next, the model was used to do a sensitivity analysis and study the effect of some operating parameters (Inlet temperature, flashed off vapour velocity and flashed off vapour composition) and design parameter (face permeability of the medium). The face permeability is defined as the capacity of the porous media face for transmitting a fluid. It is largely dependent on the size and shape of the pores in the substance.

As shown in Figure 7.12, as the velocity increases the pressure drop increases and the reason behind that was discussed in the previous section. Also, it is shown the temperature has no direct effect on the pressure drop if the velocity was maintained. In other words, the increase in temperature will lead to an increase in the vapour specific volume and that will lead to an increase in the vapour velocity. Again the pressure drop will be affected by the change in velocity.

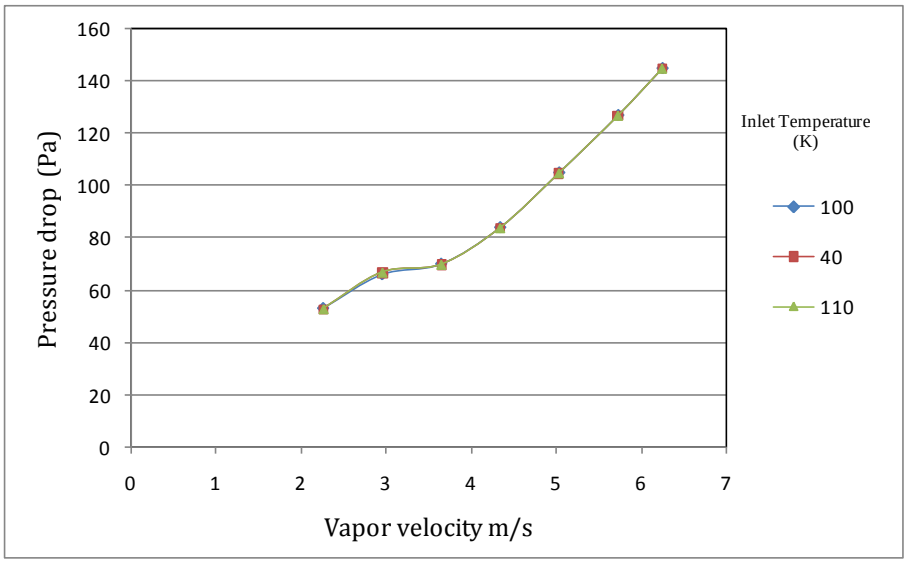

Figure 7.12 Effect of the vapour inlet temperature on the Pressure drop per across the demister at different values of vapour velocities

As shown in Figure 7.13, as the face permeability increases the pressure drop decreases. That is because as the face permeability increases it will reduce the amount of resistance force applied on the flow and less pressure drop will result.

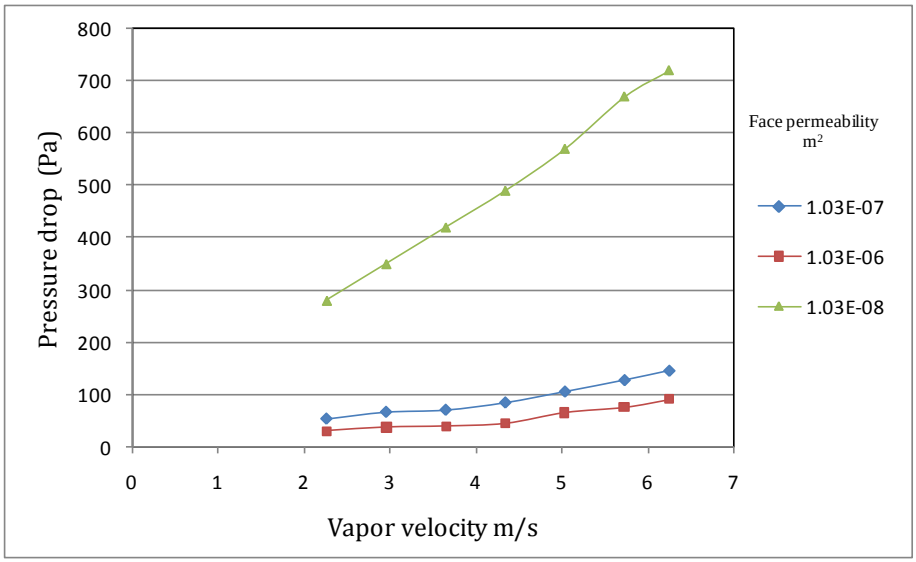

Figure 7.13 Effect of the face permeability on the Pressure drop across the demister at different values of vapour velocities

As shown in Figure 7.14, as the volume fraction of the water droplet increases in the flashed off vapour passing through the demister, the pressure drop increases. That is because as the number of droplets in the vapour stream increases, more liquid

will accumulate in the demister until it settles down and that will lead to an increase in the resistance force at the vapour flow resulting in the increase of the pressure drop.

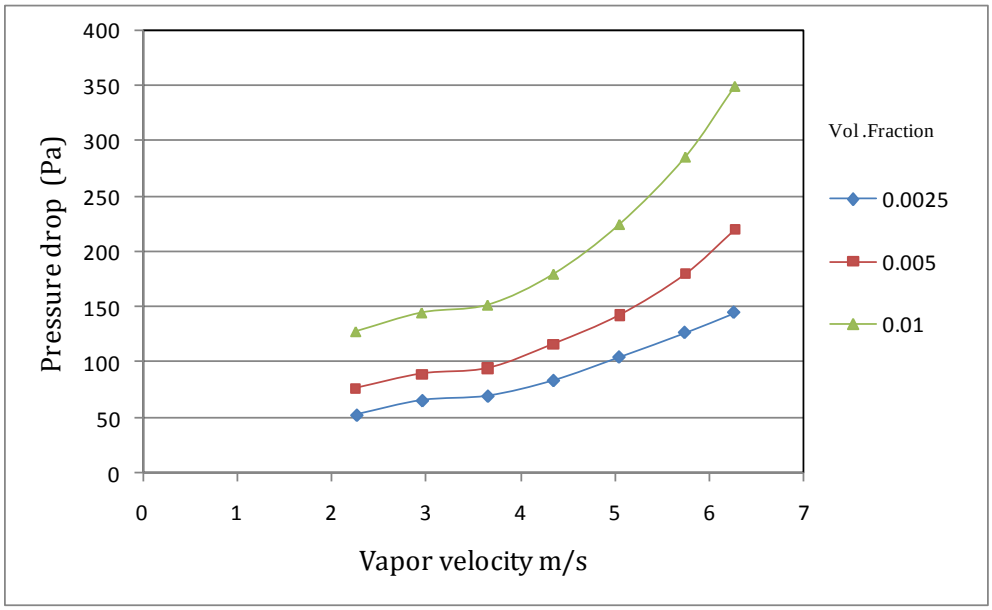

Figure 7.14 Effect of the liquid volume fraction in the inlet stream on the Pressure drop across the demister at different values of vapour velocities

7.3 Tube Banks – Multi Phase Model Approach

The tube bank with multi phase flow model approach follows the Eulerian-Eulerian model presented in section 6.4 in the same way as the porous media approach. In this approach a constant sink value is also set for the fluid region around the tubes in order to prevent brine droplet accumulation in the demister through simulations. As mentioned previously, this value depends on the design removal efficiency of the demister which should be known before running the simulator. Thus this approach is useful and important for operating and troubleshooting purposes. An example is studying the effect of changing some of the operating parameters (velocity, brine droplet concentration and temperature) on the pressure/temperature drop. This approach is not applicable for design purposes where the removal efficiency needs to be evaluated.

To run the simulations, the commercial CFD code Fluent 6.3 was employed. Before starting simulations of the runs, grid analysis should be done. Next the simulation will be applied for an experimental demister and a demister installed in the flashing stages of real plants in order to validate the model.

7.3.1 Grid Sensitivity Analysis

For the geometry in this study, the Quad scheme (Figure 7.15(b)) was selected because it is the most accurate and easiest to converge. But around the wires (Figure 7.15(c)) the Tri scheme was selected because the Quad scheme was not able to be done due to the complexity in the geometry.

The grid analysis was done in the same way as mentioned for the porous media approach in section 7.2.1 and for the same input operating and design conditions mentioned in table 7.1. In all simulations, the residual values were set to a maximum value of 1×10^{-8}. For the steady state model the simulation stops when the residual is less than the set value. For the transient model, the simulations end up with a residual less than 1×10^{-9} which is very good.

As shown in Figures (7.16-7.19), the separation efficiency, the pressure drop, and the x and y velocity components of the flow for both steady state and transient model remain constant and unaffected by the number of grid points at 204481 cells. That means that the model can be simulated with 204481 grid points without the need of further grid points. Using a minimum number of grid points will speed the simulation without affecting the results. That is applicable for both steady state and transient models.

As mentioned previously, steady state models can be used when no change occurs in the operating or design parameters with time while, transient models can be used to study the effect of any disturbance on the system behaviour.

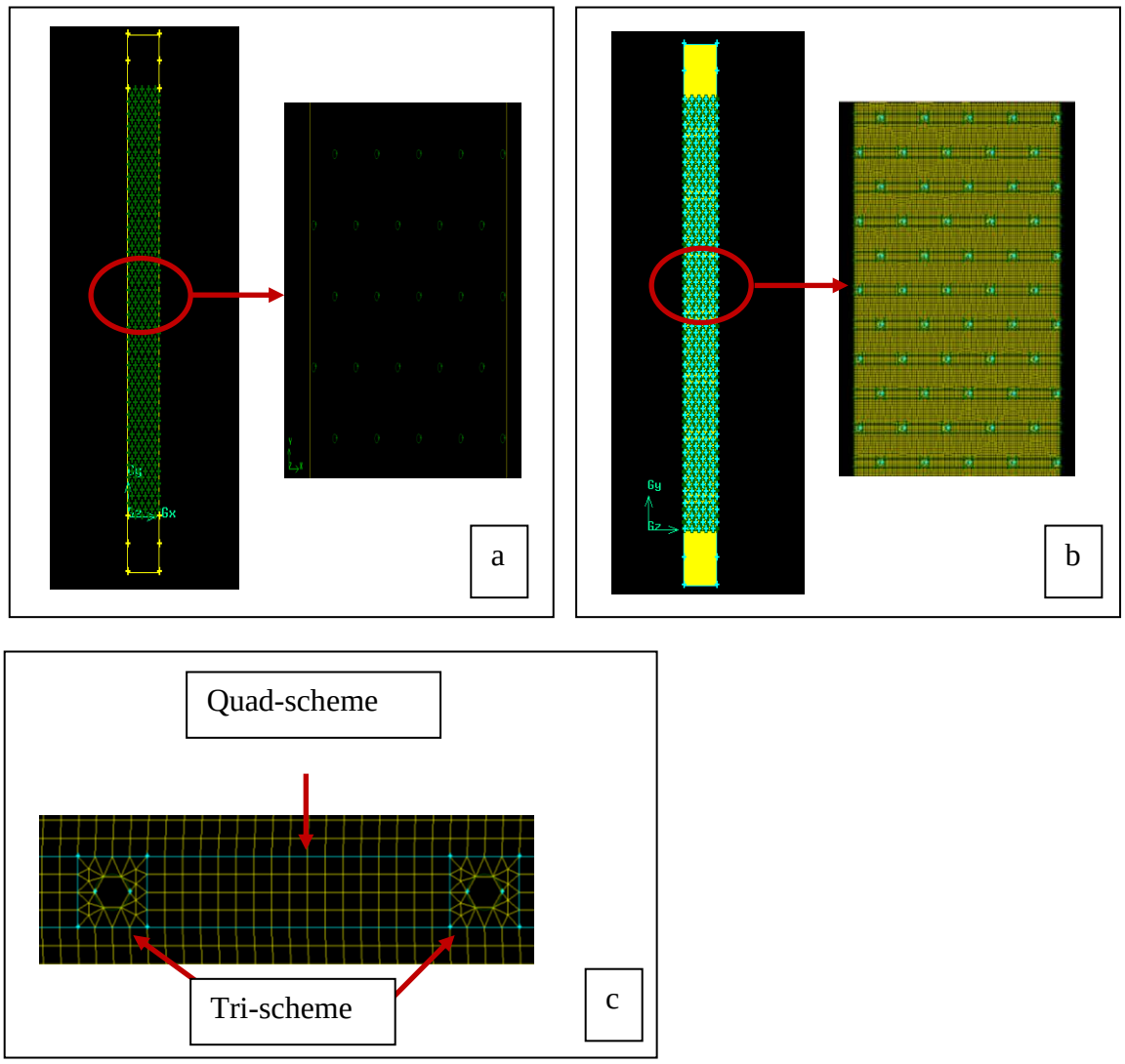

Figure 7.15 Schematic diagram of the tube-banks geometry (a) before meshing (b) after meshing (c) types of meshing

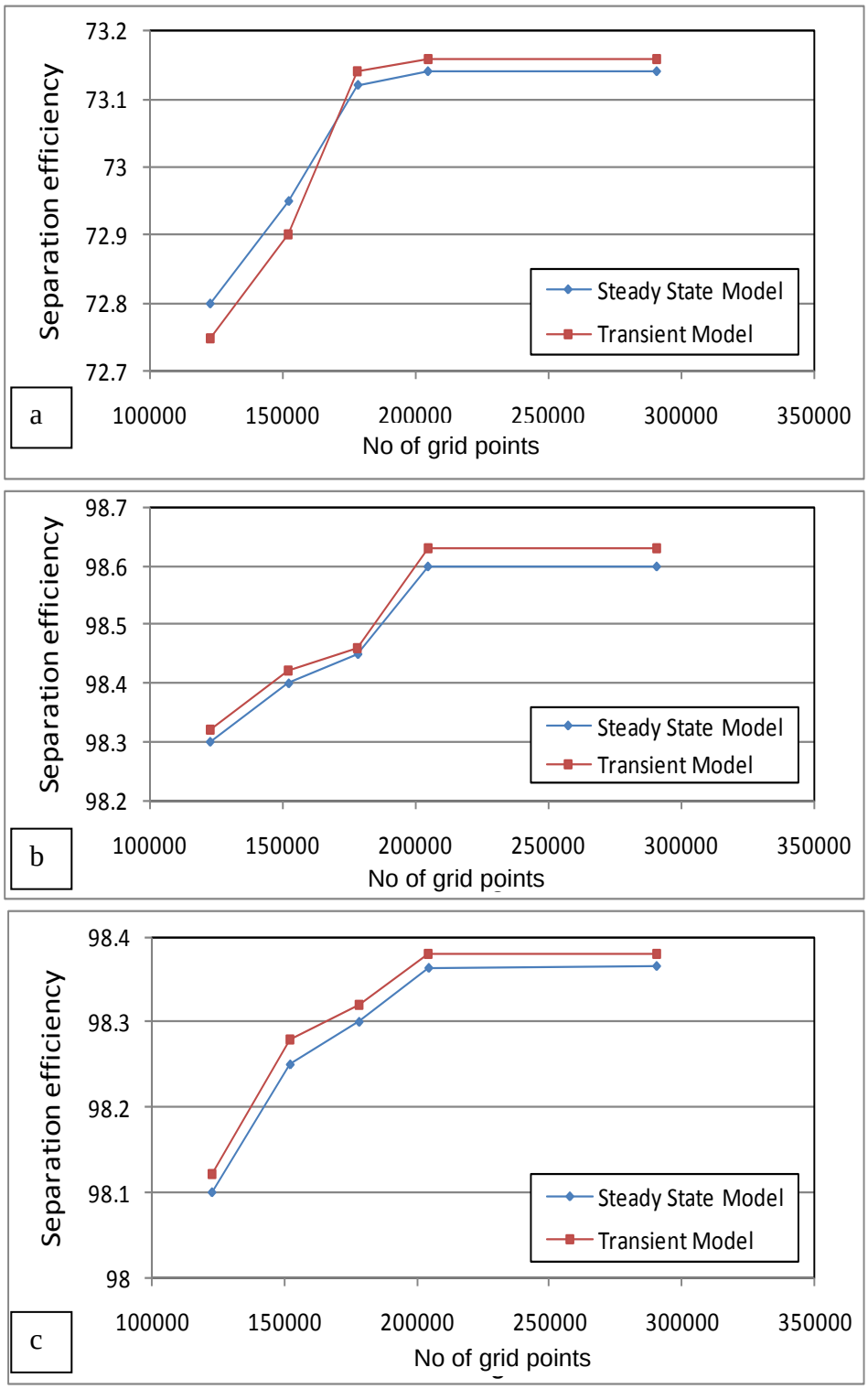

Figure 7.16 Separation efficiency values obtained for tube banks with multi-phase flow approach geometry of different gird number (a) lab scale demister (b) high temperature stage demister (c) low temperature stage demister

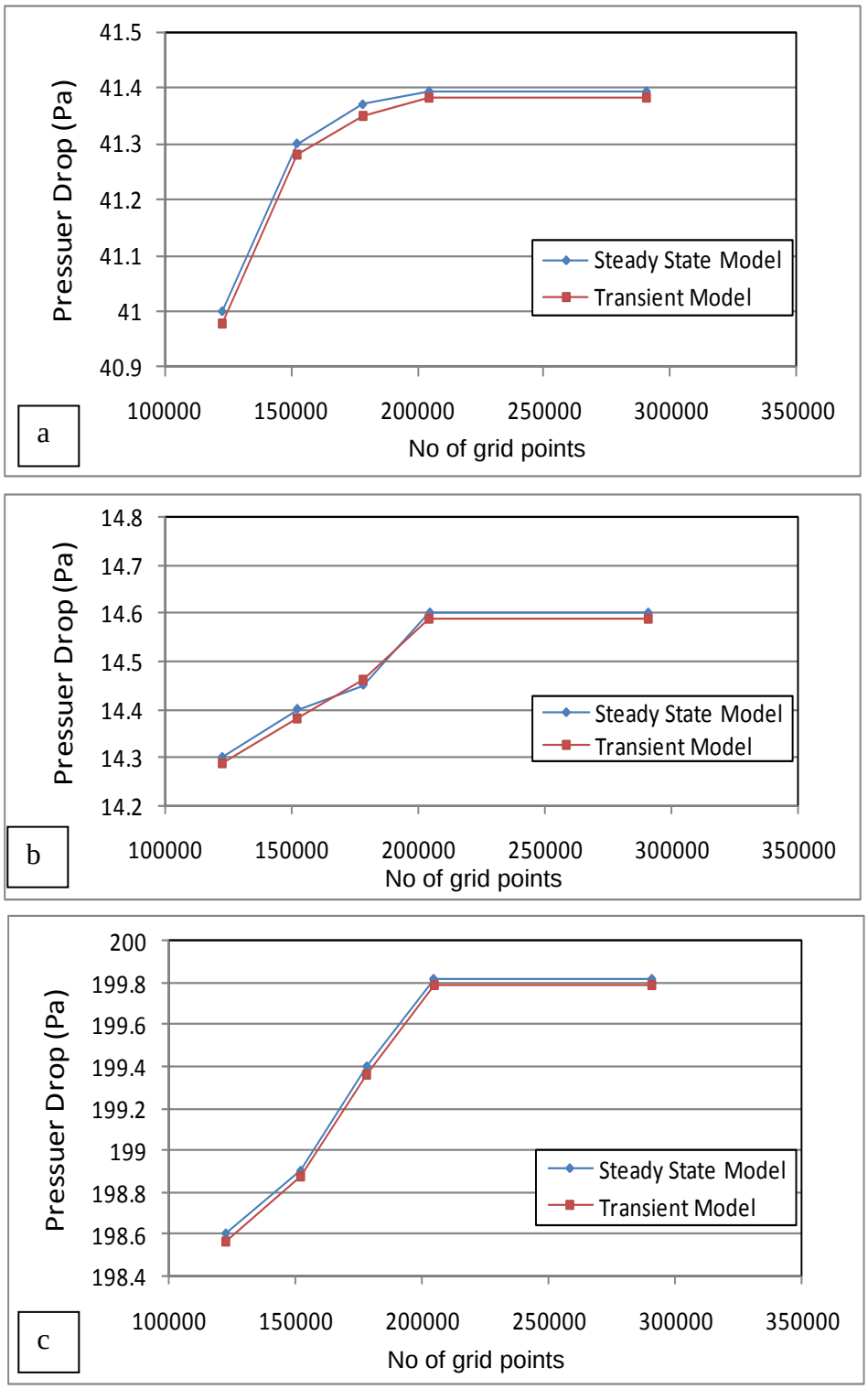

Figure 7.17, Pressure drop values obtained for tube banks with multi-phase flow approach geometry of different gird number (a) lab scale demister (b) high temperature stage demister (c) low temperature stage demister

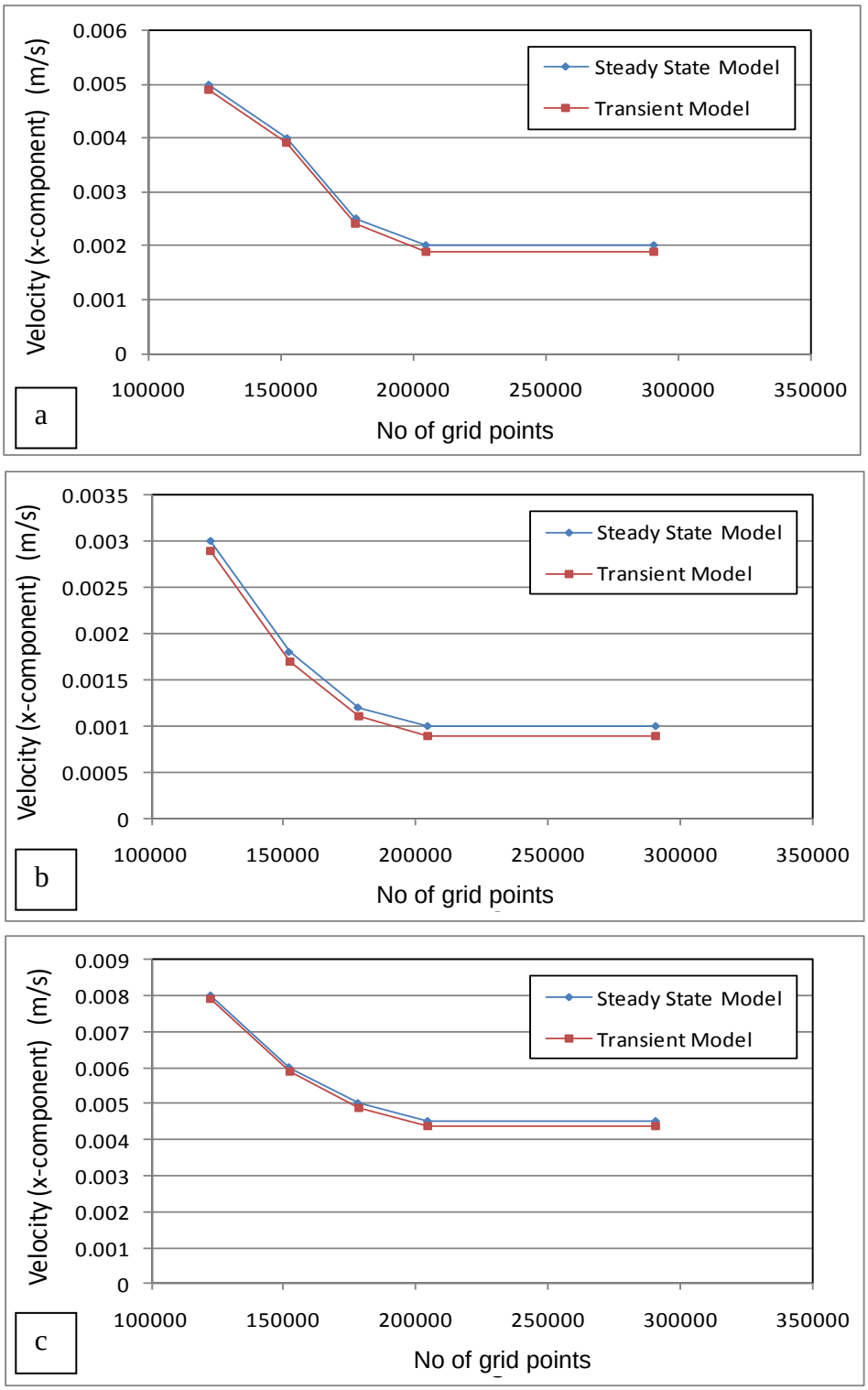

Figure 7.18 Velocity (x-component) values obtained for tube banks with multi-phase flow approach geometry of different gird number (a) lab scale demister (b) high temperature stage demister (c) low temperature stage demister

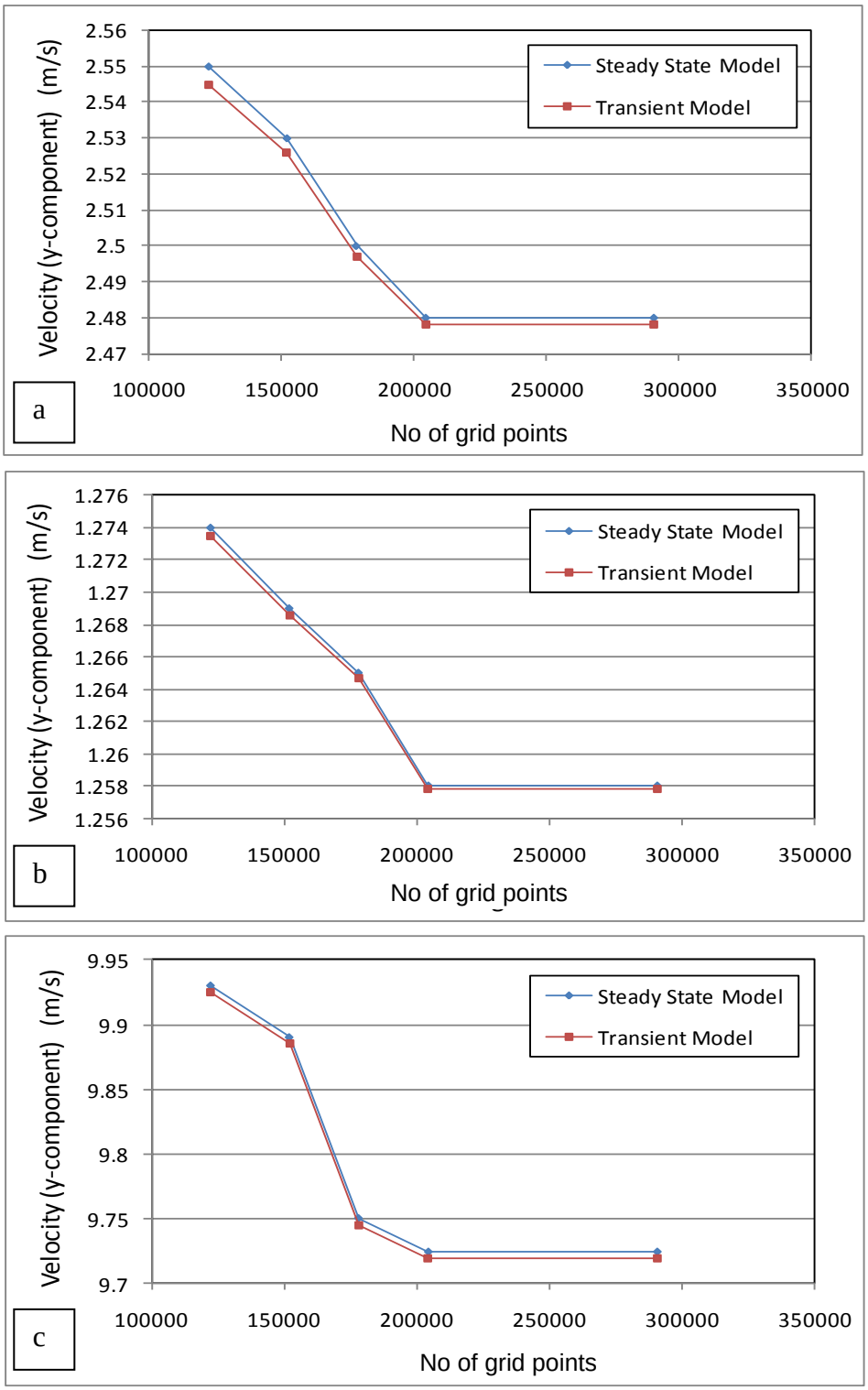

Figure 7.19 Velocity (y-component) values obtained for tube banks with multi-phase flow approach geometry of different gird number (a) lab scale demister (b) high temperature stage demister (c) low temperature stage demister

7.3.2 Cases investigated, geometries and boundary conditions

The CFD FLUENT code was used to simulate two lab scale wire mesh demisters. One demister had a packing density equal to 80.317 kg/m^{3}and 0.28 mm wire diameter. The other had a packing density equals to 176.35 kg/m^{3}and 0.24 mm wire diameter. The experiment was done by El-Dessouky et al (2000) (see section 7.2.2).

The experiment was repeated for different vapour velocities. The CFD model was applied to each run. Table 7.6 includes the operating condition and design parameters of the demister which are used as input to the simulator.

Table 7.6: Input operating conditions and design parameter to the FLUENT code.

Velocity range (m/s)	2.4-6.7
Packing density (kg/m^3)	80.317-176.35
Water droplet volume fraction in the inlet stream	1.0E-5
Droplet diameter	10 μm = 10E-6 m

In addition, CFD FLUENT code was used to simulate a wire mesh demister installed in multistage flashing (MSF) desalination plant. The demister used in this plant has a packing density = 80.317 kg/m^3. Table 7.3 includes the operating conditions of the flashing stage of real MSF-BC plant operating at low temperature which are used as input to the model. The Simulation was applied for the demister in each flashing stage with different operating conditions but the same design. This is essential to prove that the model is applicable for a wide range of conditions.

7.3.3 Model validation

The tube banks multi phase model has been simulated for different conditions of the experiment done by El-Dessouky et al (2000) to validate the model. As shown in Figure 7.20-7.21, validation of the model showed very good agreement between the CFD results and the experimental data with an error less than 5.32%.

As shown in tables (7.7-7.8), comparison between the experimental data, CFD results and the empirical correlation values obtained by El-Dessouky et al (2000) showed that the difference between the CFD results and the experimental data in all runs did not exceed 5.32% while for the empirical correlation it reached 16%. That makes the CFD model more accurate.

As shown in Figures 7.20-7.21, the pressure drop values predicted by the CFD model is less than the experimental values. That is because in this model a uniform sink value for the droplets was assumed. In reality, the droplets accumulated on the wires of the demister and then it settles causing more resistance to the upcoming flow and more pressure drop. In the model the sink value decreases to overcome the accumulation phenomenon, the simulation will stop because of the accumulation of the brine droplets in the demister.

Table 7.7: CFD results using tube banks multiphase model and empirical correlation results for lab scale demister with packing density equals to 80.317 kg/m^3 and 0.28 mm wire diameter.

Packing Density	Vapour Velocity	Experimental El-Dessouky et al. (2000)	CFD (This Work)		Correlation El-Dessouky et al (2000)	
kg/m^3	m/s	Pressure Drop (Pa)	Pressure Drop (Pa)	% Error	Pressure Drop (Pa)	% Error
80.317	2.435	41.667	41.393	0.656	45.527	9.264
	3.096	56.000	56.933	1.666	55.345	1.171
	3.652	63.333	61.742	2.512	63.308	0.040
	4.087	66.667	64.226	3.661	69.372	4.057
	4.870	83.333	79.987	4.015	79.994	4.008
	5.652	94.333	90.012	4.581	90.300	4.275
	6.052	100.000	95.018	4.982	95.463	4.537
	6.696	120.000	113.760	**5.200**	103.638	**13.635**

Table 7.8: CFD results using tube banks multiphase model and empirical correlation results for lab scale demister with packing density equals to 176.35 kg/m3 and 0.24 mm wire diameter.

Packing Density	Vapour Velocity	Experimental El-Dessouky et al. (2000)	CFD (this Work)		Correlation El-Dessouky et al (2000)	
kg/m^3	m/s	Pressure Drop (Pa)	Pressure Drop (Pa)	% Error	Pressure Drop (Pa)	% Error
176.350	1.422	60.000	59.58	0.7	50.266	**16.224**
	1.956	64.333	63.3603	1.512	65.123	1.228
	2.453	71.667	69.5084	3.012	78.311	9.271
	2.756	80.000	76.9776	3.778	86.069	7.587
	3.342	90.000	86.4018	3.998	100.696	11.885
	3.911	101.667	97.217	4.377	114.426	12.550
	4.356	113.333	107.471	5.172	124.892	10.199
	4.711	126.667	119.94	**5.311**	133.121	5.096

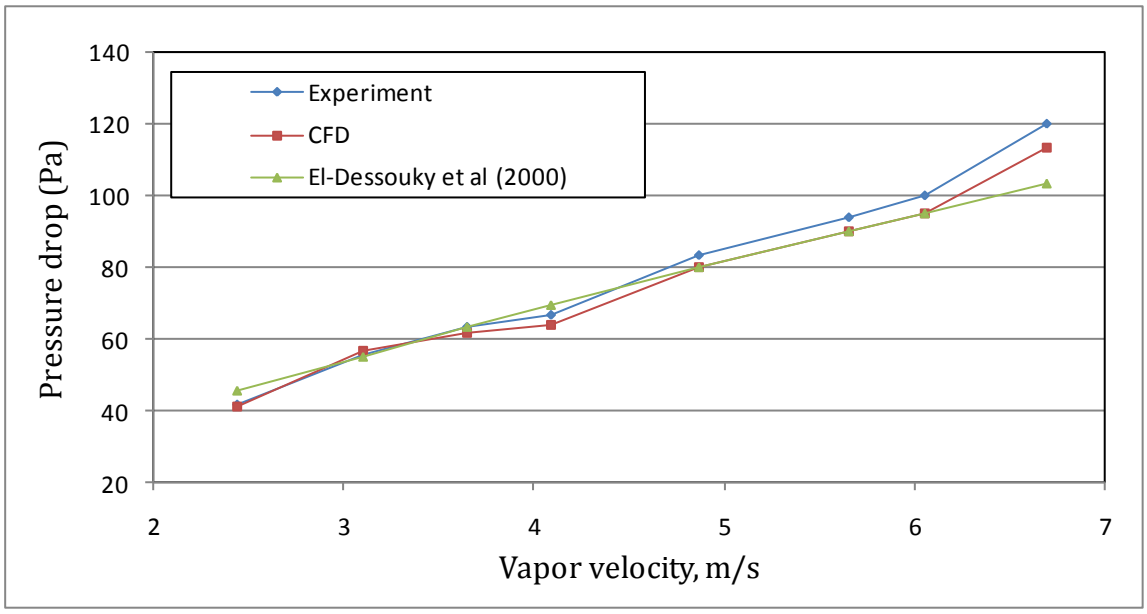

Figure 7.20 Variation in pressure drop as a function of vapour velocity for demister with packing density =80.317 kg/m^{3}and 0.28 mm wire diameter

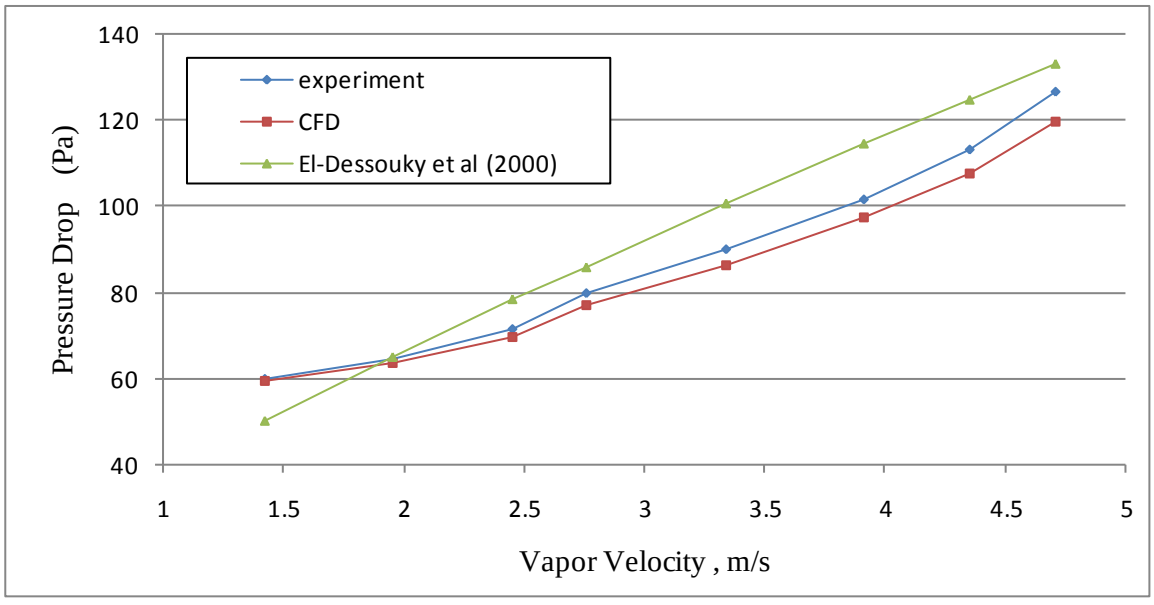

Figure 7.21 Variation in pressure drop as a function of vapour velocity for demister with packing density =176.35 kg/m^{3}and 0.24 mm wire diameter

As shown in Table 7.9 and Figures 7.22-7.23, the validation showed very good agreement between the CFD results and the real plant data with an error less than 12% except for the last two stages in reached 31.89 %. On the other hand the empirical correlation results were far away from the real data with an error which had exceeded 52%. For the last stages, the difference increases between the predicted values and the real plant values. That is because as the temperature decreases, the vapour specific volume and velocity increase resuting in increasing the amount of the entrained brine droplets. That will result in increasing the resistance on the upward flashed vapour as it flows through the demister and increasing the pressure drop. This increases in the resistance is not accounted in the CFD model.

Table 7.9: Comparison of CFD results using tube banks multiphase model, real plant (Plant D) unit data and correlation values

Stage	Vapour Pressure below demister	Vapour Pressure above demister	ΔP demister (Real)	CFD (This Work)		Correlation El-Dessouky et al (2000)	
	kPa	kPa	Pa	Pressure Drop (Pa)	% Error	Pressure Drop (Pa)	% Error
1	66.377	66.352	25.442	23.918	5.988	36.076	41.798
2	60.421	60.386	35.277	34.053	3.472	51.086	44.812
3	54.981	54.938	43.462	43.306	0.361	54.037	24.330
4	50.017	49.973	44.161	43.183	2.216	56.606	28.179
5	45.488	45.432	55.600	53.195	4.324	59.839	7.625
6	41.359	41.290	68.419	64.100	6.313	63.258	7.543
7	37.596	37.526	69.445	65.875	5.140	68.870	0.828
8	34.168	34.095	72.791	70.199	3.561	70.697	2.876
9	31.047	30.967	80.542	78.120	3.007	74.999	6.883
10	28.207	28.121	86.621	83.886	3.158	76.205	12.025
11	25.624	25.532	91.236	88.895	2.565	76.784	15.840
12	23.274	23.169	105.062	100.551	4.293	78.044	25.716
13	21.139	21.032	106.465	102.050	4.147	78.750	26.032
14	19.199	19.083	115.871	111.842	3.477	80.740	30.319
15	17.436	17.305	131.285	126.285	3.809	81.931	37.593
16	15.836	15.700	135.978	130.258	4.206	89.012	34.539
17	14.383	14.223	159.851	152.992	4.291	93.805	41.317
18	13.065	12.879	185.376	181.457	2.115	98.860	46.670
19	11.868	11.680	188.249	183.122	2.723	102.895	45.341
20	10.783	10.583	200.225	190.225	4.994	109.676	45.224
21	9.799	9.595	204.146	189.592	7.129	115.224	43.558
22	8.907	8.701	206.173	181.649	11.895	123.478	40.110
23	8.098	7.879	219.094	188.456	13.984	127.183	41.950
24	7.365	7.071	293.358	199.819	**31.885**	140.308	**52.17**

In the above table, the differences between the CFD result and the real plant data increase in the last stages. The reason behind this is that at lower temperature the specific volume increases and as a result the vapour velocity increase and that will increase the amount of entrained droplets. That will lead to an increase in the resistance towards the upward vapour flow. This additional resistance was not

accounted in the CFD model. However in the future it can be added as a user defiend function in the CFD model to get more accurate results.

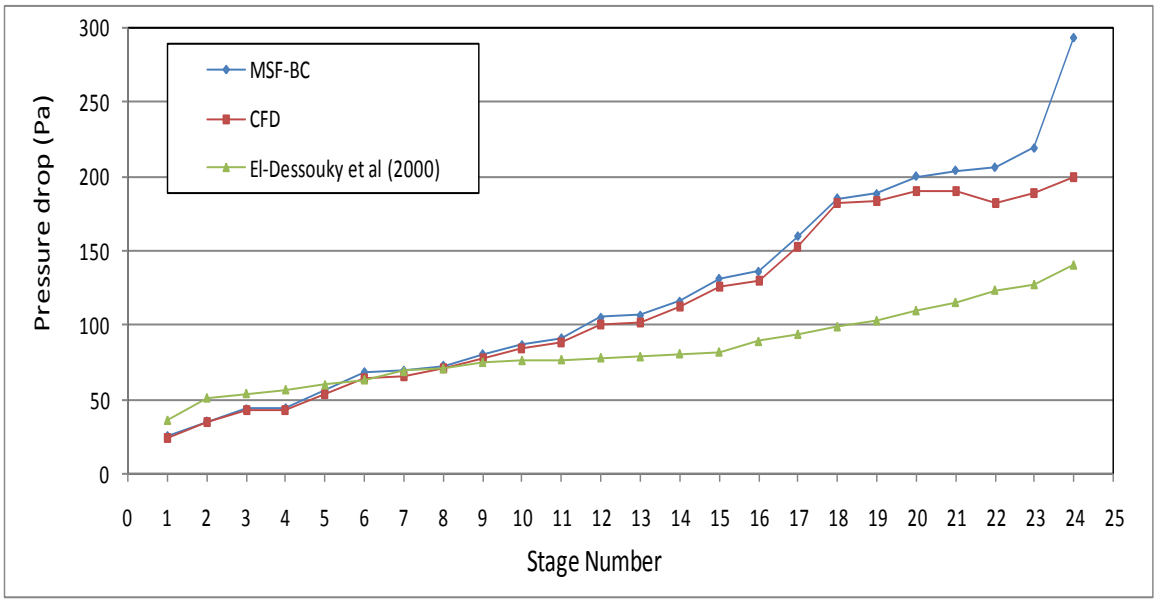

Figure 7.22 Variation in pressure drop as a function of MSF-BC stage number for demister with packing density =80.317 kg/m3

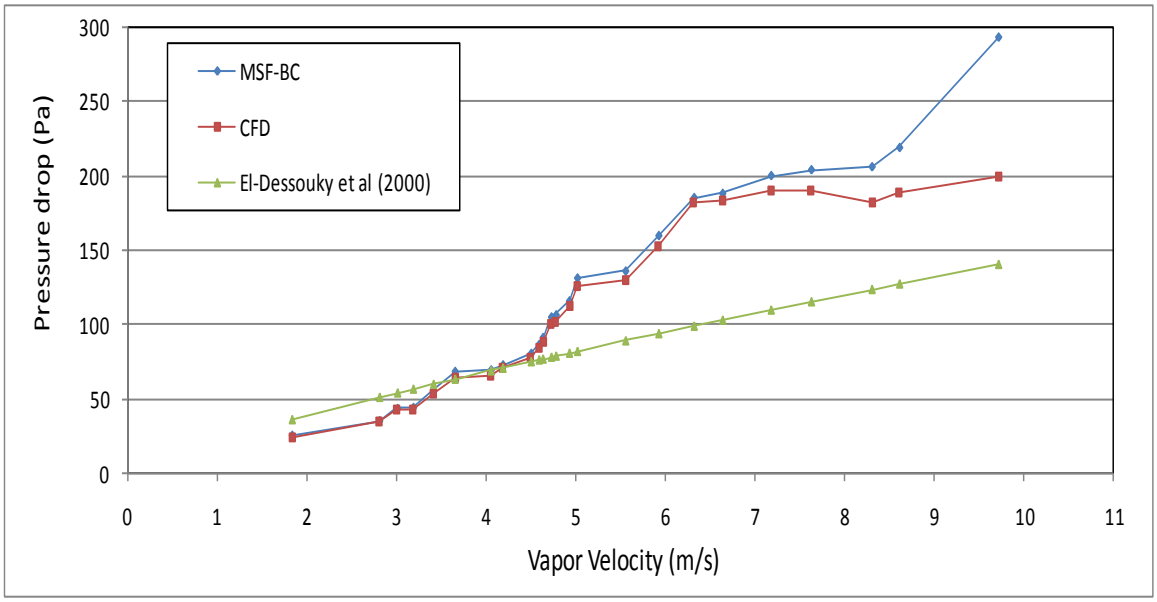

Figure 7.23 Variation in pressure drop as a function of MSF stage vapour velocity for demister with packing density =80.317 kg/m3

7.4 Tube Banks –Discrete phase model Approach

The tube banks – discrete phase model approach follows the Eulerian-Lagrangian modelling method mentioned previously in section 6.5. This approach is important for design purposes where only the operating parameters are assigned to the simulator without the need of any other design values (such as the removal efficiency in the previous methods). This makes the model more general and applicable for operating, trouble shooting and design purposes.

The results for the two dimensional model include grid sensitivity analysis, model validation against experimental and real plant data. At the end of this section, new demisters are designed and the best demister is selected to see how it would affect the heat transfer area of the flashing stages of MSF plant

7.4.1 Grid Sensitivity Analysis

The geometry was constructed using GAMBIT (See section 7.2.1). To run the simulations, Fluent 6.3 was employed. And the simulator was applied for three different operating conditions listed in table 7.1. The grid of this geometry is same as that presented is section 7.3.1. As shown in Figures (7.24-7.27), the separation efficiency, the pressure drop, and the x and y velocity components of the flow for both steady state and transient model remain constant and unaffected by the number of grid cells at 204481 cells. That means that the model can be simulated with 204481 grid points without the need of further grid refinement. In all simulations, the residual values were set to a maximum value of 1×10^{-8}. For both the steady state and transient model the simulation stops when the residual is less than the set value.

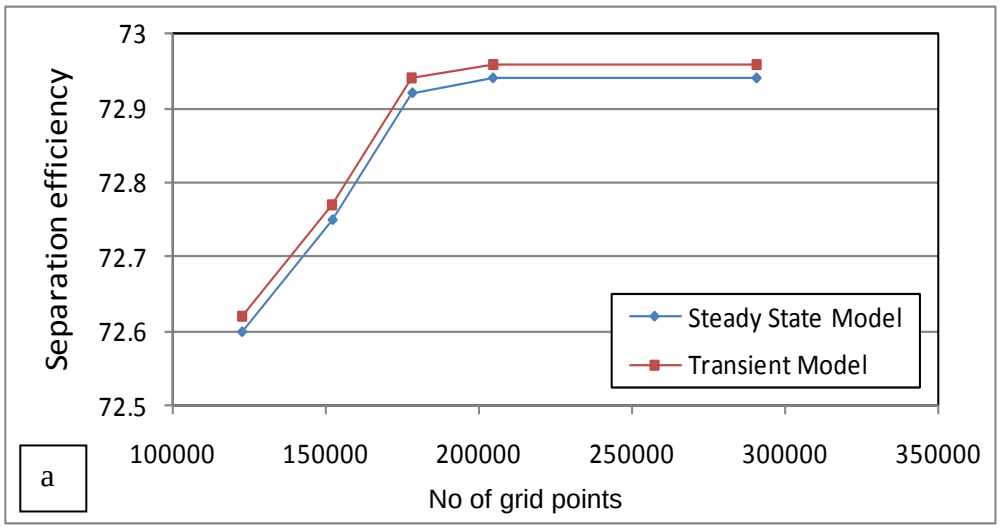

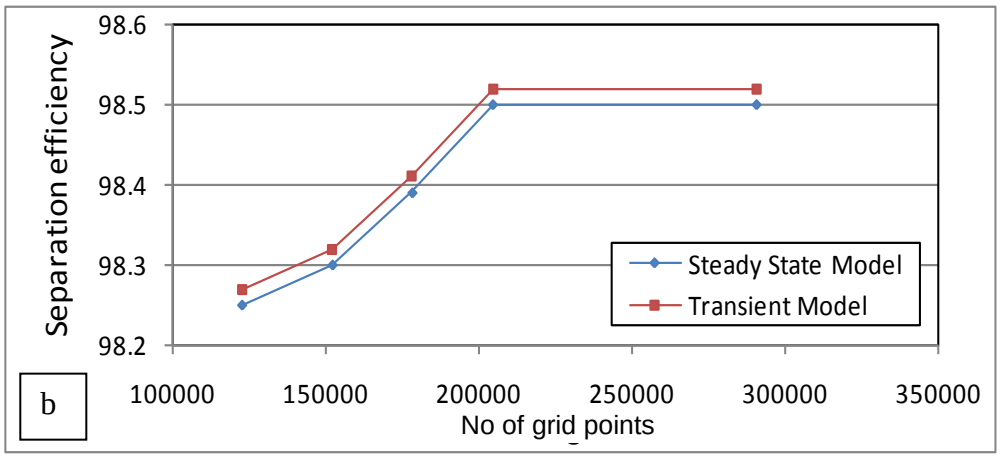

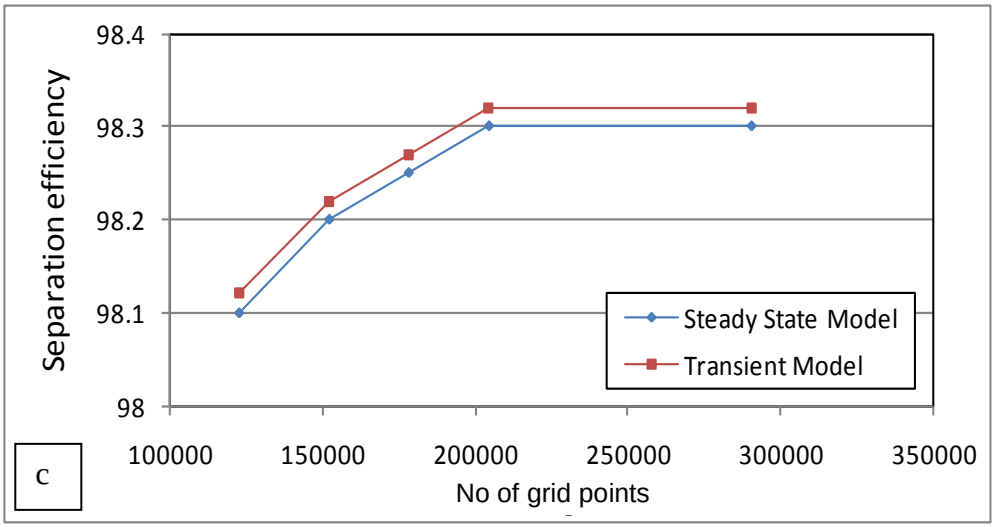

Figure 7.24 Separation efficiency values obtained for porous media geometry of different gird number (a) lab scale demister (b) high temperature stage demister (c) low temperature stage demister

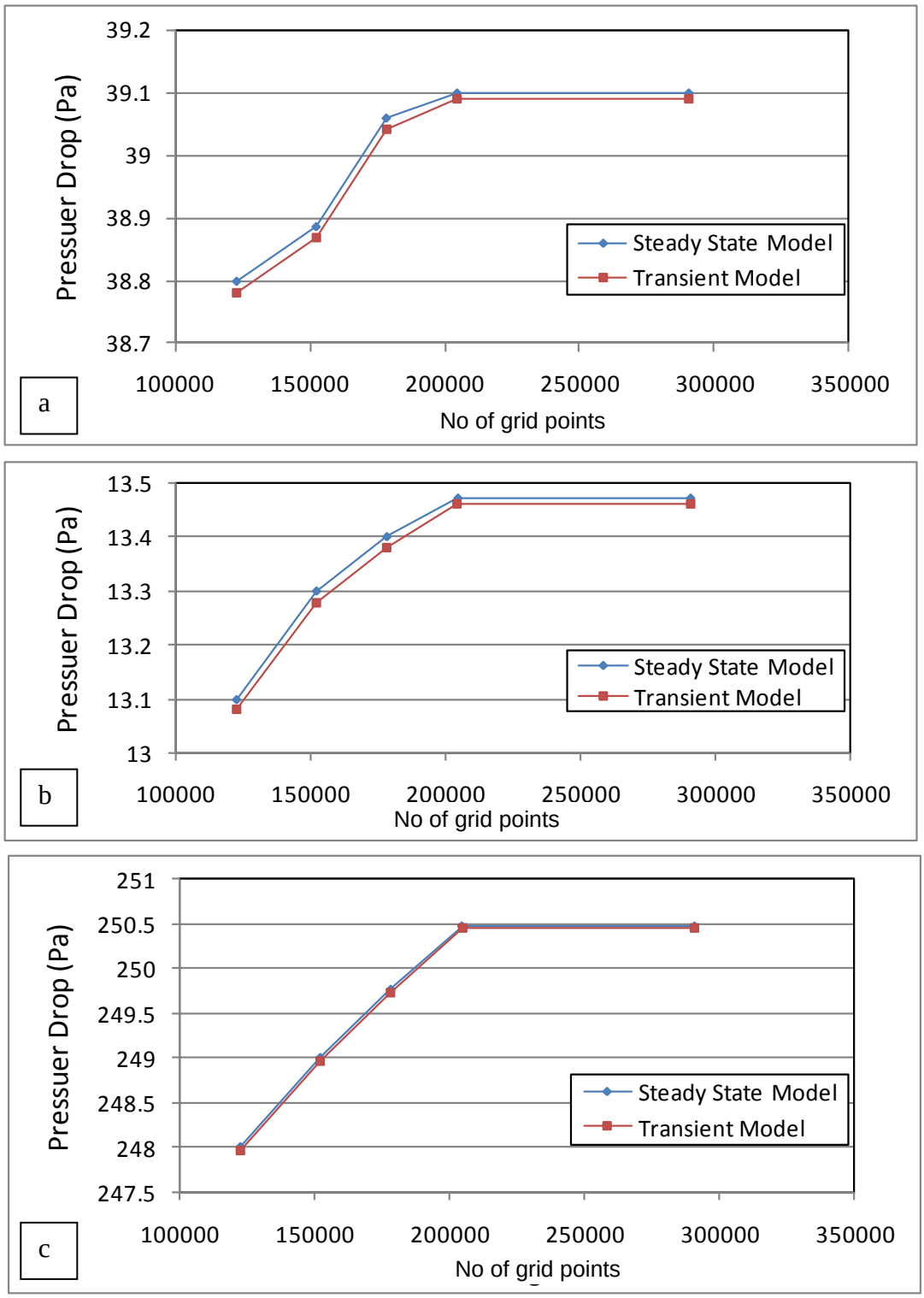

Figure 7.25 Pressure drop values obtained for porous media geometry of different gird number. (a) lab scale demister (b) high temperature stage demister (c) low temperature stage demister

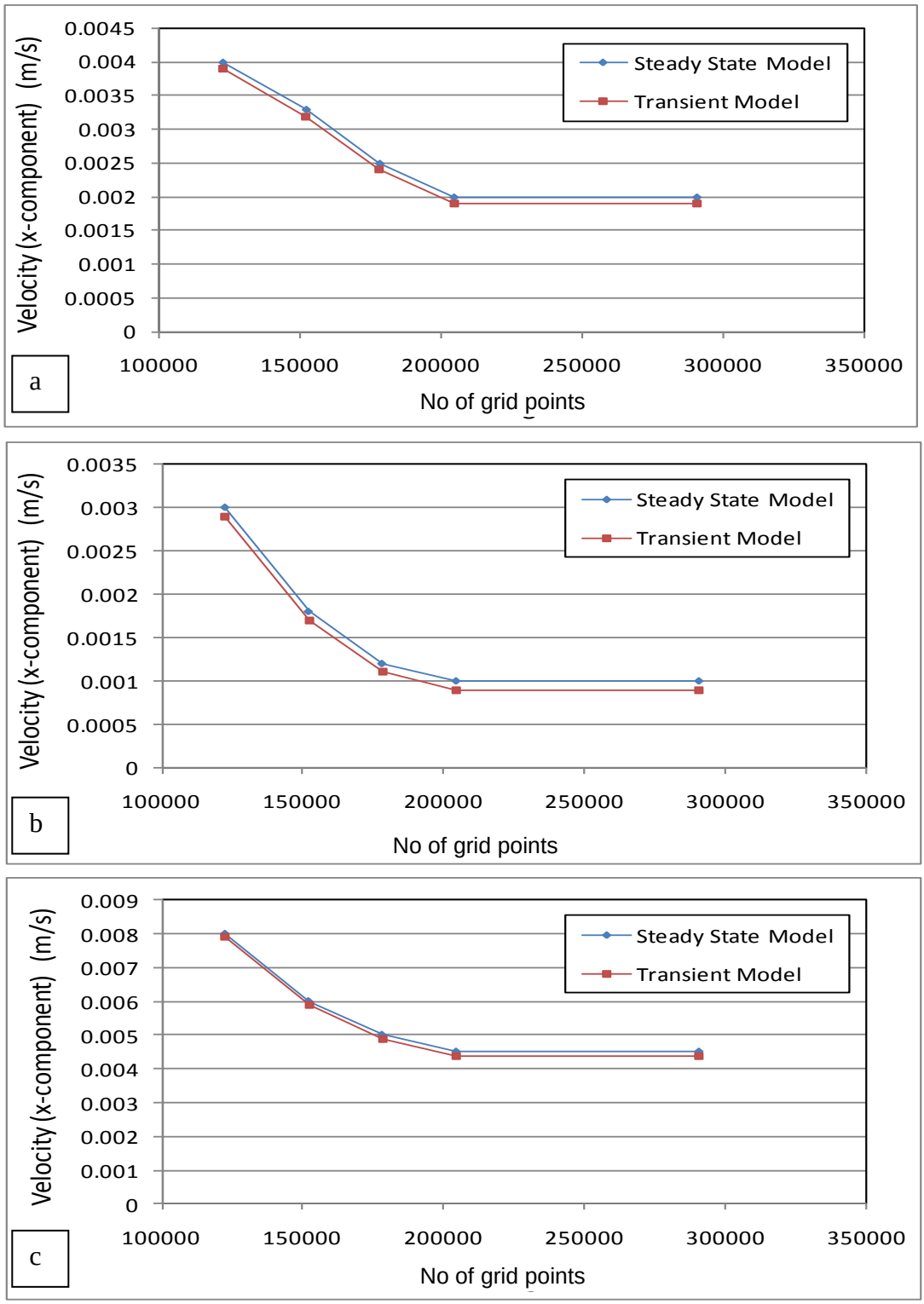

Figure 7.26 Velocity (x-component) values obtained for porous media geometry of different gird number. (a) lab scale demister (b) high temperature stage demister (c) low temperature stage demister

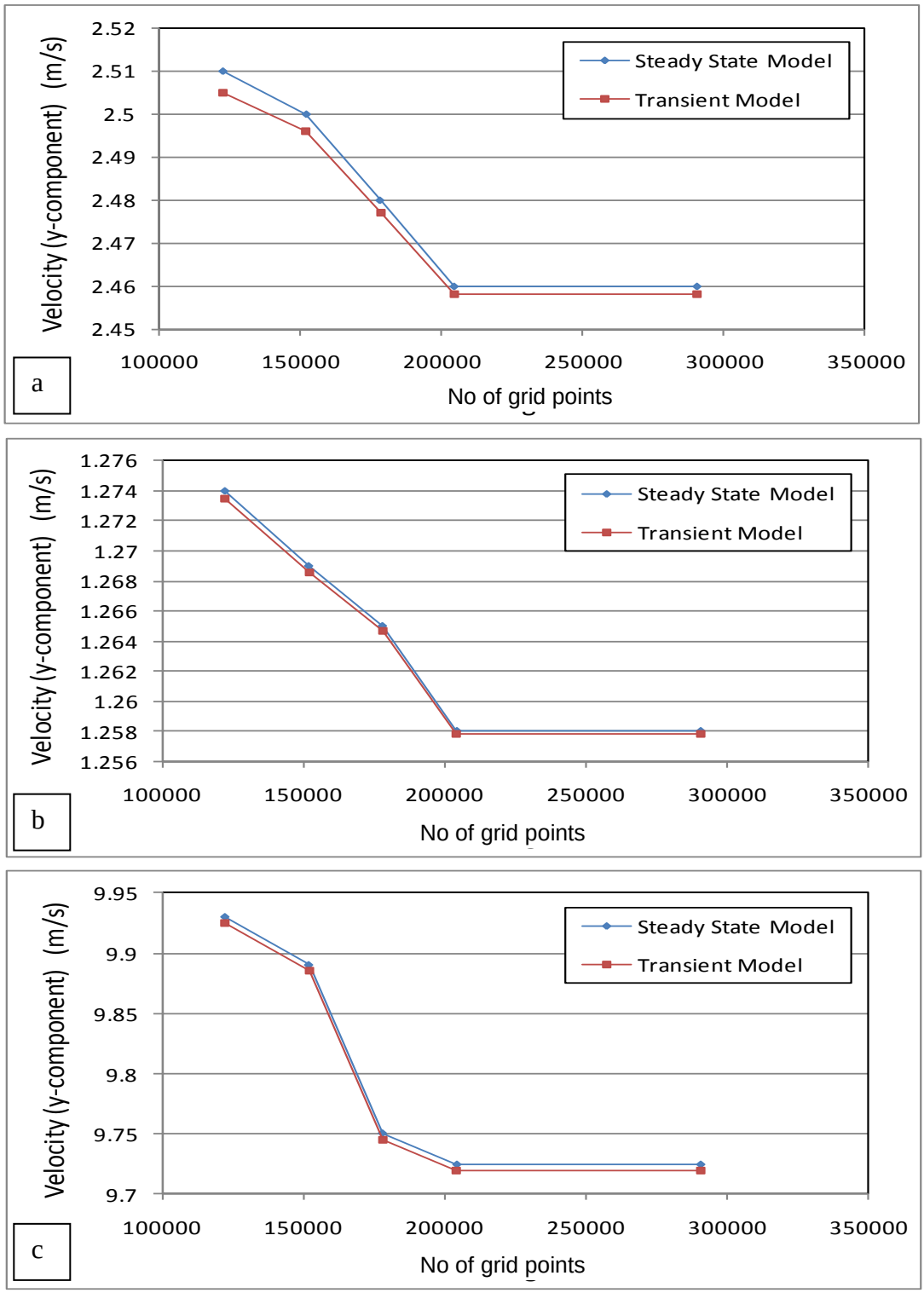

Figure 7.27 Velocity (y-component) values obtained for porous media geometry of different gird number. (a) lab scale demister (b) high temperature stage demister (c) low temperature stage demister

7.4.2 Cases investigated, geometries and boundary conditions

The CFD FLUENT code was used to simulate two lab scale wire mesh demisters. The first demister was having a packing density equals to 80.317 kg/m^{3}and 0.28 mm wire diameter. The second was having a packing density equals to 176.35 kg/m^{3}and 0.24 mm wire diameter. The experiment was done by El-Dessouky et al (2000) (see section 7.2.2).

As mentioned previously in section 7.3.2, the experiment was repeated for different vapour velocities. The CFD model was applied to each run. Table 7.6 includes the operating condition and design parameters of the demister which are used as input to the simulator.

Also, CFD FLUENT code is also used to simulate wire mesh demisters installed in the flashing stages of three different multistage flashing (MSF) desalination plants. The three plants are operating at different conditions and have different designs. This is essential in order to prove that the model is general and applicable for any demister in any plant in the world. The first plant is MSF-BC operating at low top brine temperature (Table 7.3). The second is MSF-OT operating at low top brine temperature (Table 7.10). The thirds plant is MSF-BC operating at high top brine temperature (Table 7.11). The demister used in these plants are having a packing density = 80.317 kg/m^3. Tables (7.3, 7.10, 7.11) include the operating condition of the flashing stage which is used as input to the simulator.

Table 7.10: Operating conditions of the flashing stages in MSF-OT plant operating at low temperature (Plant A- Kuwait- MEW)

Stage	Vapour temperature below demister (^oK)	Vapour density (kg/m^3)	Droplet density (kg/m^3)	Flashed off Vapour Velocity (m/s)	Inlet Volume Fraction of Droplet in Flashed off Vapour
1	361.89	0.405	995.0	1.336	5.078E-06
2	359.1422	0.367	996.9	3.296	4.568E-06
3	356.4338	0.332	998.7	3.557	4.108E-06
4	353.7654	0.300	1000.5	3.800	3.695E-06
5	351.137	0.272	1002.3	4.101	3.322E-06
6	348.5486	0.246	1003.9	4.421	2.987E-06
7	346.0002	0.222	1005.6	4.974	2.686E-06
8	343.4918	0.201	1007.1	5.164	2.415E-06
9	341.0234	0.182	1008.6	5.576	2.172E-06
10	338.595	0.164	1010.1	5.730	1.953E-06
11	336.2066	0.149	1011.5	5.843	1.757E-06
12	333.8582	0.134	1012.8	6.013	1.580E-06
13	331.5498	0.122	1014.1	6.118	1.422E-06
14	329.2814	0.110	1015.4	6.379	1.280E-06
15	327.053	0.099	1016.6	6.485	1.152E-06
16	324.8646	0.090	1017.7	7.234	1.038E-06
17	322.7162	0.081	1018.8	7.801	9.348E-07
18	320.6078	0.074	1019.9	8.355	8.426E-07
19	318.5394	0.067	1020.9	8.952	7.599E-07
20	316.511	0.061	1021.8	9.625	6.856E-07
21	314.5226	0.055	1022.8	10.327	6.191E-07

Table 7.11: Operating conditions of the flashing stages in MSF-BC plant operating at high temperature (Plant B- Kuwait- MEW)

Stage	Vapour temperature below demister (K)	Vapour density (kg/m^3)	Droplet density (kg/m^3)	Flashed off Vapour Velocity (m/s)	Inlet Volume Fraction of Droplet in Flashed off Vapour
1	377.548	0.691	1002.500	1.252	5.319E-06
2	373.671	0.608	1005.600	2.414	4.637E-06
3	369.871	0.535	1008.500	2.650	4.041E-06
4	366.146	0.471	1011.400	2.888	3.522E-06
5	362.497	0.414	1014.100	3.177	3.069E-06
6	358.923	0.364	1016.700	3.500	2.675E-06
7	355.426	0.320	1019.200	4.037	2.331E-06
8	352.004	0.281	1021.600	4.250	2.032E-06
9	348.658	0.247	1023.900	4.659	1.772E-06
10	345.388	0.217	1026.000	4.841	1.546E-06
11	342.194	0.191	1028.100	5.056	1.349E-06
12	339.075	0.168	1030.100	5.351	1.178E-06
13	336.033	0.148	1032.000	5.461	1.029E-06
14	333.066	0.130	1033.800	5.890	8.998E-07
15	330.175	0.114	1035.500	6.019	7.875E-07
16	327.359	0.101	1037.100	6.890	6.900E-07
17	324.620	0.089	1038.700	7.423	6.052E-07
18	321.956	0.079	1040.200	8.123	5.315E-07
19	319.368	0.070	1041.500	8.782	4.675E-07
20	316.856	0.062	1042.900	9.518	4.118E-07
21	314.420	0.055	1044.100	10.363	3.634E-07
22	312.059	0.048	1045.300	11.574	3.212E-07
23	309.775	0.043	1046.400	11.887	2.845E-07
24	307.566	0.038	1047.500	12.212	2.525E-07

7.4.3 Model validation

The tube banks discrete phase model has been simulated for different conditions of the experiment done by El-Dessouky et al (2000) to validate the model. As shown in Figures 7.28-7.29 validation of the model showed very good agreement between the CFD results and the experimental data with an error less than 6.3%. Tables 7.12-7.13, show comparison between the experimental data, CFD results and the empirical correlation values by El-Dessouky et al (2000). As shown, the difference between the CFD results and the experimental data in all runs did not exceed 6.3% while for the empirical correlation it reached 16.5%. That makes the CFD model more accurate.

As shown in Figure 7.29, the pressure drop values predicted by the CFD model is less than the experimental values. That is because in this model it was assumed that the droplets escape and vanish as soon as they reach the demister wires. In reality, the droplets accumulated on the wires of the demister and then it settles causing more resistance to the upcoming flow and more pressure drop. This resistance can not be determind or included in the CFD model because it is not possible to have upward and downward flow in the same zone (void space in the demister) and account the interaction between them.

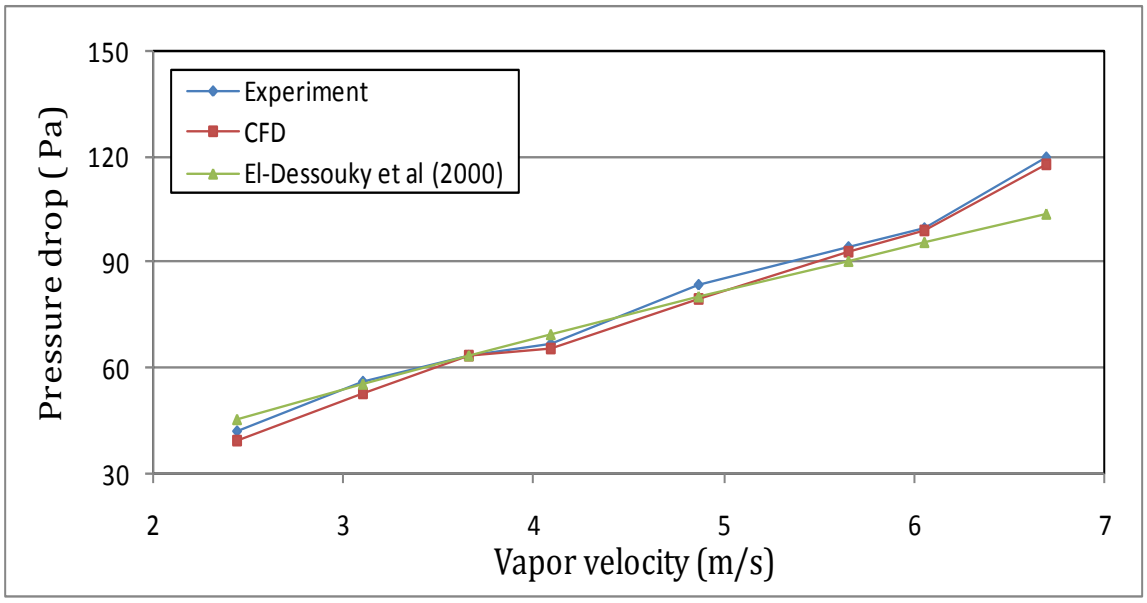

Figure 7.28, Variation in pressure drop as a function of vapour velocity for demister with packing density = 80.317 kg/m^3.

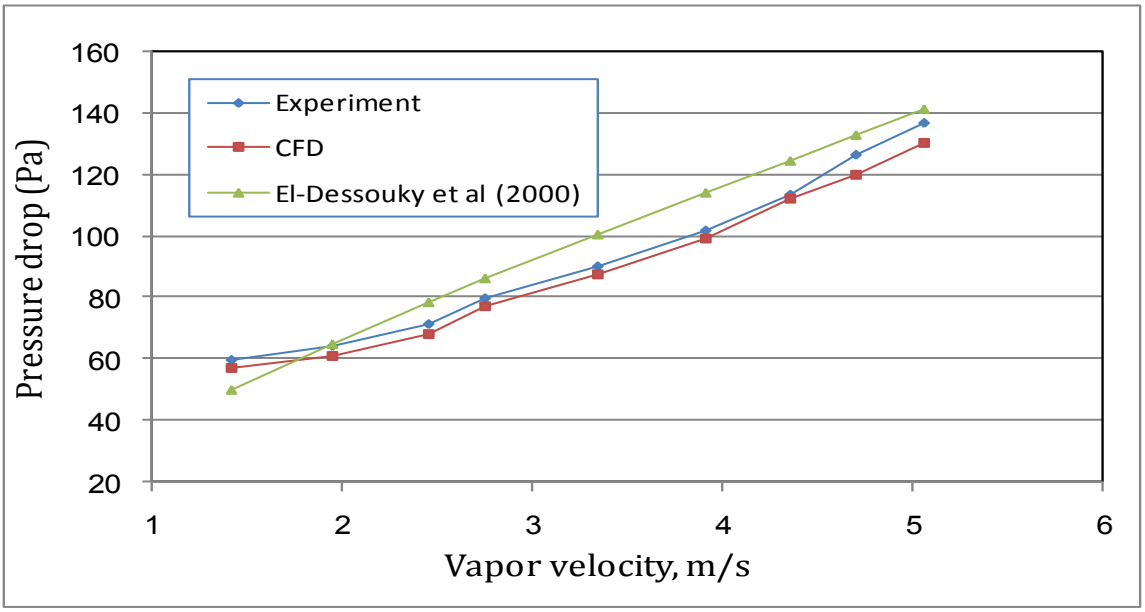

Figure 7.29, Variation in pressure drop as a function of vapour velocity for demister with packing density =176.35 kg/m^3 and 0.24 mm wire diameter

Table 7.12: CFD model and empirical correlation results for lab scale demister with packing density equals to 80.317 kg/m3 and 0.28 mm wire diameter

Packing Density	Vapour Velocity	Experimental El-Dessouky et al. (2000)	CFD (This Work)		Correlation El-Dessouky et al (2000)	
kg/m^3	m/s	Pressure Drop (Pa)	Pressure Drop (Pa)	% Error	Pressure Drop (Pa)	% Error
80.317	2.435	41.667	39.100	6.160	45.527	9.264
	3.096	56.000	52.500	**6.250**	55.345	1.171
	3.652	63.333	63.672	0.535	63.308	0.040
	4.087	66.667	65.351	1.973	69.372	4.057
	4.870	83.333	79.653	4.416	79.994	4.008
	5.652	94.333	93.182	1.220	90.300	4.275
	6.052	100.000	99.007	0.993	95.463	4.537
	6.696	120.000	118.000	1.667	103.638	**13.635**

Table 7.13: CFD model and empirical correlation results for lab scale demister with packing density equals to 176.35 kg/m3 and 0.24 mm wire diameter.

Packing Density	Vapour Velocity	Experimental El-Dessouky et al. (2000)	CFD (This Work)		Correlation El-Dessouky et al (2000)	
kg/m^3	m/s	Pressure Drop (Pa)	Pressure Drop (Pa)	% Error	Pressure Drop (Pa)	% Error
176.350	1.422	60.000	57.000	5.000	50.266	**16.224**
	1.956	64.333	61.384	4.585	65.123	1.228
	2.453	71.667	68.194	4.846	78.311	9.271
	2.756	80.000	77.129	3.589	86.069	7.587
	3.342	90.000	87.931	2.299	100.696	11.885
	3.911	101.667	99.347	2.282	114.426	12.550
	4.356	113.333	112.276	0.933	124.892	10.199
	4.711	126.667	120.029	**5.240**	133.121	5.096

As shown in Table 7.14 and Figure 7.30, the validation showed very good agreement between the CFD results and the real plant data (Table 7.3) with an error less than 6% except for the last stage it reached 14.62%. On the other hand the empirical correlation results were far away from the real data with an error which had exceeded 52%. This model is also validated against other two plants to prove its generality, the first is MSF-OT (Table 7.10) and the other is MSF-BC operating at high temperature (Table-7.11). As shown in Table 7.15-7.16 and Figure 7.31-7.32, the validation showed good agreement between the CFD results and real plant data with a difference less than 8.7% while the empirical correlation differences exceed 98%.

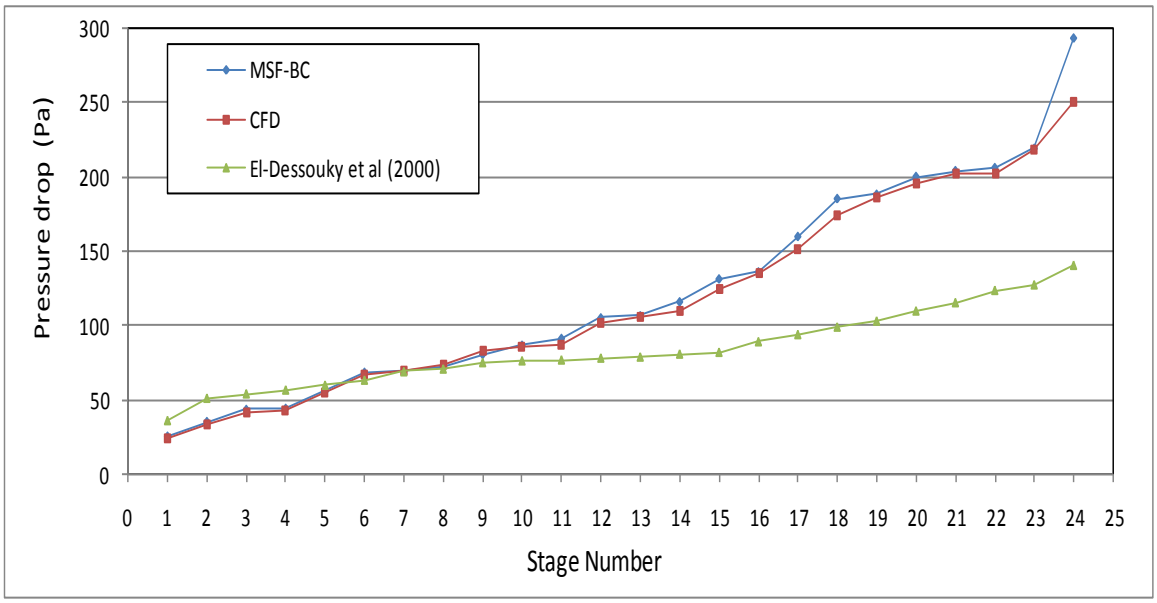

Figure 7.30 Variation in pressure drop as a function of MSF stage number for demister with packing density =80.317 kg/m^3 in MSF-BC plant operating at low temperature

Table 7.14: Comparison between CFD results using tube banks discrete phase model and real plant unit data for MSF-BC plant operating at low temperature (Plant D)

Stage	Vapour Pressure below demister	Vapour Pressure above demister	ΔP demister (Real)	CFD (This Work)		Correlation El-Dessouky et al (2000)	
	kPa	kPa	Pa	Pressure Drop (Pa)	% Error	Pressure Drop (Pa)	% Error
1	66.377	66.352	25.442	24.000	5.668	36.076	41.798
2	60.421	60.386	35.277	33.362	5.430	51.086	44.812
3	54.981	54.938	43.462	41.644	4.183	54.037	24.330
4	50.017	49.973	44.161	42.232	4.369	56.606	28.179
5	45.488	45.432	55.600	54.473	2.027	59.839	7.625
6	41.359	41.290	68.419	66.276	3.133	63.258	7.543
7	37.596	37.526	69.445	69.587	0.206	68.870	0.828
8	34.168	34.095	72.791	73.490	0.960	70.697	2.876
9	31.047	30.967	80.542	82.686	2.662	74.999	6.883
10	28.207	28.121	86.621	86.234	0.446	76.205	12.025
11	25.624	25.532	91.236	87.472	4.125	76.784	15.840
12	23.274	23.169	105.062	101.735	3.167	78.044	25.716
13	21.139	21.032	106.465	105.431	0.971	78.750	26.032
14	19.199	19.083	115.871	109.221	5.738	80.740	30.319
15	17.436	17.305	131.285	124.386	5.255	81.931	37.593
16	15.836	15.700	135.978	134.777	0.883	89.012	34.539
17	14.383	14.223	159.851	151.565	5.183	93.805	41.317
18	13.065	12.879	185.376	174.365	5.940	98.860	46.670
19	11.868	11.680	188.249	186.170	1.104	102.895	45.341
20	10.783	10.583	200.225	195.834	2.193	109.676	45.224
21	9.799	9.595	204.146	201.709	1.194	115.224	43.558
22	8.907	8.701	206.173	202.450	1.806	123.478	40.110
23	8.098	7.879	219.094	217.925	0.534	127.183	41.950
24	7.365	7.071	293.358	250.475	14.618	140.308	52.17

Table 7.15: Comparison of CFD results using tube banks discrete phase model and real plant unit data for MSF-OT plant (Plant A)

Stage	Vapour Pressure below demister	Vapour Pressure above demister	ΔP demister (Real)	CFD (This Work)		Correlation El-Dessouky et al (2000)	
	kPa	kPa	Pa	Pressure Drop (Pa)	% Error	Pressure Drop (Pa)	% Error
1	66.889	66.875	14.084	13.471	4.352	27.940	98.381
2	60.153	60.106	46.858	43.636	6.876	58.234	24.277
3	54.079	54.023	55.718	55.542	0.315	61.966	11.214
4	48.606	48.547	58.783	55.603	5.410	65.382	11.226
5	43.677	43.600	77.000	73.782	4.179	69.559	9.664
6	39.241	39.147	93.247	89.442	4.080	73.947	20.698
7	35.250	35.145	104.588	99.065	5.280	81.380	22.189
8	31.662	31.553	109.146	105.744	3.117	83.908	23.123
9	28.438	28.313	124.531	120.593	3.162	89.311	28.282
10	25.541	25.411	130.707	125.648	3.871	91.306	30.145
11	22.941	22.806	134.837	130.879	2.936	92.767	31.200
12	20.607	20.446	160.815	154.811	3.733	94.959	40.952
13	18.512	18.347	165.698	159.477	3.754	96.310	41.876
14	16.634	16.461	173.189	168.772	2.550	99.633	42.471
15	14.950	14.752	197.372	182.598	7.485	100.975	48.840
16	13.440	13.211	228.940	212.760	7.067	110.365	51.793
17	12.086	11.818	268.740	245.552	8.629	117.350	56.333
18	10.874	10.572	301.824	283.658	6.019	124.083	58.889
19	9.787	9.456	331.337	312.107	5.804	131.246	60.389
20	8.813	8.475	338.222	333.812	1.304	139.214	58.840
21	7.941	7.572	369.634	346.197	6.341	147.412	60.119

Table 7.16: Comparison between CFD results using tube banks discrete phase model and real plant unit data for MSF-BC plant operating at high temperature (Plant B)

Stage	Vapour Pressure below demister	Vapour Pressure above demister	ΔP demister (Real)	CFD (This Work)		Correlation El-Dessouky et al (2000)	
	kPa	kPa	Pa	Pressure Drop (Pa)	% Error	Pressure Drop (Pa)	% Error
1	118.406	118.391	15.633	14.705	5.935	26.501	69.526
2	103.320	103.283	36.752	35.180	4.278	45.212	23.020
3	90.109	90.068	41.014	38.993	4.927	48.769	18.908
4	78.553	78.508	45.374	42.273	6.834	52.305	15.276
5	68.456	68.406	49.593	46.438	6.361	56.523	13.976
6	59.641	59.588	53.501	50.635	5.356	61.150	14.297
7	51.953	51.899	53.877	53.674	0.376	68.678	27.474
8	45.254	45.195	59.048	58.361	1.163	71.608	21.271
9	39.420	39.354	65.709	63.223	3.782	77.174	17.449
10	34.344	34.278	65.803	63.514	3.478	79.618	20.995
11	29.930	29.863	66.382	65.486	1.349	82.481	24.253
12	26.093	26.021	71.830	69.985	2.569	86.363	20.233
13	22.760	22.684	76.322	75.960	0.475	87.805	15.046
14	19.866	19.779	87.237	82.547	5.376	93.383	7.045
15	17.353	17.263	89.982	87.078	3.228	95.034	5.614
16	15.172	15.063	109.308	106.203	2.840	106.074	2.958
17	13.279	13.124	155.737	148.740	4.493	112.708	27.629
18	11.636	11.469	167.838	165.627	1.317	121.274	27.743
19	10.211	10.009	201.274	197.591	1.830	129.218	35.800
20	8.973	8.762	211.170	206.223	6.758	137.957	37.624
21	7.898	7.684	214.409	208.118	2.934	147.828	31.053
22	6.965	6.743	221.476	220.116	0.614	161.738	26.972
23	6.154	5.925	228.290	223.214	2.223	165.281	27.601
24	5.448	5.196	252.047	245.714	2.513	168.950	32.969

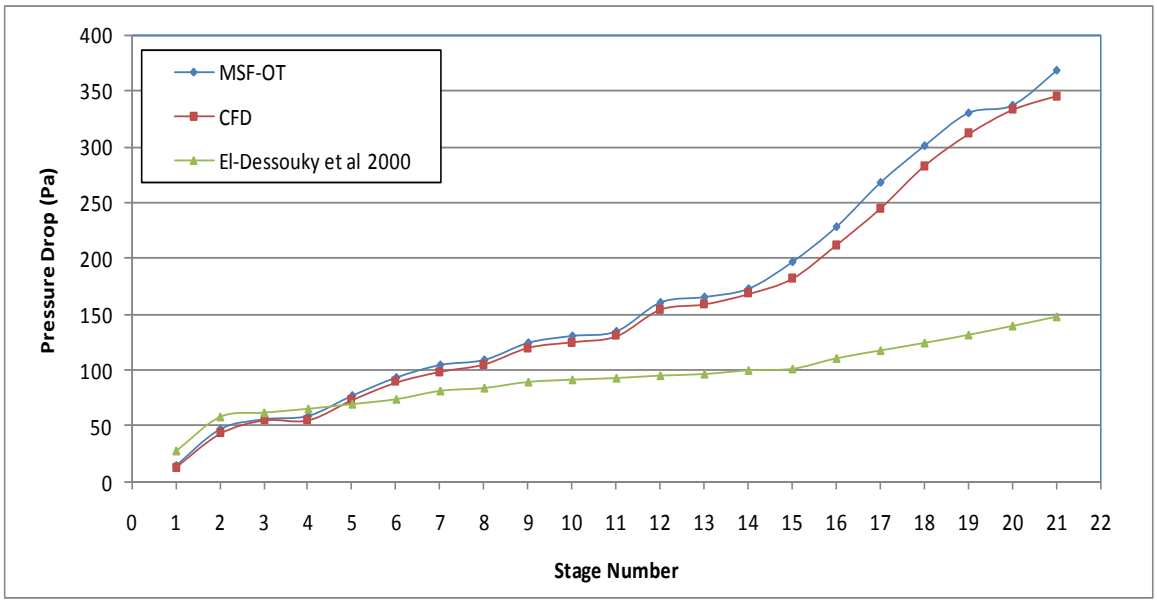

Figure 7.31 Variation in pressure drop as a function of MSF stage number for demister with packing density =80.317 kg/m^3 in MSF-OT plant

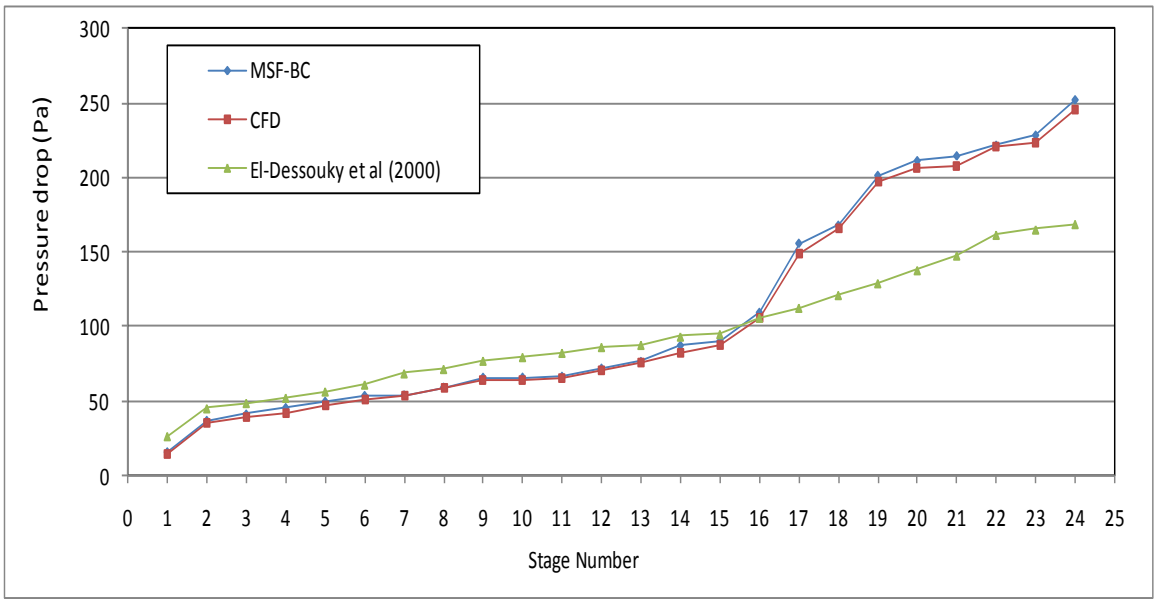

Figure 7.32 Variation in pressure drop as a function of MSF stage number for demister with packing density =80.317 kg/m^3 in MSF-BC plant operating at high temperature

7.4.4 Comparison between performance of different demisters

The demister which was previously validated against experimental data and real plant data consists of steel wires with 0.28 mm diameter. In this section new demisters were designed with the same geometry (spacing between the wires and arrangement) but with different wire diameter. The first demister has 0.24 mm diameter wires while the other is 0.2 mm diameter. The choice of these wires is not random but depends on the available wire specifications in the industry. That will reduce the cost of the demister rather than producing a new demister with specific wire diameter.

As shown in Figures 7.33-7.34, as the wire diameter decreases the pressure drop decreases. The separation efficiency remained almost unaffected for the 0.24 mm diameter demister but it decreased for the 0.20 mm diameter allowing the droplets to escape through the demister. Particle distribution within each demister type is shown Figure 7.35. The pressure drop kinks at stage 15 and that is due to many reasons such as the increase in vapour velocity, decrease in vapour density and increase in droplet density. Among these factors, the main cause for the increase in the pressure drop is the increase in the specific volume due to the decrease in the stage temperature. Therefore, a new driving force is initiated due to an increase in the rate of droplet re-entrainment at higher velocities. Thus the inlet droplet concentration in the inlet vapour to the demister increases and that is directly proportional to the pressure drop in the demister. As shown in table 7.11 the difference in temeprature which results in difference in velocity between stages 20 and 15 is much higher than the differences between stages 15 and 10. That causes the kink on stage 15.

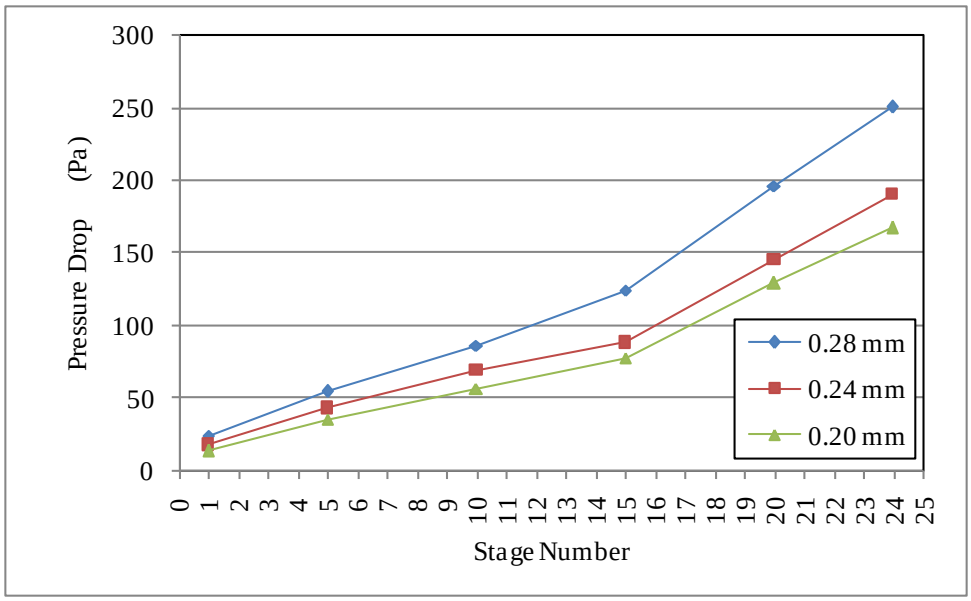

Figure 7.33 Variation in pressure drop as a function of the demister wire diameter for stages 1, 5, 10, 15, 20, 24 in the MSF-BC plant

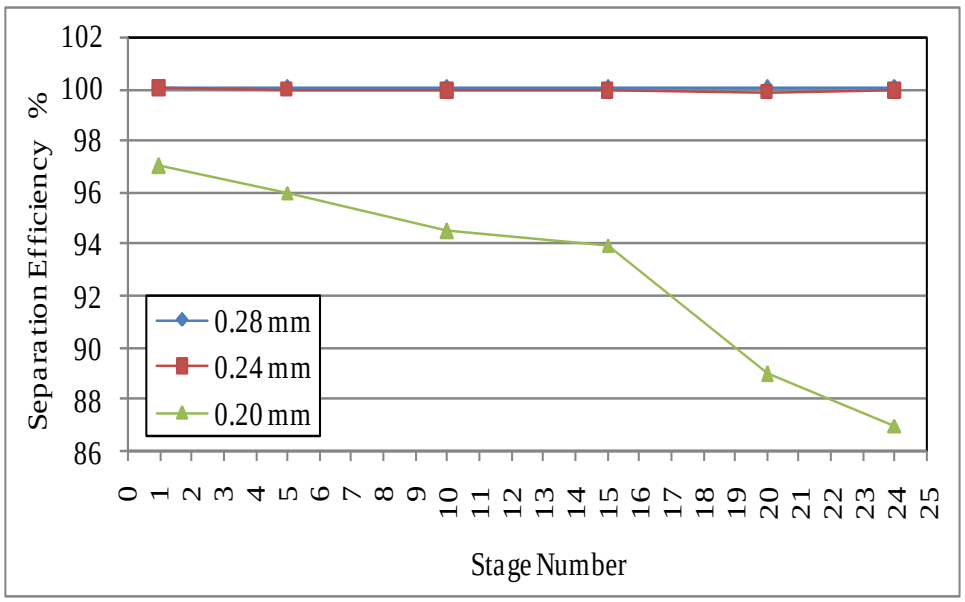

Figure 7.34 Variation in the demister separation efficiency as a function of the demister wire diameter for stages 1, 5, 10, 15, 20, 24 in the MSF-BC plant

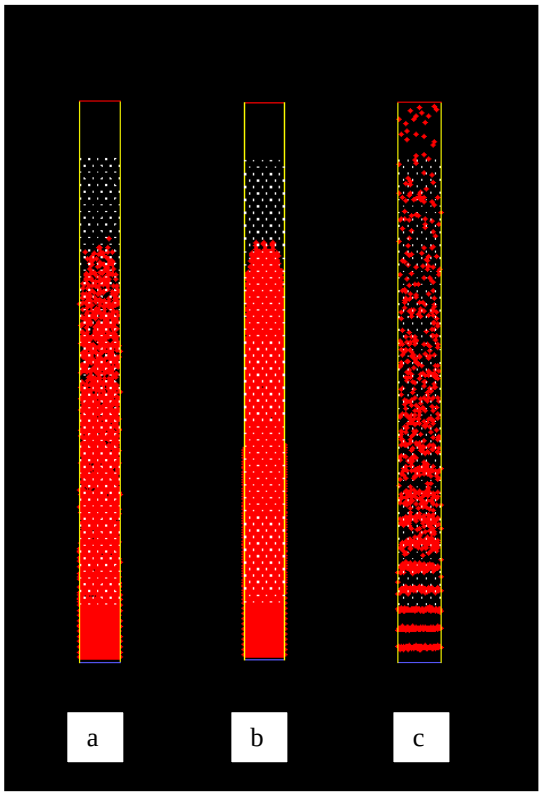

Figure 7.35 Droplet distribution in the demister with wire diameter: (a) 0.28 mm (b) 0.24 mm (c) 0.20 mm

From the obtained results, 0.24 mm wire diameter demister will be used to improve the efficiency of the MSF plant because it reduces the pressure drop across the demister with a negligible effect on the separation efficiency (within the design and acceptable range).

7.5 Conclusion

In this chapter a CFD model results were predicted for different conditions and validated following three approaches: (1) porous media- multi phase model approach (2) tube banks –multi phase model approach (3) tube banks- discrete phase model approach. All approaches showed a very good agreement with the experimental data

and real MSF plants data. The models were then used to do a sensitivity analysis and see the effect of some operating and design parameters on the demister performance (pressure drop and separation efficiency). The CFD results also showed more accurate results in comparison with an empirical correlation developed by El-Dessouky et al (2000) which was valid for the entire region of parameters.

The first two approaches can be used for simulation and troubleshooting purpose. In other words, by knowing the separation efficiency or the removal ratio of the liquid droplets, the pressure drop can be calculated. It is also useful for understanding the physics in the demister. The third approach can be used for both simulation and design purposes which makes it more useful.

Then new demisters with the same geometry and less wire diameter are designed and modeled using FLUENT and modeled by the third approach to predict their performance (pressure drop and separation efficiency). 0.24 mm wire diameter was selected because it reduces the pressure drop without affecting the separation efficiency

In the next chapter, the new demister is installed in the MSF-BC model constructed in gPROMS in order to predict the effect of the new demister on the required heat transfer area of the flashing stage condenser tubes and the product quality.

Chapter 8
Improving MSF Plant Performance

8.1 Introduction

A detailed mathematical model was presented in chapter 6 for the demister. Three approaches were followed to design the demister which are: (1) Porous media-Multi Phase Flow Model. (2) Tube –Banks Multi Phase Flow Model. (3) Tube- banks Discrete phase Model. The first two approaches have similar mathematical models (Eulerian-Eulerian) but with different boundary conditions and geometry. The third approach follows the (Eulerian-Lagrangian) approach as was described previously. The three approaches were validated in chapter 7 and showed good results in comparison with the available empirical correlation and real plant data. After validation new demisters with different wire diameter were designed and simulated using the third approach (section 7.4.4) to predict their effect on the pressure drop and separation efficiency. As mentioned in chapter 7, the third approach is more general and applicable for design purposes since it doesn't need the value of the removal efficiency in advance just like the other two approaches.

This work is motivated by the strong effect of the demister performance on the capital and operating costs of the plant. The demister performance has a strong effect on the total heat transfer area in the plant, which accounts for more than 70% of the plant capital cost, ((Al-Deffeeri, 2009), (Ettouney, El-Dessouky, & Faibish, 2002)). Also, the demister performance affects the product quality, which is strongly related to unit product cost. The newly designed demister will be used to perform the following: (1) predict steady state design/operating features to determine variations in the condenser heat transfer area and the product quality, (2) compare the effect of the new designed demister and the currently used demister on the MSF plant dynamics, i.e., determine the increase/decrease in time to reach new steady state upon imposing system disturbance.

To achieve the above tasks, the simulations performed in this chapter combine the predictions of the demister CFD model and the gPROMS simulation of the MSF plants.

In this chapter, the effect of the newly designed demisters on the MSF-OT and MSF- BC plant performance is predicted. That includes their effect on the flashing stages pressure drop, separation efficiency and product quality. This is followed by studying the effect of the current/new demisters on the system dynamics. At the end of this chapter, main conclusion will be shown.

8.2 Effect of improved demister on the MSF-OT plant performance

The effect of the newly designed demisters on the MSF-OT plant shown in Figure 2.9 will be presented in this section. The newly designed demisters will be included in the gPROMS model of the MSF-OT (section 4.4) plant to predict their effect on the product quality, plant heat transfer area and system dynamics.

8.2.1 Effect of new demister on the product quality

The product quality is measured by the amount of TDS (total dissolved solids) or salt content in the distillate product. As shown in table 8.1, the product qualities for the three demisters are calculated using gPROMS model. For the current demister (0.28mm wire diameter) the product quality is the best (lowest TDS). The new demister with 0.24 mm wire diameter almost did not affect the product quality while the demister with 0.20 mm diameter reduced the product quality and thus it is not used. The effect of increasing TDS will not affect the product quality only, but also it will cause corrosion of the tube banks as the salts will accumulate on its outer surface and that will cause tube damage.

Table 8.1: Product quality for different types of demisters installed in MSF-OT plant

Demister Wire Diameter (mm)	Product Quality (TDS) ppm
0.28	2
0.24	3
0.20	47

8.2.2 Effect of new demister on the flashing stage condenser area.

Two newly designed demisters with different wire diameter will be used to simulate MSF-OT plant (Tables 5.1, 7.10) using gPROMS. In this section, the effect of varying the demisters on the heat transfer area of the flashing stage was obtained. As shown the tube number, inner and outer diameter mentioned in table 5.1 is for the MSF plant with current demister (0.28 mm wire diameter). The reduced heat transfer area which will be obtained by using the new demister (0.24 mm wire diameter) is not related to the current tube parameter (0.28 mm wire diameter).

The pressure drops across the demister in all stages are listed in table 8.2. The pressure drop is given for the installed demister with 0.28 mm wire diameter and the new demister with 0.24 mm wire diameter. As shown in table 8.2 and Figure 8.1, the pressure drop across the demister for the MSF plant flashing stages is lower for the demister with 0.24 mm wire diameter.

As shown in table 8.3 and Figure 8.2, as the demister wire diameter decreases, the heat transfer required to condense the same amount of water vapor decreases. This is because as the pressure drop decreases the vapor temperature above the demister will increase. That will lead to an increase in the heat transfer driving force for the heat transfer around the condenser tubes and from equation (4.23), less area will be required to transfer the same amount of heat. The reduction in the heat transfer area increases across the stages until it exceeds 39% for the last stage. This is important because the condenser tubes account for almost 70 % of the plant capital cost, so any small reduction will directly affect the plant cost (Al-Zubaidi, 1987). As shown, the heat transfer area for the current plant is constant from stage 1 to 21. The reason

behind having constant values is a design feature which simplifies plant manufacturing.

Table 8.2: Pressure drop across demisters in MSF-OT (Plant A) flashing stages

Stage No	Pressure Drop (Pa)		Reduction %
	0.28 mm diameter (Current Demister)	0.24 mm diameter (New Demister)	
1	14.084	9.500	32.55
2	46.858	35.010	25.29
3	55.718	37.547	32.61
4	58.783	39.424	32.93
5	77.000	42.023	45.42
6	93.247	44.758	52.00
7	104.588	50.593	51.63
8	109.146	52.659	51.75
9	124.531	59.230	52.44
10	130.707	62.635	52.08
11	134.837	65.066	51.75
12	160.815	67.892	57.78
13	165.698	69.863	57.84
14	173.189	74.618	56.92
15	197.372	76.670	61.15
16	228.940	86.259	62.32
17	268.740	97.339	63.78
18	301.824	104.254	65.46
19	331.337	116.603	64.81
20	338.222	127.446	62.32
21	369.634	142.805	61.37

Table 8.3: Heat transfer area reduction in MSF-OT (Plant A) flashing stages

Stage No	Heat Transfer Area (m^2)		Reduction
	0.28 mm diameter (Current Demister)	0.24 mm diameter (New Demister)	%
1	3676.4	3674	0.054
2	3676.4	3671	0.158
3	3676.4	3666	0.273
4	3676.4	3664	0.327
5	3676.4	3652	0.665
6	3676.4	3638	1.040
7	3676.4	3628	1.309
8	3676.4	3620	1.544
9	3676.4	3602	2.017
10	3676.4	3589	2.376
11	3676.4	3575	2.754
12	3676.4	3524	4.153
13	3676.4	3498	4.845
14	3676.4	3469	5.652
15	3676.4	3387	7.863
16	3676.4	3284	10.662
17	3676.4	3133	14.787
18	3676.4	2952	19.713
19	3676.4	2749	25.229
20	3676.4	2598	29.333
21	3676.4	2235	39.213

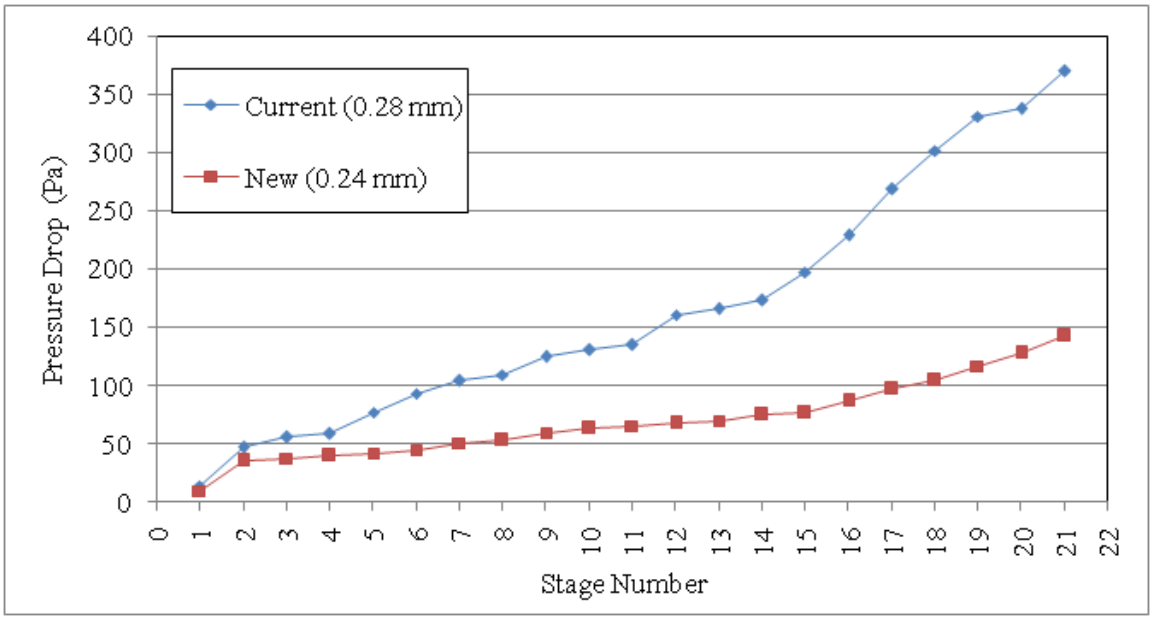

Figure 8.1 Pressure drop across current and new demister for MSF-OT plant flashing stages

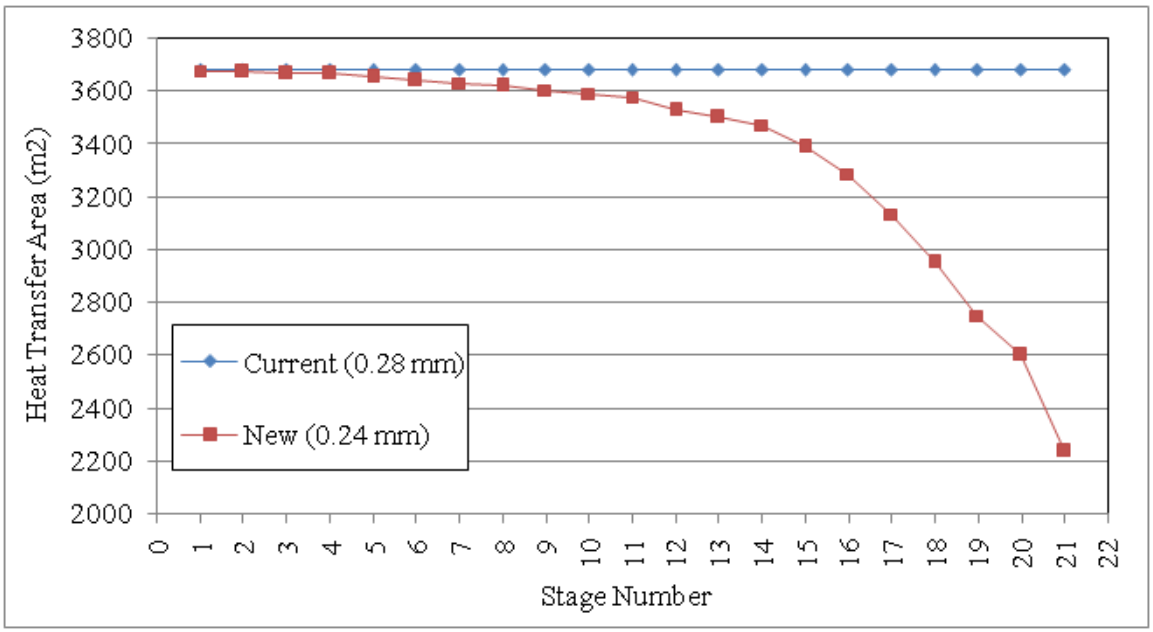

Figure 8.2 Condenser heat transfer areas required to transfer the same amount of heat using current and new demister for MSF-OT plant flashing stages

8.3 Effect of improved demister on the MSF-BC plant performance

The effect of the newly designed demisters on the MSF-BC plant shown in Figure 2.10 will be presented in this section. The new designed demisters will be installed in the gPROMS model of the MSF-BC (section 4.5) plants to predict their effect on the plant heat transfer area, product quality and system dynamics.

8.3.1 Effect of new demister on the product quality

The performance ratio (amount of distillate product per unit mass of steam fed to the brine heater) when an average value of 3332 m^2 for the heat gain section stages and 3241 m^2 for the heat rejection section stages was used with the new designed demister equals 7.0 and for the current MSF-BC plant is 7.005. That means that the performance ratio was almost not affected with the reduction in the heat transfer area. That proves that installing the new demister will not affect the plant performance ratio. As shown in table 8.4, using a demister with 0.24 mm wire diameter will not affect the product quality but the demister with 0.20 mm wire diameter has a big effect on the product quality. As was mentioned in section 8.2.2, the effect of increasing TDS will not affect the product quality only, but also it will cause corrosion of the tube banks as the salts will accumulate on its outer surface and that will cause tube damage.

Table 8.4: Product quality for different types of demisters installed in MSF-BC plant

Demister Wire Diameter (mm)	Product Quality (TDS) ppm
0.28	5
0.24	7
0.20	89

8.3.2 Effect of new demister on the flashing stage condenser area

Two demisters with different wire diameter will be used to simulate two MSF-BC plants. One operates at high temperature (Plant B) and other at low temperature (Plant D) using gPROMS. In this section, the effect of varying the demisters on the heat transfer area of the flashing stage was obtained. As shown, the tube number, inner and outer diameter mentioned in tables 5.3, 5.4 is for the MSF plant with current demister (0.28 mm wire diameter). The reduced heat transfer area which will be obtained by using the new demister (0.24 mm wire diameter) is not related to the current tube parameter (0.28 mm wire diameter).

The pressure drop across the demister in all stages for both plants are listed in tables 8.5, 8.7. The pressure drop is given for the installed demister with 0.28 mm wire diameter and the new demister with 0.24 mm wire diameter. As shown in tables 8.5, 8.7 and Figures 8.3, 8.5, the pressure drop across the demister for the MSF plant flashing stages is lower for the demister with 0.24 mm wire diameter.

As shown in Figures 8.4, 8.6, as the demister wire diameter decreases, the heat transfer required to condense the same amount of water vapor decreases. That is because as the pressure drop decreases the vapor temperature above the demister will increase. That will lead to an increase in the heat transfer driving force around the condenser tubes and from equation (4.23), less area will be required to transfer the same amount of heat. The reduction in the heat transfer area increases across the stages until it exceeds 8.5% for the last stage. That is important because the condenser tubes account for almost 70 % of the plant capital cost, so any small reduction will directly affect the plant cost. As shown, the heat transfer area for the current plant is constant from stage 1 to 21 (heat gain section) and then increases and remains constant for stages 22, 23 and 24 (heat rejection section). The reason behind having constant values is a design feature which simplifies plant manufacturing.

Comparing the results of the effect of the newly designed demister on the MSF-BC plants operating at high and low temperature, the following observations are found:

1. From Tables (8.5 and 8.7), the maximum reduction in the pressure drop for the MSF-BC operating at low temperature is lower than that of the MSF-BC plant operating at high temperature. That is due to the fact that at low temperature the vapour specific volume increases resulting in increasing the vapour velocity. The high velocity causes higher pressure drop as was mentioned in chapter 7. Using the newly designed demister in will reduce the pressure drop but less than that of high temperature operation.
2. From Tables (8.6 and 8.8) the reduction in the heat transfer area for the MSF-BC operating at low temperature is higher than that of the MSF-BC plant operatig at high temperature. That is due to the fact that at low temperature the latent heat of evaporation is higher than the enthalpy at high temperature and that will increase the driving force for heat transfer and reduce the required heat transfer area.

Table 8.5: Pressure drop across demisters in MSF-BC (Plant D) operating at low temperature

Stage	Pressure Drop (Pa)		Reduction %
	0.28 mm diameter (Current Demister)	0.24 mm diameter (New Demister)	
1	25.442	17.880	29.723
2	35.277	26.104	26.003
3	43.462	31.996	26.382
4	44.161	32.460	26.496
5	55.600	43.156	22.381
6	68.419	50.574	26.082
7	69.445	52.714	24.092
8	72.791	55.544	23.694
9	80.542	62.341	22.598
10	86.621	68.938	20.414
11	91.236	70.676	22.535
12	105.062	84.547	19.527
13	106.465	85.547	19.648
14	115.871	87.448	24.530
15	131.285	88.027	32.950
16	135.978	101.170	25.598
17	159.851	113.588	28.941
18	185.376	130.794	29.444
19	188.249	139.458	25.918
20	200.225	145.354	27.405
21	204.146	150.215	26.418
22	206.173	150.623	26.943
23	219.094	163.182	25.520
24	293.358	190.798	34.961

Table 8.6: Heat transfer area reduction in MSF-BC (Plant D) flashing stages operating at low temperature

Stage No	Heat Transfer Area (m^2)		Reduction %
	0.28 mm diameter (Current Demister)	0.24 mm diameter (New Demister)	
1	3482	3364	3.389
2	3482	3363	3.418
3	3482	3361	3.475
4	3482	3361	3.475
5	3482	3360	3.504
6	3482	3357	3.590
7	3482	3357	3.590
8	3482	3355	3.647
9	3482	3354	3.676
10	3482	3353	3.705
11	3482	3349	3.820
12	3482	3348	3.848
13	3482	3345	3.935
14	3482	3336	4.193
15	3482	3315	4.796
16	3482	3310	4.940
17	3482	3301	5.198
18	3482	3282	5.744
19	3482	3270	6.088
20	3482	3266	6.203
21	3482	3257	6.462
22	3508	3268	6.842
23	3508	3245	7.497
24	3508	3210	8.495

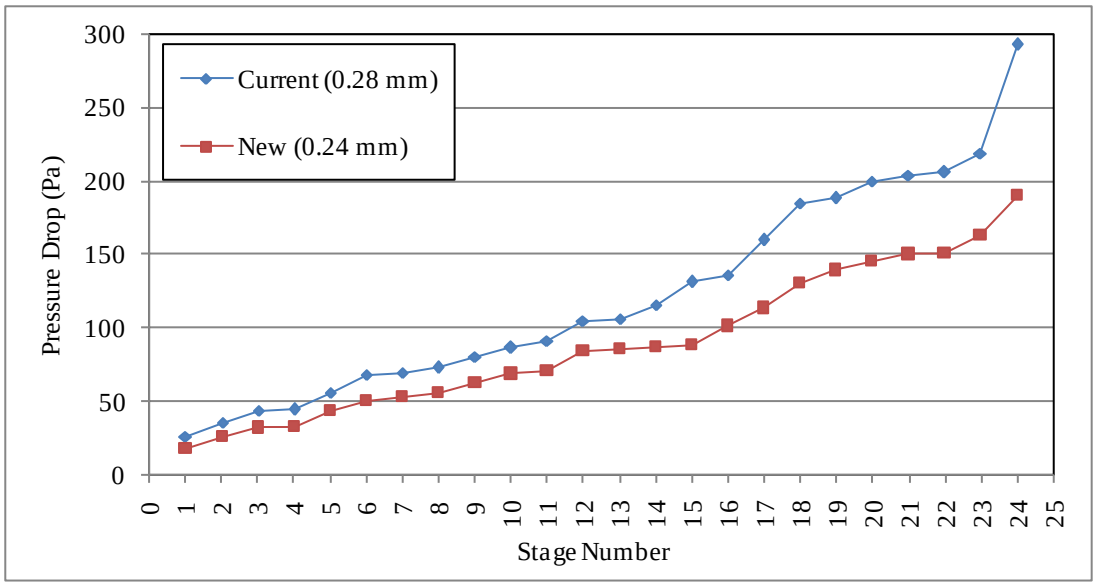

Figure 8.3 Pressure drop across current and new demister for MSF-BC plant flashing stages operating at low temperature

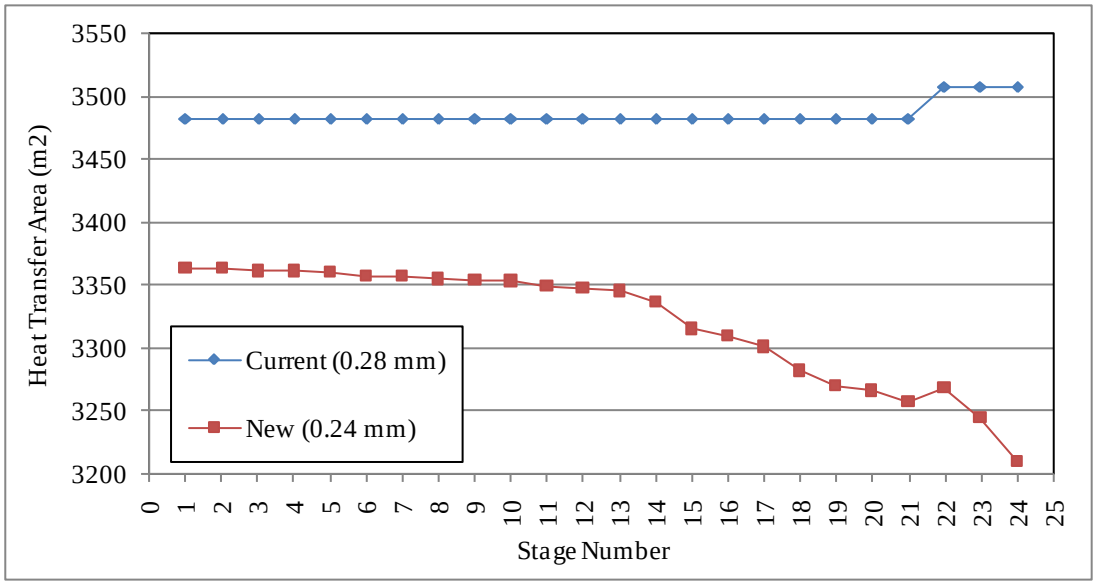

Figure 8.4 Condenser heat transfer area required to transfer the same amount of heat using current and new demister for MSF-BC plant flashing stages operating at low temperature

Table 8.7: Pressure drop across demisters in MSF-BC (Plant B) operating at high temperature

Stage	Pressure Drop (Pa)		Reduction %
	0.28 mm diameter (Current Demister)	0.24 mm diameter (New Demister)	
1	15.633	10.082	35.508
2	36.752	21.536	41.402
3	41.014	24.907	39.272
4	45.374	28.774	36.584
5	49.593	33.565	32.319
6	53.501	39.317	26.512
7	53.877	46.090	14.452
8	59.048	50.162	15.048
9	65.709	53.387	18.752
10	65.803	57.025	13.340
11	66.382	57.720	13.048
12	71.830	60.242	16.133
13	76.322	60.885	20.226
14	87.237	66.512	23.757
15	89.982	76.471	15.015
16	109.308	81.000	25.897
17	155.737	92.387	40.678
18	167.838	107.401	36.010
19	201.274	121.069	39.849
20	221.170	140.434	36.504
21	214.409	162.419	24.248
22	221.476	177.655	19.786
23	228.290	178.906	21.632
24	252.047	182.027	27.781

Table 8.8: Heat transfer area reduction in MSF-BC (Plant B) flashing stages operating at high temperature

Stage No	Heat Transfer Area (m^2)		Reduction %
	0.28 mm diameter (Current Demister)	0.24 mm diameter (New Demister)	
1	3676	3675	0.049
2	3676	3671	0.158
3	3676	3669	0.203
4	3676	3667	0.253
5	3676	3665	0.322
6	3676	3665	0.315
7	3676	3669	0.201
8	3676	3667	0.268
9	3676	3661	0.428
10	3676	3664	0.331
11	3676	3663	0.358
12	3676	3657	0.527
13	3676	3649	0.737
14	3676	3638	1.041
15	3676	3649	0.738
16	3676	3619	1.559
17	3676	3541	3.670
18	3676	3542	3.655
19	3676	3491	5.033
20	3676	3481	5.323
21	3676	3544	3.597
22	3148	3047	3.185
23	3148	3033	3.656
24	3148	2978	5.377

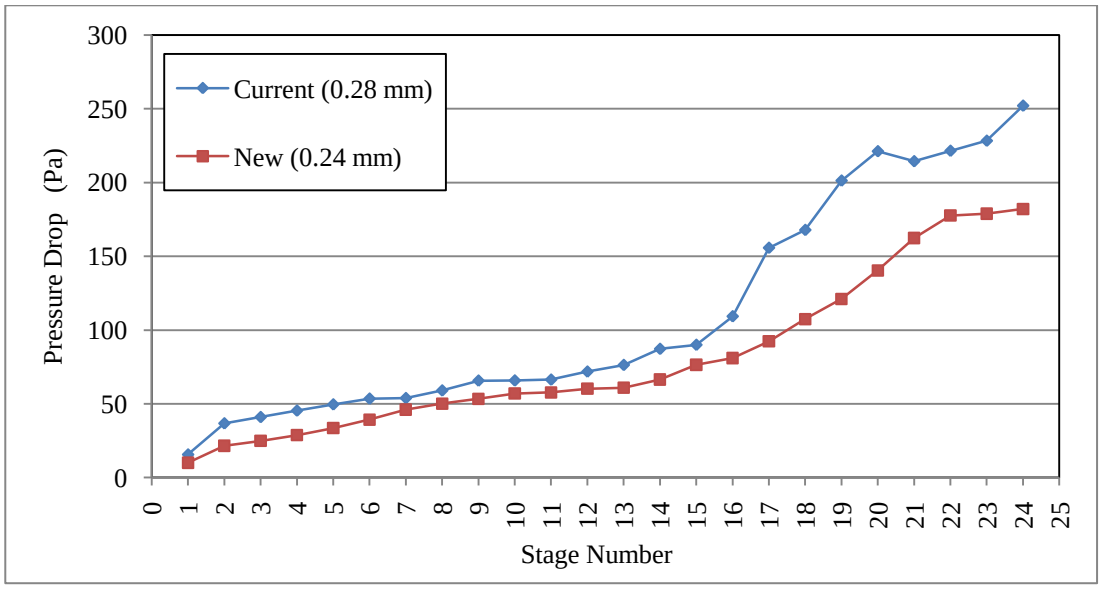

Figure 8.5 Pressure drop across current and new demister for MSF-BC plant stages operating at high temperature

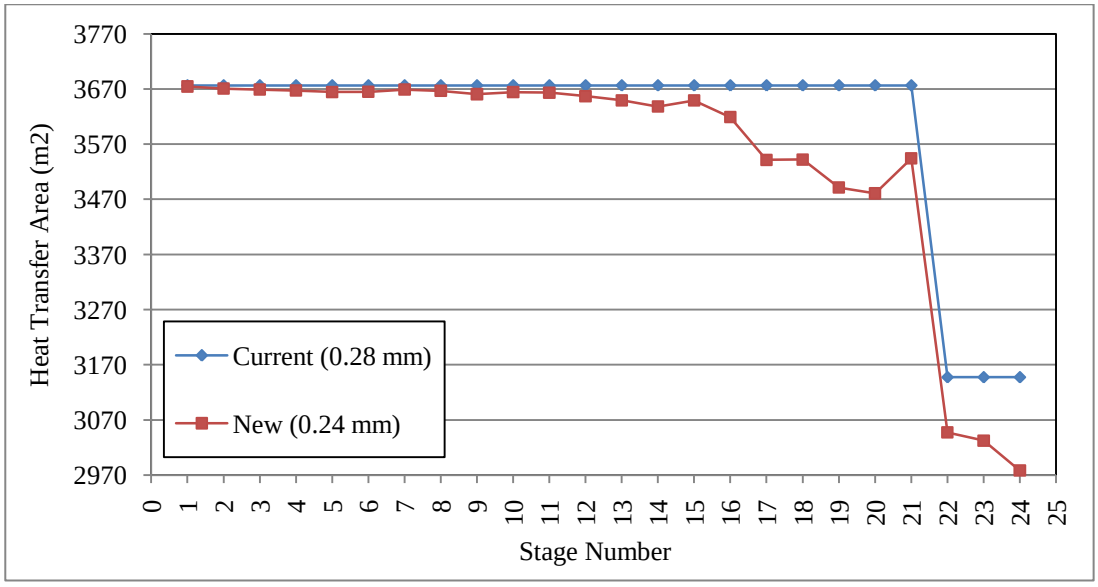

Figure 8.6 Condenser heat transfer area required to transfer the same amount of heat using current and new demister for MSF-BC plant stages operating at high temperature

8.3.3 Effect of new demister on system dynamics

The new demister with 0.24 mm wire diameter is installed in the MSF-BC model built in gPROMS. The effect of the new demister on the system dynamics will be studied in this section; in other words, how long it will take the system to reach steady state after applying a disturbance. Two disturbances are applied: the first changes the cooling water flow rate by decreasing it by 70 % and then going back to the original value. The second is reducing the top brine temperature (by changing either the steam flow rate or temperature) by 2 ^{o}C and going back to the original value. The system behaviour is studied for three different stages (stages 1 , 15 , 23).

As shown in Figure 8.7, the new and current demisters undergo the same response for the cooling water flow rate disturbance without any delay in the new demister. The same behaviour is shown in Figure 8.8, when the top brine temperature disturbance is applied. That proves that the new demister will not delay the steady state condition if any disturbance occurs in the operating condition of the plant.

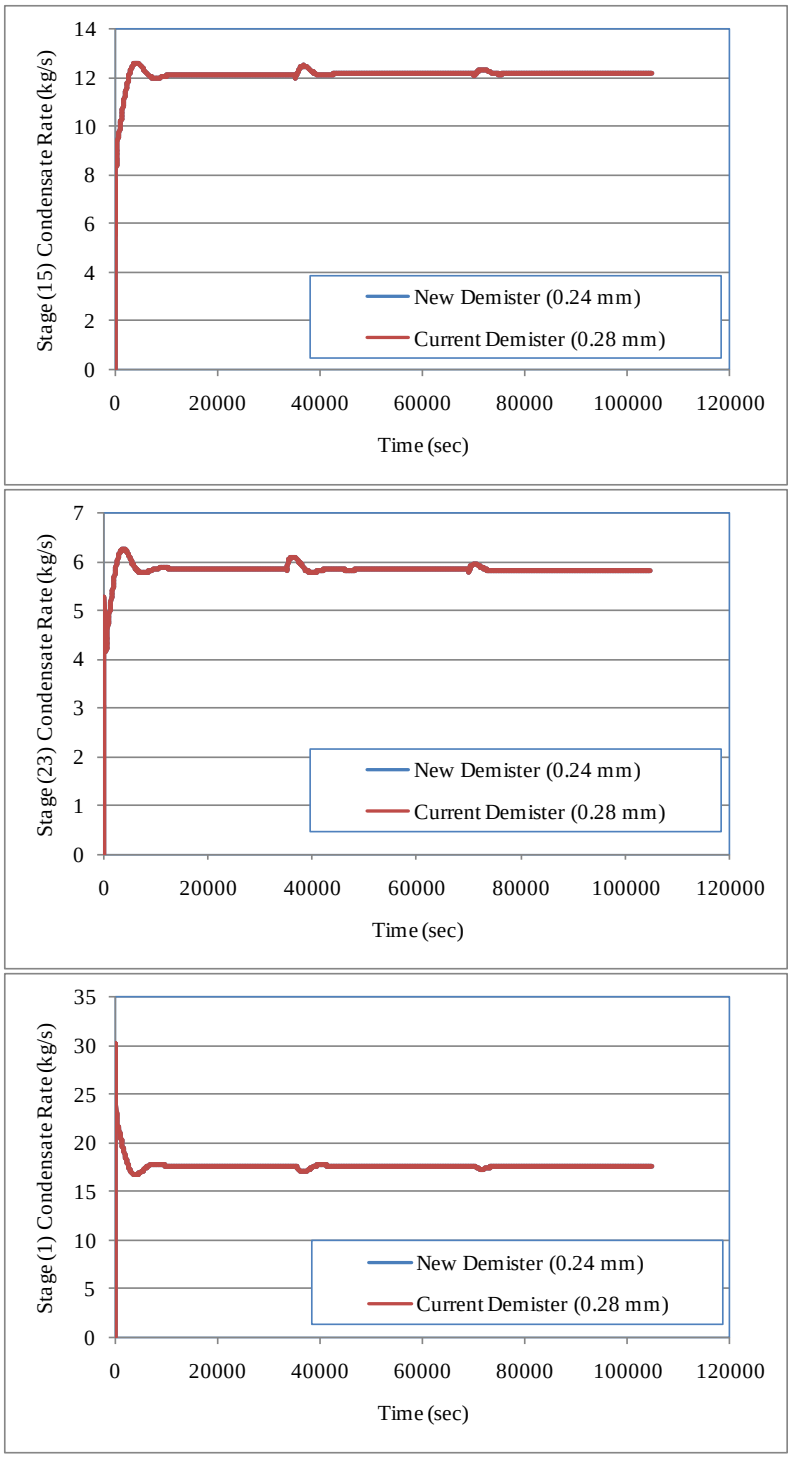

Figure 8.7 Dynamics of the condensate rate in stages 1, 15, and 23 for step decrement in the cooling water flow rate for new and current used demisters

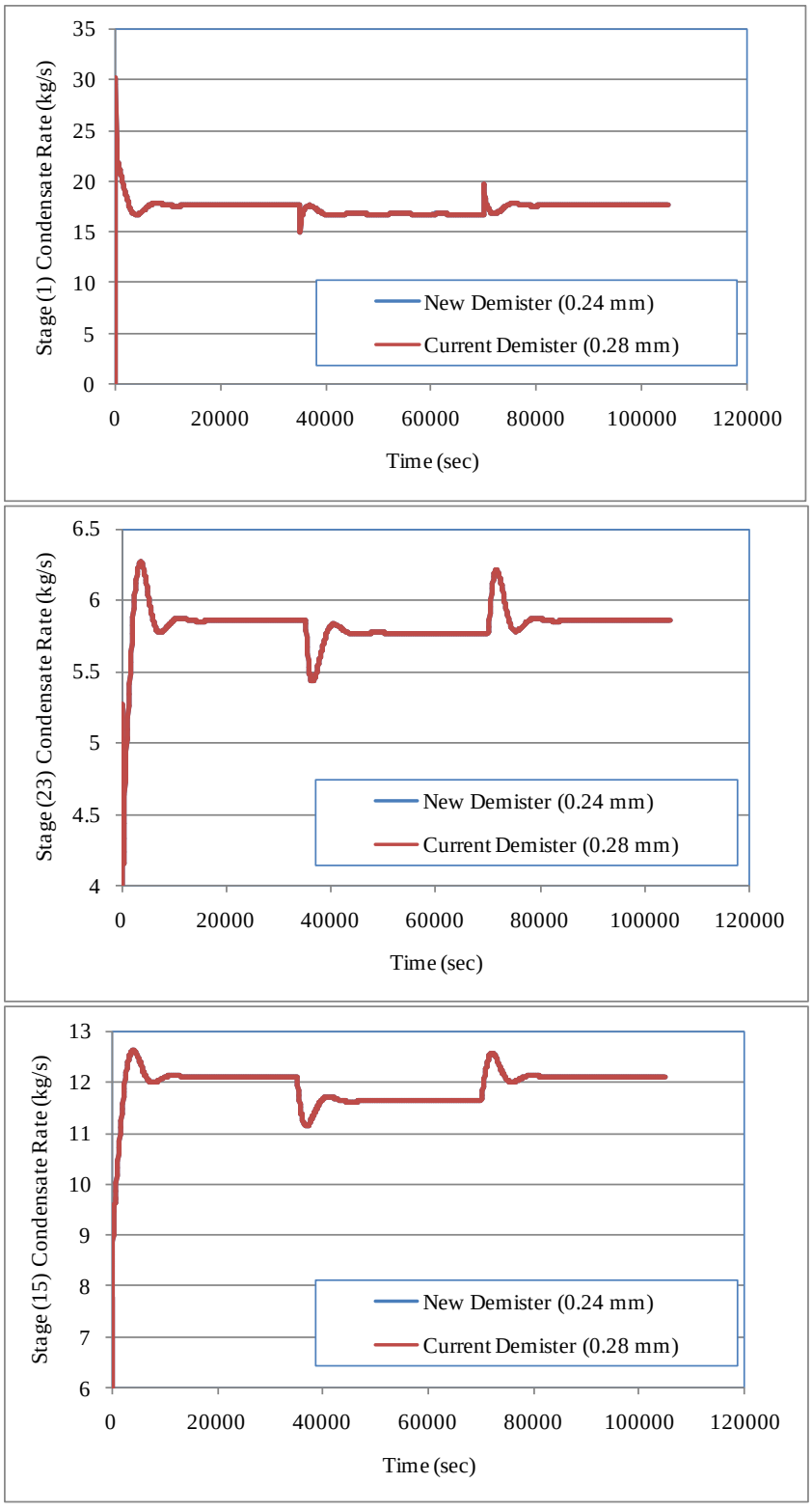

Figure 8.8 Dynamics of the condensate rate in stages 1, 15, and 23 for step decrement in the top brine temperature for new and current used demisters

8.4 Conclusion

A newly designed demister was simulated using CFD tool (FLUENT) and installed in MSF plants model build in gPROMS simulator to predict the effect of the new demister on the plants performance. The new demister was first installed in MSF-OT gPROMS model, and then, the same procedure was repeated for two MSF-BC plants. One is operating at high temperature and other is operating at low temperature in order to predict the effect of the new demister on different plants operating at different conditions. The results showed that the new demister reduced the pressure drop across the demister in all flashing stages without affecting the product quality. As a result the heat transfer area of the condenser tubes was reduced and that will reduce the plant capital and unit product cost. On the other hand, installing the new demister did not cause any delay in reaching the steady state condition after applying disturbances to the plant. That gives the newly designed demister another strength point.

The selection between operating at high temperature or low temperature is tied up with the antiscalent and weather it is capable to withstand the high temperature or not. The new units are all built to operate in the high temperature range. On the other hand, the older units were built to operate in the low temperature range because the antiscalent technology could not support high temperature operation. These days a unit is found with high/low temperature operation range and usually such unit is old and is modified to operate in the high temperature range in order to increase the production capacity. So it is better to operate at high temperature as long as the antiscalent allows because higher temperatures increase the flashing range, the performance ratio or GOR and the production capacity.

Chapter 9
Conclusions and Future work

9.1 Conclusions

Desalination has proved that it is a feasible and economical process to solve the water shortage problem in many regions around the world. There are many desalination technologies but Multi Stage Flashing (MSF) and Reverse Osmosis (RO) processes are the leading techniques in this industry. The MSF process accounts for 50% of desalination market worldwide and more than 90% for the desalination industry in Kuwait and the Gulf countries. Thus, MSF was selected as the topic for research in this thesis where it focused on developing models which include the dynamics of the MSF process and CFD modeling of the demister. The studies conducted in this thesis are novel and new to the literature. This adds and contributes to enhancement of knowledge and understanding of the MSF process. In addition, results of this work can be used to improve the process efficiency and reduce the capital and product unit cost.

To begin our study, in Chapter 2, the need for water desalination and different types of desalination technologies was presented. That was followed by a comprehensive literature review on steady state and dynamic modeling of MSF processes in Chapter 3. The review provided the weaknesses and strengths of the available models in the literature and helped in developing the new models presented in this thesis. The newly developed models were based on a fewer number of assumptions and more details were added to the model to increase its accuracy.

Detailed and comprehensive dynamic mathematical models for both MSF-OT and MSF-BC processes were developed in Chapter 4 aiming to fulfill some of the weaknesses of the existing published models. Extensive literature review showed that most of the published dynamic models are limited to the once through configuration (MSF-OT). Other model details include modeling of the dynamics of the brine heater, which have a strong effect on the gain output ratio. Also, effects of the demister on

the pressure drop in the vapour and the effect of distillate flashing were included in the dynamic model.

In chapter 5, the MSF models (steady state and dynamics) were solved using the gPROMS software. This computer package enables constructing the model in a hierarchical structure where the lower hierarchy includes the flashing stages while the higher hierarchy combines the flashing stages together and also combine them with the brine heater. The gPROMS software facilitates solution of the non-linear set of equations forming either of the steady state or the dynamic models. The predictions of the steady state and dynamic models for both MSF-OT and MSF-BC processes were carefully validated against several sets of data obtained from large MSF plants operating at different conditions and having different design characteristics. That was essential to prove the generality of the models and that are applicable to any MSF plant in the world. They can be useful for operating, troubleshooting and design purposes. This process showed very good agreement for both steady state and dynamic models. The other part of the validation was made through examining the expected system behavior as well as known physical phenomena, i.e., lower vapour temperature than brine temperature because of thermodynamic losses, increase in vapour velocity and demister pressure drop in low temperature stage. For all of the simulation conditions it was found that the model predictions are physically sound and follow known and expected behavior.

An important part of this study was the analysis of the MSF dynamic response upon making step changes in the system operating parameters. This was motivated by the fact that most of the previous literature studies of MSF dynamics were limited to model testing or examining a limited range of operating parameters. Therefore, it was necessary to make use of the dynamic model over a wide range of operating conditions. The findings of this analysis are new to the literature and would provide valuable insights into limits of operating conditions. In turn, plant operators can avoid unnecessary increase or decrease in the operating parameters that may lead to system shut down, which is costly. This is due to loss of production (throughout the duration of the system shutdown and startup) and the cost incurred during a new startup.

The second part of this work involved CFD modeling of the MSF demisters. This task is novel to the MSF desalination literature. As the vapour and entrained brine droplets flow upward across the demister, its temperature and pressure drop. That in turn reduces the heat transfer driving force between the condensed vapour and the brine flowing in the condenser tubes and as a result more heat transfer area is required which in turn increases the plant cost. Thus, this study focused on design of a wire mesh demister that gives a maximum removal efficiency and minimum pressure drop. The new demister design resulted in smaller pressure drop with negligible effect on the separation efficiency. Simultaneously, the temperature drop through the demister was smaller. In turn, a smaller heat transfer area was necessary to achieve the same degree of feed preheating. This resulted in a decrease of the plant capital as well as the unit product cost.

To begin solving this task, three different approaches were used to model the demister. The first is the porous media approach. Second is the tube bank-multi phase flow model. Third is tube bank-discrete phase model approach. The first two approaches followed Eulerian-Eulerian modeling method and the third approach followed Eulerian-Lagrangian modeling method. The three approaches have been simulated using the CFD software (FLUENT) and the predicted results were validated against experimental and data from real MSF plants that covered a wide range of operating conditions. All approaches showed a very good agreement with the experimental data and operating plant data. These models can be used to see the effect of some operating and design parameters on the demister performance (pressure drop and separation efficiency). The first two approaches could be used for simulation and troubleshooting purposes since both depend on a prior knowledge of the demister removal efficiency. The third approach could be used for simulation troubleshooting as well as design purposes, because it does not require knowledge of the demister removal efficiency. This made the third approach more general than the other two methods. On the other hand, the third approach did not account for the brine droplet resistance to the vapour flow because it was not possible to include both upward and downward flows in the same zone and calculate the interaction between them.

New demisters were designed and simulated using FLUENT to predict their pressure drop and removal efficiency. The values of the predicted pressure drop by FLUENT for the new demisters were fed as input to the gPROMS simulator to predict their effect on the MSF-OT and MSF-BC plants performance. The new demister with 0.24 mm wire diameter reduced the pressure drop across the demister in all flashing stages without affecting the product quality. On the other hand, the new designed demister with 0.20 mm wire diameter reduced the pressure drop but increased the water salinity and affected the product quality. As a result, (0.24 mm wire diameter demister) was selected. That reduced the heat transfer area of the condenser tubes as well as the plant capital cost and product unit cost. On the other hand, installing the new demister did not cause any delay in reaching the steady state condition after applying disturbances to the plant. That gives the new designed demister another strength point.

The modelling approach presented in this thesis enables design of thermal desalination units to determine optimal heat transfer area and operating conditions. The gPROMS software was developed to simulate the MSF steady and dynamic behaviour. For the first time CFD modelling of demister steady and dynamics were developed and analyzed for the MSF process. These models can be extended to simulate and design other desalination and chemical processes.

9.2 Future work

In this thesis, steady state, dynamic, and CFD models are developed and used to simulate/design the MSF process. The steady state and dynamic models were based on well established procedures in the literature; however, in the developed model, several new features were added to the model to improve the accuracy in predicting the system behaviour such as the pressure drop across the demister, distillate flashing and the venting system. These models were solved using the gPROMS software, which is an equation oriented simulator. This simplified simulation of the multistage process in a hierarchical structure. This also, allows for addition/removal of other

process elements and details. This is done without having to modify the entire code for the process.

Several future studies can be done on steady state and dynamic modeling on the MSF process and other similar thermal desalination or separation processes. These studies include the following:

1. Further relaxation of the model assumptions, i.e., thermal energy losses from the system, extensive and detailed modeling for the release of the non-condnesable gases, salt entrainment in the product water, fouling resistance, etc. Relaxation of these assumptions will improve the model prediction abilities of various elements of the process. This will improve the accuracy in process simulation and design and will give more realistic picture of the process elements. This task will be achieved as a result of rapid progress and advancement in computing hard/soft ware.
2. Exergy analysis is also another useful development that can be made for the models developed in this study. Therefore, addition of the entropy balance equation to various elements of the process can be done in order to determine exergetic efficiency (2^{nd} law efficiency) of the system, which is more accurate than the first law efficiency. Exergy can be used as well to determine what is known as exergetic economics (Sharaf, Nafey, & Lourdes, 2011).
3. Optimizing the developed model to predict the optimal operating and design condition which will lead to a higher gain output ratios in the plant.
4. The model development and analysis presented in this study can be adopted to simulate other thermal desalination processes (multiple effect evaporation) as well as chemical separation processes. This is to take advantage of the hierarchal structure and the simple coding of the gPROMS simulator.

The second part of the work focused on CFD simulation of the MSF demister, which is the first time this task is undertaken in open literature. Three modeling approaches are used in the CFD analysis that include use of porous media (Eulerian-Eulerian models for the continuous and brine droplets) and tube bank arrangement that used the same Eulerian-Eulerian approach as in the porous media and the

Eulerian-Lagrangian approach for the vapour phase (continuous phase) and the brine droplets (discrete phase). Several schemes are proposed to continue the novel CFD study and analysis presented in this thesis. These schemes include the following:

1. Relaxation of the model assumptions in the demister model. This may include any of the following: 1) upward/downward movement of the brine droplets or re-entrainment/detachement/settling, where different pathes are assigned for rising and falling droplets, 2) fouling accumulation and build on the demister wire and how it would affect separation efficiency, pressure, vapour/droplet flow, and 3) dropletet growth or disintegration during upward/downward flow. These are some of ideas that can be pursued to improve the demister CFD model.
2. CFD modeling and analysis of the condenser tube, which is a novel approach in MSF literature studies. This study will built on similar studies developed other system and processes (Hu & Zhang, 2007), (Zhang & Zhang, 1993). CFD model for the condenser tubes which includes identifying the dead zones and the effect of the different tube arrangements on the efficiency of the condensation process. Although similar studies are done in this topic (in other processes and application) but it will be the first of its type in desalination.
3. CFD model for the brine pool and orifice which includes bubbles formation, growth and release. Limited numbers of studies are available on orifice flow. Most of the available literature studies are limited to isothermal flow without bubble formation, growth, and release. Therefore, this study will be novel and new to the literature of MSF, desalination, and chemical processes (Lior, Chung, & Miyatake, 2002), (Rautenbach & Schafer, 1999).
4. CDF model for the vapour flow in the vapour space above the brine pool, through the demister, and around the condenser tubes. This model will combine the demister model presented in this thesis together with the condenser model mentioned in the previous point.
5. Link of CFD and gPROMS can be used to combine the effect of the previous points on the MSF plant performance and get more detailed and flexible model. That will help in understanding the effect of the behaviour of the vapour and liquid streams in the flashing stage on the whole plant performance

and how any change in the design of the flashing stage details may affect the plant behaviour.

Notation

A	Area, m^2.
A_{do}	Total projected area of droplets in a given control volume, m^2
A_p	Demister specific area, m^2/ m^3
B	Flow rate of flashing brine between stages, kg/s.
BPE	Boiling point elevation, ^oC
C	Salt concentration, kg/m^3
C_1	Constant in *k-ε* model
C_2	Constant in *k-ε* model
C_{p2}	Pressure jump coefficient
Cd	Discharge coefficient
C_{DC}	Drag coefficient
C_f	Interphase friction coefficient
C_p	Specific heat at constant pressure, kJ/kg ^oC
C_{phase}	Constant
C_μ	Constant in *k-ε* model
D	Flow rate of the distillate between stages, kg/s.
D_{to}	Outer diameter of condenser tubes, m
D_{do}	Droplet diameter, m
D_i	Mass flow rate of the distillate in stage I, kg/s
D_{ot}	Outer diameter of the demister wires, mm
e	Specific enthalpy, kJ/kg
E	Total enthalpy, kJ
F	additional acceleration (force/unit particle mass)
f	Friction factor
f_d	Friction factor
G	Generation of turbulent kinetic energy
g	gravity acceleration, m/s^2
H	Height, m
H1, H2	Flash box dimension (m)
Hg	gate height, m

H_p	Thickness of demister pad, m
H_{sp}	set point for the brine height in the last stage, m
k	Turbulent kinetic energy, m^2/ s^2
K_{c-b}	Proportional controller gain, kg/s m
L	Length of condenser tubes, m
L_p	Length of demister pad, m
m	Mass flow rate, kg/s
$\dot{m}$	Mass rate of collected liquid droplet per unit volume, kg/s. m^3
M	Total mass, kg
MCW	Cooling water flow rate, kg/s
MD	Total plant production kg/s
MF	Intake seawater flow rate, kg/s
MS	Steam fluorite in the brine heater, kg/s
N	Number of the condenser tubes
NC	Mass flow rate of non-condensable gases, kg/s
NEA	Non-equilibrium allowance, ^oC
P	pressure, kPa
P_t	Tube pitch, m
ΔP	Pressure drop between stages, Pa
ΔP_p	demister pressure drop, Pa
Re_1	Reynolds number at orifice gate
Re_2	Reynolds number at brine level height
R	Source term due to tube bundles
S	Source term due to the interphase friction
T	Temperature, ^oC.
t	Time, s
TBT	Top brine temperature, ^oC
TF1	Brine temperature entering the brine heater, ^oC
U	Overall heat transfer coefficient, $kW/m^2\ ^oC$.
U_g	Vapour Velocity magnitude = $(u^2 + v^2)^{0.5}$, m/s
U_l	Liquid Velocity magnitude = $(u^2 + v^2)^{0.5}$, m/s
u	Velocity component in the x-direction, m/s

V	Volume, m^3
$\vec{v}$	Velocity vector
v1	Velocity (m/s) = $B_o(i-1) / [\rho b(i-1)\ h_b(i-1)]$
v2	Velocity (m/s) = $B_o(i) / [\rho b(i)\ h_b(i)]$
v	Velocity component in the y-direction, m/s
v_f	Fluid phase velocity, m/s
v_{pt}	Particle velocity, m/s
VL	brine velocity in the tube bundle, m/s
VR	Mass flow rate of released vapour stream, kg/s
VV	Mass flow rate of vented stream, kg/s
Vv	Vapour velocity across the demister , m/s
W	Stage width, m.
W_p	Width of demister pad, m
X	Mass fraction of gases in the brine
Y	Mass fraction of non-condensable gases in the vented vapour

Greek Letters

λ	Latent heat of vaporization, kJ/kg.
ρ	Mass density, kg/m^3.
ρ_p	demister packing density, kg/m^3.
ρ_m	two phase density (equation 46), kg/m^3
γ	Efficiency of degassing process
α	venting line orifice discharge coefficient.
α’	gas phase discharge coefficient
ψ	Volume fraction
ω	Local porosity
ω_{td}	Tube bundle porosity
τ	Shear stress, Pa
δ	permeability, m^2
μ	Laminar dynamic viscosity, cp

μ_t Turbulent viscosity, cp

μ_{eg} effective viscosity, cp

σ Fluid surface tension, N/m

ζ Rate of brine re-entrainment, kg/s

φ_f thickness of the liquid film, m

ϕ_2 the fraction of the demister area covered by liquid brine

ϕ fraction of the droplet perimeter which is attached to the demister wires

Subscripts

a air

b Brine

bg Gases in the brine

cw sew water

d distillate

e Equilibrium

ε Parameter for turbulent kinetic energy dissipation rate

f Brine stream flowing inside the condenser tubes

g Gas phase (vapour water)

i stage number i

k Parameter for turbulent kinetic energy

l Liquid phase (entrained liquid droplets)

n last stage

nc Non-condensable gases

ncr Released non-condensable gases

ncv vented non-condensable gases

out discharged from the plant (Rejected Brine)

p Packing of the demister

pt particle

r Recycle brine stream flowing inside the condenser tubes

ref reference

s Salt

st	Flashing stage
stm	steam
t	Condenser tubes
td	Wires of the demister
v	Vapour
vr	Released vapour
vv	vented stream
w	Wire
x	x- direction
y	y- direction

Bibliography

Abdel-Jabbar, N. M., Qiblawy, H. M., Mjalli, F. S., & Ettouny, H. (2007). Simulation of large capacity MSF brine circulation plants. *Desallination* , 501-514 (204).

Abu-Eid, Z. M., & Fakhoury, A. G. (1974). Some special design features of Kuwait MSF plants. *Desalination* , 263-284 (23).

Alatiqi, I., Ettouney, H., El-Dessouky, H., & Al-Hajri, K. (2004). Measurments of dynamic behavior of a multistage flash water desalination system. *Desalination* , 233-251 (160).

AlBahou, M., Al-Rakkaf, Z., Zaki, H., & Ettouney, H. (2007). Desalination experience in Kuwait. *Desalination* , 403-415 (204).

Al-Deffeeri, N. (2009). Chemical Section Head,Doha West Power Station, Ministry of Water and Electricity. *Kuwait , Personal Communication* .

Al-Fulaij, H. (2002). *Analysis of MSF Flashing Chambers, Master thesis.* Kuwait: Kuwait University.

Al-Mutaz, I. S., & Soliman, M. A. (1989). Simulation of MSF desalination plants. *Desalination* , 317-326 (74).

Al-Sanea, S., Rhodes, N., Tatchell, D. G., & Wilkinson, T. S. (1983). A computer model for detailed calculation of the flow in power station condensers. In *Condensers: Theory and Practice, The Institution of Chemical Engineers Symposium* (pp. 70-88). Oxford: Pergamon Press.

Al-Shuaib, A., Al-Bahu, M., El-Dessouky, H., & Ettouney, H. (1999). Progress of the Desalination Industry in Kuwait. *IDA World Congress on Desalination and Water Reuse.* San Diego, USA.

Aly, N. H., & Marwan, M. A. (1995). Dynamic behavior of MSF desalination plants. *Desalination* , 287-293 (101).

Al-Zubaidi, A. A. (1987). Sea water desalination in Kuwait - A report on 33 years experience. *Desalination* , 1-55 (63).

Anon. (1995). *Selecting and sizing ACS mesh pad mist eliminators.* Houston: Bulletin SA-12, ACS Industries, Inc.

ANSYS. (n.d.). *ANSYS FLUENT*. Retrieved January 16, 2011, from ANSYS: http://www.ansys.com/Products/Simulation+Technology/Fluid+Dynamics/ANSYS+FLUENT

Aspen Technology. (2010). *ASPEN PLUS User's Guide*. Retrieved 2010, from http://www.aspentech.com

Bogle, D., Cipollina, A., & Micale, G. (2009). Dynamic modeling tools for solar powered desalination process during transient operations. *Solar Desalination for the 21st Century* (pp. 43-67). Tunisia: Springer.

Borsani, R., & Rebagliati, S. (2005). Fundamentals and costing of MSF desalination plants and comparison with other technologies. *Desalination* , 29-37 (182).

Brennen, C. (2005). In *Fundamentals of multiphase flow* (pp. 1-29). New York: Cambridge University Press.

Brunazzi, E., & Paglianti, A. (2000). Design of Complex wire mesh-mist eliminatos. *AIChE J.* , 1131-1137 (46).

Brunazzi, E., & Paglianti, A. (1998). Design of wire mesh mist eliminators. *AIChE J.* , 505-512 (44).

Buekholz, A. (1986). Die Beschreibung der partiklelabscheidung durch tragheitskrafte mit hilfe einer dimensionsanalytisch abgeleiteten kennzahl. *Chem. Eng. Techol.* , 548-556(58).

Buerkholz, A. (1989). *Droplet Separation.* New York: VCH.

Bush, A. W., Marshell, G. S., & Wilkinson, T. S. (1990). The prediction of steam condensation using three component solution algorithm. *Proceedings of the Second International Symposium on Condensers and Condensation* (pp. 223-234). UK: University of Bath.

Cameron, I. T., Hangos, K., & Stephanopoulos, G. (2001). *Process Modelling and Model Analysis, Process System Engineering.* London, UK: Academic Press.

Carpenter, C. L., & Othmer, D. F. (1955). Entrainment removal by a wire-mesh separator. *AIChE J.* , 549.

Chapra, S. C., & Canale, R. P. (2006). *Numerical Methods for Engineers.* NY (USA): McGraw-Hill .

Cipollina, A. (2004-2005). *Experimental study and dynamic modelling of Multi stage flash desalination units.* Palermo, Italy: PhD Thesis.

Cipollina, A., Micale, G., & Rizzuti, L. (2009). *Seawater Desalination Conventional and Renewable Energy Processes.* Verlag Berlin Heidelberg: Springer.

Clift, R., Grace, J. R., & Weber, M. E. (1978). *Bubbles, Drops and Particles* . New York: Academic Press.

Corbett, J. O. (1988). Particle capture by interception and its relevance to nuclear reactor containment sprays . *International Journal of Multiphase Flow* , 459-472 .

Darwish, M. A. (1991). Thermal analysis of multi stage flash desalination systems. *Desalination* , 59-79 (81).

Davidson, B. J., & Rowe, M. (1981). Simulation of power condenser performance by computation method: an overview. In P. Marto, & R. Nunn, *In Power Condenser Heat Transfer Technology* (pp. 17-49). Washington: Hemisphere.

Drake, F. A. (1986). Chapter 2.1 Measurements and control in flash evaporator plants. *Desalination* , 241-262 (59).

Durst, F., Miloievic, D., & Schonung, B. (1984). Eulerian and Lagrangian predictions of particulate two-phase flows: a numerical study. *Applied Mathematical Modelling* , 101-115 (8).

El-Bairouty, M., Fath, H., Saddiqi, M., & El-Rabghy, O. (2005). Design, Construction and Testing of an Experimental Educational MSF Desalination Unit. *Proceedings of IDA Congress in Desalination & Water Reuse.* Singapore.

El-Dessouky, H. T., & Ettouney, H. M. (2002). *Fundamentals of salt water desalination.* USA: Elsevier.

El-Dessouky, H. T., Alatiqi, I. M., Ettouney, H. M., & Al-Deffeeri, N. S. (2000). Performance of wire mesh mist eliminator. *Chemical Engineering and Processing* , 129-139 (39).

El-Dessouky, H. T., Alatiqi, I., & Ettouney, H. M. (1998). Process synthesis: The multi-stage flash desalination system. *Desalination* , 155-179 (115).

El-Dessouky, H. T., Ettouney, H. M., Al-Fulaij, H., & Mandani, F. (2000). Multistage flash desalination combined with thermal vapor compression. *Chem. Eng. & Proc.* , 343-356 (39).

El-Dessouky, H., & Bingulac, S. (1996). Solving equations simulating the steady state behavior of the multi stage flash desalination process. *Desalination* , 171-193 (107).

El-Dessouky, H., Ettouney, H., Al-Juwayhel, F., & Al-Fulaij, H. (2004). Analysis of multistage flash desalination flashing chambers,. *IChemE* , 82(A8): 967-978.

El-Dessouky, H., Ettouney, H., Al-Juwayhel, F., & Al-Fulaij, H. (2004). Analysis of multistage flash desalination flashing chambers,. *IChemE* , 82(A8): 967-978.

El-Dessouky, H., Shaban, H. I., & Al-Ramadan, H. (1995). El-Dessouky, H., Shaban, H.I., and Al-Ramadan, H., Steady-state analysis of multi-stage flash desalination process. *Desalination* , 271-287 (103).

El-Khatib, K. M., Eissa, A. H., & Khedr, M. A. (2005). Transient model, simulation and control of a Multi-Stage Flash Evaporation (MSF) desalination system. *The Transaction of the Egyptian Society of Chemical Engineering Journal* , Vol. 32, No. 1.

Ergun, S., & Orning, A. A. (1952). Fluid Flow Through Packed Columns. In *Chemical Engineering Progress* (pp. 89-94). New York: American Institute of Chemical Engineers.

Ettouney, H. (2005). Brine entrainment in multistage flash desalination. *Desalination* , 87-97(182).

Ettouney, H. M., El-Dessouky, H. T., & Alatiqi, I. (1999). Understand thermal desalination. *Chemical Eng. Prog.* , 43-54 (95).

Ettouney, H. M., El-Dessouky, H. T., & Al-Juwayhel, F. (2002). Performance of the once through multistage flash desalination. *Proc. Instn. Mech. Engrs. Part A, Power and Energy* , 229-242 (216).

Ettouney, H. M., El-Dessouky, H. T., & Faibish, R. S. (2002). Evaluating the economics of desalination,. *Chem. Eng. Prog.* , 32-39 (98).

Ettouny, H. M., & El-Dessouky, H. (1999). A simulator for thermal desalination processes. *Desalination* , 277-291 (125).

Fabian, P., Van Dessel, P., Hennessey, P., & Neuman, M. (1993a). Demystifying the selection of mist eliminators, Part I: The basics. *Chemical engineering* , 148-156(11).

Fabian, P., Van Dessel, P., Hennessey, P., & Neuman, M. (1993b). Demystifying the selection of mist eliminators, Part II: The Apllications. *Chemical Engineering* , 106-111(12).

Falcetta, M. F., & Sciubba, E. (1999). Falcetta, M. F., and Sciubba, E., Transient simulation of a real multi-stage flashing desalination process. *Desalination* , 263-269 (122).

Felder, R., & Rousseau, R. (2000). *Elementary principles of chemical processes.* Wiley and Sons.

Feord, D., Wilcock, E., & Davies, G. A. (1993). A stochastis model to describe the operation of knitted mesh mist eliminators, computation of separation efficiency . *Trans.Ind.Chem.Eng.* , 282(71).

Fluent_Inc. (2006). *Fluent 6.3 Manual.* Centerra Resource Park: Fluent Inc.

Fritzmann, C., Löwenberg, J., Wintgens, T., & Melin, T. (2007). State-of-the-art of reverse osmosis desalination. *Desalination* , 1-76 (216).

Fumagalli, B., & Ghiazza, E. (1994). 50. Fumagalli, B., and Ghiazza, E., Mathematical modelling and expert systems integration for optimum control strategy of MSF desalination plants. *Desalination* , 547-554 (97).

Galletti, C., Brunazzi, E., & Tognotti, L. (2008). Anumerical model for gas flow and droplet motion in wave drainage channels. *Chemical Engineering Science* , 5639-5652 (63).

Gambier, A., & Badreddin, E. (2002). Application of hybrid modeling and control techniques to desalination plants. *Desalination* , 175-184 (152).

Gambier, A., & Badreddin, E. (2004). Dynamic modeling of MSF plants for automatic control and simulation purposes: a survey. *Desalination* , 191-204 (166).

Gambit 2.3 Manual. Fluent, Incorporated. 2006.

Gerrard, M. G., PUC, G., & Simpson, E. (1986). Optimize the design of wire-mesh separators. *Chem. Eng.* , 91.

Gillandt, I., Riehle, C., & Fritsching, U. (1996). Gas-particle flow in a comparison of measurments and simulations. *Forschung Im Ingenieurwesen - Engineering Research* , 315-321(62).

Glueck, A. R., & Bradshaw, R. W. (1970). A mathematical model for a multistage flash distillation plant. *3rd international symposium on fresh water from the sea*, (pp. 95-108). Dubrovnik.

Hangos, K. M., & Cameron, I. T. (2001). *Process Modelling and Model Analysis.* Academic Press.

Harvey, B., & Mercusot, M. (2007). Cooperation between Mediterranean countries of Europe and the southern rim of the Mediterranean. *Desalination* , 20-26 (203).

Hassan, A. M., Al-Sofi, M. A., Al-Amoudi, A. S., Jamaluddin, A. T., Farooque, A. M., Rowaili, A., et al. (1998). A new approach to membrane and thermal seawater desalination processes using nanofiltration membranes (Part 1). *Desalination* , 35-51 (118).

Helal, A. M. (2004). Once-through and brine recirculation MSF designs – a comparative study. *Desalination* , 33-60 (171).

Helal, A. M. (2003). Uprating of Umm Al Nar East 4-6 MSF desalination plants. *Desalination* , 43-60 (159).

Helal, A. M., Medani, M. S., Soliman, M. A., & Flower, J. R. (1986). A Tridiagonal matrix model for multi-stage flash desalination plants. *Comp. & Chem. Eng.* , 327-342 (10).

Hinkebein, T. E., & Price, M. K. (2005). Progress with the desalination and water purification technologies US roadmap. *Desalination* , 19-28 (182).

Holmes, T. L., & Chen, G. K. (1984). Design and selection of spray/mist elimination equipment. *Chemical Engineering* , 82-89(91).

Horn, R. A., & Johnson, C. R. (1985). *Matrix Analysis.* Cambridge University Press.

Hu, H. G., & Zhang, C. A. (2007). A modified k–ε turbulence model for the simulation of two-phase flow and heat transfer in condensers . *International Journal of Heat and Mass Transfer* , 1641-1648(50).

Hung, L. S., & Yao, S. C. (1999). Experimental investigation of the impaction of water droplets on cylindrical objects . *International Journal of Multiphase Flow* , 1545-1559.

Husain, A., Hassan, A., Al-Gobaisi, D. M., Al-Radif, A., Woldai, A., & Sommariva, C. (1993). Modelling, simulation, optimization and control of multistage flashing (MSF) desalination plants Part I: Modelling and simulation. *Desalination* , 21-41 (92).

Husain, A., Reddy, K. V., & Woldai, A. (1994). Modelling,simulation and optimization of a MSF desalinationplant. *Proc. Eurotherm Seminar*, (p. 40).

Husain, A., Woldai, A., Al-Radif, A., Kesou, A., Borsani, R., Sultan, H., (1994). Modelling and simulation of a multistage flash (MSF) desalination plant. *Desalination* , 555-586 (97).

Husain, A., Woldai, A., Al-Radif, A., Kesou, A., Borsani, R., Sultan, H., (1994a). Modelling and simulation of a multistage flash (MSF) desalination plant. *Desalination* , 555-586 (97).

IDA. (2006). *The 19th IDA worldwide desalting plant inventory*. Topsfield, MA, USA,: International desalination association .

Incropera, F. P., DeWitt, D. P., Bergman, T. L., & Lavine, A. S. (2006). *Fundamentals of Heat and Mass Transfer*. New York: Wiley.

James, P. W., Azzopardi, B. J., Wang, Y., & Hughes, J. P. (2005). A model for liquid film flow and separation in a wave-plate ist eliminator. *Chemical Engineering Research and Design* , 469-477(83).

James, P. W., Wang, Y., Azzopardi, B. J., & Hughes, J. P. (2003). The role of drainage channels in the performnace of wave-plate mist eliminators. *Chemical Engineering Research and Design* , 639-648(81).

Khawaji, A. D., Kutubkhanah, I. K., & Wie, J. M. (2007). A 13.3 MGD seawater RO desalination plant for Yanbu Industrial City. *Desalination* , 176-188 (203).

Langmuir, I., & Blodgett, K. B. (1946). *U.S. Army Air Forces Technical Report, 5418.*

Lerner, B. J. (1986). High-tech mist elimination in multi-stage evaporators. *Plant/Operations Progress* , 52-56(5).

Lior, N., Chung, R., & Miyatake, O. (2002). Correlations (updated) for predicting the flow through MSF plant interstage orifices. *Desalination* , 209-216 (151).

Malin, M. R. (1997). Modelling flow in an experimental marine condenser . *International Communications in Heat and Mass Transfer* , 597-608.

Mazzei, L., Casillo, A., Lattieri, P., & Salatino, P. (2010). CFD simluations of segregating fluidized bidisperse mixtures of particles differing in size. *ChemicalEngineering Journal* , 432-445 (156).

Mazzotti, M., Rosso, M., Beltramini, A., & Morbidelli, M. (2000). Dynamic modeling of multistage flash desalination plants. *Desalination* , 207-218 (127).

McCabe, W., Smith, J., & Harriott, P. (2000). *Unit Operations of Chemical Engineering.* New York: McGraw-Hill.

Micale, G. (1993). *Introduction to Computational Fluid Dynamics (CFD) Physical Models and Numerical Methods with applications to Engineering Problems; Presentation at the UCL* .

Morsi, S. A., & Alexander, A. J. (1972). An investigation of particle trajectories in two-phase flow systems. *J. Fluid Mech.* , 193-208(55).

Mussati, S. F., Aguirre, P. A., & Scenna, N. J. (2004). Improving the efficiency of the MSF once through (MSF-OT) and MSF-mixer (MSF-M) evaporators. *Desalination* , 141-151 (166).

Oldfield, J. W., & Todd, B. (1999). Technical and economic aspects of stainless steels in MSF desalination plants. *Desalination* , 75-84 (124).

Omar, A. M. (1983). Simulation of M.S.F. desalination plants. *Desalination* , 65-76 (45).

Ounis, H., Ahmadi, G., & McLaughlin, G. B. (1991). Brownian Diffusion of Submicrometer Particles in the Viscous Sublayer. *Journal of Colloid and Interface Science* , 266-277(143).

Pich, J. (1966). *aerpsp Science, Chap. 9. C.N. Davies, ed.,.* New York: Academic Press.

PSE. (1997). *PSE - World technology and services for model-based engineering*. Retrieved 2010, from gPROMS: http://www.psenterprise.com/gproms/

Rahbar, M. T. (1993). Improvement of the design and operation of desalination plants by computer modelling and simulation. *Desalination* , 253-269 (92).

Rahimi, R., & Abbaspour, D. (2008). Determination of pressure drop in wire mesh mist eliminator by CFD. *Chemical Engineering and Processing* , 1504-1508 (47).

Rautenbach, R., & Schafer, S. (1999). Experimental and theoretical studies on interstage brine orifices for MSF desalination plants. *Proceeding of the IDA World Congress on Desalination and Water Sciences*, (pp. 47-63 (Vol. I)). San Diego , USA.

Reddy, K. V., Husain, A., Woldai, A., & Al-Gopaisi, D. M. (1995). Dynamic modelling of the MSF desalination process. *Proc. IDA and WRPC World Congress on Desalination and Water Treatment*, (pp. 227-242). Abu Dhabi.

Rhodes, D. B., & Carlucci, L. N. (1983). Predicted and measured velocity distribution in a model heat exchanger. *International Conference on Numerical Methods in Nuclear Engineering.* Montreal: Canadian Nuclear Society-American Nuclear Society.

Rimawi, M. A., Ettouny, H. M., & Aly, G. S. (1989). Transient model of multistage flash desalination. *Desalination* , 327-338 (74).

Rosso, M., Beltramini, A., Mazzotti, M., & Morbidelli, M. (1997). Modeling multistage flash desalination plants. *Desalination* , 365-374 (108).

Schiffler, M. (2004). Perspectives and challenges for desalination in the 21st century. *Desalination* , 1-9 (165).

Sharaf, M. A., Nafey, A. S., & Lourdes, G. (2011). Exergy and thermo-economic analyses of a combined solar organic cycle with multi effect distillation (MED) desalination process. *Desalination* , 135-147.

Shiklomanov, I. A., & Rodda, J. C. (2003). *World Water Resources at the Beginning of the Twenty-First Century*. Cambridge, UK: Cambridge University Press.

Shivayyanamath, S., & Tewari, P. K. (2003). Simulation of start-up characteristics of multi-stage flash desalination plants. *Desalination* , 277-286 (155).

Silver, R. S. (1970). Multi-stage flash distillation – The first 10 years. *3rd Int. Sym. On Fresh Water from the Sea*, (pp. 191-206). Athens, Greece.

Soliman, M. A. (1981). A mathematical model for multi-stage, flash desalination plants. *J. Eng. Sci.* , 2-10 (7).

Tanvir, M. S., & Mujtaba, I. M. (2006b). Modelling and Simulation of MSF Desalination Process using gPROMS and Neural Network based Physical Property Correlation. *Computer aided chemical engineering* (p. 315). Marquardt and Pantelides (Eds.), Elsevier.

Tanvir, M. S., & Mujtaba, I. M. (2006a). Neural network based correlations for estimating temperature elevation for seawater in MSF desalination process. *Desalination* , 251-272(195).

Tanvir, M. S., & Mujtaba, I. M. (2008). Optimisation of design and operation of MSF desalination process using MINLP technique in gPROMS. *Desalination* , 419-430 (222).

Tarifa, E. E., Humana, D., Franco, S., & Scenna, N. J. (2004). A new method to process algebraic equation systems used to model a MSF desalination plant. *Desalination* , 113-121 (166).

Tarifa, E., & Scenna, J. (2001). A dynamic simulator for MSF plants. *Desalination* , 349-364 (138).

Thirumeni, C., & Deutsche, B. (2005). Rehabilitation and uprating of Ras Abu Fontas MSF, desalination units: process optimisation and life extension. *Desalination* , 63–67 (182).

Thomas, P. J., Bhattacharyya, S., Petra, A., & Rao, G. P. (1998). Steady state and dynamic simulation of multi-stage flash desalination plants: A case study. *Computers Chem. Engng* , 1515-1529 (22).

Ulrich, J. (1997). *Dynamic behaviours of MSF plants forseawater desalination. Dissertation (in German).* University of Hannover.

UN. (2010b). *United Nations, Department of Economic and Social Affairs, Population Division, Population Estimates and Projections Sections*. Retrieved 2010, from http://esa.un.org/unpd/wpp2008/

UN. (2006). *UN-Water Thematic Initiative: Coping with Water Scarcity*. Retrieved from ftp://ftp.fao.org/agl/aglw/docs/waterscarcity.pdf

UN. (2001). *Water Desalination Technologies in the ESCWA Member Countries.* New York.

UN. (2010a). *Water For Life, 2005-2015*. Retrieved 2010, from www.un.org/waterforlifedecade/

Ustun, A. P., & Corvalan, C. (2006). *Preventing Disease Through Healthy Environments, Towards an estimate of the environmental burden of disease.* World Health Organization, WHO.

Van Wachem, B. G., & Almstedt, A. E. (2003). Methods for multiphase computational fluid dynamics. *Chem. Eng. J.*, , 81-98(96).

Verlaan, C. C. (1991). *Performance of Novel Mist Eliminators, PhD Thesis.* The Netherlands: Delft University of Technology.

Versteeg, H. K., & Malalasekera, W. (2007). *An Introduction to Compuational Fluid Dynamics , The finite Volume Method.* England: Pearson Education Limited.

Wade, N. M. (2001). Distillation plant development and cost update. *Desalination* , 3-12 (136).

Wang, Y., & Davies, G. A. (1996). CFD Studies of separation of mists from gases using vane-type separators. *Chemical Engineering Research & Design* , 232-238(74).

Wang, Y., & James, P. W. (1999). Assesment of an eddy-interaction model and its refinements using predictions of droplet deposition in wave plate demister. *Chemical Engineering Research & Design* , 692-698(77).

Wang, Y., & James, P. W. (1998). The Calculation of Wave-Plate Demister Efficiencies Using Numerical Simulation of the Flow Field and Droplet Motion . *Chemical Engineering Research and Design* , 980-985(76).

Wangnick, K. (1995). How incorrectly determined physical and constructional properties in the seawater and brine regimesinfluence the design and size of an MSF desalination plant-stimulus for further thoughts. *Proceedings of the*

IDA, World Congress on Desalination and Water Science, (pp. 201-218(2)). Abu Dhabi.

York, O. H. (1954). Performance of Wire-Mesh Demisters. *Chem. Eng. Prog.* , 421 (50).

Zhang, C., & Bokil, A. (1997). A quasi-three dimensional approach to simulate the two-phase fluid flow and heat transfer in condensers. *International Journal Of Heat and Mass Transfer* , 3537-3546.

Zhang, C., & Zhang, Y. (1993). A quasi-three dimensional approach to predict the performance of steam surface condensers. *Journal of Energy Resources Technology* , 213-220.

Zhao, J., Jin, B., & Zhong, Z. (2007). Study of separation efficiency of a demister vane with response surface technology. *Journal of Hazardous Materials* , 363-369(147).

Publications

REFEREED JOURNAL PUBLICATIONS:

1. Al-Fulaij, H., Cipollina, A., Bogle, D., and Ettouney, H., Once through Multistage Flash Desalination: gPROMS Dynamic and Steady State Modeling, Desalination and Water Treatment, 18 (2010) 46-60.
2. Al-Fulaij, H., Cipollina, A., Bogle, D., and Ettouney, H., Steady State and Dynamic Models of Multistage Flash Desalination: A Review, Desalination and Water Treatment, 13 (2010) 42-52.
3. Al-Fulaij, H., Cipollina, A , Micale, G., Bogle, D., and Ettouney, H., CFD modeling of the demister in the multistage flash desalination plant, Proceedings of the 21st European Symposium on Computer Aided Process Engineering – ESCAPE21, Chalkidiki, Greece, (2011) 1618-1622.
4. Al-Fulaij, H., Micale, G., Cipollina, A., Bogle, D., and Ettouney, H., Porous media approach (Eulerian-Eulerian) for CFD modeling of demisters in multistage flash desalination, Computers and Chemical Engineering, in print, 2011.
5. Al-Fulaij, H., Micale, G., Cipollina, A., Bogle, D., and Ettouney, H., Eulerian-Lagrangian CFD modeling of wire mesh demisters in MSF plants, Trans. IChemE, in print, 2011.
6. Al-Fulaij, H., Cipollina, A., Bogle, D., and Ettouney, H., Simulation of Stability and Dynamics of Multistage Flash Desalination, Desalination, in print, 2011

CONFERENCE PRESENTATIONS:

1. Al-Fulaij, H., Cipollina, A., Bogle, D., and Ettouney, H., Review of steady state and dynamic models of MSF, Desalination for the Environment, Baden-Baden, Germany, 17-20 May, 2009.

2. Al-Fulaij, H., Cipollina, A., Bogle, D., and Ettouney, H., gPROMS steady and dynamic simulation of the MSF once through desalination process, Desalination for the Environment, Baden-Baden, Germany, 17-20 May, 2009.
3. Al-Fulaij, H., Micale, G., Cipollina, A., Bogle, D., and Ettouney, H., CFD modeling of demisters in MSF processes, 21st European Symposium on Computer Aided Process Engineering – ESCAPE21, Chalkidiki, Greece, 31 May – 1 June, 2011.
4. Al-Fulaij, H., Cipollina, A., Bogle, D., and Ettouney, H., Simulation of Stability and Dynamics of Multistage Flash Desalination. The 2011 International Conference on Water: Environmental Sustainability, United Arab Emirates, 14-17 November 2011.

Appendix A
Model Physical Properties Correlations

Seawater density

The density correlation for seawater is given by El-Dessouky and Ettouney (2002):

$$\rho = 10^3 (A_1 F_1 + A_2 F_2 + A_3 F_3 + A_4 F_4) \quad \text{(A.1)}$$

where

$B = ((2)(C)/1000 - 150)/150$

$G_1 = 0.5$

$G_2 = B$

$G_3 = 2 B^2 - 1$

$A_1 = 4.032219 G_1 + 0.115313 G_2 + 3.26\times10^{-4} G_3$

$A_2 = - 0.108199 G_1 + 1.571\text{x}10^{-3} G_2 - 4.23\times10^{-4} G_3$

$A_3 = - 0.012247 G_1 + 1.74\times10^{-3} G_2 - 9\times10^{-6} G_3$

$A_4 = 6.92\times10^{-4} G_1 - 8.7\times10^{-5} G_2 - 5.3\times10^{-5} G_3$

$A = ((2)(T) - 200)/160$

$F_1 = 0.5$, $F_2 = A$, $F_3 = 2 A^2 - 1$, $F_4 = 4 A^3 - 3 A$

In the above equations ρ is the seawater density in kg/m^3, C is the seawater salinity in ppm, and T is the seawater temperature in ^oC. This correlation is valid over the following ranges: $0 \leq C \leq 160000$ ppm and $10 \leq T \leq 180\ ^oC$.

Seawater Specific Heat at Constant Pressure

The seawater specific heat at constant pressure is given by the following correlation, (El-Dessouky & Ettouney, Fundamentals of salt water desalination, 2002):

$$C_p = (A + B\,T + C\,T^2 + D\,T^3)\times 10^{-3} \quad \text{(A.2)}$$

The variables A, B, C and D are evaluated as a function of the water salinity as follows:

$$A = 4206.8 - 6.6197\,s + 1.2288\times 10^{-2}\,s^2$$

$$B = -1.1262 + 5.4178\times 10^{-2}\,s - 2.2719\times 10^{-4}\,s^2$$

$$C = 1.2026\times 10^{-2} - 5.3566\times 10^{-4}\,s + 1.8906\times 10^{-6}\,s^2$$

$$D = 6.8777\times 10^{-7} + 1.517\times 10^{-6}\,s - 4.4268\times 10^{-9}\,s^2$$

where Cp in kJ/kg ^{o}C, T in ^{o}C, and s is the water salinity in gm/kg. The above correlation is valid over salinity and temperature ranges of $20000 \leq s \leq 160000$ ppm and $20 \leq T \leq 180$ ^{o}C, respectively.

Seawater Dynamic Viscosity

The correlation for the dynamic viscosity of seawater is given by El-Dessouky and Ettouney (2002):

$$\mu = (\mu_W)\,(\mu_R) \times 10^3 \quad \text{(A.3)}$$

with

$$\mathrm{Ln}(\mu_W) = -3.79418 + 604.129/(139.18+T)$$

$$\mu_R = 1 + A\,s + B\,s^2$$

$$A = 1.474\times10^{-3} + 1.5\times10^{-5}\,T - 3.927\times10^{-8}\,T^2$$

$$B = 1.0734\times10^{-5} - 8.5\times10^{-8}\,T + 2.23\times10^{-10}\,T^2$$

where μ in kg/m s, T in ^{o}C, and s in gm/kg. The above correlation is valid over the following ranges $0 \le s \le 130$ gm/kg and $10 \le T \le 180\ ^{o}$C.

Latent Heat of Water Evaporation

The correlation for latent heat of water evaporation is given by El-Dessouky and Ettouney (2002):

$$\lambda = 2501.897149 - 2.407064037\,T + 1.192217\times10^{-3}\,T^2 - 1.5863\times10^{-5}\,T^3 \quad \text{(A.4)}$$

In the above equation, T is the saturation temperature in °C and λ is the latent heat in kJ/kg. The percentage errors for the calculated versus the steam table values are less than 0.026%.

Saturation Pressure of Water Vapour containing gases

The correlation for the (water vapour/gas) saturation pressure is given by Antoine's Equation, (Cipollina, Experimental study and dynamic modelling of Multi stage flash desalination units, 2004-2005):

$$LOG(1-Ymol) = Aant - \frac{Bant}{(Tvap + Cant)}$$

(A.5)

where ,

Ymol is the non condensable gases mol fraction in the vapor/gas phase

Aant is Antoine's equation coefficient = 23.2256

Bant is Antoine's equation coefficient = 3835.18

Cant is Antoine's equation coefficient = 45.343

where P is Pa and Tvap is K. The percentage errors for the calculated versus the steam table values are less than 0.05%.

Boiling Point Elevation

The correlation for the boiling point elevation of seawater is El-Dessouky and Ettouney (2002):

$$BPE = A\,X + B\,X^2 + C\,X^3 \quad \text{(A 6)}$$

with

$$A = (8.25\times10^{-2} + 1.883\times10^{-2}\,T + 4.02\times x10^{-6}\,T^2)$$

$$B = (-\,7.625x10^{-4} + 9.02\times10^{-5}\,T - 5.2\times10^{-7}\,T^2)$$

$$C = (1.522\times10^{-4} - 3\times10^{-6}\,T - 3\times10^{-8}\,T^2)$$

where T is the temperature in ^{o}C and X is the salt weight percentage. The above equation is valid over the following ranges: $1 \leq X \leq 16\%$, $10 \leq T \leq 180°C$.

Vapour/gas density

The correlation for the vapour/gas phase density is given by El-Dessouky and Ettouney (2002):

$$Dvap = \frac{P}{R \quad Tvap} \frac{1}{\left[\left(\frac{(1-Y)}{H_2O\_mol\_mass}\right)+\left(\frac{Y}{AIR\_mol\_mass}\right)\right]1000} \quad \text{(A 7)}$$

where P is the vapour pressure,

Pa, R is the universal gas constant,

Tvap is the vapour temperature,

Y is the non condensable gas mass fraction in the vapor/gas phase,

$H_2O_{mol\text{-}mass}$ is the water molecular weight,

$AIR_{molmass}$ is the air molecular weight, and

Dvap is the vapour density in kg/m^3

Appendix B

Degree of Freedom in gPROMS Models

The degree of freedom should be determined before starting the gPROMS simulation. It represents the difference between the available model equations and the number of variables. Thus:

$$Degree\ of\ freedom = n_{equations} - n_{variables}$$

$$degree\ of\ freedom \begin{cases} = 0 & \text{the problem is well established and can be solved} \\ \leq -1 & \text{the problem is underspecified and initial condition should be stated} \\ \geq 1 & \text{the problem is overspecified and many variables are assigned} \end{cases}$$

Example:

For a flashing stage in MSF-OT plant, the following mass, energy and constituve equations apply:

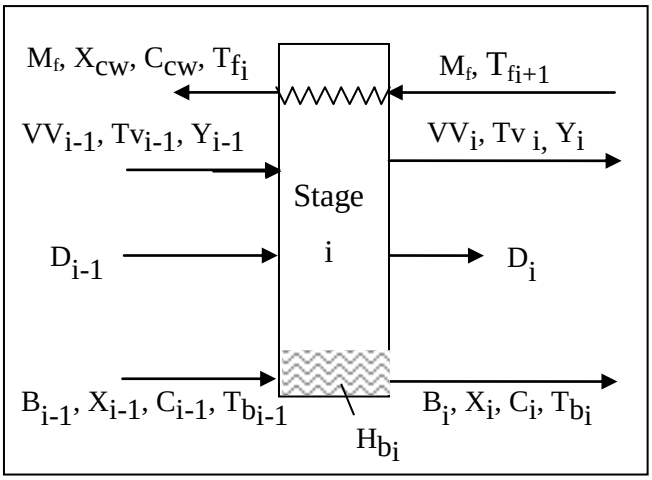

$$\frac{dM_{b_i}}{dt} = B_{i-1} - B_i - VR_i - NC_i \quad (1)$$

$$\frac{dM_{V_i}}{dt} = VR_i + NC_i + D_{i-1} + VV_{i-1} - D_i - VV_i \quad (2)$$

$$D_i = D_{i-1} + [VR_i - VV_i(1 - Y_i)] + VV_{i-1}(1 - Y_{i-1}) \quad (3)$$

$$\frac{dM_{s_i}}{dt} = B_{i-1}\, C_{i-1} - B_i\, C_i \quad (4)$$

$$\frac{dM_{nc_i}}{dt} = NC_i + VV_{i-1}\, Y_{i-1} - VV_i\, Y_i \quad (5)$$

$$\frac{dM_{bg_i}}{dt} = B_{i-1}X_{i-1} - B_iX_i - NC_i \quad (6)$$

$$\frac{dE_{v_i}}{dt} = VR_i\ e_{vr_i} + NC_i\ e_{ncr_i} + VV_{i-1}Y_{i-1}\ e_{ncr_{i-1}} + VV_{i-1}(1 - Y_{i-1})\ e_{vv_{i-1}} + D_{i-1}\, e_{d_{i-1}} - D_i\, e_{d_i} - VV_i\, Y_i\ e_{ncr_i} - VV_i(1 - Y_i)\ e_{vv_i} \quad (7)$$

$$\frac{dE_{b_i}}{dt} = B_{i-1}\, e_{b_{i-1}} - B_i\, e_{b_i} - VR_ie_{vr_i} - NC_ie_{ncr_i} \quad (8)$$

$$M_b = \rho_b\, V_b \quad (8)$$

$$V_b = A_{st}\, H_b \quad (10)$$

$$M_v = \rho_v V_v \quad (11)$$

$$V_v = A_{st}\left(H_{st} - H_b\right) \quad (12$$

$$M_s = C\, M_b \quad (13)$$

$$M_{bg} = X\, M_b \quad (14)$$

$$M_{nc} = Y\, M_v \quad (15)$$

$$NC = B\left(X - X_e\right)\gamma \quad (16)$$

$e = C_P\ (T - T_{ref})$ (9 equations) (17-25)

$$T_{vr} = T_b - BPE - NEA \quad (26)$$

$$T_{vv} = T_{vr} - \Delta T_p - \Delta T_{fr} \tag{27}$$

$$\Delta P_p = 3.9\,(\rho_p)^{0.38}(V_v)^{0.81}(d_w)^{-1.56} \tag{28}$$

Antoine equation (29)

$$D_{i-1}\left(e_{d_{i-1}} - e_{d_i}\right) + \left(VR_i - VV_i(1 - Y_i)\right)\lambda_{V_i} + VV_{i-1}(1 - Y_{i-1})\left((e_{VV_{i-1}} - e_{VV_i}) + \lambda_{V_i}\right) + VV_{i-1}\,Y_{i-1}\left(e_{ncv_{i-1}} - e_{ncv_i}\right) = M_f\,Cp_{b_i}(T_{f_i} - T_{f_{i+1}}) \tag{30}$$

$$D_{i-1}\left(e_{d_{i-1}} - e_{d_i}\right) + \left(VR_i - VV_i(1 - Y_i)\right)\lambda_{V_i} + VV_{i-1}(1 - Y_{i-1})\left((e_{VV_{i-1}} - e_{VV_i}) + \lambda_{V_i}\right) + VV_{i-1}\,Y_{i-1}\left(e_{ncv_{i-1}} - e_{ncv_i}\right) = U_i A_{t_i}\left[\frac{\left(T_{VV_i} - T_{f_{i+1}}\right) + \left(T_{VV_i} - T_{f_i}\right)}{2}\right] \tag{31}$$

$$A_t = N_t\,\pi\,D_{to}\,L_t \tag{32}$$

$$NEA = 1667 \times 10^5 \;\; T_{b_i}^{-4.84124} \times \left(T_{b_{i-1}} - T_{b_i}\right)^{-0.04486} \;\; H_{b_i}^{1.150576} \;\; Re_{1_i}^{-0.18218} \;\; Re_{2_i}^{0.204095} \tag{33}$$

$$U_i = 0.107309 \times T_{v_i}^{0.773247} \times VL^{0.484958} \tag{34}$$

Brine density = *f* (Temperature , salinity) (35)

Vapour density = *f* (Temperature, Pressure) (36)

$\lambda_{V_i} = f$ (Temperature, Salinity) (37)

BPE = f (Temperature) (Appendix A) (38)

Re_{2_i} , Re_{1_i} (39-40)

List of variables:

1	M_{b_i}	19	C_{i-1}	37	λ_{V_i}
2	Bi-1	20	C_i	38	BPE
3	Bi	21	M_{nc_i}	39	NEA
4	VRi	22	C_{i-1}	40	E_{b_i}
5	NCi	23	C_i	41	T_{vv}
6	M_{V_i}	24	M_{bg_i}	42	T_{vr}
7	Di-1	25	X_{i-1}	43	ΔT_p
8	Di	26	X_i	44	Vv
9	VVi-1	27	E_{v_i}	45	Re_{1_i}
10	VVi	28	e_{vr_i}	46	Re_{2_i}
11	Y_i	29	e_{ncr_i}	47	e_{ncv_i}
12	Y_{i-1}	30	$e_{ncr_{i-1}}$	48	$e_{ncv_{i-1}}$
13	ρ_b	31	$e_{vv_{i-1}}$	49	M_f
14	V_b	32	$e_{d_{i-1}}$	50	T_{f_i}
15	Hb	33	e_{d_i}	51	$T_{f_{i+1}}$
16	ρ_v	34	e_{vv_i}	52	U_i
17	V_v	35	e_{b_i}	53	A_t
18	M_{s_i}	36	$e_{b_{i-1}}$		

$$Degree\ of\ freedom = n_{equations} - n_{variables}$$

$$Degree\ of\ freedom = 40 - 53$$

$$Degree\ of\ freedom = -13$$

This means that more 13 equations are needed in order to solve the model or it may be a equations and initial conditions for some variables. Some equations are found in the higher level model which connects the flashing stages to each other such as those for calucalting (B) and (VV). Also initial conditions were set for some variables such as the brine temperature and vapour pressure and the brine height. At this point the degree of freedom had reached zero and the model was solved.

Appendix C

(MSF-OT) gPROMS code

```
#============================================================#
#                                                            #
#             Model of a Single Falshing Stage               #
#   -with condensation of vapour;                            #
#   - with demister losses;                                  #
#   - with vapour production rate;                           #
#   - with non condensable gases ;                           #
#   - With Thermodynamic properties correlations ;           #
#   - With Distillate Tray;                                  #
#   - With distillate and vapor interconnection between stages#
#============================================================#


PARAMETER

  W              AS REAL #STAGE WIDTH
  L              AS REAL #STAGE LENGTH
  H              AS REAL #STAGE HEIGHT
  A              AS REAL #STAGE FLOOR AREA
  Horifice1      AS REAL #WEIR GATE HIEGHT
  Horifice2      AS REAL #FLASH BOX OPENING
  R              AS REAL #UNIVERSAL GAS CONSTANT
  H2O_mol_mass   AS REAL #MOLECULAR MASS OF WATER
  AIR_mol_mass   AS REAL #MOLECULAR MASS OF AIR
  Pvent          AS REAL #PRESSURE IN VENT SYSTEM
  Br_vel         AS Real #brine velocity in tubes

  #Physical parmaeters correlations
  Aant           AS REAL #ANTOINE EQUATION
  Bant           AS REAL #ANTOINE EQUATION
  Cant           AS REAL #ANTOINE EQUATION

  G1             AS REAL #BRINE DENSITY CORRELATION
  F1             AS REAL #BRINE DENSITY CORRELATION

  #Condensing zone parameters
  Wtube          AS REAL    #LENGTH
  NoTubes        AS INTEGER #NUMBER OF CONDENSER TUBES
  Diam_Tube_out  AS REAL    #EXTERNAL DIAMETER OF ONE TUBE
  Diam_Tube_in   AS REAL    #INTERNAL DIAMETER OF ONE TUBE

  #Demister parameters
  Demisterdensity AS REAL
  wire_diam       AS REAL



VARIABLE
  vel                   AS distillate_flow_rate
  Acp                   AS param_corr
  Bcp                   AS param_corr
  Ccp                   AS param_corr
  Dcp                   AS param_corr
  Cp_br                AS specific_heat #SPECIFIC HEAT OF BRINE
  Cp_dist                 AS  specific_heat  #SPECIFIC  HEAT  OF
DISTILLATE WATER
```

```
        Cp_air                AS specific_heat
        Re1                  AS Reynolds_Number #REYNOLD'S NUMBER AT
Horifice1
        Re2                   AS Reynolds_Number #REYNOLD'S NUMBER AT
Hbrine
        Diam                  AS Diameter_RE
        Diam2                 AS Diameter_RE
        Viscosity             AS Viscosity
        Bin, Bout             AS brine_flowrate
        Vin, Vout             AS vapour_flowrate
        Hbrine                AS length # BRINE HEIGHT IN THE STAGE
        Peevap          AS pressure
        Teevap          AS Temperature

        DPdemister                AS pressure
        Vap_Vel                   AS vapor_velocity
        Area_demister             AS area
        Cbr_in, Cbr               AS mass_fraction_ppm
        Dbr                       AS brine_density
        Dvap                      AS vapour_density
        DRec_br                   AS brine_density
        P,Pevap                   AS pressure
        Tdin                      AS temperature
        Tbr_in,Tbr                AS temperature
        Tvap_in, Tvap, Tevap      AS temperature
        NEA, BPE                  AS param_corr
        Mbr, Mvap, Msalt          AS mass
        Vol_vap, Vol_br           AS volume
        Ebr_tot                   AS enthalpy
        Ebr_in, Ebr               AS specific_enthalpy
        Vap_rate                  AS vapour_flowrate
        Vap_heat                  AS latent_heat
        Vap_heat_in               AS latent_heat
        Vap_heat_down             AS latent_heat
        Din                       AS condensate_flowrate
        Dout                      AS condensate_flowrate
        Mdis                      AS condensate_flowrate
        Ddist                     AS distillate_density

        Abd                       AS param_corr
        Bbd                       AS param_corr
        Ab                        AS param_corr
        Bb                        AS param_corr
        Cd                        AS param_corr
        Abr                       AS param_corr
        Bbr                       AS param_corr

        Utot                      AS heat_transf_coeff
        Cond_rate                 AS condensate_flowrate
        Tc_in, Tc_out             AS temperature
        Rec_br                    AS brine_flowrate
        Tfeed_avg                 AS temperature

        Xgas                      AS mass_fraction
        Xgas_in                   AS mass_fraction
        Xgas_eq                   AS mass_fraction
        Xeq_mol                   AS mass_fraction
        Y                         AS mass_fraction
        Ymol                      AS mass_fraction
        Yin                       AS mass_fraction
```

```
        Henry                       AS param_corr
        Mnncond                     AS mass
        Mbr_gas                     AS mass
        Non_cond_rate               AS vapour_flowrate
                                 #actually   non-condensable   gases
flowrate
        Gamma                         AS param_corr
                               #efficency  coefficient  of  degassing
process

        ALPHA                       AS param_corr
        NCin                        AS vapour_flowrate
        NCout                       AS vapour_flowrate

      STREAM
        brine_inlet    : Cbr_in, Xgas_in, Tbr_in  AS   CTStream
        brine_outlet   : Cbr, Xgas, Tbr           AS   CTStream
        vap_inlet      : Yin, Tvap_in             AS   VapStream
        vap_outlet     : Y, Tvap                  AS   VapStream
        feed_inlet     : Tc_in                    AS   TStream
        feed_outlet    : Tc_out                   AS   TStream


      SELECTOR
        Evaporation    AS (present, notpresent) DEFAULT notpresent
        Condensation   AS (present, notpresent) DEFAULT notpresent
        Brine_flow     AS (flow, noflow)        DEFAULT flow


      EQUATION

      ##Brine phase, Vapor phase & distllate tray mass balances ##
        $Mbr    = Bin - Bout - Vap_rate - Non_cond_rate ;
        $Mvap    = Din + Vap_rate + Non_cond_rate + Vin   - Vout    -
Dout  ;
        $Mdis   = Din + (cond_rate –Vout (1-Yout))+Vin*(1-Yin) - Dout
;
                        # almost steady state since the distillate
tray height is very small
        Mbr     = Vol_br * Dbr ;
        Mvap    = Vol_vap * Dvap  ;
        Mdis    = 2.048*0.1*0.8 * W  * Ddist;
           # distillate tray dimension L=2048mm , H = 10 mm ,
fraction occupied = 0.8
        Vol_br  = A * Hbrine ;
        Vol_vap = A * (H-Hbrine) ;

      ##Brine salt balance##
        $Msalt = Bin * Cbr_in/1E6 - Bout * Cbr/1E6 ;
        Msalt  = Mbr * Cbr/1E6 ;

      ##Non-Condensables Mass Balance Equation in the vap phase##
        $Mnncond = Non_cond_rate + Vin * Yin - Vout * Y  ;
        Mnncond  = Mvap * Y  ;
        NCin     = Yin * Vin ;
        NCout    = Y * Vout  ;


      ##Non-Condensables Mass Balance Equation in the  brine phase ##
```

```
      #Henry's Constant value
        Henry = -7.9E+5*Tbr^2 + 5.8E+8*Tbr - 9.499E+10;
                                        #PERRY, Henry [Pa] & T[K]

      #Liquid mass fraction at equilibium with gas phase in the stage
        Ymol  =  Y  /  AIR_mol_mass  /  (Y  /  AIR_mol_mass  +  (1-Y)  /
H2O_mol_mass);
        Xeq_mol = Xgas_eq / AIR_mol_mass / (Xgas_eq / AIR_mol_mass
                                  + (1-Xgas_eq) / H2O_mol_mass);
        Ymol = Henry * Xeq_mol / P;
                    #molar_Xgas calculated neglecting the presence of
the salt



      ##Brine Enthalpy balance Equation in the stage##
        $Ebr_tot     =  Bin*Ebr_in  -  Bout*Ebr  -  Vap_rate*(Cp_br  *
(Tevap-273.15)
                     +  Vap_heat_down)  -Non_cond_rate*cp_air*(Tevap-
273.15) ;
        Ebr_tot    = Ebr*Mbr                        ;
        Ebr_in     = Cp_br * (Tbr_in - 273.15)    ;
        Ebr        = Cp_br * (Tbr    - 273.15)    ;

      ##Physical Parameters Correlations##
       #Brine Density#
        Ab     = ((2*(Tbr-273.15)-200))/160 ;
        Bb     = ((2*Cbr/1000)-150)/150 ;
        Dbr      = 1000  *  ((4.032219*G1+0.115313*Bb+3.26E-4*(2*Bb^2-
1))*F1 +
                          (-0.108199*G1+1.571E-3*Bb-4.23E-4*(2*Bb^2-
1))*Ab +
                          (-0.012247*G1+1.74E-3*Bb-9E-6*(2*Bb^2-
1))*(2*Ab^2-1)
                   +(6.92E-4*G1-8.7E-5*Bb-5.3E-5*(2*Bb^2-1))*(4*Ab^3-
3*Ab)) ;

       #Distillate density#
        Abd    = (2*(Tvap-273.15)-200)/160;
        Bbd    = -1;
        Ddist   = 1000 ;      # assumed constant (Not affecting the
model since distillate tray balance is S.S)

       #Vapor density#
        Dvap  =  (P/R/Tevap)/((1-Y)/H2O_mol_mass+Y/AIR_mol_mass)/1000
;
                                                  # mass averaged ideal
gas law
        Vap_heat_down  =  (2501.89714  -  2.40706*(Tevap-273.15)     +
1.192217e-3*(Tevap-273.15)^2   - 1.5863E-5*(Tevap-273.15)^3)*1E-3   ;
#ETTOUNEY
        Vap_heat_in     =  (2501.89714  -  2.40706*(Tvap_in-273.15)  +
1.192217e-3*(Tvap_in-273.15)^2 - 1.5863E-5*(Tvap_in-273.15)^3)*1E-3 ;
#ETTOUNEY
        Vap_heat        =  (2501.89714  -  2.40706*(Tvap-273.15)     +
1.192217e-3*(Tvap-273.15)^2    - 1.5863E-5*(Tvap-273.15)^3)*1E-3    ;
#ETTOUNEY
```

```
      ##Boiling Point Elevation##
        BPE =(-4.584e-4*(Tbr-273.15)^2+2.823e-1*(Tbr-273.15)+17.95)
        *(cbr/1e6)^2+ (1.536e-4*(Tbr-273.15)^2+5.267e-2*(Tbr-273.15)
              +6.56)*(cbr/1e6);# Sharqawy, M el al.

      ##Specific Heat Correlations##
      Acp = 4206.8 - 6.6197 * Cbr/1000 + 1.2288e-2 * (Cbr/1000)^2 ;
      Bcp = -1.1262 + 5.4178e-2 * Cbr/1000 - 2.2719e-4 * (Cbr/1000)^2
;
      Ccp  =  1.2026e-2  -  5.3566e-4  *  Cbr/1000  +  1.8906e-6  *
(Cbr/1000)^2 ;
      Dcp  =  6.8777e-7  +  1.517e-6  *  Cbr/1000  -  4.4268e-9  *
(Cbr/1000)^2 ;


      Cp_br   = (Acp + Bcp*(Tbr-273.15) + Ccp * (Tbr-273.15)^2
               + Dcp * (Tbr-273.15)^3) *1e-6; # ETTOUNEY   MJ/Kg K
      Cp_dist = (4206.8 -1.1262 *   (Tdin - 273.15) +   1.2026e-2 *
(Tdin-
      273.15)^2 + 6.8777e-7 *(TDin-273.15)^3)*1e-6;
                                        #  ETTOUNEY     MJ/Kg  K  (SALT
CONC=0 )
      Cp_air = 1.009E-3; #MJ/kg.K

      ##Demister losses##

      DPdemister =    0.2*3.9 * Demisterdensity^ 0.38 *Vap_Vel^0.81 *
                                              wire_diam^(-1.56)
;#Pa
      Vap_Vel = Vap_rate / Dvap / Area_demister      ;# m/sec
      Area_demister = 1.11* W       ;#m2
      DPdemister = Pevap - P   ;#Pa


      LOG(Peevap*(1-Ymol))     = Aant - (Bant/(Teevap-Cant))    ;
                #(Antoine Eq. applied to the vapour partial pressure
above demister)
```

```
#=====================================================================#
#                                                                     #
#                      Model of a Multi-stages unit                   #
#   - vapour and brine passing from one stage to the subsequent       #
#   - with condensation of vapour;                                    #
#   - with non-condensable gases                                      #
#   - withOUT vapour by-pass through the gate                         #
#   - with controllers for brine height at the last stage             #
#   - with controllers for pressure at the last stage                 #
#   - With Thermodynamic properties correlations                      #
#   - With Distillate Tray                                            #
#   - With NEW Correlations  For Cd, NEA , U  From AlFulaij 2002      #
#     Based on real plant data                                        #
#=====================================================================#

PARAMETER

  NoStages       AS INTEGER # NUMBER OF STAGES PRESENT IN THE UNIT
  g              AS REAL    # Gravitational accelaration

  W              AS REAL #STAGE WIDTH
  L              AS REAL #STAGE LENGTH
  R              AS REAL #UNIVERSAL GAS CONSTANT
  H2O_mol_mass   AS REAL #MOLECULAR MASS OF WATER
  AIR_mol_mass   AS REAL #MOLECULAR MASS OF AIR

  Bant           AS REAL #ANTOINE EQUATION
  Cant           AS REAL #ANTOINE EQUATION
  Aant           AS REAL #ANOTINE EQAUTION

  G1             AS REAL #BRINE DENSITY CORRELATION
  F1             AS REAL #BRINE DENSITY CORRELATION

  Wtube          AS REAL #LENGTH OF TUBES IN THE CONDENSER


##Venting line parameters##
  Pvent          AS REAL #PRESSURE IN VENT SYSTEM
  Pvent1         AS REAL #PRESSURE IN VENT SYSTEM
  Pvent7         AS REAL #PRESSURE IN VENT SYSTEM
  Pvent12        AS REAL #PRESSURE IN VENT SYSTEM

##CONTROL LOOP PARAMETERS##
  Hsp       AS REAL # SET POINT FOR THE BRINE HEIGHT IN THE LAST
STAGE
  ALPHA_sp  AS REAL # initial value of ALPHA in the last stage



VARIABLE
  Kc_b      AS param_corr # Proportional controller gain [kg/sm]
  Kc_p      AS param_corr # Proportional controller gain [kg/sm]
  Psp       AS pressure # SET POINT FOR THE PRESSURE IN THE LAST
STAGE
  distcapacity       AS distillate_flow_rate
  Msteam         AS steam_flowrate # steam flowrate to the brine
heater
  PerformanceRatio   AS Performance # SYSTEM PERFORMANCE RATIO
  Tsteam             AS Temperature #STEAM TEMP.
  Steam_heat         AS enthalpy #STEAM ENTHALPY
```

```
UNIT
 FS AS ARRAY (NoStages) OF FLASHING_STAGE



STREAM
  brine_inlet    IS  FS(1).brine_inlet
  brine_outlet   IS  FS(NoStages).brine_outlet
  vap_inlet      IS  FS(1).vap_inlet
  vap_outlet     IS  FS(NoStages).vap_outlet
  feed_inlet     IS  FS(NoStages).feed_inlet
  feed_outlet    IS  FS(1).feed_outlet


EQUATION

##Discharge coefficient correlations##
 #Flash Box Stages#
For i:=2 to 9 do

FS(i).Cd= 0.49* (FS(i).Horifice1/((FS(i-1).P-FS(i).P)/FS(i-
1).Dbr/9.81+FS(i-1).Hbrine))   ^(-0.058)*(FS(i-1).Bout/FS(i-
1).Dbr/FS(i-1).Hbrine /(FS(i).Bout/FS(i).Dbr /FS(i).Hbrine))^0.188
*(FS(i-1).Dbr/(FS(i-1).Dbr/((1-(1-FS(i-1).Dbr/Fs(i-1).Dvap)*FS(i-
1).Cond_rate/(FS(i-1).cond_rate+fs(i-1).Bout)))))^(-
0.234)*(FS(i).Horifice1/FS(i).Horifice2)^0.2;  # AlFulaij 2002
end

FS(1).Cd=0.775;
#Assumed to be constant since No correlation available for the first
stage Cd

 #Weir orifice stages#
FOR i:=10 to nostages do
FS(i).Cd= 0.14* (FS(i).Horifice1/((FS(i-1).P-FS(i).P)/FS(i-
1).Dbr/9.81+FS(i-1).Hbrine))   ^(0.147)*(FS(i-1).Bout/FS(i-
1).Dbr/FS(i-1).Hbrine/(FS(i).Bout
/FS(i).Dbr/FS(i).Hbrine))^1.33*(FS(i-1).Dbr/(FS(i-1).Dbr/((1-(1-FS(i-
1).Dbr/Fs(i-1).Dvap)*FS(i-1).Cond_rate/(FS(i-1).cond_rate+fs(i-
1).Bout)))))^(0.362);
                                                    #  AlFulaij 2002
end

##Non-Equilibrium Allowancw NEA Correlations##
 #NEA correlation for flash box stages#
For i:=1 to 9 do
FS(i).Viscosity = EXP(-3.79418+604.129/(139.18+(FS(i).Tbr-273.15)))*
                      (1+(1.474e-3 +1.5e-5*(FS(i).Tbr-273.15)-
3.927e-8*(FS(i).Tbr-273.15)^2) *FS(i).Cbr/1000+(1.0734e-5-8.5e-
8*(FS(i).Tbr-273.15)+2.23e-10*(FS(i).Tbr-
273.15)^2)*(FS(i).Cbr/1000)^2)* 1e-3;
FS(i).Diam  = 4*FS(i).Horifice1*W/(2*FS(i).Horifice1+2*W);
FS(i).Diam2 = 4*FS(i).Hbrine*FS(i).W/(2*FS(i).Hbrine+2*FS(i).W);
FS(i).Re1 = FS(i).Bin*FS(i).Diam /(FS(i).Horifice1*FS(i).W)/
FS(i).Viscosity;
FS(i).Re2 = FS(i).Bin*FS(i).Diam2/(FS(i).Hbrine/3.25   *FS(i).W)/
FS(i).Viscosity;
```

```
FS(i).NEA = (166714689.5* (FS(i).Tbr_IN-273.15)^(-4.841)
*(FS(i).Tbr_IN-FS(i).Tbr)^(-0.045) * (FS(i).Hbrine/3.25)^(1.150) *
FS(i).Re1^(-0.182) * FS(i).Re2^(0.204) ) ;   # AlFulaij 2002}

end

 #NEA correlation for weir orifice#
For i:=10 to nostages do
FS(i).Viscosity = EXP(-3.79418+604.129/(139.18+(FS(i).Tbr-273.15)))*
                       (1+(1.474e-3 +1.5e-5*(FS(i).Tbr-273.15)-
3.927e-8*(FS(i).Tbr-273.15)^2)*FS(i).Cbr/1000+ (1.0734e-5-8.5e-
8*(FS(i).Tbr-273.15)+2.23e-10*(FS(i).Tbr-
273.15)^2)*(FS(i).Cbr/1000)^2)* 1e-3;
FS(i).Diam  = 4*FS(i).Horifice1*W/(2*FS(i).Horifice1+2*W);
FS(i).Diam2 = 4*FS(i).Hbrine*FS(i).W/(2*FS(i).Hbrine+2*FS(i).W);
FS(i).Re1 = FS(i).Bin*FS(i).Diam /(FS(i).Horifice1*FS(i).W)/
FS(i).Viscosity;
FS(i).Re2 = FS(i).Bin*FS(i).Diam2/(FS(i).Hbrine/3.25   *FS(i).W)/
FS(i).Viscosity;
FS(i).NEA = ( 6998.338* (FS(i).Tbr_IN-273.15)^(-3.137)
*(FS(i).Tbr_IN-FS(i).Tbr)^(-.21) * (FS(i).Hbrine/3.25)^(0.683) *
FS(i).Re1^(0.174) * FS(i).Re2^(0.042))  ;   # AlFulaij 2002}

end

##Blow Through Calculation (Cipollina)##
FOR i := 1 TO 1 DO

    CASE FS(i).Brine_flow OF
      WHEN FS(i).flow   : FS(i).Bout = FS(i).Cd *
(FS(i).Horifice1*FS(i).w) *
        (ABS(2*(FS(i).P-FS(i+1).P + (FS(i).Hbrine-FS(i+1).Hbrine)*
g*FS(i).Dbr)*FS(i).Dbr))^0.5 * SGN(2*(FS(i).P-FS(i+1).P +
(FS(i).Hbrine-FS(i+1).Hbrine)*g*FS(i).Dbr)*FS(i).Dbr)        ;
                          FS(i).Vout = FS(i).ALPHA *
(ABS(FS(i).Dvap*(FS(i).P-Pvent1)))^0.5 * SGN(FS(i).Dvap*(FS(i).P-
Pvent1))        ;
         SWITCH TO FS(i).noflow  IF FS(i).Hbrine <
(FS(i+1).Horifice1+0.05 ) ;
      WHEN FS(i).noflow : FS(i).Bout = FS(i).Cd *
(FS(i).Hbrine*FS(i+1).w) *
                                      (ABS(2*(FS(i).P-FS(i+1).P +
(FS(i).Hbrine-FS(i+1).Hbrine)*g*FS(i).Dbr)*FS(i).Dbr))^0.5 *
                                       SGN(2*(FS(i).P-FS(i+1).P +
(FS(i).Hbrine-FS(i+1).Hbrine)*g*FS(i).Dbr)*FS(i).Dbr)        ;
                          FS(i).Vout =
(FS(i).ALPHA+(FS(i+1).Horifice1-FS(i).Hbrine)*FS(i).W) *
(ABS(FS(i).Dvap*(FS(i).P-Pvent1)))^0.5 *
                                       SGN(FS(i).Dvap*(FS(i).P-
Pvent1))        ;
         SWITCH TO FS(i).flow    IF FS(i).Hbrine > (FS(i+1).Horifice1
+0.03) ;
    END #CASE

END #FOR

FOR i := 2 TO 6 DO

    CASE FS(i).Brine_flow OF
```

```
      WHEN FS(i).flow   : FS(i).Bout = FS(i).Cd *
(FS(i).Horifice1*FS(i).w) *
                                        (ABS(2*(FS(i).P-FS(i+1).P +
(FS(i).Hbrine-FS(i+1).Hbrine)*g*FS(i).Dbr)*FS(i).Dbr))^0.5 *
                                         SGN(2*(FS(i).P-FS(i+1).P +
(FS(i).Hbrine-FS(i+1).Hbrine)*g*FS(i).Dbr)*FS(i).Dbr)        ;
                          FS(i).Vout = FS(i).ALPHA *
(ABS(FS(i).Dvap*(FS(i).P-FS(i+1).P)))^0.5 *
                                         SGN(FS(i).Dvap*(FS(i).P-
FS(i+1).P))        ;
         SWITCH TO FS(i).noflow  IF FS(i).Hbrine <
(FS(i+1).Horifice1+0.05 ) ;
      WHEN FS(i).noflow : FS(i).Bout = FS(i).Cd *
(FS(i).Hbrine*FS(i+1).w) *
                                        (ABS(2*(FS(i).P-FS(i+1).P +
(FS(i).Hbrine-FS(i+1).Hbrine)*g*FS(i).Dbr)*FS(i).Dbr))^0.5 *
                                         SGN(2*(FS(i).P-FS(i+1).P +
(FS(i).Hbrine-FS(i+1).Hbrine)*g*FS(i).Dbr)*FS(i).Dbr)        ;
                          FS(i).Vout =
(FS(i).ALPHA+(FS(i+1).Horifice1-FS(i).Hbrine)*FS(i).W) *
(ABS(FS(i).Dvap*(FS(i).P-FS(i+1).P)))^0.5 *
                                         SGN(FS(i).Dvap*(FS(i).P-
FS(i+1).P))        ;
         SWITCH TO FS(i).flow    IF FS(i).Hbrine > (FS(i+1).Horifice1
+0.03) ;
    END #CASE

END #FOR

FOR i := 7 TO 7 DO

    CASE FS(i).Brine_flow OF
      WHEN FS(i).flow   : FS(i).Bout = FS(i).Cd *
(FS(i).Horifice1*FS(i).w) *
                                        (ABS(2*(FS(i).P-FS(i+1).P +
(FS(i).Hbrine-FS(i+1).Hbrine)*g*FS(i).Dbr)*FS(i).Dbr))^0.5 *
                                         SGN(2*(FS(i).P-FS(i+1).P +
(FS(i).Hbrine-FS(i+1).Hbrine)*g*FS(i).Dbr)*FS(i).Dbr)        ;
                          FS(i).Vout = FS(i).ALPHA *
(ABS(FS(i).Dvap*(FS(i).P-Pvent7)))^0.5 *
                                         SGN(FS(i).Dvap*(FS(i).P-
Pvent7))        ;
         SWITCH TO FS(i).noflow  IF FS(i).Hbrine <
(FS(i+1).Horifice1+0.005 ) ;
      WHEN FS(i).noflow : FS(i).Bout = FS(i).Cd *
(FS(i).Hbrine*FS(i+1).w) *
                                        (ABS(2*(FS(i).P-FS(i+1).P +
(FS(i).Hbrine-FS(i+1).Hbrine)*g*FS(i).Dbr)*FS(i).Dbr))^0.5 *
                                         SGN(2*(FS(i).P-FS(i+1).P +
(FS(i).Hbrine-FS(i+1).Hbrine)*g*FS(i).Dbr)*FS(i).Dbr)        ;
                          FS(i).Vout =
(FS(i).ALPHA+(FS(i+1).Horifice1-FS(i).Hbrine)*FS(i).W) *
(ABS(FS(i).Dvap*(FS(i).P-Pvent7)))^0.5 *
                                         SGN(FS(i).Dvap*(FS(i).P-
Pvent7))        ;
         SWITCH TO FS(i).flow    IF FS(i).Hbrine > (FS(i+1).Horifice1
+0.03) ;
    END #CASE

END #FOR
```

```
FOR i := 8 TO 11 DO

    CASE FS(i).Brine_flow OF
      WHEN FS(i).flow   : FS(i).Bout = FS(i).Cd *
(FS(i).Horifice1*FS(i).w) *
                                        (ABS(2*(FS(i).P-FS(i+1).P +
(FS(i).Hbrine-FS(i+1).Hbrine)*g*FS(i).Dbr)*FS(i).Dbr))^0.5 *
                                         SGN(2*(FS(i).P-FS(i+1).P +
(FS(i).Hbrine-FS(i+1).Hbrine)*g*FS(i).Dbr)*FS(i).Dbr)        ;
                           FS(i).Vout = FS(i).ALPHA *
(ABS(FS(i).Dvap*(FS(i).P-FS(i+1).P)))^0.5 *
                                         SGN(FS(i).Dvap*(FS(i).P-
FS(i+1).P))        ;
         SWITCH TO FS(i).noflow  IF FS(i).Hbrine <
(FS(i+1).Horifice1+0.005 ) ;
      WHEN FS(i).noflow : FS(i).Bout = FS(i).Cd *
(FS(i).Hbrine*FS(i+1).w) *
                                        (ABS(2*(FS(i).P-FS(i+1).P +
(FS(i).Hbrine-FS(i+1).Hbrine)*g*FS(i).Dbr)*FS(i).Dbr))^0.5 *
                                         SGN(2*(FS(i).P-FS(i+1).P +
(FS(i).Hbrine-FS(i+1).Hbrine)*g*FS(i).Dbr)*FS(i).Dbr)        ;
                           FS(i).Vout =
(FS(i).ALPHA+(FS(i+1).Horifice1-FS(i).Hbrine)*FS(i).W) *
(ABS(FS(i).Dvap*(FS(i).P-FS(i+1).P)))^0.5 *
                                         SGN(FS(i).Dvap*(FS(i).P-
FS(i+1).P))        ;
         SWITCH TO FS(i).flow    IF FS(i).Hbrine > (FS(i+1).Horifice1
+0.03) ;
    END #CASE

END #FOR

FOR i := 12 TO 12 DO

    CASE FS(i).Brine_flow OF
      WHEN FS(i).flow   : FS(i).Bout = FS(i).Cd *
(FS(i).Horifice1*FS(i).w) *
                                        (ABS(2*(FS(i).P-FS(i+1).P +
(FS(i).Hbrine-FS(i+1).Hbrine)*g*FS(i).Dbr)*FS(i).Dbr))^0.5 *
                                         SGN(2*(FS(i).P-FS(i+1).P +
(FS(i).Hbrine-FS(i+1).Hbrine)*g*FS(i).Dbr)*FS(i).Dbr)        ;
                           FS(i).Vout = FS(i).ALPHA *
(ABS(FS(i).Dvap*(FS(i).P-Pvent12)))^0.5 *
                                         SGN(FS(i).Dvap*(FS(i).P-
Pvent12))        ;
         SWITCH TO FS(i).noflow  IF FS(i).Hbrine <
(FS(i+1).Horifice1+0.005 ) ;
      WHEN FS(i).noflow : FS(i).Bout = FS(i).Cd *
(FS(i).Hbrine*FS(i+1).w) *
                                        (ABS(2*(FS(i).P-FS(i+1).P +
(FS(i).Hbrine-FS(i+1).Hbrine)*g*FS(i).Dbr)*FS(i).Dbr))^0.5 *
                                         SGN(2*(FS(i).P-FS(i+1).P +
(FS(i).Hbrine-FS(i+1).Hbrine)*g*FS(i).Dbr)*FS(i).Dbr)        ;
                           FS(i).Vout =
(FS(i).ALPHA+(FS(i+1).Horifice1-FS(i).Hbrine)*FS(i).W) *
(ABS(FS(i).Dvap*(FS(i).P-Pvent12)))^0.5 *
                                         SGN(FS(i).Dvap*(FS(i).P-
Pvent12))        ;
```

```
         SWITCH TO FS(i).flow    IF FS(i).Hbrine > (FS(i+1).Horifice1
+0.03) ;
    END #CASE

END #FOR

FOR i := 13 TO nostages-1 DO

    CASE FS(i).Brine_flow OF
      WHEN FS(i).flow   : FS(i).Bout = FS(i).Cd *
(FS(i).Horifice1*FS(i).w) *
                                      (ABS(2*(FS(i).P-FS(i+1).P +
(FS(i).Hbrine-FS(i+1).Hbrine)*g*FS(i).Dbr)*FS(i).Dbr))^0.5 *
                                       SGN(2*(FS(i).P-FS(i+1).P +
(FS(i).Hbrine-FS(i+1).Hbrine)*g*FS(i).Dbr)*FS(i).Dbr)        ;
                           FS(i).Vout = FS(i).ALPHA *
(ABS(FS(i).Dvap*(FS(i).P-FS(i+1).P)))^0.5 *
                                       SGN(FS(i).Dvap*(FS(i).P-
FS(i+1).P))        ;
         SWITCH TO FS(i).noflow  IF FS(i).Hbrine <
(FS(i+1).Horifice1+0.005 ) ;
      WHEN FS(i).noflow : FS(i).Bout = FS(i).Cd *
(FS(i).Hbrine*FS(i+1).w) *
                                      (ABS(2*(FS(i).P-FS(i+1).P +
(FS(i).Hbrine-FS(i+1).Hbrine)*g*FS(i).Dbr)*FS(i).Dbr))^0.5 *
                                       SGN(2*(FS(i).P-FS(i+1).P +
(FS(i).Hbrine-FS(i+1).Hbrine)*g*FS(i).Dbr)*FS(i).Dbr)        ;
                           FS(i).Vout =
(FS(i).ALPHA+(FS(i+1).Horifice1-FS(i).Hbrine)*FS(i).W) *
(ABS(FS(i).Dvap*(FS(i).P-FS(i+1).P)))^0.5 *
                                       SGN(FS(i).Dvap*(FS(i).P-
FS(i+1).P))        ;
         SWITCH TO FS(i).flow    IF FS(i).Hbrine > (FS(i+1).Horifice1
+0.03) ;
    END #CASE

END #FOR



##outlet flow conditions (Cipollina)##

      #control loop for the brine height in the last stage
      Kc_b=0.90*FS(1).Bin;
      FS(NoStages).Bout = 0.90*FS(1).Bin + Kc_b*(FS(NoStages).Hbrine-
Hsp)/Hsp;

      #control loop for the pressure in the last stage
      Kc_p=ALPHA_sp/2000;

      FS(NoStages).ALPHA = ALPHA_sp + Kc_p*(FS(NoStages).P-Psp);
      FS(NoStages).Vout  = FS(NoStages).ALPHA *
(ABS(FS(NoStages).Dvap*(FS(NoStages).P-Pvent)))^0.5 *

SGN(FS(NoStages).Dvap*(FS(NoStages).P-Pvent))      ;


##condensation around the tube bundle ##
For i:=1 to nostages do
```

```
  FS(i).Tfeed_avg = (FS(i).Tc_in+FS(i).Tc_out)/2;
  FS(i).Abr     = ((2*(FS(i).Tfeed_avg-273.15)-200))/160 ;
  FS(i).Bbr     = ((2*FS(1).Cbr_in/1000)-150)/150 ;
  FS(i).DRec_br = 1000 *
((4.032219*FS(i).G1+0.115313*FS(i).Bbr+3.26E-4*(2*FS(i).Bbr^2-
1))*FS(i).F1 +
                   (-0.108199*FS(i).G1+1.571E-3*FS(i).Bbr-4.23E-
4*(2*FS(i).Bbr^2-1))*FS(i).Abr +
                   (-0.012247*FS(i).G1+1.74E-3*FS(i).Bbr-9E-
6*(2*FS(i).Bbr^2-1))*(2*FS(i).Abr^2-1) +
                   (6.92E-4*FS(i).G1-8.7E-5*FS(i).Bbr-5.3E-
5*(2*FS(i).Bbr^2-1))*(4*FS(i).Abr^3-3*FS(i).Abr)) ;
  FS(i).Utot =(1e-3*( 0.107*(FS(i).Tvap-273.15)^0.773*
(FS(i).Rec_br/FS(i).DRec_br/(3.14/4*FS(i).Diam_Tube_in^2
*FS(i).Notubes))^0.485)); # MJ/Kg.K, AlFulaij 2002 }
  FS(i).Vel =
FS(i).Rec_br/FS(i).DRec_br/(3.14/4*FS(i).Diam_Tube_in^2*
FS(i).Notubes);
end

FOR i := 1 TO nostages DO
  CASE FS(i).Condensation OF
    WHEN FS(i).present    :

  FS(i).Din*FS(i).Cp_dist*(FS(i).Tdin-FS(i).Tvap) +
(FS(i).Cond_rate*FS(i).Vap_heat)+FS(i).Vin*(1-FS(i).Yin)*(1.88e-
3*(FS(i).Tvap_in-FS(i).Tvap)+FS(i).Vap_heat) +
FS(i).Vin*FS(i).Yin*FS(i).Cp_air*(FS(i).Tvap_in-FS(i).Tvap)
                                    =
FS(i).Rec_br*FS(i).Cp_br*(FS(i).Tc_out-FS(i).Tc_in) ;


FS(i).Din*FS(i).Cp_dist*(FS(i).Tdin-FS(i).Tvap) +
(FS(i).Cond_rate*FS(i).Vap_heat)+FS(i).Vin*(1-FS(i).Yin)*(1.88e-
3*(FS(i).Tvap_in-FS(i).Tvap)+FS(i).Vap_heat)+
FS(i).Vin*FS(i).Yin*FS(i).Cp_air*(FS(i).Tvap_in-FS(i).Tvap)
                                    =
FS(i).Utot * FS(i).NoTubes*(FS(i).Wtube*FS(i).Diam_Tube_out*3.1416) *
((FS(i).Tvap-FS(i).Tc_in)+(FS(i).Tvap-FS(i).Tc_out))/2 ;


      SWITCH TO FS(i).notpresent   IF  (FS(i).Tvap < FS(i).Tc_out) ;
    WHEN FS(i).notpresent :
                      FS(i).Cond_rate =   0.0001          ;
                      FS(i).Tc_out    = FS(i).Tc_in  ;

      SWITCH TO FS(i).present      IF  (FS(i).Tvap >
FS(i).Tc_out+0.2)  ;
  END #CASE
END #FOR


##connecting two subsequent stages##
For i :=1 to Nostages-1 Do
      FS(i+1).Tdin = FS(i).Tvap ;
      FS(i+1).Din  = FS(i).Dout;
      FS(i).feed_inlet  = FS(i+1).feed_outlet  ;
      FS(i).Rec_br      = FS(i+1).Rec_br ;
      FS(i).brine_outlet = FS(i+1).brine_inlet ;
      FS(i).Bout         = FS(i+1).Bin         ;
```

```
END

FOR i :=2 TO 2 DO
    FS(i).Vin=0;
    FS(i).Yin=FS(i-1).Y;
    FS(i).Tvap_in=FS(i-1).Tvap;
END #FOR

FOR i :=3 TO 7 DO
    FS(i).Vin=FS(i-1).Vout;
    FS(i).Yin=FS(i-1).Y;
    FS(i).Tvap_in=FS(i-1).Tvap;
END #FOR

FOR i :=8 TO 8 DO
    FS(i).Vin=0;
    FS(i).Yin=FS(i-1).Y;
    FS(i).Tvap_in=FS(i-1).Tvap;
END #FOR

FOR i :=9 TO 12 DO
    FS(i).Vin=FS(i-1).Vout;
    FS(i).Yin=FS(i-1).Y;
    FS(i).Tvap_in=FS(i-1).Tvap;
END #FOR

FOR i :=13 TO 13 DO
    FS(i).Vin=0;
    FS(i).Yin=FS(i-1).Y;
    FS(i).Tvap_in=FS(i-1).Tvap;
END #FOR

FOR i :=14 TO nostages DO
    FS(i).Vin=FS(i-1).Vout;
    FS(i).Yin=FS(i-1).Y;
    FS(i).Tvap_in=FS(i-1).Tvap;
END #FOR


##Total Plant Capacity and Performance Ratio##
  distcapacity     = FS(nostages).Dout;
  PerformanceRatio = distcapacity/Msteam;


##BRINE HEATER energy balanc##
  Steam_heat = (2501.89714 - 2.40706*(Tsteam-273.15) + 1.192217e-
3*(Tsteam-273.15)^2 - 1.5863E-5*(Tsteam-273.15)^3)*1E-3 ;#Ettuney;
  Msteam * Steam_heat = FS(1).Rec_br * FS(1).Cp_br  * (FS(1).Tbr_in -
FS(1).Tc_out);


#########################################################################
#                                                                       #
#                         SCHEDULED PROCESS                             #
#                                                                       #
#########################################################################


UNIT
  MSF   AS    MSF_PLANT
```

```
MONITOR
  MSF.FS(*).DPdemister   ;
  MSF.FS(*).Yin          ;
  MSF.FS(*).Re1          ;
  MSF.FS(*).Re2          ;
  MSF.FS(*).Peevap       ;
  MSF.FS(*).Teevap       ;
  MSF.FS(*).NCin         ;
  MSF.FS(*).NCout        ;
  MSF.FS(*).Mnncond      ;
  MSF.FS(*).P            ;
  MSF.FS(*).Bout         ;
  MSF.FS(*).Vout         ;
  MSF.FS(*).Dbr          ;
  MSF.FS(*).Ddist        ;
  MSF.FS(*).Vin          ;
  MSF.FS(*).Hbrine       ;
  MSF.FS(*).Cbr          ;
  MSF.FS(*).Cp_br        ;
  MSF.FS(*).Cp_dist      ;
  MSF.FS(*).Tvap         ;
  MSF.FS(*).Tevap        ;
  MSF.FS(*).Tbr          ;
  MSF.FS(*).NEA          ;
  MSF.FS(*).Cond_rate    ;
  MSF.FS(*).Tc_in        ;
  MSF.FS(*).Tc_out       ;
  MSF.FS(*).Vap_rate     ;
  MSF.FS(*).Mvap         ;
  MSF.FS(*).Cd           ;
  MSF.FS(*).Y            ;
  MSF.FS(*).Non_cond_rate;
  MSF.FS(*).ALPHA        ;
  MSF.FS(*).Utot         ;
  MSF.FS(*).BPE          ;
  MSF.FS(*).vel          ;
  MSF.FS(*).Din          ;
  MSF.FS(*).Dout         ;
  MSF.distcapacity       ;
  MSF.PerformanceRatio   ;

SET # Parameter Values
  MSF.NoStages         := 21      ; #
  MSF.g                := 9.81    ; # m/s2
  MSF.W                := 17.66   ; # m
  MSF.L                := 4       ; # m
  MSF.Wtube            := 17.66   ; # m

  FOR i:=1 TO MSF.NOSTAGES do
  MSF.FS(i).H          := 4       ; # m
  MSF.FS(i).Demisterdensity := 80 ; #kg/m3
  MSF.FS(i).wire_diam  := 0.254   ; #mm
  MSF.FS(i).Br_vel     := 2.044   ; #m/s
  END

  FOR i:=1 TO MSF.NoStages DO
    MSF.FS(i).A        := MSF.FS(i).L * MSF.FS(i).W ; #m2
  END #FOR
```

```
# FLASH BOX DIMENSIONS FOR EACH STAGE (REAL PLANT DATA)
  MSF.FS(1).HORIFICE1  :=0.098;
  MSF.FS(2).Horifice1  :=0.220;
  MSF.FS(3).Horifice1  :=0.228;
  MSF.FS(4).Horifice1  :=0.237;
  MSF.FS(5).Horifice1  :=0.262;
  MSF.FS(6).Horifice1  :=0.293;
  MSF.FS(7).Horifice1  :=0.355;
  MSF.FS(8).Horifice1  :=0.355;
  MSF.FS(9).Horifice1  :=0.388;
  MSF.FS(10).Horifice1 :=0.224;
  MSF.FS(11).Horifice1 :=0.307;
  MSF.FS(12).Horifice1 :=0.310;
  MSF.FS(13).Horifice1 :=0.400;
  MSF.FS(14).Horifice1 :=0.304;
  MSF.FS(15).Horifice1 :=0.310;
  MSF.FS(16).Horifice1 :=0.354;
  MSF.FS(17).Horifice1 :=0.361;
  MSF.FS(18).Horifice1 :=0.409;
  MSF.FS(19).Horifice1 :=0.429;
  MSF.FS(20).Horifice1 :=0.443;
  MSF.FS(21).Horifice1 :=0.488;


  MSF.FS(1).Horifice2  :=0.155;
  MSF.FS(2).Horifice2  :=0.234;
  MSF.FS(3).Horifice2  :=0.240;
  MSF.FS(4).Horifice2  :=0.230;
  MSF.FS(5).Horifice2  :=0.270;
  MSF.FS(6).Horifice2  :=0.339;
  MSF.FS(7).Horifice2  :=0.428;
  MSF.FS(8).Horifice2  :=0.496;
  MSF.FS(9).Horifice2  :=0.562;

  FOR i :=10 to msf.nostages do
  MSF.FS(i).Horifice2 := MSF.FS(i).Horifice1;# Horifice2 for these
stages will not occur in the solution
  END#for

  MSF.R                := 8.314   ; # J/mol/K
  MSF.H2O_mol_mass     := 18      ; # kg/kmol
  MSF.AIR_mol_mass     := 29      ; # kg/kmol
  MSF.Pvent            := 7000    ; # Pa
  MSF.Pvent1           := 60000   ; # Pa
  MSF.Pvent7           := 30000   ; # Pa
  MSF.Pvent12          := 12000    ; # Pa


#Physical parmaeters corerlations
  MSF.Aant := 23.2256 ; #ANTOINE EQUATION, P[Pa] & T[K]
  MSF.Bant := 3835.18 ; #ANTOINE EQUATION, P[Pa] & T[K]
  MSF.Cant := 45.343  ; #ANTOINE EQUATION, P[Pa] & T[K]

  MSF.G1 := 0.5 ; #BRINE DENSITY CORRELATION
  MSF.F1 := 0.5 ; #BRINE DENSITY CORRELATION

#Condensing zone parameters

  FOR i := 1 TO MSF.NoStages DO
```

```
  MSF.FS(i).NoTubes        := 1410    ; # NUMBER OF CONDENSER TUBES
  MSF.FS(i).Diam_Tube_out  := 0.0445  ; # m
  MSF.FS(i).Diam_Tube_in   := 0.04197 ; # m
  END #FOR

# CONTROL LOOP PARAMETERS
  MSF.Hsp         := 0.688 ;    # SET POINT FOR THE BRINE HEIGHT IN
THE LAST STAGE
  MSF.ALPHA_sp    := 0.5e-1;    # initial value of ALPHA in the last
stage [m2]


ASSIGN # Degrees of Freedom

  MSF.FS(1).Tdin        := 250         ;#No Distillate entering
stage1
  MSF.FS(1).Din         := 0           ;#No Distillate entering
stage1
  MSF.FS(1).Tbr_in      := 91.1+273.15   ; # K , TOP BRINE
TEMPERATURE
  MSF.FS(1).Bin         := 4025.27     ; # kg/s , FEED BRINE TO STAGE
1
  MSF.FS(1).Cbr_in      :=40000 {64528}       ; # ppm , FEED SALINITY
  MSF.FS(1).Xgas_in     := 9E-5        ; # ppm , FEED GAS CONTENT
  MSF.FS(MSF.NoStages).Tc_in := 37.7+273.15;# K , SEA WATER
TEMPERATURE
  MSF.Psp               := 10000       ;
                            # Pa SET POINT FOR THE PRESSURE IN THE
LAST STAGE (calculated after setting the outlet temperature)
  MSF.FS(1).Rec_br    := 4025.27     ;
           # Kg/sec , recycle brine flow rate in the condensing tubed
  MSF.Tsteam          := 100+273.15  ;
               #K ,steam condensation temperature in the brine heater

  FOR i:=1 to (msf.nostages-1) do
  MSF.FS(i).ALPHA      := 0.5E-1     ; # m2
  END#FOR

  FOR i :=1 TO 1 DO
  MSF.FS(i).Vin       :=0  ;
  MSF.FS(i).Yin       :=0  ;
  MSF.FS(i).Tvap_in   :=300;
  END #FOR



INITIAL # Initial Conditions

  MSF.FS(1).Tbr       = 359.11884  ; # K
  MSF.FS(2).Tbr       = 354.68817  ; # K
  MSF.FS(3).Tbr       = 351.1259   ; # K
  MSF.FS(4).Tbr       = 347.67465  ; # K
  MSF.FS(5).Tbr       = 344.33075  ; # K
  MSF.FS(6).Tbr       = 341.06503  ; # K
  MSF.FS(7).Tbr       = 337.84268  ; # K
  MSF.FS(8).Tbr       = 334.8511   ; # K
  MSF.FS(9).Tbr       = 332.3038   ; # K
  MSF.FS(10).Tbr      = 330.85046  ; # K
  MSF.FS(11).Tbr      = 329.1478   ; # K
  MSF.FS(12).Tbr      = 327.4673   ; # K
```

```
  MSF.FS(13).Tbr      = 325.7794   ; # K
  MSF.FS(14).Tbr      = 324.4019   ; # K
  MSF.FS(15).Tbr      = 323.09088  ; # K
  MSF.FS(16).Tbr      = 321.80408  ; # K
  MSF.FS(17).Tbr      = 320.58362  ; # K
  MSF.FS(18).Tbr      = 319.43323  ; # K
  MSF.FS(19).Tbr      = 318.39032  ; # K
  MSF.FS(20).Tbr      = 317.4546   ; # K
  MSF.FS(21).Tbr      = 316.60742  ; # K

  MSF.FS(1) .Hbrine      = 1.2676916  ; # m
  MSF.FS(2) .Hbrine      = 1.9961544  ; # m
  MSF.FS(3) .Hbrine      = 1.9977281  ; # m
  MSF.FS(4) .Hbrine      = 1.8446163  ; # m
  MSF.FS(5) .Hbrine      = 1.6556592  ; # m
  MSF.FS(6) .Hbrine      = 1.3906261  ; # m
  MSF.FS(7) .Hbrine      = 1.0352969  ; # m
  MSF.FS(8) .Hbrine      = 1.6980833  ; # m
  MSF.FS(9) .Hbrine      = 1.6668056  ; # m
  MSF.FS(10).Hbrine      = 1.5893252  ; # m
  MSF.FS(11).Hbrine      = 1.3468597  ; # m
  MSF.FS(12).Hbrine      = 1.1631613  ; # m
  MSF.FS(13).Hbrine      = 1.0557262  ; # m
  MSF.FS(14).Hbrine      = 1.0495183  ; # m
  MSF.FS(15).Hbrine      = 0.9989856  ; # m
  MSF.FS(16).Hbrine      = 0.91079885 ; # m
  MSF.FS(17).Hbrine      = 0.84954417 ; # m
  MSF.FS(18).Hbrine      = 0.80167437 ; # m
  MSF.FS(19).Hbrine      = 0.78042215 ; # m
  MSF.FS(20).Hbrine      = 0.76704156 ; # m
  MSF.FS(21).Hbrine      = 0.7462217  ; # m

  MSF.FS(1).Pevap         = 62742.383    ; # Pa
  MSF.FS(2).Pevap         = 50170.133    ; # Pa
  MSF.FS(3).Pevap         = 44160.668    ; # Pa
  MSF.FS(4).Pevap         = 38927.12     ; # Pa
  MSF.FS(5).Pevap         = 34696.26     ; # Pa
  MSF.FS(6).Pevap         = 31925.96     ; # Pa
  MSF.FS(7).Pevap         = 30601.58     ; # Pa
  MSF.FS(8).Pevap         = 20352.328    ; # Pa
  MSF.FS(9).Pevap         = 17940.615    ; # Pa
  MSF.FS(10).Pevap        = 15339.161    ; # Pa
  MSF.FS(11).Pevap        = 14226.41     ; # Pa
  MSF.FS(12).Pevap        = 13130.971    ; # Pa
  MSF.FS(13).Pevap        = 11945.176    ; # Pa
  MSF.FS(14).Pevap        = 10995.577    ; # Pa
  MSF.FS(15).Pevap        = 10215.243    ; # Pa
  MSF.FS(16).Pevap        = 9543.536     ; # Pa
  MSF.FS(17).Pevap        = 8913.589     ; # Pa
  MSF.FS(18).Pevap        = 8340.192     ; # Pa
  MSF.FS(19).Pevap        = 7811.212     ; # Pa
  MSF.FS(20).Pevap        = 7346.776     ; # Pa
  MSF.FS(21).Pevap        = 7006.4883    ; # Pa


FOR i :=1 TO MSF.NoStages DO
    MSF.FS(i).Cbr      = 40000          ; # ppm
    MSF.FS(i).Xgas     = 9E-5           ; # kg/kg
    MSF.FS(i).Y        = 0.05          ; # kg/kg
```

```
END #FOR

SOLUTIONPARAMETERS
  REPORTINGINTERVAL    := 100   ;
  OUTPUTLEVEL          := 4       ;
  DIAGNOSTICS          := OFF     ;
  IndexReduction       := ON      ;
  ABSOLUTEACCURACY     := 1E-4    ;

#For dynamic behavior#
SCHEDULE  # Operating procedure

SEQUENCE

    CONTINUE FOR 14400
RESET
    MSF.FS(1).Bin    := 4048.33 ;
    MSF.FS(1).Rec_br := 4048.33 ;
    MSF.FS(21).Tc_in := 37.82 +273.15 ;
    MSF.FS(1).Tbr_in := 91.2+273.15   ;
END
    CONTINUE for 14400
RESET
    MSF.FS(1).Bin    := 4025.3 ;
    MSF.FS(1).Rec_br := 4025.3 ;
    MSF.FS(21).Tc_in := 37.8 +273.15 ;
    MSF.FS(1).Tbr_in := 89.9+273.15   ;
END
    CONTINUE for 14400
RESET
    MSF.FS(1).Bin    := 4048.33 ;
    MSF.FS(1).Rec_br := 4048.33 ;
    MSF.FS(21).Tc_in := 37.9 +273.15 ;
    MSF.FS(1).Tbr_in := 89.9+273.15   ;
END
    CONTINUE for 14400
RESET
    MSF.FS(1).Bin    := 4013.9 ;
    MSF.FS(1).Rec_br := 4013.9 ;
    MSF.FS(21).Tc_in := 37.86 +273.15 ;
    MSF.FS(1).Tbr_in := 91+273.15   ;
END
    CONTINUE for 14400
RESET
    MSF.FS(1).Bin    := 4025.3 ;
    MSF.FS(1).Rec_br := 4025.3 ;
    MSF.FS(21).Tc_in := 37.68 +273.15 ;
    MSF.FS(1).Tbr_in := 91.1+273.15   ;
END
    CONTINUE for 14400
RESET
    MSF.FS(1).Bin    := 4037 ;
    MSF.FS(1).Rec_br := 4037 ;
    MSF.FS(21).Tc_in := 37.7 +273.15 ;
    MSF.FS(1).Tbr_in := 91.2+273.15   ;
END
    CONTINUE for 14400
END #SEQUENCE

      #For steady state behavior
```

```
SCHEDULE  # Operating procedure
SEQUENCE
    CONTINUE FOR 150000
END #SEQUENCE

#For Feed disturbance
SCHEDULE  # Operating procedure
SEQUENCE
    CONTINUE FOR 55000
RESET
    MSF.FS(1).Bin    := 4010 ;
    MSF.FS(1).Rec_br := 4010 ;
END
CONTINUE for 55000
RESET
    MSF.FS(1).Bin    := 4048 ;
    MSF.FS(1).Rec_br := 4048 ;
END
Continue for 55000
END #SEQUENCE
#for Top brine temperature disturbance
SCHEDULE # Operating procedure
SEQUENCE
    CONTINUE FOR 100000
RESET
    MSF.FS(1).Tbr_in    := 89.0+273.15 ;
END
CONTINUE for 100000
RESET
    MSF.FS(1).Tbr_in    := 91+273.15 ;
END
Continue for 100000
END #SEQUENCE
```

Appendix D

(MSF-BC) gPROMS code

```
#============================================================#
#                                                            #
#                   Model of a Single Falshing Stage         #
#   - with condensation of vapour;                           #
#   - with demister losses;                                  #
#   - with vapour production rate;                           #
#   - with non condensable gases ;                           #
#   - With Thermodynamic properties correlations ;           #
#   - With Distillate Tray;                                  #
#   - With distillate and vapor interconnection              #
#      between stages;                                       #
#============================================================#


PARAMETER

  W              AS REAL #STAGE WIDTH
  L              AS REAL #STAGE LENGTH
  H              AS REAL #STAGE HEIGHT
  A              AS REAL #STAGE FLOOR AREA
  Horifice1      AS REAL #WEIR GATE HIEGHT
  Horifice2      AS REAL #FLASH BOX OPENING
  R              AS REAL #UNIVERSAL GAS CONSTANT
  H2O_mol_mass   AS REAL #MOLECULAR MASS OF WATER
  AIR_mol_mass   AS REAL #MOLECULAR MASS OF AIR
  Pvent          AS REAL #PRESSURE IN VENT SYSTEM


  #Physical parmaeters correlations
  Aant           AS REAL #ANTOINE EQUATION
  Bant           AS REAL #ANTOINE EQUATION
  Cant           AS REAL #ANTOINE EQUATION

  G1             AS REAL #BRINE DENSITY CORRELATION
  F1             AS REAL #BRINE DENSITY CORRELATION

  #Condensing zone parameters
  Wtube          AS REAL    #LENGTH
  NoTubes        AS INTEGER #NUMBER OF CONDENSER TUBES
  Diam_Tube_out  AS REAL    #EXTERNAL DIAMETER OF ONE TUBE
  Diam_Tube_in   AS REAL    #INTERNAL DIAMETER OF ONE TUBE

  #Demister parameters
  Demisterdensity AS REAL
  wire_diam       AS REAL
  Tdemister         AS real


VARIABLE
  Area                      As area
  Acp                       AS param_corr
  Bcp                       AS param_corr
  Ccp                       AS param_corr
  Dcp                       AS param_corr
  Cp_br                     AS specific_heat #SPECIFIC HEAT OF
BRINE
```

```
        Cp_dist                     AS specific_heat #SPECIFIC HEAT OF
DISTILLATE
                                       WATER
        Cp_air                      AS specific_heat
        Re1                              AS Reynolds_Number #REYNOLD'S
NUMBER AT
                                 Horifice1
        Re2                              AS Reynolds_Number #REYNOLD'S
NUMBER AT Hbrine
        Diam                        AS Diameter_RE
        Diam2                       AS Diameter_RE
        Viscosity                   AS Viscosity
        Bin, Bout                   AS brine_flowrate
        Vin, Vout                   AS vapour_flowrate
        Hbrine                        AS length # BRINE HEIGHT IN THE
STAGE

        Peevap                      AS pressure
        Teevap                      AS Temperature

        DPdemister                  AS pressure
        Vap_Vel                     AS vapor_velocity
        Area_demister               AS area
        Cbr_in, Cbr                 AS mass_fraction_ppm
        Dbr                         AS brine_density
        Dvap                        AS vapour_density
        DRec_br                     AS brine_density
        P,Pevap                     AS pressure
        Tdin                        AS temperature
        Tbr_in,Tbr                  AS temperature
        Tvap_in, Tvap, Tevap        AS temperature
        NEA, BPE                    AS param_corr
        Mbr, Mvap, Msalt            AS mass
        Vol_vap, Vol_br             AS volume
        Ebr_tot                     AS enthalpy
        Ebr_in, Ebr                 AS specific_enthalpy
        Vap_rate                    AS vapour_flowrate
        Vap_heat                    AS latent_heat
        Vap_heat_in                 AS latent_heat
        Vap_heat_down               AS latent_heat
        Din                         AS condensate_flowrate
        Dout                        AS condensate_flowrate
        Mdis                        AS condensate_flowrate
        Ddist                       AS distillate_density

        Abd                         AS param_corr
        Bbd                         AS param_corr
        Ab                          AS param_corr
        Bb                          AS param_corr
        Cd                          AS param_corr
        Abr                         AS param_corr
        Bbr                         AS param_corr

        Utot                        AS heat_transf_coeff
        Cond_rate                   AS condensate_flowrate
        Tc_in, Tc_out               AS temperature
        Rec_br                      AS brine_flowrate
        Tfeed_avg                   AS temperature
        Q_rate                      as  heat_load
```

```
        Xgas                        AS mass_fraction
        Xgas_in                     AS mass_fraction
        Xgas_eq                     AS mass_fraction
        Xeq_mol                     AS mass_fraction
        Y                           AS mass_fraction
        Ymol                        AS mass_fraction
        Yin                         AS mass_fraction

        Henry                       AS param_corr
        Mnncond                     AS mass
        Mbr_gas                     AS mass
        Non_cond_rate                AS vapour_flowrate #actually non-
condensable
                                 gases flowrate
        gamma                           AS param_corr       #efficency
coefficient of
                                 degassing process

        ALPHA                       AS param_corr
        NCin                        AS vapour_flowrate
        NCout                       AS vapour_flowrate

      STREAM
        brine_inlet    : Cbr_in, Xgas_in, Tbr_in   AS   CTStream
        brine_outlet   : Cbr, Xgas, Tbr            AS   CTStream
        vap_inlet      : Yin, Tvap_in              AS   VapStream
        vap_outlet     : Y, Tvap                   AS   VapStream


      SELECTOR
        Evaporation    AS (present, notpresent) DEFAULT notpresent
        Condensation   AS (present, notpresent) DEFAULT notpresent
        Brine_flow     AS (flow, noflow)        DEFAULT flow


      EQUATION

      ##Brine phase, Vapor phase & distllate tray mass balances ##
        $Mbr    = Bin - Bout - Vap_rate - Non_cond_rate ;
        $Mvap    = Din + Vap_rate + Non_cond_rate + Vin   - Vout    -
Dout    ;
        $Mdis   = Din + cond_rate + Vin*(1-Yin)- Dout ;
              # almost steady state since the distillate tray height
is very small
        Mbr     = Vol_br * Dbr ;
        Mvap    = Vol_vap * Dvap  ;
        Mdis    = 2.048*0.1*0.8 * W  * Ddist;
         # distillate tray dimension L=2048mm , H = 10 mm , fraction
occupied = 0.8
        Vol_br  = A * Hbrine ;
        Vol_vap = A * (H-Hbrine) ;

      ##Brine salt balance##
        $Msalt = Bin * Cbr_in/1E6 - Bout * Cbr/1E6 ;
        Msalt  = Mbr * Cbr/1E6 ;

      ##Non-Condensables Mass Balance Equation in the vap phase##
        $Mnncond = Non_cond_rate + Vin * Yin - Vout * Y  ;
        Mnncond  = Mvap * Y  ;
        NCin     = Yin * Vin ;
```

```
        NCout    = Y * Vout  ;


      ##Non-Condensables Mass Balance Equation in the  brine phase ##
        $Mbr_gas = Bin * Xgas_in - Bout * Xgas - Non_cond_rate ;
        Mbr_gas  = Mbr * Xgas ;

      #Henry's Constant value
        Henry = -7.9E+5*Tbr^2 + 5.8E+8*Tbr - 9.499E+10; #PERRY, Henry
[Pa] & T[K]

      #Liquid mass fraction at equilibium with gas phase in the stage
        Ymol  =  Y  /  AIR_mol_mass  /  (Y  /  AIR_mol_mass  +  (1-Y)  /
H2O_mol_mass);
        Xeq_mol = Xgas_eq / AIR_mol_mass / (Xgas_eq / AIR_mol_mass +
(1-Xgas_eq) / H2O_mol_mass);
        Ymol  =  Henry  *  Xeq_mol  /  P;        #molar_Xgas  calculated
neglecting the presence of the salt



      ##Brine Enthalpy balance Equation in the stage##
        $Ebr_tot     =  Bin*Ebr_in  -  Bout*Ebr  -  Vap_rate*(Cp_br  *
(Tevap-273.15) + Vap_heat_down)
      - non_cond_rate *cp_air*(Tevap-273.150);
        Ebr_tot    = Ebr*Mbr                      ;
        Ebr_in     = Cp_br * (Tbr_in - 273.15)   ;
        Ebr        = Cp_br * (Tbr    - 273.15)   ;

      ##Physical Parameters Correlations##
       #Brine Density#
        Ab     = ((2*(Tbr-273.15)-200))/160 ;
        Bb     = ((2*Cbr/1000)-150)/150 ;
        Dbr      =  1000  *  ((4.032219*G1+0.115313*Bb+3.26E-4*(2*Bb^2-
1))*F1 +
                        (-0.108199*G1+1.571E-3*Bb-4.23E-4*(2*Bb^2-
1))*Ab +
                        (-0.012247*G1+1.74E-3*Bb-9E-6*(2*Bb^2-
1))*(2*Ab^2-1) +
                        (6.92E-4*G1-8.7E-5*Bb-5.3E-5*(2*Bb^2-
1))*(4*Ab^3-3*Ab)) ;

       #Distillate density#
        Abd    = (2*(Tvap-273.15)-200)/160;
        Bbd    = -1;
        Ddist   = 1000 ; # assumed constant (Not affecting the model
since distillate tray balance is S.S)

       #Vapor density#
        Dvap  =  (P/R/Tevap)/((1-Y)/H2O_mol_mass+Y/AIR_mol_mass)/1000
; # mass averaged ideal gas law
        Vap_heat_down  =  (2501.89714  -  2.40706*(Tevap-273.15)     +
1.192217e-3*(Tevap-273.15)^2   - 1.5863E-5*(Tevap-273.15)^3)*1E-3   ;
#ETTOUNEY
        Vap_heat_in     =  (2501.89714  -  2.40706*(Tvap_in-273.15)  +
1.192217e-3*(Tvap_in-273.15)^2 - 1.5863E-5*(Tvap_in-273.15)^3)*1E-3 ;
#ETTOUNEY
        Vap_heat        =  (2501.89714  -  2.40706*(Tvap-273.15)     +
1.192217e-3*(Tvap-273.15)^2    - 1.5863E-5*(Tvap-273.15)^3)*1E-3    ;
#ETTOUNEY
```

```
      ##Efficiency Parameters Correlations##
        LOG(P*(1-Ymol))      = Aant - (Bant/(Tvap-Cant))  ; #(Antoine
Eq. applied to the vapour partial pressure above demister)

        LOG(Pevap*(1-Ymol)) = Aant - (Bant/(Tevap-Cant)) ; #(Antoine
Eq. applied to the vapour partial pressure below demister)


      ##rate of vapour production in the stage##
        CASE Evaporation OF
          WHEN present    :
                            Vap_rate*(Cp_br*(Tevap-
Tbr)+Vap_heat_down) = Bin*Cp_br*(Tbr_in-(Tevap+BPE+NEA)) ;
          SWITCH TO notpresent IF Tbr_in < (Tevap+BPE+NEA) ;
          WHEN notpresent :
                            Vap_rate = 0.0001 ;
          SWITCH TO present    IF Tbr_in > (Tevap+BPE+NEA)+0.2  ;
        END #CASE



      ##rate of non-condensable gases released in the stage##
        IF (Xgas-Xgas_eq) > 0 THEN
          Non_cond_rate = Bin*(Xgas-Xgas_eq)*gamma ;
      # gamma related to the effciency of the degassing process &
0<gamma<1
          ELSE
          Non_cond_rate = 0.0 ;
        END #IF

        gamma = 0.90 ; #imposing a 85% efficiency of degassing
process


      ##Boiling Point Elevation##
       BPE                  =(-4.584e-4*(Tbr-273.15)^2+2.823e-1*(Tbr-
273.15)+17.95)*(cbr/1e6)^2+
             (1.536e-4*(Tbr-273.15)^2+5.267e-2*(Tbr-
273.15)+6.56)*(cbr/1e6);

      ##Specific Heat Correlations##
      Acp = 4206.8      - 6.6197      * Cbr/1000 + 1.2288e-2       *
(Cbr/1000)^2 ;
      Bcp = -1.1262     + 5.4178e-2   * Cbr/1000 - 2.2719e-4       *
(Cbr/1000)^2 ;
      Ccp = 1.2026e-2   - 5.3566e-4   * Cbr/1000 + 1.8906e-6       *
(Cbr/1000)^2 ;
      Dcp = 6.8777e-7   + 1.517e-6    * Cbr/1000 - 4.4268e-9       *
(Cbr/1000)^2 ;


      Cp_br    = (Acp + Bcp*(Tbr-273.15) + Ccp * (Tbr-273.15)^2 + Dcp
* (Tbr-273.15)^3) *1e-6; # ETTOUNEY   MJ/Kg K
      Cp_dist = (4206.8 -1.1262 *   (Tdin - 273.15) +  1.2026e-2 *
(Tdin-273.15)^2 + 6.8777e-7 *(TDin-273.15)^3)*1e-6;# ETTOUNEY   MJ/Kg
K (SALT CONC=0 )
      Cp_air = 1.01E-3; #MJ/kg.K
```

```
      ##Demister losses##

      DPdemister  =       0.2  *3.9*  Demisterdensity^  0.38  *Vap_Vel
^0.81*wire_diam^(-1.56)  ;#Pa
      Vap_Vel = Vap_rate / Dvap / Area_demister + 0.0001   ;# m/sec

      Area_demister = 1.11* W       ;#m2

      DPdemister = Pevap - P   ;#Pa

      Tvap = Tevap - Tdemister ;
      LOG(Pevap*(1-Ymol))     = Aant - (Bant/(Tevap-Cant))    ;
       #(Antoine  Eq.  applied  to  the  vapour  partial  pressure  above
demister)
```

```
      #============================================================#
      #                                                            #
      #  Model of the Last Falshing Stage of Heat Rejection Section #
      #   - with condensation of vapour;                           #
      #   - with vapour production rate;                           #
      #   - with non condensable gases ;                           #
      #   - With Thermodynamic properties correlations ;           #
      #   - With Distillate Tray;                                  #
      #============================================================#


      PARAMETER

        W              AS REAL #STAGE WIDTH
        L              AS REAL #STAGE LENGTH
        H              AS REAL #STAGE HEIGHT
        A              AS REAL #STAGE FLOOR AREA
        Horifice1      AS REAL #WEIR GATE HIEGHT
        Horifice2      AS REAL #FLASH BOX OPENING
        R              AS REAL #UNIVERSAL GAS CONSTANT
        H2O_mol_mass   AS REAL #MOLECULAR MASS OF WATER
        AIR_mol_mass   AS REAL #MOLECULAR MASS OF AIR
        Pvent          AS REAL #PRESSURE IN VENT SYSTEM
        Tdemister as real
        #Physical parmaeters correlations
        Aant           AS REAL #ANTOINE EQUATION
        Bant           AS REAL #ANTOINE EQUATION
        Cant           AS REAL #ANTOINE EQUATION

        G1             AS REAL #BRINE DENSITY CORRELATION
        F1             AS REAL #BRINE DENSITY CORRELATION

        #Condensing zone parameters
        Wtube          AS REAL    #LENGTH
        NoTubes        AS INTEGER #NUMBER OF CONDENSER TUBES
        Diam_Tube_out  AS REAL    #EXTERNAL DIAMETER OF ONE TUBE
        Diam_Tube_in   AS REAL    #INTERNAL DIAMETER OF ONE TUBE

        #Demister parameters
        Demisterdensity AS REAL
        wire_diam       AS REAL



      VARIABLE
        Q_rate                    As  heat_load
        Area                      As area
        Feed_Mcw                  AS brine_flowrate
                                #INLET SEAWATER FEED TO THE PLANT
        Mcw                         AS brine_flowrate #COOLING WATER
FLOWRATE
        Acp                       AS param_corr
        Bcp                       AS param_corr
        Ccp                       AS param_corr
        Dcp                       AS param_corr
        Cp_br                     AS specific_heat #SPECIFIC HEAT OF
BRINE

        Cp_dist                   AS specific_heat
```

```
                        #SPECIFIC HEAT OF DISTILLATE WATER
        Cp_air                    AS specific_heat
                                #SPECIFIC  HEAT  OF  noncondensable
                        gases
        Cp_br_in                  AS specific_heat
                                #SPECIFIC HEAT OF brine entering the stage
        Cp_br_feed                AS specific_heat
                                #SPECIFIC  HEAT  OF  seawater  entering  the
                  last stage
        Re1                       AS Reynolds_Number
                                #REYNOLD'S NUMBER AT Horifice1
        Re2                       AS Reynolds_Number
                                #REYNOLD'S NUMBER AT Hbrine
        Diam                      AS Diameter_RE
        Diam2                     AS Diameter_RE
        Viscosity                 AS Viscosity
        Bin, Bout                 AS brine_flowrate
        Vin, Vout                 AS vapour_flowrate
        Hbrine                      AS length # BRINE HEIGHT IN THE
STAGE
        Feed_Last                 AS brine_flowrate
        Cbr_in, Cbr, Cbr_feed     AS mass_fraction_ppm
        Cbr_rec                   AS mass_fraction_ppm
        Dbr                       AS brine_density
        Dvap                      AS vapour_density
        DRec_br                   AS brine_density
        P                         AS pressure
        Tdin                      AS temperature
        Tbr_in,Tbr,Tbr_feed,Tevap AS temperature
        Tvap_in, Tvap             AS temperature
        NEA, BPE                  AS param_corr
        Mbr, Mvap, Msalt          AS mass
        Vol_vap, Vol_br           AS volume
        Ebr_tot                   AS enthalpy
        Ebr_in, Ebr,Ebr_feed      AS specific_enthalpy
        Vap_rate                  AS vapour_flowrate
        Vap_heat                  AS latent_heat
        Vap_heat_in               AS latent_heat
        Din                       AS condensate_flowrate
        Dout                      AS condensate_flowrate
        Mdis                      AS condensate_flowrate
        Ddist                     AS distillate_density

        Abd                       AS param_corr
        Bbd                       AS param_corr
        Ab                        AS param_corr
        Bb                        AS param_corr
        Cd                        AS param_corr
        Abr                       AS param_corr
        Bbr                       AS param_corr

        Utot                      AS heat_transf_coeff
        Cond_rate                 AS condensate_flowrate
        Tc_in, Tc_out             AS temperature
        Rec_br                    AS brine_flowrate
        Tfeed_avg                 AS temperature

        Xgas                      AS mass_fraction
        Xgas_in, Xgas_feed        AS mass_fraction
        Xgas_eq                   AS mass_fraction
```

```
        Xeq_mol                     AS mass_fraction
        Y                           AS mass_fraction
        Ymol                        AS mass_fraction
        Yin                         AS mass_fraction

        Henry                       AS param_corr
        Mnncond                     AS mass
        Mbr_gas                     AS mass
        Non_cond_rate               AS vapour_flowrate
                          #actually non-condensable gases flowrate
        gamma                       AS param_corr
                          #efficency coefficient of degassing process

        ALPHA                       AS param_corr

        Peevap,Pevap                AS pressure
        Teevap                      AS Temperature

        DPdemister                  AS pressure
        Vap_Vel                     AS vapor_velocity
        Area_demister               AS area

      STREAM
        brine_inlet   : Cbr_in, Xgas_in, Tbr_in  AS   CTStream
        brine_outlet  : Cbr, Xgas, Tbr           AS   CTStream
        vap_inlet     : Yin, Tvap_in             AS   VapStream
        vap_outlet    : Y, Tvap                  AS   VapStream



      SELECTOR
        Evaporation    AS (present, notpresent) DEFAULT notpresent
        Condensation   AS (present, notpresent) DEFAULT notpresent
        Brine_flow     AS (flow, noflow)        DEFAULT flow


      EQUATION

      ##Brine phase, Vapor phase & distllate tray mass balances ##
        $Mbr     = {Feed_Last + } Bin - Bout { -REC_BR } - Vap_rate -
Non_cond_rate ;
        $Mvap    = Din + Vap_rate + Vin - Vout - Dout  + Non_cond_rate
;
        $Mdis    = Din + cond_rate + Vin*(1-Yin)- Dout;# almost steady
state since the height is very small
        Mbr      = Vol_br * Dbr ;
        Mvap     = Vol_vap * Dvap ;
        Mdis       = 2.048*0.1*0.8 * W   * Ddist; # distillate tray
dimension L=2048mm , H = 10 mm , fraction occupied = 0.8
        Vol_br   = A * Hbrine ;
        Vol_vap  = A * (H-Hbrine) ;
        Feed_Last = Feed_Mcw - Mcw;



      ##Brine salt balance##
        #$Msalt = Feed_Last * Cbr_feed/1E6  + Bin * Cbr_in/1E6 - Bout
* Cbr/1E6 - Rec_br *Cbr_rec/1E6 ;
        Msalt  = Mbr * Cbr/1E6 ;
        $Msalt = Bin * Cbr_in/1E6 - Bout * Cbr/1E6 ;
```

```
      ##Non-Condensables Mass Balance Equation in the vap phase##
        $Mnncond = Non_cond_rate + Vin*Yin - Vout*abs(Y)  ;
        Mnncond  = Mvap*Y  ;


      ##Non-Condensables Mass Balance Equation in the  brine phase ##
        $Mbr_gas = Feed_Last * Xgas_feed + Bin*Xgas_in - Bout*Xgas -
Non_cond_rate - Rec_br * Xgas ;
        Mbr_gas  = Mbr*Xgas ;


      ##Brine Enthalpy balance Equation in the stage##
        $Ebr_tot    = Feed_last* Ebr_feed + Bin*Ebr_in - Bout*Ebr -
Rec_br * Ebr -
                        Vap_rate*(Cp_br * (Tvap-273.15) + Vap_heat)
;
        Ebr_tot    = Ebr*Mbr                    ;
        Ebr_in     = Cp_br_in * (Tbr_in-273.15)   ;
        Ebr        = Cp_br * (Tbr-273.15)      ;
        Ebr_feed   = Cp_br_feed * (Tbr_feed-273.15)    ;
        Tbr_feed   = Tc_in + 5;


      ##Physical Parameters Correlations##
       #Brine Density#
        Ab     = ((2*(Tbr-273.15)-200))/160 ;
        Bb     = ((2*Cbr/1000)-150)/150 ;
        Dbr      = 1000 * ((4.032219*G1+0.115313*Bb+3.26E-4*(2*Bb^2-
1))*F1 +
                        (-0.108199*G1+1.571E-3*Bb-4.23E-4*(2*Bb^2-
1))*Ab +
                        (-0.012247*G1+1.74E-3*Bb-9E-6*(2*Bb^2-
1))*(2*Ab^2-1) +
                        (6.92E-4*G1-8.7E-5*Bb-5.3E-5*(2*Bb^2-
1))*(4*Ab^3-3*Ab)) ;
       #Distillate density#
        Abd    = ((2*(Tvap-273.15)-200))/160;
        Bbd    = -1;
        Ddist   = 1000 * ((4.032219*G1+0.115313*Bbd+3.26E-4*(2*Bbd^2-
1))*F1 +
                        (-0.108199*G1+1.571E-3*Bbd-4.23E-4*(2*Bbd^2-
1))*Abd +
                        (-0.012247*G1+1.74E-3*Bbd-9E-6*(2*Bbd^2-
1))*(2*Abd^2-1) +
                        (6.92E-4*G1-8.7E-5*Bbd-5.3E-5*(2*Bbd^2-
1))*(4*Abd^3-3*Abd)) ;
        #Vapor density#
        Dvap   =   (P/R/Tvap)/((1-Y)/H2O_mol_mass+Y/AIR_mol_mass)/1000
; # mass averaged ideal gas law
        Vap_heat         =  (2501.89714  -  2.40706*(Tvap-273.15)  +
1.192217e-3*(Tvap-273.15)^2   -   1.5863E-5*(Tvap-273.15)^3)*1E-3   ;
#Ettuney
        Vap_heat_in   =   (2501.89714   -   2.40706*(Tvap_in-273.15)   +
1.192217e-3*(Tvap_in-273.15)^2 - 1.5863E-5*(Tvap_in-273.15)^3)*1E-3 ;
#Ettuney
       #Henry's Constant value
        Henry = -7.9E+5*Tbr^2 + 5.8E+8*Tbr - 9.499E+10; #PERRY, Henry
[Pa] & T[K]
```

```
       ##Boiling Point Elevation##
      BPE                    =(-4.584e-4*(Tbr-273.15)^2+2.823e-1*(Tbr-
273.15)+17.95)*(cbr/1e6)^2+
             (1.536e-4*(Tbr-273.15)^2+5.267e-2*(Tbr-
273.15)+6.56)*(cbr/1e6);

      ##Specific Heat Correlations##
      Acp = 4206.8       - 6.6197       * Cbr/1000 + 1.2288e-2       *
(Cbr/1000)^2 ;
      Bcp = -1.1262      + 5.4178e-2    * Cbr/1000 - 2.2719e-4       *
(Cbr/1000)^2 ;
      Ccp = 1.2026e-2    - 5.3566e-4    * Cbr/1000 + 1.8906e-6       *
(Cbr/1000)^2 ;
      Dcp = 6.8777e-7    + 1.517e-6     * Cbr/1000 - 4.4268e-9       *
(Cbr/1000)^2 ;
      Cp_br    = (Acp + Bcp*(Tbr-273.15) + Ccp * (Tbr-273.15)^2 + Dcp
* (Tbr-273.15)^3) *1e-6; # ETTOUNEY   MJ/Kg K
      Cp_br_in =(Acp + Bcp*(Tbr_in-273.15) + Ccp * (Tbr_in-273.15)^2
+ Dcp * (Tbr_in-273.15)^3) *1e-6; # ETTOUNEY   MJ/Kg K
      Cp_br_feed =(Acp  + Bcp*(Tbr_feed-273.15)  + Ccp  *  (Tbr_feed-
273.15)^2 + Dcp * (Tbr_feed-273.15)^3) *1e-6; # ETTOUNEY   MJ/Kg K
      Cp_dist = (4206.8 -1.1262 *   (Tdin - 273.15) +   1.2026e-2 *
(Tdin-273.15)^2 + 6.8777e-7 *(TDin-273.15)^3)*1e-6;# ETTOUNEY   MJ/Kg
K (SALT CONC=0 )
      Cp_air = 1.01E-3; #kJ/kg.K ^



      #Liquid mass fraction at equilibium with gas phase in the stage
        Ymol = Y/AIR_mol_mass/(Y/AIR_mol_mass+(1-Y)/H2O_mol_mass);
        Xeq_mol    =    Xgas_eq/AIR_mol_mass/(Xgas_eq/AIR_mol_mass+(1-
Xgas_eq)/H2O_mol_mass);
        Ymol = Henry*Xeq_mol/P;     #molar_Xgas calculated neglecting
the presence of the salt

      ##Efficiency Parameters Correlations##
        LOG(P*(1-Ymol)) = Aant  -  (Bant/(Tvap-Cant))  ;  #(Antoine Eq.
applied to the vapour partial pressure)
        LOG(Pevap*(1-Ymol)) = Aant - (Bant/(Tevap-Cant)) ; #(Antoine
Eq. applied to the vapour partial pressure below demister)

      ##rate of vapour production in the stage##
        CASE Evaporation OF
          WHEN present    :
                           Vap_rate*(Cp_br*(Tvap-Tbr)+Vap_heat)    =
Bin*Cp_br*(Tbr_in-(Tvap+BPE+NEA)) ;
          SWITCH TO notpresent IF Tbr_in < (Tvap+BPE+NEA) ;
          WHEN notpresent :
                           Vap_rate = 0.0 ;
          SWITCH TO present    IF Tbr_in > (Tvap+BPE+NEA)+0.3  ;
        END #CASE


      ##rate of non-condensable gases released in the stage##
        IF (Xgas-Xgas_eq)>0 THEN
          Non_cond_rate = Bin*(Xgas-Xgas_eq)*gamma ; # gamma related
to the effciency of the degassing process & 0<gamma<1
          ELSE
          Non_cond_rate = 0 ;
        END #IF
```

```
        gamma = 0.85 ; #imposing a 90% efficiency of degassing
process

      ##Demister losses##

      DPdemister =    0.2 * 3.9*Demisterdensity^ 0.38 *Vap_Vel^0.81 *
wire_diam^(-1.56)  ;#Pa
      Vap_Vel = Vap_rate / Dvap / Area_demister + 0.0001   ;# m/sec

      Area_demister = 1.11* W       ;#m2
      DPdemister = Pevap - P   ;#Pa

      Tvap = Tevap - Tdemister ;

      LOG(Pevap*(1-Ymol))       = Aant  -  (Bant/(Teevap-Cant))     ;
#(Antoine Eq. applied to the vapour partial pressure above demister)

      #============================================================#
      #                                                            #
      #                    Model of a Multi-stages unit            #
      #   vapour and brine passing from one stage to the subsequent #
      #   - with condensation of vapour;                           #
      #   - with non-condensable gases                             #
      #   - withOUT vapour by-pass through the gate                #
      #   - with controllers for brine height at the last stage    #
      #   - with controllers for pressure at the last stage        #
      #   - With Thermodynamic properties correlations             #
      #   - With Distillate Tray                                   #
      #   With NEW Correlations  For Cd, NEA , U  From AlFulaij 2002#
      #     Based on real plant data                               #
      #============================================================#

      PARAMETER

        NoStages        AS INTEGER # NUMBER OF STAGES PRESENT IN THE
UNIT
        g               AS REAL    # Gravitational accelaration

        W               AS REAL #STAGE WIDTH
        L               AS REAL #STAGE LENGTH
        R               AS REAL #UNIVERSAL GAS CONSTANT
        H2O_mol_mass    AS REAL #MOLECULAR MASS OF WATER
        AIR_mol_mass    AS REAL #MOLECULAR MASS OF AIR

        Bant            AS REAL #ANTOINE EQUATION
        Cant            AS REAL #ANTOINE EQUATION
        Aant            AS REAL #ANOTINE EQAUTION

        G1              AS REAL #BRINE DENSITY CORRELATION
        F1              AS REAL #BRINE DENSITY CORRELATION

        Wtube           AS REAL #LENGTH OF TUBES IN THE CONDENSER


      ##Venting line parameters##
        Pvent           AS REAL #PRESSURE IN VENT SYSTEM
        Pvent1          AS REAL #PRESSURE IN VENT SYSTEM
        Pvent7          AS REAL #PRESSURE IN VENT SYSTEM
        Pvent12         AS REAL #PRESSURE IN VENT SYSTEM
```

```
      ##CONTROL LOOP PARAMETERS##
        Hsp              AS REAL # SET POINT FOR THE BRINE HEIGHT IN
THE LAST STAGE
        ALPHA_sp        AS REAL # initial value of ALPHA in the last
stage



      VARIABLE
        Kc_b                        AS param_corr
                          # Proportional controller gain [kg/sm]
        Kc_p                        AS param_corr
                               # Proportional controller gain [kg/sm]
        Psp                         AS pressure
                               #  SET  POINT  FOR  THE  PRESSURE  IN  THE
                          LAST STAGE
        distcapacity                AS distillate_flow_rate

      Msteam                      AS steam_flowrate
                          # steam flowrate to the brine heater
        PerformanceRatio            AS Performance # SYSTEM PERFORMANCE
RATIO
        Tsteam                      AS Temperature #STEAM TEMP.
        Steam_heat                  AS enthalpy #STEAM ENTHALPY



      UNIT
       FS AS ARRAY (NoStages) OF FLASHING_STAGE
       FSRL   AS ARRAY (1) Of Flashing_stage_rejection_last


      STREAM
        brine_inlet    IS  FS(1).brine_inlet
        brine_outlet   IS  FS(NoStages).brine_outlet
        vap_inlet      IS  FS(1).vap_inlet
        vap_outlet     IS  FS(NoStages).vap_outlet



      EQUATION

      ##Discharge coefficient correlations##
       #Flash Box Stages#
      For i:=2 to 14 do

      FS(i).Cd=0.49*      (FS(i).Horifice1/((FS(i-1).P-FS(i).P)/FS(i-
1).Dbr/9.81+FS(i-1).Hbrine))   ^(-0.058)
                  *(FS(i-1).Bout/FS(i-1).Dbr/FS(i-
1).Hbrine/(FS(i).Bout/FS(i).Dbr/FS(i).Hbrine))^0.188
                  *(FS(i-1).Dbr/(FS(i-1).Dbr/((1-(1-FS(i-
1).Dbr/Fs(i-1).Dvap)
                  *FS(i-1).Cond_rate/(FS(i-1).cond_rate+fs(i-
1).Bout)))))^(-0.234)
                  *(FS(i).Horifice1/FS(i).Horifice2)^0.2;          #
AlFulaij 2002
      end

      FS(1).Cd=0.7; #Assumed to be constant since No correlation
available for the first stage Cd
```

```
       #Weir orifice stages#
      FOR i:=15 to nostages do
      FS(i).Cd=0.14*      (FS(i).Horifice1/((FS(i-1).P-FS(i).P)/FS(i-
1).Dbr/9.81+FS(i-1).Hbrine))   ^(0.147)
                  *(FS(i-1).Bout/FS(i-1).Dbr/FS(i-
1).Hbrine/(FS(i).Bout/FS(i).Dbr/FS(i).Hbrine))^1.33
                  *(FS(i-1).Dbr/(FS(i-1).Dbr/((1-(1-FS(i-
1).Dbr/Fs(i-1).Dvap)
                  *FS(i-1).Cond_rate/(FS(i-1).cond_rate+fs(i-
1).Bout)))))^(0.362);   #  AlFulaij 2002
      end
      FOR i:=nostages+1 to nostages+1 do

      FSRL(1).Cd=0.14*                (FSRL(1).Horifice1/((FS(i-1).P-
FSRL(1).P)/FS(i-1).Dbr/9.81+FS(i-1).Hbrine))   ^(0.147)
                  *(FS(i-1).Bout/FS(i-1).Dbr/FS(i-
1).Hbrine/(FSRL(1).Bout/FSRL(1).Dbr/FSRL(1).Hbrine))^1.33
                  *(FS(i-1).Dbr/(FS(i-1).Dbr/((1-(1-FS(i-
1).Dbr/Fs(i-1).Dvap)
                  *FS(i-1).Cond_rate/(FS(i-1).cond_rate+FS(i-
1).Bout)))))^(0.362);   #  AlFulaij 2002
      end


      ##Non-Equilibrium Allowancw NEA Correlations##
       #NEA correlation for flash box stages#
      For i:=1 to 14 do
             FS(i).Viscosity                =                  EXP(-
3.79418+604.129/(139.18+(FS(i).Tbr-273.15)))*
                           (1+(1.474e-3 +1.5e-5*(FS(i).Tbr-273.15)-
3.927e-8*(FS(i).Tbr-273.15)^2)*FS(i).Cbr/1000+
                           (1.0734e-5-8.5e-8*(FS(i).Tbr-
273.15)+2.23e-10*(FS(i).Tbr-273.15)^2)*(FS(i).Cbr/1000)^2)*
                             1e-3;
               FS(i).Diam                                          =
4*FS(i).Horifice1*W/(2*FS(i).Horifice1+2*W);
               FS(i).Diam2                                         =
4*FS(i).Hbrine*FS(i).W/(2*FS(i).Hbrine+2*FS(i).W);
             FS(i).Re1          =          FS(i).Bin*3600*FS(i).Diam
/(FS(i).Horifice1*FS(i).W)/FS(i).Viscosity;
               FS(i).Re2  =  FS(i).Bin*3600*FS(i).Diam2/(FS(i).Hbrine
*FS(i).W)/FS(i).Viscosity;
               FS(i).NEA   =   0.1   *   166714689.5*   (FS(i).Tbr_IN-
273.15)^(-4.841) *(FS(i).Tbr_IN-FS(i).Tbr)^(-0.045) *
                        FS(i).Hbrine^(1.150)  *  FS(i).Re1^(-0.182)  *
FS(i).Re2^(0.204)  ;   # AlFulaij 2002}

      end

       #NEA correlation for weir orifice#
      For i:=15 to nostages do
             FS(i).Viscosity                =                  EXP(-
3.79418+604.129/(139.18+(FS(i).Tbr-273.15)))*
                           (1+(1.474e-3 +1.5e-5*(FS(i).Tbr-273.15)-
3.927e-8*(FS(i).Tbr-273.15)^2)*FS(i).Cbr/1000+
                           (1.0734e-5-8.5e-8*(FS(i).Tbr-
273.15)+2.23e-10*(FS(i).Tbr-273.15)^2)*(FS(i).Cbr/1000)^2)*
                             1e-3;
```

```
               FS(i).Diam                                                =
4*FS(i).Horifice1*W/(2*FS(i).Horifice1+2*W);
               FS(i).Diam2                                               =
4*FS(i).Hbrine*FS(i).W/(2*FS(i).Hbrine+2*FS(i).W);
            FS(i).Re1          =          FS(i).Bin*3600*FS(i).Diam
/(FS(i).Horifice1*FS(i).W)/FS(i).Viscosity;
               FS(i).Re2  =  FS(i).Bin*3600*FS(i).Diam2/(FS(i).Hbrine
*FS(i).W)/FS(i).Viscosity;
               FS(i).NEA  =  0.1  *6998.338*  (FS(i).Tbr_IN-273.15)^(-
3.137) *(ABS(FS(i).Tbr_IN-FS(i).Tbr))^(-.021) *
                        FS(i).Hbrine^(0.683)  *  FS(i).Re1^(0.174)  *
FS(i).Re2^(0.042)  ;   # AlFulaij 2002}

      end

       #Last Stage NEA#
            FSRL(1).Viscosity                =                EXP(-
3.79418+604.129/(139.18+(FSRL(1).Tbr-273.15)))*
                           (1+(1.474e-3       +1.5e-5*(FSRL(1).Tbr-
273.15)-3.927e-8*(FSRL(1).Tbr-273.15)^2)*FSRL(1).Cbr/1000+
                           (1.0734e-5-8.5e-8*(FSRL(1).Tbr-
273.15)+2.23e-10*(FSRL(1).Tbr-273.15)^2)*(FSRL(1).Cbr/1000)^2)*
                             1e-3;
               FSRL(1).Diam                                              =
4*FSRL(1).Horifice1*W/(2*FSRL(1).Horifice1+2*W);
               FSRL(1).Diam2                                             =
4*FSRL(1).Hbrine*FSRL(1).W/(2*FSRL(1).Hbrine+2*FSRL(1).W);
            FSRL(1).Re1        =       FSRL(1).Bin*3600*FSRL(1).Diam
/(FSRL(1).Horifice1*FSRL(1).W)/FSRL(1).Viscosity;
               FSRL(1).Re2                                               =
FSRL(1).Bin*3600*FSRL(1).Diam2/(FSRL(1).Hbrine
*FSRL(1).W)/FSRL(1).Viscosity;
               FSRL(1).NEA   =   0.1   *6998.338*   (FSRL(1).Tbr_IN-
273.15)^(-3.137) *(FSRL(1).Tbr_IN-FSRL(1).Tbr)^(-.021) *
                        FSRL(1).Hbrine^(0.683) * FSRL(1).Re1^(0.174)
* FSRL(1).Re2^(0.042)  ;   # AlFulaij 2002}


      ##Blow Through Calculation (Cipollina)##
      FOR i := 1 TO 1 DO

          CASE FS(i).Brine_flow OF
            WHEN   FS(i).flow        :   FS(i).Bout   =   FS(i).Cd   *
(FS(i).Horifice1*FS(i).w) *
                                          (ABS(2*(FS(i).P-FS(i+1).P
+ (FS(i).Hbrine-FS(i+1).Hbrine)*g*FS(i).Dbr)*FS(i).Dbr))^0.5 *
                                           SGN(2*(FS(i).P-FS(i+1).P
+ (FS(i).Hbrine-FS(i+1).Hbrine)*g*FS(i).Dbr)*FS(i).Dbr)        ;
                                 FS(i).Vout     =     FS(i).ALPHA     *
(ABS(FS(i).Dvap*(FS(i).P-Pvent1)))^0.5 *
                                           SGN(FS(i).Dvap*(FS(i).P-
Pvent1))        ;
               SWITCH   TO   FS(i).noflow      IF   FS(i).Hbrine   <
(FS(i+1).Horifice1+0.05 ) ;
            WHEN   FS(i).noflow   :   FS(i).Bout   =   FS(i).Cd   *
(FS(i).Hbrine*FS(i+1).w) *
                                          (ABS(2*(FS(i).P-FS(i+1).P
+ (FS(i).Hbrine-FS(i+1).Hbrine)*g*FS(i).Dbr)*FS(i).Dbr))^0.5 *
                                           SGN(2*(FS(i).P-FS(i+1).P
+ (FS(i).Hbrine-FS(i+1).Hbrine)*g*FS(i).Dbr)*FS(i).Dbr)        ;
```

```
                                    FS(i).Vout                                =
(FS(i).ALPHA+(FS(i+1).Horifice1-FS(i).Hbrine)*FS(i).W)                        *
(ABS(FS(i).Dvap*(FS(i).P-Pvent1)))^0.5 *
                                                        SGN(FS(i).Dvap*(FS(i).P-
Pvent1))        ;
                SWITCH   TO   FS(i).flow           IF   FS(i).Hbrine   >
(FS(i+1).Horifice1 +0.03) ;
           END #CASE

      END #FOR

      FOR i := 2 TO 6 DO

           CASE FS(i).Brine_flow OF
             WHEN   FS(i).flow        :   FS(i).Bout   =   FS(i).Cd   *
(FS(i).Horifice1*FS(i).w) *
                                                       (ABS(2*(FS(i).P-FS(i+1).P
+ (FS(i).Hbrine-FS(i+1).Hbrine)*g*FS(i).Dbr)*FS(i).Dbr))^0.5 *
                                                        SGN(2*(FS(i).P-FS(i+1).P
+ (FS(i).Hbrine-FS(i+1).Hbrine)*g*FS(i).Dbr)*FS(i).Dbr)        ;
                                    FS(i).Vout     =     FS(i).ALPHA     *
(ABS(FS(i).Dvap*(FS(i).P-FS(i+1).P)))^0.5 *
                                                        SGN(FS(i).Dvap*(FS(i).P-
FS(i+1).P))        ;
                SWITCH   TO   FS(i).noflow       IF   FS(i).Hbrine   <
(FS(i+1).Horifice1+0.05 ) ;
             WHEN   FS(i).noflow   :   FS(i).Bout   =   FS(i).Cd   *
(FS(i).Hbrine*FS(i+1).w) *
                                                       (ABS(2*(FS(i).P-FS(i+1).P
+ (FS(i).Hbrine-FS(i+1).Hbrine)*g*FS(i).Dbr)*FS(i).Dbr))^0.5 *
                                                        SGN(2*(FS(i).P-FS(i+1).P
+ (FS(i).Hbrine-FS(i+1).Hbrine)*g*FS(i).Dbr)*FS(i).Dbr)        ;
                                    FS(i).Vout                                =
(FS(i).ALPHA+(FS(i+1).Horifice1-FS(i).Hbrine)*FS(i).W)                        *
(ABS(FS(i).Dvap*(FS(i).P-FS(i+1).P)))^0.5 *
                                                        SGN(FS(i).Dvap*(FS(i).P-
FS(i+1).P))        ;
                SWITCH   TO   FS(i).flow           IF   FS(i).Hbrine   >
(FS(i+1).Horifice1 +0.03) ;
           END #CASE

      END #FOR

      FOR i := 7 TO 7 DO

           CASE FS(i).Brine_flow OF
             WHEN   FS(i).flow        :   FS(i).Bout   =   FS(i).Cd   *
(FS(i).Horifice1*FS(i).w) *
                                                       (ABS(2*(FS(i).P-FS(i+1).P
+ (FS(i).Hbrine-FS(i+1).Hbrine)*g*FS(i).Dbr)*FS(i).Dbr))^0.5 *
                                                        SGN(2*(FS(i).P-FS(i+1).P
+ (FS(i).Hbrine-FS(i+1).Hbrine)*g*FS(i).Dbr)*FS(i).Dbr)        ;
                                    FS(i).Vout     =     FS(i).ALPHA     *
(ABS(FS(i).Dvap*(FS(i).P-Pvent7)))^0.5 *
                                                        SGN(FS(i).Dvap*(FS(i).P-
Pvent7))        ;
                SWITCH   TO   FS(i).noflow       IF   FS(i).Hbrine   <
(FS(i+1).Horifice1+0.005 ) ;
             WHEN   FS(i).noflow   :   FS(i).Bout   =   FS(i).Cd   *
(FS(i).Hbrine*FS(i+1).w) *
```

```
                                                (ABS(2*(FS(i).P-FS(i+1).P
+ (FS(i).Hbrine-FS(i+1).Hbrine)*g*FS(i).Dbr)*FS(i).Dbr))^0.5 *
                                                 SGN(2*(FS(i).P-FS(i+1).P
+ (FS(i).Hbrine-FS(i+1).Hbrine)*g*FS(i).Dbr)*FS(i).Dbr)        ;
                                  FS(i).Vout                              =
(FS(i).ALPHA+(FS(i+1).Horifice1-FS(i).Hbrine)*FS(i).W)                    *
(ABS(FS(i).Dvap*(FS(i).P-Pvent7)))^0.5 *
                                                 SGN(FS(i).Dvap*(FS(i).P-
Pvent7))        ;
               SWITCH   TO   FS(i).flow           IF   FS(i).Hbrine   >
(FS(i+1).Horifice1 +0.03) ;
          END #CASE

      END #FOR

      FOR i := 8 TO 11 DO

          CASE FS(i).Brine_flow OF
            WHEN   FS(i).flow        :   FS(i).Bout   =   FS(i).Cd   *
(FS(i).Horifice1*FS(i).w) *
                                                (ABS(2*(FS(i).P-FS(i+1).P
+ (FS(i).Hbrine-FS(i+1).Hbrine)*g*FS(i).Dbr)*FS(i).Dbr))^0.5 *
                                                 SGN(2*(FS(i).P-FS(i+1).P
+ (FS(i).Hbrine-FS(i+1).Hbrine)*g*FS(i).Dbr)*FS(i).Dbr)        ;
                                  FS(i).Vout     =     FS(i).ALPHA     *
(ABS(FS(i).Dvap*(FS(i).P-FS(i+1).P)))^0.5 *
                                                 SGN(FS(i).Dvap*(FS(i).P-
FS(i+1).P))        ;
               SWITCH   TO   FS(i).noflow      IF   FS(i).Hbrine   <
(FS(i+1).Horifice1+0.005 ) ;
            WHEN   FS(i).noflow   :   FS(i).Bout   =   FS(i).Cd   *
(FS(i).Hbrine*FS(i+1).w) *
                                                (ABS(2*(FS(i).P-FS(i+1).P
+ (FS(i).Hbrine-FS(i+1).Hbrine)*g*FS(i).Dbr)*FS(i).Dbr))^0.5 *
                                                 SGN(2*(FS(i).P-FS(i+1).P
+ (FS(i).Hbrine-FS(i+1).Hbrine)*g*FS(i).Dbr)*FS(i).Dbr)        ;
                                  FS(i).Vout                              =
(FS(i).ALPHA+(FS(i+1).Horifice1-FS(i).Hbrine)*FS(i).W)                    *
(ABS(FS(i).Dvap*(FS(i).P-FS(i+1).P)))^0.5 *
                                                 SGN(FS(i).Dvap*(FS(i).P-
FS(i+1).P))        ;
               SWITCH   TO   FS(i).flow           IF   FS(i).Hbrine   >
(FS(i+1).Horifice1 +0.03) ;
          END #CASE

      END #FOR

      FOR i := 12 TO 12 DO

          CASE FS(i).Brine_flow OF
            WHEN   FS(i).flow        :   FS(i).Bout   =   FS(i).Cd   *
(FS(i).Horifice1*FS(i).w) *
                                                (ABS(2*(FS(i).P-FS(i+1).P
+ (FS(i).Hbrine-FS(i+1).Hbrine)*g*FS(i).Dbr)*FS(i).Dbr))^0.5 *
                                                 SGN(2*(FS(i).P-FS(i+1).P
+ (FS(i).Hbrine-FS(i+1).Hbrine)*g*FS(i).Dbr)*FS(i).Dbr)        ;
                                  FS(i).Vout     =     FS(i).ALPHA     *
(ABS(FS(i).Dvap*(FS(i).P-Pvent12)))^0.5 *
                                                 SGN(FS(i).Dvap*(FS(i).P-
Pvent12))        ;
```

```
              SWITCH   TO   FS(i).noflow      IF   FS(i).Hbrine   <
(FS(i+1).Horifice1+0.005 ) ;
            WHEN   FS(i).noflow   :   FS(i).Bout   =   FS(i).Cd   *
(FS(i).Hbrine*FS(i+1).w) *
                                                (ABS(2*(FS(i).P-FS(i+1).P
+ (FS(i).Hbrine-FS(i+1).Hbrine)*g*FS(i).Dbr)*FS(i).Dbr))^0.5 *
                                                 SGN(2*(FS(i).P-FS(i+1).P
+ (FS(i).Hbrine-FS(i+1).Hbrine)*g*FS(i).Dbr)*FS(i).Dbr)        ;
                                  FS(i).Vout                              =
(FS(i).ALPHA+(FS(i+1).Horifice1-FS(i).Hbrine)*FS(i).W)                    *
(ABS(FS(i).Dvap*(FS(i).P-Pvent12)))^0.5 *
                                                 SGN(FS(i).Dvap*(FS(i).P-
Pvent12))        ;
              SWITCH   TO   FS(i).flow          IF   FS(i).Hbrine   >
(FS(i+1).Horifice1 +0.03) ;
          END #CASE

      END #FOR

      FOR i := 13 TO nostages-1 DO

          CASE FS(i).Brine_flow OF
            WHEN   FS(i).flow        :   FS(i).Bout   =   FS(i).Cd   *
(FS(i).Horifice1*FS(i).w) *
                                                (ABS(2*(FS(i).P-FS(i+1).P
+ (FS(i).Hbrine-FS(i+1).Hbrine)*g*FS(i).Dbr)*FS(i).Dbr))^0.5 *
                                                 SGN(2*(FS(i).P-FS(i+1).P
+ (FS(i).Hbrine-FS(i+1).Hbrine)*g*FS(i).Dbr)*FS(i).Dbr)        ;
                                  FS(i).Vout     =     FS(i).ALPHA     *
(ABS(FS(i).Dvap*(FS(i).P-FS(i+1).P)))^0.5 *
                                                 SGN(FS(i).Dvap*(FS(i).P-
FS(i+1).P))        ;
              SWITCH   TO   FS(i).noflow      IF   FS(i).Hbrine   <
(FS(i+1).Horifice1+0.005 ) ;
            WHEN   FS(i).noflow   :   FS(i).Bout   =   FS(i).Cd   *
(FS(i).Hbrine*FS(i+1).w) *
                                                (ABS(2*(FS(i).P-FS(i+1).P
+ (FS(i).Hbrine-FS(i+1).Hbrine)*g*FS(i).Dbr)*FS(i).Dbr))^0.5 *
                                                 SGN(2*(FS(i).P-FS(i+1).P
+ (FS(i).Hbrine-FS(i+1).Hbrine)*g*FS(i).Dbr)*FS(i).Dbr)        ;
                                  FS(i).Vout                              =
(FS(i).ALPHA+(FS(i+1).Horifice1-FS(i).Hbrine)*FS(i).W)                    *
(ABS(FS(i).Dvap*(FS(i).P-FS(i+1).P)))^0.5 *
                                                 SGN(FS(i).Dvap*(FS(i).P-
FS(i+1).P))        ;
              SWITCH   TO   FS(i).flow          IF   FS(i).Hbrine   >
(FS(i+1).Horifice1 +0.03) ;
          END #CASE

      END #FOR
      FOR i := nostages TO nostages DO

          CASE FS(i).Brine_flow OF
            WHEN   FS(i).flow        :   FS(i).Bout   =   FS(i).Cd   *
(FS(i).Horifice1*FS(i).w) *
                                                (ABS(2*(FS(i).P-FSRL(1).P
+ (FS(i).Hbrine-FSRL(1).Hbrine)*g*FS(i).Dbr)*FS(i).Dbr))^0.5 *
                                                 SGN(2*(FS(i).P-FSRL(1).P
+ (FS(i).Hbrine-FSRL(1).Hbrine)*g*FS(i).Dbr)*FS(i).Dbr)        ;
```

```
                                    FS(i).Vout     =     FS(i).ALPHA     *
(ABS(FS(i).Dvap*(FS(i).P-FSRL(1).P)))^0.5 *
                                                SGN(FS(i).Dvap*(FS(i).P-
FSRL(1).P))        ;
                SWITCH    TO    FS(i).noflow       IF    FS(i).Hbrine    <
(FSRL(1).Horifice1+0.005 ) ;
             WHEN    FS(i).noflow    :    FS(i).Bout    =    FS(i).Cd    *
(FS(i).Hbrine*FSRL(1).w) *
                                               (ABS(2*(FS(i).P-FSRL(1).P
+ (FS(i).Hbrine-FSRL(1).Hbrine)*g*FS(i).Dbr)*FS(i).Dbr))^0.5 *
                                                SGN(2*(FS(i).P-FSRL(1).P
+ (FS(i).Hbrine-FSRL(1).Hbrine)*g*FS(i).Dbr)*FS(i).Dbr)        ;
                                    FS(i).Vout                                =
(FS(i).ALPHA+(FSRL(1).Horifice1-FS(i).Hbrine)*FS(i).W)                 *
(ABS(FS(i).Dvap*(FS(i).P-FSRL(1).P)))^0.5 *
                                                SGN(FS(i).Dvap*(FS(i).P-
FSRL(1).P))        ;
                SWITCH    TO    FS(i).flow           IF    FS(i).Hbrine    >
(FSRL(1).Horifice1 +0.03) ;
             END #CASE

      END #FOR


      ##outlet flow conditions (Cipollina)##

            #control loop for the brine height in the last stage
            Kc_b=0.9*FS(1).Bin;
            FSRL(1).Bout   =   0.9*FS(1).Bin   +   Kc_b*(FSRL(1).Hbrine-
Hsp)/Hsp;

            #control loop for the pressure in the last stage
            Kc_p=ALPHA_sp/20000;

            FSRL(1).ALPHA = ALPHA_sp + Kc_p*(FSRL(1).P-Psp);
            FSRL(1).Vout                =        FSRL(1).ALPHA        *
(ABS(FSRL(1).Dvap*(FSRL(1).P-Pvent)))^0.5 *

SGN(FSRL(1).Dvap*(FSRL(1).P-Pvent))      ;


      ##condensation around the tube bundle ##
      #Overall heat transfer coefficient HGS#
      For i:=1 to nostages-2 do
        FS(i).Tfeed_avg = (FS(i).Tc_in+FS(i).Tc_out)/2;
        FS(i).Abr     = ((2*(FS(i).Tfeed_avg-273.15)-200))/160 ;
        FS(i).Bbr     = ((2*FS(1).Cbr_in/1000)-150)/150 ;
        FS(i).DRec_br               =               1000               *
((4.032219*FS(i).G1+0.115313*FS(i).Bbr+3.26E-4*(2*FS(i).Bbr^2-
1))*FS(i).F1 +
                          (-0.108199*FS(i).G1+1.571E-3*FS(i).Bbr-
4.23E-4*(2*FS(i).Bbr^2-1))*FS(i).Abr +
                          (-0.012247*FS(i).G1+1.74E-3*FS(i).Bbr-9E-
6*(2*FS(i).Bbr^2-1))*(2*FS(i).Abr^2-1) +
                          (6.92E-4*FS(i).G1-8.7E-5*FS(i).Bbr-5.3E-
5*(2*FS(i).Bbr^2-1))*(4*FS(i).Abr^3-3*FS(i).Abr)) ;
        FS(i).Utot                                                =1e-3*(
0.107*FS(i).Tvap^0.773*(FS(i).Rec_br/FS(i).DRec_br/
```

```
(3.14/4*FS(i).Diam_Tube_in*FS(i).Notubes))^0.485);     #     MJ/Kg.K,
AlFulaij 2002

      end
      #Overall heat transfer coefficient HRS#
      For i:=nostages-1 to nostages do
        FS(i).Tfeed_avg = (FS(i).Tc_in+FS(i).Tc_out)/2;
        FS(i).Abr     = ((2*(FS(i).Tfeed_avg-273.15)-200))/160 ;
        FS(i).Bbr     = ((2*FS(1).Cbr_in/1000)-150)/150 ;
        FS(i).DRec_br               =              1000              *
((4.032219*FS(i).G1+0.115313*FS(i).Bbr+3.26E-4*(2*FS(i).Bbr^2-
1))*FS(i).F1 +
                          (-0.108199*FS(i).G1+1.571E-3*FS(i).Bbr-
4.23E-4*(2*FS(i).Bbr^2-1))*FS(i).Abr +
                          (-0.012247*FS(i).G1+1.74E-3*FS(i).Bbr-9E-
6*(2*FS(i).Bbr^2-1))*(2*FS(i).Abr^2-1) +
                          (6.92E-4*FS(i).G1-8.7E-5*FS(i).Bbr-5.3E-
5*(2*FS(i).Bbr^2-1))*(4*FS(i).Abr^3-3*FS(i).Abr)) ;
        FS(i).Utot                                              =1e-3*(
0.00392*FS(i).Tvap^1.1509*(FS(i).Rec_br/FS(i).DRec_br/

(3.14/4*FS(i).Diam_Tube_in*FS(i).Notubes))^0.2864);     #     MJ/Kg.K,
AlFulaij 2002
      end
      #Overall heat transfer coefficient Last stage#
        FSRL(1).Tfeed_avg = (FSRL(1).Tc_in+FSRL(1).Tc_out)/2;
        FSRL(1).Abr     = ((2*(FSRL(1).Tfeed_avg-273.15)-200))/160 ;
        FSRL(1).Bbr     = ((2*FS(1).Cbr_in/1000)-150)/150 ;
        FSRL(1).DRec_br             =             1000              *
((4.032219*FSRL(1).G1+0.115313*FSRL(1).Bbr+3.26E-4*(2*FSRL(1).Bbr^2-
1))*FSRL(1).F1 +
                          (-0.108199*FSRL(1).G1+1.571E-3*FSRL(1).Bbr-
4.23E-4*(2*FSRL(1).Bbr^2-1))*FSRL(1).Abr +
                          (-0.012247*FSRL(1).G1+1.74E-3*FSRL(1).Bbr-
9E-6*(2*FSRL(1).Bbr^2-1))*(2*FSRL(1).Abr^2-1) +
                          (6.92E-4*FSRL(1).G1-8.7E-5*FSRL(1).Bbr-5.3E-
5*(2*FSRL(1).Bbr^2-1))*(4*FSRL(1).Abr^3-3*FSRL(1).Abr)) ;

        FSRL(1).Utot                                            =1e-3*(
0.00392*FSRL(1).Tvap^1.1509*(FSRL(1).Rec_br/FSRL(1).DRec_br/

(3.14/4*FSRL(1).Diam_Tube_in*FSRL(1).Notubes))^0.2864);   #   MJ/Kg.K,
AlFulaij 2002

      FOR i := 1 TO nostages-2 DO
        CASE FS(i).Condensation OF
          WHEN FS(i).present    :

        FS(i).Din*FS(i).Cp_dist*(FS(i).Tdin-FS(i).Tvap)             +
(FS(i).Cond_rate*FS(i).Vap_heat)+FS(i).Vin*(1-FS(i).Yin)*(1.88e-
3*(FS(i).Tdin-FS(i).Tvap)+(FS(i).Vap_heat                          ))+
FS(i).Vin*FS(i).Yin*FS(i).Cp_air*(FS(i).Tvap_in-FS(i).Tvap)
       {- FS(i).Vout*FS(i).Y*FS(i).Cp_air*(FS(i).Tvap-273.15)}
                                  =
FS(i).Rec_br*FS(i).Cp_br*(FS(i).Tc_out-FS(i).Tc_in) ;
            FS(i).Din*FS(i).Cp_dist*(FS(i).Tdin-FS(i).Tvap)         +
(FS(i).Cond_rate*FS(i).Vap_heat)+FS(i).Vin*(1-FS(i).Yin)*(1.88e-
3*(FS(i).Tdin-FS(i).Tvap)+(FS(i).Vap_heat                          ))+
FS(i).Vin*FS(i).Yin*FS(i).Cp_air*(FS(i).Tvap_in-FS(i).Tvap)
```

```
       {- FS(i).Vout*FS(i).Y*FS(i).Cp_air*(FS(i).Tvap-273.15)}
                                          = FS(i).Utot * FS(i).Area *
                                                  ((FS(i).Tvap-
FS(i).Tc_in)+(FS(i).Tvap-FS(i).Tc_out))/2 ;
              FS(i).Q_rate  = FS(i).Rec_br*FS(i).Cp_br*(FS(i).Tc_out-
FS(i).Tc_in) ;

            SWITCH  TO  FS(i).notpresent       IF     (FS(i).Tvap  <
FS(i).Tc_out) ;
          WHEN FS(i).notpresent :
                           FS(i).Cond_rate =   0.0001          ;
                           FS(i).Tc_out    = FS(i).Tc_in  ;
                           FS(i).Q_rate = 0;
            SWITCH  TO  FS(i).present            IF    (FS(i).Tvap  >
FS(i).Tc_out+0.2)  ;
        END #CASE
      END #FOR
      FOR i := nostages-1 TO nostages DO
        CASE FS(i).Condensation OF
          WHEN FS(i).present    :

        FS(i).Din*FS(i).Cp_dist*(FS(i).Tdin-FS(i).Tvap)             +
(FS(i).Cond_rate*FS(i).Vap_heat)+FS(i).Vin*(1-FS(i).Yin)*(1.88e-
3*(FS(i).Tdin-FS(i).Tvap)+(FS(i).Vap_heat                          ))+
FS(i).Vin*FS(i).Yin*FS(i).Cp_air*(FS(i).Tvap_in-FS(i).Tvap)
       {- FS(i).Vout*FS(i).Y*FS(i).Cp_air*(FS(i).Tvap-273.15)}
                                          =
FS(i).Rec_br*FS(i).Cp_br*(FS(i).Tc_out-FS(i).Tc_in) ;
            FS(i).Din*FS(i).Cp_dist*(FS(i).Tdin-FS(i).Tvap)         +
(FS(i).Cond_rate*FS(i).Vap_heat)+FS(i).Vin*(1-FS(i).Yin)*(1.88e-
3*(FS(i).Tdin-FS(i).Tvap)+(FS(i).Vap_heat                          ))+
FS(i).Vin*FS(i).Yin*FS(i).Cp_air*(FS(i).Tvap_in-FS(i).Tvap)
       {- FS(i).Vout*FS(i).Y*FS(i).Cp_air*(FS(i).Tvap-273.15)}
                                          = FS(i).Utot *FS(i).Area*
                                                  ((FS(i).Tvap-
FS(i).Tc_in)+(FS(i).Tvap-FS(i).Tc_out))/2 ;

            FS(i).Q_rate    =  FS(i).Rec_br*FS(i).Cp_br*(FS(i).Tc_out-
FS(i).Tc_in) ;
            SWITCH  TO  FS(i).notpresent       IF     (FS(i).Tvap  <
FS(i).Tc_out) ;
          WHEN FS(i).notpresent :
                           FS(i).Cond_rate =   0.0001          ;
                           FS(i).Tc_out    = FS(i).Tc_in  ;
                           FS(i).Q_rate = 0;
            SWITCH  TO  FS(i).present            IF    (FS(i).Tvap  >
FS(i).Tc_out+0.2)  ;
        END #CASE
      END #FOR
      CASE FSRL(1).Condensation OF
          WHEN FSRL(1).present    :

        FSRL(1).Din*FSRL(1).Cp_dist*(FSRL(1).Tdin-273.15)           +
(FSRL(1).Cond_rate+FSRL(1).Vin*(1-FSRL(1).Yin))*FSRL(1).Vap_heat    +
FSRL(1).Vin*FSRL(1).Yin*FSRL(1).Cp_air*(FSRL(1).Tvap_in-FSRL(1).Tvap)
      -     FSRL(1).Dout*FSRL(1).Cp_dist*(FSRL(1).Tvap-273.15)     {-
FSRL(1).Vout*FSRL(1).Y*FSRL(1).Cp_air*(FSRL(1).Tvap-273.15)}
                                          =
FSRL(1).Feed_Mcw*FSRL(1).Cp_br*(FSRL(1).Tc_out-FSRL(1).Tc_in) ;
```

```
            FSRL(1).Din*FSRL(1).Cp_dist*(FSRL(1).Tdin-273.15)        +
(FSRL(1).Cond_rate+FSRL(1).Vin*(1-FSRL(1).Yin))*FSRL(1).Vap_heat     +
FSRL(1).Vin*FSRL(1).Yin*FSRL(1).Cp_air*(FSRL(1).Tvap_in-FSRL(1).Tvap)
      -     FSRL(1).Dout*FSRL(1).Cp_dist*(FSRL(1).Tvap-273.15)     {-
FSRL(1).Vout*FSRL(1).Y*FSRL(1).Cp_air*(FSRL(1).Tvap-273.15)}
                                          =       FSRL(1).Utot       *
FSRL(1).area *
                                                 ((FSRL(1).Tvap-
FSRL(1).Tc_in)+(FSRL(1).Tvap-FSRL(1).Tc_out))/2 ;
      FSRL(1).Q_rate =FSRL(1).Feed_Mcw*FSRL(1).Cp_br*(FSRL(1).Tc_out-
FSRL(1).Tc_in) ;

            SWITCH  TO  FSRL(1).notpresent      IF    (FSRL(1).Tvap  <
FSRL(1).Tc_out) ;
          WHEN FSRL(1).notpresent :
                           FSRL(1).Cond_rate =   0.0001          ;
                           FSRL(1).Tc_out    = FSRL(1).Tc_in  ;
                          FSRL(1).Q_rate = 0;
            SWITCH  TO  FSRL(1).present          IF    (FSRL(1).Tvap  >
FSRL(1).Tc_out+0.2)  ;
       END #CASE


      ##connecting two subsequent stages##
      For i :=1 to Nostages-1 Do
            FS(i+1).Tdin = FS(i).Tvap ;
            FS(i+1).Din  = FS(i).Dout;
            FS(i).brine_outlet = FS(i+1).brine_inlet ;
            FS(i).Bout         = FS(i+1).Bin         ;
      END
      For i :=nostages to Nostages Do
            FSRL(1).Tdin = FS(i).Tvap ;
            FSRL(1).Din  = FS(i).Dout;
            FS(i).brine_outlet = FSRL(1).brine_inlet ;
            FS(i).Bout         = FSRL(1).Bin         ;
      END


      For i:=1 to Nostages-3 Do
           FS(i).Tc_in       = FS(i+1).Tc_out;
           FS(i).Rec_br      = FS(i+1).Rec_br ;
      END

      For i:=Nostages-1 to Nostages-1 Do
           FS(i).Tc_in       = FS(i+1).Tc_out;
           FS(i).Rec_br      = FS(i+1).Rec_br ;
      END
      For i:=Nostages to Nostages Do
           FS(i).Tc_in       = FSRL(1).Tc_out;
           FS(i).Rec_br      = FSRL(1).feed_mcw ;
      END
      FOR i :=1 TO 1 DO
          FS(i).Vin       =0  ;
          FS(i).Yin       =0  ;
          FS(i).Tvap_in   =300;
      END #FOR

      FOR i :=2 TO 2 DO
          FS(i).Vin=0;
          FS(i).Yin=FS(i-1).Y;
```

```
        FS(i).Tvap_in=FS(i-1).Tvap;
    END #FOR

    FOR i :=3 TO 7 DO
        FS(i).Vin=FS(i-1).Vout;
        FS(i).Yin=FS(i-1).Y;
        FS(i).Tvap_in=FS(i-1).Tvap;
    END #FOR

    FOR i :=8 TO 8 DO
        FS(i).Vin=0;
        FS(i).Yin=FS(i-1).Y;
        FS(i).Tvap_in=FS(i-1).Tvap;
    END #FOR

    FOR i :=9 TO 12 DO
        FS(i).Vin=FS(i-1).Vout;
        FS(i).Yin=FS(i-1).Y;
        FS(i).Tvap_in=FS(i-1).Tvap;
    END #FOR

    FOR i :=13 TO 13 DO
        FS(i).Vin=0;
        FS(i).Yin=FS(i-1).Y;
        FS(i).Tvap_in=FS(i-1).Tvap;
    END #FOR

    FOR i :=14 TO nostages DO
        FS(i).Vin=FS(i-1).Vout;
        FS(i).Yin=FS(i-1).Y;
        FS(i).Tvap_in=FS(i-1).Tvap;
    END #FOR

        FSRL(1).Vin=FS(nostages).Vout;
        FSRL(1).Yin=FS(nostages).Y;
        FSRL(1).Tvap_in=FS(nostages).Tvap;

    ##Total Plant Capacity and Performance Ratio##
      distcapacity     = FSRL(1).Dout;
      PerformanceRatio = distcapacity/Msteam;


    ##BRINE HEATER energy balanc##
      Steam_heat   =   (2501.89714   -   2.40706*(Tsteam-273.15)   +
1.192217e-3*(Tsteam-273.15)^2   -   1.5863E-5*(Tsteam-273.15)^3)*1E-3
;#Ettuney;
      Msteam   *   Steam_heat   =   FS(1).Rec_br   *   FS(1).Cp_br     *
(FS(1).Tbr_in - FS(1).Tc_out);




    #Recycles tream salinity

    FSRL(1).Feed_Last *FSRL(1).Cbr_feed + FSRL(1).Bout+ FSRL(1).Cbr
=
    FSRL(1).Rec_br   *   FSRL(1).Cbr_rec   +   (FSRL(1).Feed_Last   -
distcapacity)*70000 ;

    FS(1).Cbr_in =  FSRL(1).Cbr_rec
```

```
##################################################################
#                          SCHEDULED PROCESS                     #
#                                                                #
##################################################################


UNIT
  MSF   AS    MSF_PLANT


MONITOR
  MSF.FS(*).DPdemister   ;
  MSF.FS(*).Peevap       ;
  MSF.FS(*).Teevap       ;
  MSF.FS(*).NCin         ;
  MSF.FS(*).NCout        ;
  MSF.FS(*).Mnncond      ;
  MSF.FS(*).P            ;
  MSF.FS(*).Bout         ;
  MSF.FS(*).Vout         ;
  MSF.FS(*).Dbr          ;
  MSF.FS(*).Ddist        ;
  MSF.FS(*).Vin          ;
  MSF.FS(*).Hbrine       ;
  MSF.FS(*).Cbr          ;
  MSF.FS(*).Tvap         ;
  MSF.FS(*).Tevap        ;
  MSF.FS(*).Tbr          ;
  MSF.FS(*).NEA          ;
  MSF.FS(*).Cond_rate    ;
  MSF.FS(*).Tc_in        ;
  MSF.FS(*).Tc_out       ;
  MSF.FS(*).Vap_rate     ;
  MSF.FS(*).Mvap         ;
  MSF.FS(*).Cd           ;
  MSF.FS(*).Y            ;
  MSF.FS(*).Non_cond_rate;
  MSF.FS(*).ALPHA        ;
  MSF.FS(*).Utot         ;
  MSF.FS(*).BPE          ;
  MSF.FSRL(1).Cbr        ;
  MSF.FSRL(1).Bout       ;
  MSF.FSRL(1).Cond_rate  ;
  MSF.FSRL(1).Tbr        ;
  MSF.distcapacity       ;
  MSF.PerformanceRatio   ;
  MSF.Msteam             ;

SET # Parameter Values
  MSF.NoStages         := 23      ; #Without the last stage
  MSF.g                := 9.81    ; # m/s2
  MSF.W                := 17.66   ; # m
  MSF.L                := 4       ; # m
  MSF.Wtube            := 17.66   ; # m

  FOR i:=1 TO MSF.NOSTAGES do
  MSF.FS(i).H          := 4       ; # m
  MSF.FS(i).Demisterdensity := 80 ; #kg/m3
  MSF.FS(i).wire_diam  := 0.254   ; #mm
```

```
        END
        MSF.FSRL(1).H          := 4       ; # m
        MSF.FSRL(1).Demisterdensity := 80 ; #kg/m3
        MSF.FSRL(1).wire_diam  := 0.254   ; #mm

        FOR i:=1 TO MSF.NoStages DO
          MSF.FS(i).A        := MSF.FS(i).L * MSF.FS(i).W ; #m2
        END #FOR
           MSF.FSRL(1).A          := MSF.FSRL(1).L * MSF.FSRL(1).W ;
#m2
       # FLASH BOX DIMENSIONS FOR EACH STAGE (REAL PLANT DATA)
        MSF.FS(1).HORIFICE1  :=0.098;
        MSF.FS(2).Horifice1  :=0.220;
        MSF.FS(3).Horifice1  :=0.228;
        MSF.FS(4).Horifice1  :=0.237;
        MSF.FS(5).Horifice1  :=0.262;
        MSF.FS(6).Horifice1  :=0.293;
        MSF.FS(7).Horifice1  :=0.355;
        MSF.FS(8).Horifice1  :=0.355;
        MSF.FS(9).Horifice1  :=0.388;
        MSF.FS(10).Horifice1 :=0.224;
        MSF.FS(11).Horifice1 :=0.307;
        MSF.FS(12).Horifice1 :=0.310;
        MSF.FS(13).Horifice1 :=0.400;
        MSF.FS(14).Horifice1 :=0.304;
        MSF.FS(15).Horifice1 :=0.310;
        MSF.FS(16).Horifice1 :=0.354;
        MSF.FS(17).Horifice1 :=0.361;
        MSF.FS(18).Horifice1 :=0.409;
        MSF.FS(19).Horifice1 :=0.429;
        MSF.FS(20).Horifice1 :=0.443;
        MSF.FS(21).Horifice1 :=0.488;
        MSF.FS(22).Horifice1 :=0.488;
        MSF.FS(23).Horifice1 :=0.490;
        MSF.FSRL(1).Horifice1 :=0.495;

        MSF.FS(1).Horifice2  :=0.155;
        MSF.FS(2).Horifice2  :=0.234;
        MSF.FS(3).Horifice2  :=0.240;
        MSF.FS(4).Horifice2  :=0.230;
        MSF.FS(5).Horifice2  :=0.270;
        MSF.FS(6).Horifice2  :=0.339;
        MSF.FS(7).Horifice2  :=0.428;
        MSF.FS(8).Horifice2  :=0.496;
        MSF.FS(9).Horifice2  :=0.562;

        FOR i :=10 to msf.nostages do
        MSF.FS(i).Horifice2 := MSF.FS(i).Horifice1;
                  # Horifice2 for these stages will not occur in the
            solution
        END#for
        MSF.FSRL(1).Horifice2 := MSF.FSRL(1).Horifice1;




        MSF.R                := 8.314   ; # J/mol/K
        MSF.H2O_mol_mass     := 18      ; # kg/kmol
        MSF.AIR_mol_mass     := 29      ; # kg/kmol
        MSF.Pvent            := 7000    ; # Pa
```

```
        MSF.Pvent1          := 60800   ; # Pa
        MSF.Pvent7          := 30000   ; # Pa
        MSF.Pvent12         := 11000    ; # Pa


      #Physical parmaeters corerlations
        MSF.Aant := 23.2256 ; #ANTOINE EQUATION, P[Pa] & T[K]
        MSF.Bant := 3835.18 ; #ANTOINE EQUATION, P[Pa] & T[K]
        MSF.Cant := 45.343  ; #ANTOINE EQUATION, P[Pa] & T[K]

        MSF.G1 := 0.5 ; #BRINE DENSITY CORRELATION
        MSF.F1 := 0.5 ; #BRINE DENSITY CORRELATION

      #Condensing zone parameters

        FOR i := 1 TO MSF.NoStages-3 DO
        MSF.FS(i).NoTubes         := 1410     ; # NUMBER OF CONDENSER
TUBES
        MSF.FS(i).Diam_Tube_out  := 0.0445  ; # m
        MSF.FS(i).Diam_Tube_in   := 0.04197 ; # m
        END #FOR
        FOR i := MSF.Nostages-2 TO MSF.NoStages DO
        MSF.FS(i).NoTubes         := 1992     ; # NUMBER OF CONDENSER
TUBES
        MSF.FS(i).Diam_Tube_out  := 0.03175  ; # m
        MSF.FS(i).Diam_Tube_in   := 0.02927  ; # m
        END #FOR
        MSF.FSRL(1).NoTubes            := 1992       ; # NUMBER OF
CONDENSER TUBES
        MSF.FSRL(1).Diam_Tube_out  := 0.03175  ; # m
        MSF.FSRL(1).Diam_Tube_in   := 0.02927  ; # m



      # CONTROL LOOP PARAMETERS
        MSF.Hsp           := 0.688 ;     # SET POINT FOR THE BRINE
HEIGHT IN THE LAST STAGE
        MSF.ALPHA_sp    := 0.5e-1;    # initial value of ALPHA in the
last stage [m2]




      ASSIGN # Degrees of Freedom
        MSF.FSRL(1).feed_mcw          := 832+1400;
        MSF.FSRL(1).Mcw               := 1400 ;
        MSF.FS(1).Tdin                := 250         ;#No Distillate
entering stage1
        MSF.FS(1).Din                 := 0           ;#No Distillate
entering stage1
        MSF.FS(1).Tbr_in                 := 91.3+273.15 ; # K , TOP
BRINE TEMPERATURE
        MSF.FS(1).Bin                 := 4025.3      ; # kg/s , FEED
BRINE TO STAGE 1
        MSF.FS(21).Rec_br               := 4025.3       ; # Kg/sec ,
recycle brine flow rate in the condensing tubed
        MSF.FS(21).Tc_in              := 37.73+273.15   ;
        MSF.FS(1).Xgas_in              := 9E-5        ; # ppm , FEED
GAS CONTENT
```

```
        MSF.FSRL(1).Tc_in               := 31.87+273.15   ; # K , SEA
WATER TEMPERATURE
        MSF.FSRL(1).Rec_br             := 4025.3      ;
        MSF.FSRL(1).Cbr_feed           := 40000       ;
        MSF.FSRL(1).Xgas_feed          := 9E-4        ;

        MSF.Psp                        := 7500       ; # Pa SET POINT
FOR THE PRESSURE IN THE LAST STAGE (calculated after setting the
outlet temperature)
        MSF.Tsteam                        := 111+273.15  ; #K ,steam
condensation temperature in the brine heater

        FOR i:=1 to (msf.nostages) do
        MSF.FS(i).ALPHA      := 0.5E-1     ; # m2
        END#FOR
        For i:=1 to 21 do
        MSF.FS(i).area       :=3367   ;
        End
        For i:=22 to 23 do
        MSF.FS(i).area        :=3398 ;
        end
        MSF.FSRL(1).area     :=3398;
      INITIAL # Initial Conditions

        MSF.FS(1).Cbr_in               := 64528       ; # ppm , FEED
SALINITY


        MSF.FS(1) .Hbrine      = 1.2676916  ; # m
        MSF.FS(2) .Hbrine      = 1.9961544  ; # m
        MSF.FS(3) .Hbrine      = 1.9977281  ; # m
        MSF.FS(4) .Hbrine      = 1.8446163  ; # m
        MSF.FS(5) .Hbrine      = 1.6556592  ; # m
        MSF.FS(6) .Hbrine      = 1.3906261  ; # m
        MSF.FS(7) .Hbrine      = 1.0352969  ; # m
        MSF.FS(8) .Hbrine      = 1.6980833  ; # m
        MSF.FS(9) .Hbrine      = 1.6668056  ; # m
        MSF.FS(10).Hbrine      = 1.5893252  ; # m
        MSF.FS(11).Hbrine      = 1.3468597  ; # m
        MSF.FS(12).Hbrine      = 1.1631613  ; # m
        MSF.FS(13).Hbrine      = 1.0557262  ; # m
        MSF.FS(14).Hbrine      = 1.0495183  ; # m
        MSF.FS(15).Hbrine      = 0.9989856  ; # m
        MSF.FS(16).Hbrine      = 0.91079885 ; # m
        MSF.FS(17).Hbrine      = 0.84954417 ; # m
        MSF.FS(18).Hbrine      = 0.80167437 ; # m
        MSF.FS(19).Hbrine      = 0.78042215 ; # m
        MSF.FS(20).Hbrine      = 0.76704156 ; # m
        MSF.FS(21).Hbrine      = 0.7462217  ; # m
        MSF.FS(22).Hbrine      = 0.72042215 ; # m
        MSF.FS(23).Hbrine      = 0.70704156 ; # m
        MSF.FSRL(1).Hbrine      = 0.6862217  ; # m

        MSF.FS(1).Pevap         = 62742.383    ; # Pa
        MSF.FS(2).Pevap         = 50170.133    ; # Pa
        MSF.FS(3).Pevap         = 44160.668    ; # Pa
        MSF.FS(4).Pevap         = 38927.12     ; # Pa
        MSF.FS(5).Pevap         = 34696.26     ; # Pa
        MSF.FS(6).Pevap         = 31925.96     ; # Pa
        MSF.FS(7).Pevap         = 30601.58     ; # Pa
```

```
  MSF.FS(8).Pevap          = 20352.328    ; # Pa
  MSF.FS(9).Pevap          = 17940.615    ; # Pa
  MSF.FS(10).Pevap         = 15339.161    ; # Pa
  MSF.FS(11).Pevap         = 14226.41     ; # Pa
  MSF.FS(12).Pevap         = 13130.971    ; # Pa
  MSF.FS(13).Pevap         = 11945.176    ; # Pa
  MSF.FS(14).Pevap         = 10995.577    ; # Pa
  MSF.FS(15).Pevap         = 10215.243    ; # Pa
  MSF.FS(16).Pevap         = 9543.536     ; # Pa
  MSF.FS(17).Pevap         = 8913.589     ; # Pa
  MSF.FS(18).Pevap         = 8340.192     ; # Pa
  MSF.FS(19).Pevap         = 7811.212     ; # Pa
  MSF.FS(20).Pevap         = 7346.776     ; # Pa
  MSF.FS(21).Pevap         = 7006.4883    ; # Pa
  MSF.FS(22).Pevap         = 6811.212     ; # Pa
  MSF.FS(23).Pevap         = 6346.776     ; # Pa
  MSF.FSRL(1).Pevap        = 6006.4883    ; # Pa

FOR i :=1 TO MSF.NoStages DO
    MSF.FS(i).Cbr      = 50000          ; # ppm
    MSF.FS(i).Xgas     = 9E-5           ; # kg/kg
    MSF.FS(i).Y        = 0.05          ; # kg/kg

END #FOR

    MSF.FSRL(1).Cbr      = 50000          ; # ppm
    MSF.FSRL(1).Xgas     = 9E-5           ; # kg/kg
    MSF.FSRL(1).Y        = 0.08          ; # kg/kg


SOLUTIONPARAMETERS
  REPORTINGINTERVAL    := 100   ;
  OUTPUTLEVEL          := 4       ;
  DIAGNOSTICS          := OFF     ;
  IndexReduction       := ON      ;
  ABSOLUTEACCURACY     := 1E-4    ;


SCHEDULE  # Operating procedure

SEQUENCE

    CONTINUE FOR 55000

END #SEQUENCE
```